N° d'ordre : 2016LYSEI003 Année 2016

THÈSE

présentée devant

L'Institut National des Sciences Appliquées de Lyon

pour obtenir le grade de

Docteur

dans le cadre de

L'école doctorale Électronique Électrotechnique Automatique

par

FIRAS KHALED
Ingénieur

Contribution à la Valorisation Electrique des Piles à Combustible Microbiennes

(Contribution to Electrical Valorization of Microbial Fuel Cells)

Soutenue devant la commission d'examen

le 21 Janvier 2016

Membres du jury :

M. YVES LEMBEYE	Professeur	G2Elab (Grenoble)	Rapporteur
M. CHRISTOPHE INNOCENT	Chargé de Recherche	IEM (Montpellier)	Rapporteur
M. OLIVIER ONDEL	Maître de Conférences	Ampère (Lyon)	Encadrant
M. BRUNO ALLARD	Professeur	Ampère (Lyon)	Directeur
M. NICOLAS DEGRENNE	Docteur	MERCE (Rennes)	Examinateur
M. VINCENZO FERRARA	Professeur	DIET (Rome, Italie)	Président

Thèse préparée dans les départements bioingénierie et énergie électrique du laboratoire Ampère de Lyon

UMR CNRS 5005, 21 avenue Jean capelle – 69621 Villeurbanne cedex , France

Remerciements

La présente étude n'aurait pas été possible sans le bienveillant soutien de certaines personnes. Et je ne suis pas non plus capable de dire dans les mots qui conviennent, le rôle qu'elles ont pu jouer à mes côtés pour en arriver là. Cependant, je voudrais les prier d'accueillir ici tous mes sentiments de gratitude qui viennent du fond de mon coeur, en acceptant mes remerciements.

Mes premiers remerciements vont d'abord à mon directeur de thèse, le professeur Bruno ALLARD, qui m'a accompagné tout au long de ma formation. Sa disponibilité et ses généreux secours au cours de certains de mes moments difficiles ont été d'une très grande qualité, et d'un immense réconfort. Entre autres qualités, peu de personnes ń racontent ż comme lui la science. Je me souviendrai de l'énergie et de la motivation communicative qui se dégage de ce laboratoire. Cette énergie a définitivement marqué ma thèse tout comme le plaisir et l'honneur d'avoir travaillé au sein de laboratoire Ampère. Merci infiniment Monsieur ALLARD, votre rigueur au travail est un exemple pour moi. Je remercie Olivier Ondel qui a codirigé cette thèse en y apportant conseils et soutien. Je lui adresse mes sincères remerciements ainsi que mon plus profond respect. Je remercie aussi tous les membres de mon jury qui m'ont prodigué d'utiles conseils qui m'ont aidé à bien structurer mon étude : il s'agit de : Monsieur Yves Lembeye et Monsieur Christophe Innocent m'ont fait l'honneur d'être rapporteurs de ma thèse, ils ont pris le temps de m'écouter et de discuter avec moi. Leurs remarques m'ont permis d'envisager mon travail sous un autre angle. Pour tout cela je les remercie. Je tiens à remercier Vincenzo Ferrara pour avoir accepté de participer à mon jury de thèse et pour sa participation scientifique ainsi que le temps qu'il a consacré à ma recherche. Je remercie également Nicolas Degrenne pour l'honneur qu'il me fait d'être dans mon jury de thèse. Je sais infiniment gré à monsieur François Buret de s'être rendu disponible pour la pré-soutenance, de m'avoir prodigué maints conseils et d'avoir accepté la fonction de rapporteur.

J'adresse un grand merci à mon père, pour qui entre autres, j'ai spécialement porté cette tenue aujourd'hui, et à ma mère, pour avoir pu cimenter ma vie dans un douillet cocon familial, fait d'amour, de bravoure et de zèle au travail.

Il y a une personne de très grande importance dans ma vie, qui m'accompagne et qui me soutient tout le temps par la force et l'énergie qui lui sont disponibles. Il s'agit de KHALED Shahama, ma merveilleuse, splendide et vertueuse épouse, dont je ne pourrai mesurer l'apport dans l'accomplissement de cette formation. Dans tout ce que j'ai pu souffrir et obtenir, elle a été l'autre moi. Je te remercie infiniment ma chérie.

De plus, mes remerciements seraient incomplets, si je ne fais pas mention de mon enfant, qui a pu supporter mon éloignement et a pu continuer d'être sages en dépit de mon absence. Je t'adresse mes chaleureux remerciements, Sahar. De même, que tous les membres de la grande famille KHALED et KZO trouvent ici toute ma reconnaissance pour le soutien que chacun d'eux a pu apporter pour faire aboutir ce rêve. Heureusement que mes parents, mes frères et mes amis sont la pour me changer les idées. Ils ont tous cru en moi et ouf ! Maintenant j'y suis ! Alors merci à vous tous,

Mes remerciements vont également à mon pays qui m'a permis de terminer cette formation, en me fournissant les ressources nécessaires disponibles. Que tous ceux qui ont contribué à faciliter cette étude dans ce cadre trouvent ici le témoignage de ma sincère gratitude. Mes remerciements vont aussi à tous mes amis, qu'ils soient en France ou en Syrie, et je sais qu'ils sont nombreux. Vous m'avez tous soutenu par votre encouragement, et vos dons en prière et en nature souvent. Je vous adresse tous mes sentiments de reconnaissance renouvelée.

Abstract

Microbial **F**uel **C**ells (MFCs) are bioreactors that convert chemical energy in organic compounds to electrical energy through the metabolism of microorganisms. Organic matters are widely available in the environment that contains a huge amount of energy. This energy could be harvested, converted, by the technology of MFCs, to be used in certain applications. Energy production of a MFC is limited in low voltage value and low-power values what limits the potential applications. However this energy is still sufficient to supply low-power applications (e.g. wireless sensors) to replace batteries and overcome their (environmental and economic) limitations. An electrical model of MFCs appears useful to better understand their dynamics and to validate the design of electrical circuits before fabrication. That also helps to evaluate the internal losses what may lead to another design of MFCs for better efficiency.

To step-up the voltage of MFCs to be suitable for these applications, an efficient power management unit (PMU) is required with a specific design to deal with their characteristics. A flyback converter under discontinuous conduction mode (DCM) is the most adapted to such low-power source like MFCs, offers a simple implementation, and low losses conversion system. The DCM characteristics of the flyback converter are very attractive for impedance matching that is investigated as a maximum power point tracking algorithm. An integrated, low-voltage, low-consumption charge pump circuit is a good solution to supply start-up and the oscillator at low voltages. The flyback converter has a good efficiency that can reach 75% with one MFC and about 80% when it is supplied by a serial stack of MFCs.

Associations of MFCs are very interesting to increase the output power and expand the domain of application. Parallel association is a method to increase the output current but it imposes limitations in conversion efficiency due to the low output voltage of the stack. Contrarily, the serial association steps-up the voltage what leads to better performance of the converter. However the non-uniformities between cells in a serial stack affect negatively the performance of the stack. Voltage balancing circuits are considered as the solution to compensate this phenomenon. Alternatively connecting the MFCs in series and parallel can achieve the purpose (switched-MFCs) by exploiting the internal capacitor of the MFCs. In the switched-capacitor method, an external capacitor is used to transfer the energy from the strongest MFC(s) to the weakest one(s). The losses in the switched-capacitor circuit are less than the losses of the switched-MFCs. The switched-capacitor offers an efficient, simple, low consumption method to optimize the performance and prevent the voltage reversal of the weak cells. Integration of this circuit can optimize the efficiency.

Operating MFCs in a batch mode requires a periodic intervention to add organic matter. Continuous operation mode by hydraulically connection between MFCs overcomes this problem and can continuously refresh the substrate to give an autonomous energy harvesting system. On the other hand, in some applications, e.g. a wastewater treatment plant, MFCs could not be hydraulically isolated. In this configuration, a leakage charge between the associated MFCs will decrease the global efficiency. The flow rate has to be controlled to eliminate this problem. A flow from cathodes to anodes causes additional losses due to the oxygen leakage.

A practical investigation of the harvested energy from MFCs may prove the fact that MFCs are good candidates to replace the chemical batteries. A temperature sensor is continuously supplied by alternatively connecting two MFCs. Each MFC supplies the sensor for two days. The flyback converter is able to continuously supply the sensor from the energy harvested from one continuously-fed MFC. This could be a good example, in a wastewater treatment plant (WWTP), to supply the monitoring system or also to supply the low power application of a building from a local WWTP.

Keywords: Microbial fuel cell; energy harvesting; power management; DC/DC converter; voltage balancing; modeling; wastewater treatment plant; hydraulic coupling; low-power applications; sensors; renewable energy.

Contents

List of Figures

List of Tables

Chapter 1

Introduction

Contents

Fossil fuels have been the mainstay in providing energy during the industrial revolution. Considering that fossil fuel reserves are finite, one of the greatest challenges in this century is to manage the global energy demands necessary to support the economic growth and the population. Burning fossil fuel, such as coal, oil and natural gas, for energy production and industrial processes releases a huge amount of carbon dioxide and other greenhouse gases as CO, SO2, NOx and CH4, into the atmosphere what creates impacts dangerous to human health and environment [Mukhopadhyay and Forssell, 2005, Mohan et al., 2008]. Energy related emissions account for almost 80% of the total greenhouse gas emissions [COMMISSION, 2010]. The limitations of these sources call for more sustainable solutions. By using more renewables to meet energy needs, the word would lower its dependence on fossil fuels and makes its energy production more sustainable. No official definition has been published to the term ''renewable energy''. One definition accepted by the International Energy Agency is that "Renewable energy is the one which can be obtained from natural resources that can be constantly replenished". Green energy or renewable energy can be produced from a wide variety of natural sources including wind, solar, hydro, tidal, geothermal and various forms of biomass.

Solar energy refers to the energy produced directly from the natural light or the heat that sunlight generates [Bradford, 2006]. Solar energy is a free, inexhaustible resource. Two components are required

to have a functional solar energy generator , namely a collector and a storage unit. [Kalogirou, 2004]. The ability to use solar power for heating was the first discovery. Although producing electricity from solar energy was discovered in 1839 by Edmund Becquerel [Williams, 1960], it was not until 1954 that the first commercially viable application of the technology was demonstrated by Bell Laboratories [Chapin et al., 1954]. Even though solar energy generation represents only a small fraction of total energy production (4000 GWh generated by photovoltaic in France in 2013), markets for solar technologies are growing rapidly.

Wind power has been used for hundreds of years for pumping water and milling grains. Wind energy is then converted into electrical energy by wind turbines. This energy is growingly used in many countries like Germany, Denmark, Spain or USA.

Hydropower plants convert the kinetic energy of the natural falling or flowing water, such as a waterfall, or from a dam built across a river into electrical energy. Hydroelectric power plant is one of the most efficient, economical and environmentally friendly means of producing electric energy on a large scale.

Biomass is considered as a renewable energy resource. It refers to a product of organic matter that has stored energy and naturally regenerates at a rapid cycle. Biomass can be combusted directly as a solid fuel by thermal process to produce heat and electricity by driving a turbine. Biomass can be also converted to biogas, rich in methane, via a biological process through bacteria in the absence of oxygen under a controlled environment [Jacques K, 1999]. Natural but longer process of the solid waste is possible in landfill; a landfill gas (methane-rich-gas) will be produced and can be used as fuel for power generation [Rasi et al., 2007]. These biofuels can be converted either into mechanical energy in a combustion engine or into electrical energy in a fuel cell. In this case, gas obtained from biological materials and/or biological processes are known as bioalcohols (e.g. bioethanol). Biofuels can be candidates to replace petroleum fuel. One direct limitation is the use of land to grow resource not dedicated to feet the planet!. Production of biofuel from biomass is a good solution to reduce both consumption of oil and environmental pollution. These gases could be produced also from food [Kim et al., 2008]. For example, bioethanol could be produced through the fermentation of corn, potato, beet and wheat [Smith, 2008].

1.1 Various Energy Harvesting Techniques

In the past years, research and development works have been oriented to harnessing large-scale energy from various renewable energy sources (wind, solar, water, etc.). Small-scales energy harvesting from ambient energy (such as vibrational, thermal, wastewater, RF, etc.) are receiving more and more attention. The developments in low power design and CMOS technologies have been led to produce micropower electronic applications. Energy harvesting presents thus an important role for the alternative low power technology as it can reduce the dependency on batteries which have a number of limitations [Jiang et al., 2005]:

- The possibility of complete discharge brings negative consequences of forgetting to change the battery in safety-critical systems.
- The limited lifetime: this means that battery replacement will be required what leads to service disruptions during battery replacement and maintenance cost, especially when the system contains a large number of electronic devices or in inaccessible zone.
- Batteries contain chemicals materials which are hazardous both to the environment and to health if not carefully handled.
- The battery size often exceeds that of the system components in the electronic device.
- Batteries are non-operational in exceptional environmental conditions.
- High cost of a rechargeable battery.

Available ambient energy could be harvested, converted into usable electrical energy, stored and used for small electronics and low-power applications such as wireless and mobile electronics instead of batteries. Four energy types at least considered: thermal energy, radiant energy, mechanical and chemical energy as presented in Fig. 1.1. The sources of mechanical energy can be a moving object, a vibrating structure and vibration induced by flowing water or air [Roundy et al., 2003, Beeby et al., 2006]. Mechanical energy conversion can be achieved through three schemes, namely electromagnetic, electrostatic, and piezo- electric transductions [Arnold, 2007, Mitcheson et al., 2004, Jeon et al., 2005]. Thermoelectric conversion exploits the thermal energy carried by charges (electron and holes) near a heat source and convert temperature differences into electrical energy [Minnich et al., 2009, Böttner, 2002]. The concept of radiant energy harvesting is based on receiving RF signals (radio frequency) with frequency range from 300 GHz to as low as 3 kHz by an efficient antenna with a circuit capable of converting them into DC voltage [Visser and Vullers, 2013, Xie et al., 2013]. Microbial fuel cell is a technology to convert electrochemically the energy of organic matters (renewable biodegradable materials) into electricity, using either enzymes or microorganisms [Logan et al., 2006, Lovley, 2006].

Table 1.1 compares some features of low-power energy harvester, where it appears that the MFC, topic of this manuscript, is in the lower range of power density. To some extent, a MFC can be used as a sensor (almost autonomous in energy as will be demonstrated later). So MFC remains essentially a mean to transform organic wastes into valuable electricity. It is pertinent in the context of wastewater treatment plant WWTP but also the sensor node story and implantable medical devices. There is thus a real interest into managing the electricity generated from MFCs.

1.2 Microbial fuel cell as an energy harvester

Huge volume of wastewater from industrial and agriculture operations are produced annually. Treatment of this wastewater requires large amounts of energy. That is known in literature as “Water Energy

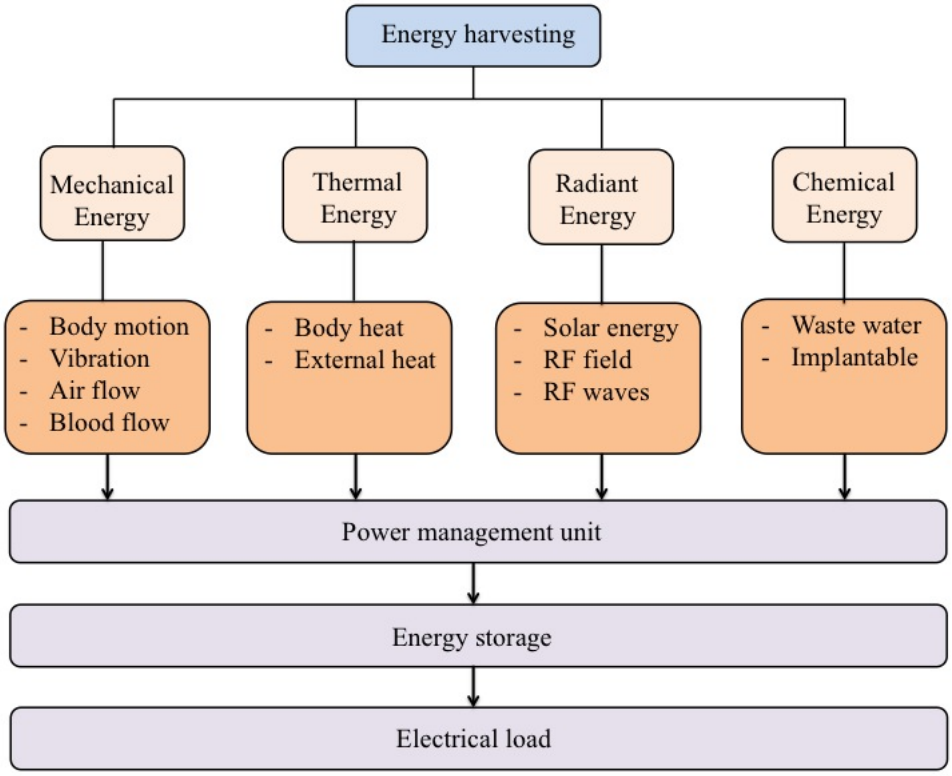

Figure 1.1: Types of ambient energy sources suitable for energy harvesting

Nexus" [Stillwell et al., 2010]. In wastewater treatment, a so-called activated sludge process is widely used. However during the degradation of organic pollutants, it produces huge amount of waste-activated sludge (WAS). Currently USA generates about 8.2 million tons of dry WAS per year and EU annually produces over 10 million tons. In China the total amount of sludge is about 4.4 million tons in 2010 and can increase to about 6 million tons in 2016 [Paul and Liu, 2012]. As the treatment and disposal of WAS accounts for 25–65% of the total plant operation cost [Zhao and Kugel, 1996], it has become a severe problem for many wastewater treatment plants (WWTPs) [Rai et al., 2004, Xiao et al., 2011]. From another perspective, the sludge contains high concentrations of organic matters that can be regarded as an available resource. A number of methods have been successfully used to recover resource/energy from WAS, e.g., anaerobic digestion for methane production [Appels et al., 2008], anaerobic fermentation for hydrogen generation [Guo, 2010], sludge composting for fertilizer utilization [Ndegwa and Thompson, 2001, U. Song, 2010], etc. Organic material in wastewater contains a huge amount of energy. Two technologies to harvest this energy are, namely, "Anaerobic hydrogen production" and "Microbial fuel cells (MFC)" [Sharma and Li, 2010, Appels et al., 2008, Li et al., 2009, U. Song, 2010]. It has been known for several years that bacteria found in wastewater could biologically convert the organic material into electricity [Allen and Bennetto, 1993]. The production of energy from wastewater provides

Table 1.1: Power density comparison of various energy harvesting sources

Energy Source	Performance (Power Density)	Notes	References
Solar (direct sunlight)	100 mW/cm^3		[Randall, 2003]
Thermoelectric	60 μW/cm^3	From 5 °C	[Stevens, 1999]
Blood Pressure	3μJ/cm^3/cycle		[Deterre et al., 2014]
Ambient airflow harvester	2.3 μW/cm^3	At 20 m/s	[S P Matova and van Schaijk, 2011]
Vibration	200 μW/cm^3		[Roundy et al., 2003, Roundy et al., 2004]
Implanted microbial fuel cell	72.3mW/m^2		[Patil, 2013]
Microbial fuel cell	1010 μW/cm^3	Continuous-flow mode wastewater	[Fan et al., 2007]

economic and environmental benefits. Besides capturing energy in the form of electricity, electricity can be used to power the wastewater treatment plant (WWTP) along cleaning the water. The aim of using this technology is to reduce the energy and cost of cleaning wastewater by using the microorganisms found in the wastewater to produce green electrical energy to operate the plant [Inc., 1999, Liu and Ramnarayanan, 2004]. This can be done by using MFCs to harvest that energy. Microbial fuel cell is a bio-electrochemical device suitable for producing electricity from wastewater. Capturing energy as a molecular biohydrogen by the fermentation of organic matter in wastewater treatment process could also be investigated to improve energy recovery in WWTP [Chong et al., 2009, Khanna and Das, 2013]. Integrating the two biotechnologies, anaerobic hydrogen production and microbial fuel cell, could optimize the energy harvesting from wastewater treatment. In this context, wastewater treatment plants could be self-sufficient and may even contribute energy to the grid. It was reported that a potential energy of 330 kWh could be produced from a WWTP that produces 7500 kg/day of waste organics [Logan, 2004b, Logan et al., 2006].

At this point, it is quite clear that MFCs in WWTP will not be considered with green energy generators from sun, wind or hydraulic storage, in terms of power density and peak power. MFCs must be seen as a mean to add value to the energy spoil in WWTP. What is true for the sludge in WWTP is also true

for a large number of organic waste matters in agriculture [Shannon et al., 2008, Samuel Raj. B, 2013]. On a small scale, a MFC should be considered as energy harvester for sensor nodes.

1.3 Conventional fuel cell technology

Fuel cells offer an exciting technology to harvest electrical energy from biomass by bridging biological components together with electrochemical devices. A fuel cell is a system that converts the chemical energy of the fuel into electrical energy [Minh and Takahashi, 1995]. Fuel cells have been developed for use with a variety of different fuels, the most common being hydrogen. Fuel cells have become a widely studied energy conversion technology due to their high efficiency: simplicity in terms of moving parts; and wide-range of configurations, fuels, and applications. A fuel cell is like a battery that converts chemical energy into electrical energy. However a battery holds a closed amount of energy and once it is depleted, the battery must be recharged. While a fuel cell uses an external source of chemical energy and can operate as long as it is supplied with a source of oxygen and a source of hydrogen. In a hydrogen fuel cell, electricity is generated efficiently from the oxidation of hydrogen, coupled to the reduction of oxygen, with water as presented in Fig. 1.2-a. Hydrogen is supplied to the anode and split into an electron and a proton via electrochemical reactions. Electrons are released in the process and flow from the anode to the cathode through an external circuit as an electric current [Edwards et al., 2008]. The most commonly used electrocatalyst in fuel cells is platinum. Platinum is very efficient in oxidizing hydrogen and enabling high currents to be produced. The major disadvantage is that platinum is expensive and its availability limited, resulting in an expensive method of energy production [Sealy, 2008]. At the cathode, oxygen reacts with electron and proton that have travelled through the electrolyte to form the water.

1.4 Biofuel cell technology

A biological fuel cell (biofuel cell) is the offspring of two technologies: biotechnology and fuel cells. Like conventional fuel cells, a biofuel cells are composed of two electrodes (anode and cathode) separated by a membrane that is selective for the passage protons. Microbial biofuel cells (abbreviated as microbial fuel cell or MFCs) employ living cells (microorganisms) to catalyze the oxidation of the fuel, whereas enzymatic biofuel cells (EFCs) use enzymes for this purpose [Minteer et al., 2007]. MFCs or EFCs transform chemical energy into electrical energy via electrochemical reactions involving microorganisms or enzymes. Enzymatic fuel cells employ enzymes as biocatalysts instead of conventional noble metal catalysts [Ivanov et al., 2010]. The operation of these cells is the same as in conventional fuel cells; fuel is oxidized at the anode side. The anode extracts electrons and hydrogen ions from the sugar (glucose) through enzymatic oxidation as follows:

$$Glucose(C_6H_{12}O_6) \rightarrow Gluconolactone(C_6H_{10}O_6) + 2H^+ + 2e^-$$

The electrons that are released are driven through an external electrical circuit to the cathode, where they combine with the final electron acceptor (typically oxygen) and protons to form water:

$^1/_2O_2 + 2H^+ + 2e^- \rightarrow H_2O$

The principle of operation of the conventional polymer electrolyte membrane (PEM) fuel cell and an enzymatic fuel cell (EFC) are presented in Fig. 1.2. Even though the BFCs have been known for almost a century since the first microbial BFC was demonstrated in 1911 [Potter, 1911], the first enzyme-based biofuel cell was reported only in 1964 using glucose as a biofuel [Yahiro et al., 1964]. Enzyme-based biofuel cells remain limited by short active lifetimes, low power densities and efficiency.

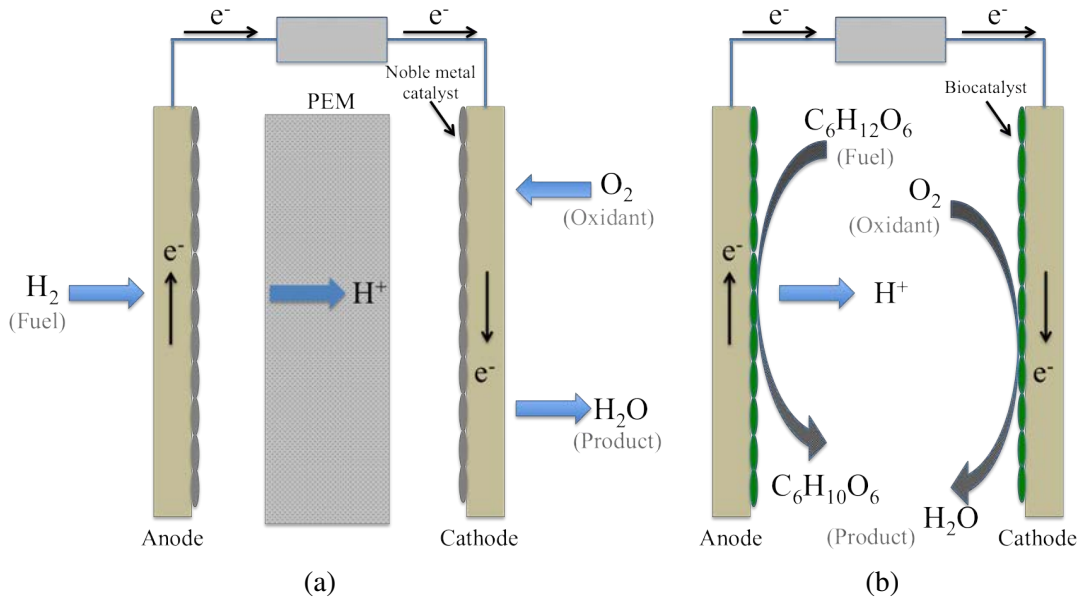

Figure 1.2: Schematic presentation of conventional PEM fuel cell (a) and enzymatic biofuel cell (b)

Microbial fuel cells (MFCs) are special types of biofuel cells, producing electric power by utilizing microorganisms, instead of isolated enzymes, to assist redox reactions. MFCs have longer lifetimes (up to several years) than EFCs. In both microbial and enzymatic fuel cells, mediators are required to transfer electrons from the oxidized fuel to the electrode surface. The drawback of utilizing a mediator is toxicity and sustainability of the system. Most mediators are not easily re-oxidized in the anodic chamber. Therefore continuous replacement of mediators is required [Logan et al., 2006]. It was found that some microorganisms have the ability to produce their own mediators to promote extracellular electron transfer (endogenous mediators). The electrons transferred to extracellular space can be utilized to generate anodic current [Schröder, 2007, Minteer et al., 2007].

1.5 Microbial Fuel Cells

Luigi Galvani observed the bioelectric phenomenon first in 1790 [Luigi, 1791] but microbial fuel cells (MFCs) were not discovered until the beginning of the 20th century. Microbial fuel cells (MFCs) have been demonstrated to generate electricity from a variety of carbon sources used as electron donors. In 1911, M.C. Potter was the first to observe and describe how microbial conversions could create power and electrical current [Potter, 1911]. He monitored the electrical effects associated with fermentation in a galvanic cell based on platinum wires and a pure culture of yeast and discovered the first bio-based battery. The concept was presented again in the literature in 1931 by Cohen by connected many cells to generate 35 volts with a low current (2mA) [Cohen, 1931]. From 1911-1960, there was very little interest or advances in this field. MFCs became popular in the 1960s, when the "NASA" in USA proposed the idea to use MFCs to supply their applications in space missions from human waste [Canfield JH, 1963]. It was discovered that current and power output could be enhanced by using electron mediators to improve the electron transfer rate from microorganisms to the anode [Allen and Bennetto, 1993, Thurston C. F. and L., 1985].

The truly research and application of MFCs were not advanced until the 1990's. Although the addition of chemical mediators as methylene blue in these first MFCs, output currents and power densities were still low. In 1999, first report was published that species *Shewanella* could transfer electrons directly in mediator-less microbial fuel cells [Kim et al., 1999]. That leaded to eliminate the mediator in MFCs. Such improvements were attributed to the minimized distance that the mediator had to travel between the electrode and bacteria and consequently minimizing the distance between electrodes of the MFC. This design exhibits a higher output current and power density resulting from using direct electron transfer bacteria. In that period, MFC's field publication released research fundamentals, methods, and only few designs [Biffinger and Ringeisen, 2008]. Contributions from material science, environmental engineering, electrical engineering, biology, microbial physiology and electrochemistry have made recently the study of MFCs a truly interdisciplinary endeavor [Lovley, 2006, Logan et al., 2006, He et al., 2006, Bullen et al., 2006].

The basic concept of a MFC incorporates anodes and cathodes connected by an electrical load, separated by a membrane (Fig.1.3). In the anode chamber, the fuel such as acetate or lactate is oxidized by a monoculture biofilms or bacterial microorganisms, releasing electrons and protons. In the anode chamber, it is essential that oxygen would not be present near the anode surface, as the electrode will function as the terminal electron acceptor for organisms associated with MFCs. The anode compartment is therefore an anaerobic region (i.e. no oxygen) where the anaerobic bacteria are located while the cathode compartment is an aerobic region (i.e. oxygen is present). An electrochemical reaction of reduction of oxygen and/or other molecules associated with wastewater, such as nitrates, occurs at the cathode of MFC [Rosenbaum et al., 2011]. The electrons produced through the oxidation of organic matter are transferred to the anode electrode, in the anode compartment, and travel through a wire and the electrical load to the cathode electrode. Protons are diffused through the membrane from the anode compartment

to the cathode to combine with the electrons and oxygen to form water. A catalyst at the cathode or a catholyte solution must be used to facilitate this reaction. The by-products of this reaction in MFCs are small amounts of carbon dioxide, from the decomposition of the organic matter and small amounts of water at the cathode.

The reactor is often divided by a proton exchange membrane into the anodic and cathodic compartments to form a two-chambered MFC. The proton exchange membrane allows the transport of positively charged ions (protons) from the anode to the cathode, thereby maintaining pH and electro-neutrality. The main drawback of using these separators is that they affect the fuel cell performance due to high Ohmic resistance contribution [Min et al., 2005]. The basic MFC which is used in MFCs research, such as examining the performance of new electrode materials, is a conventional MFC 'H' type design, dual chamber, containing two bottles separated by a tube containing the proton exchange membrane like Nafion [Logan et al., 2005, Oh et al., 2009]. This two-chamber design would be difficult to apply to larger systems for continuous wastewater treatment.

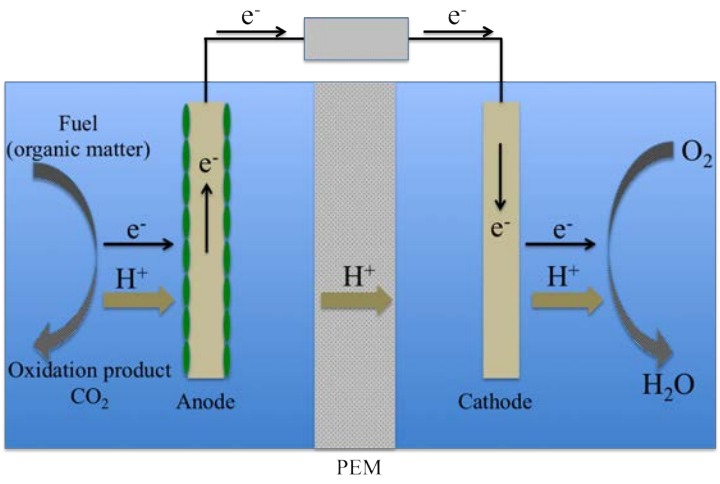

Figure 1.3: Schematic representation of dual chamber MFC system.

A simpler design where the proton exchange membrane could be eliminated will offer more perspective for energy harvesting. In a single chamber MFC design, the proton exchange membrane is either removed or pressed against the anode or cathode to form Membrane Electrode Assemblies (MEAs) as shown in Fig. 1.4. One is developed by Liu et al. [Liu and Ramnarayanan, 2004], which consisted of an anode placed at the bottom and a floating cathode placed at the top in a glass cylindrical chamber.

The basic advantage of exposing the cathode directly to air is to eliminate any limitation in oxygen supply to the electrode due to mass transport issues. These modifications minimize the internal resistance and increase the power generation [Logan et al., 2006]. Moreover this design is more suitable for large geometry scale and thus wastewater treatment [Liu and Ramnarayanan, 2004]. This design is therefore chosen in this study.

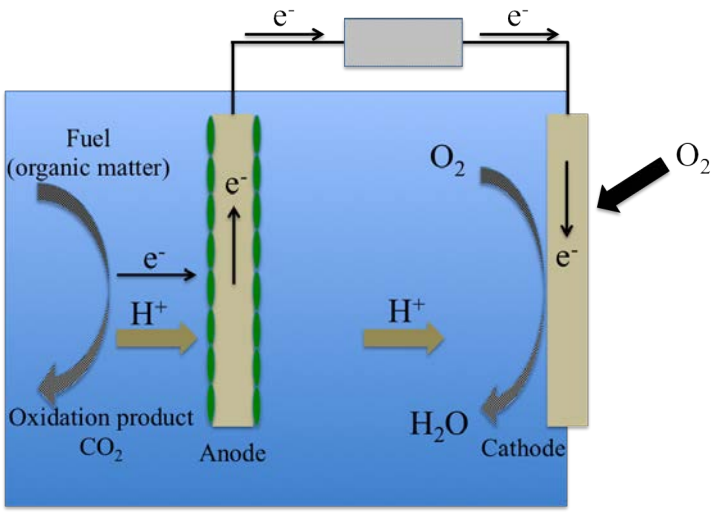

Figure 1.4: Schematic representation of single chamber MFC system.

1.6 Research efforts on MFCs

MFC technology is very attractive since it can potentially address two sustainability problems: energy production and wastewater management. It has been already proved that MFCs allow energy production from "poor" waste (e.g. sludge or wastewater) while providing inexpensive waste treatment.

In the past ten years, MFCs as a new source of bio-energy have been extensively reviewed [Pant et al., 2010] : various terminology and measurements [Logan et al., 2006], state of the art information on MFCs and recent improvements in MFC technologies [Du et al., 2007], electrodes performance and limitations in MFCs [Rismani-Yazdi et al., 2008, Pham et al., 2009] and practical implementation of BioElectrochemical Systems BESs [Rozendal et al., 2008]. The ability of the MFC to degrade a wide range of organic matters to provide efficiently the electrical energy has lead to a dramatic raise in the number of publications (see Fig. 1.5). Researches on MFCs are oriented towards four axes capabilities (Fig. 1.6):

- Configuration, design and materials
- Operating conditions
- Microorganisms and the microbial activities
- Power management unit and applications

MFCs are being fabricated using a wide variety of materials and diversity of configurations. Either single- or double-chamber MFC reactors can be constructed for electricity generation. Many materials have been studied and tested to achieve a best performance of the anode, the cathode and the membrane [Watanabe,

2008]. A more complex, stacked MFC is studied for the investigation of performances of several MFCs connected in series and in parallel [Aelterman et al., 2006a]. These systems are tested under a range of conditions including differences in temperature, pH, electron acceptor, reactor size, electrode surface areas and operation time [Hong Liu and Logan, 2005, Singh et al., 2010]. Energy harvesting from MFCs requires a specific design of power management system to deal with their characteristics (low power, low voltage). In literature, few papers are reported on electrical management of MFCs [Yang et al., 2012, Degrenne et al., 2012a]. Electrical conditioning of MFC(s) is still one critical part in the system.

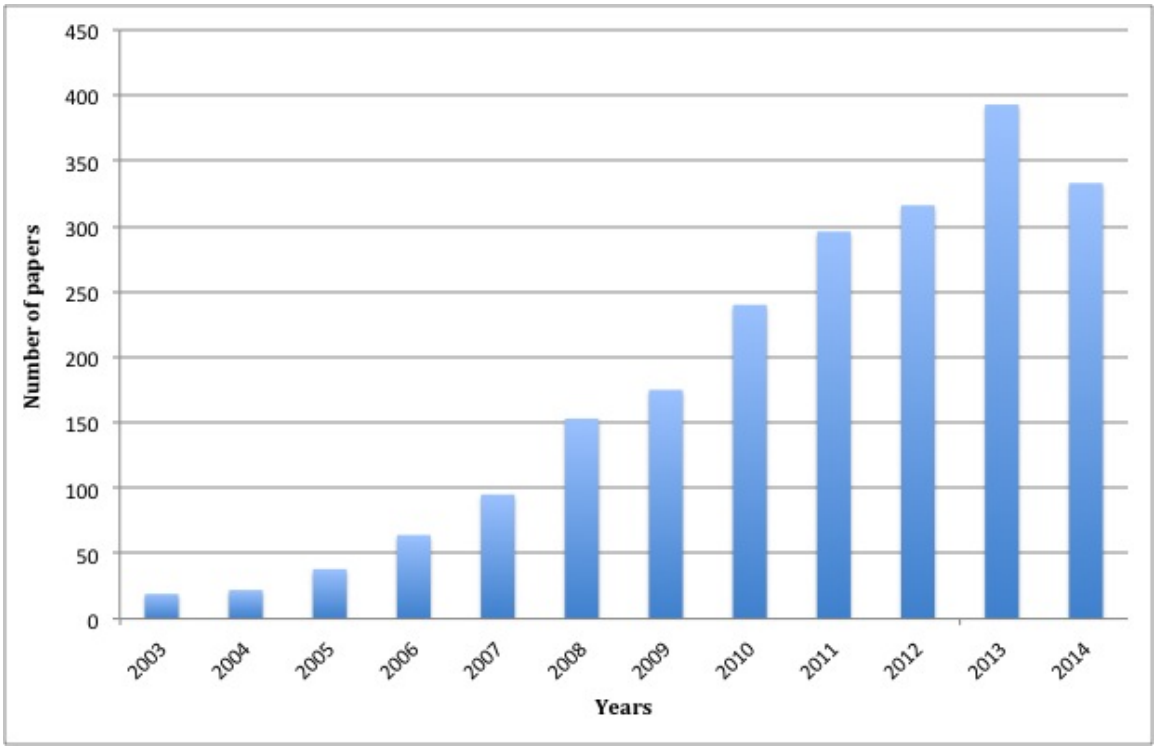

Figure 1.5: The number of articles on MFCs. The data is based on the number of articles entitled MFC in the database Google scholar in July' 2015.

1.7 Microbial fuel cells at Ampere lab

Electrical conversion related to MFCs started in 2009 with a first PhD. In this dissertation, N. Degrenne has studied the principle operation of MFCs [Degrenne, 2012]. A simple electrical model has been proposed and validated. A maximum power point tracking (MPPT) algorithm was adapted and tested with MFCs. The design of a Power Management Unit (PMU) for energy harvesting from MFCs was also studied. Another application of interest concerned the case where energy is harvested from several MFCs. It was found that the non-uniformities between the associated MFCs limit the efficiency of the stack. Many voltage balancing circuits can solve the former issue. Three of these circuits were analyzed

and evaluated by simulation. No experimental results related to voltage balancing circuit were presented in that work. The present work is a continuation of the former thesis delivered in 2012.

1.8 Scope of the thesis and objectives

Energy harvesting or energy scavenging is the conversion of ambient energy present in the environment into electrical energy. This relates to the conversion of small amounts of ambient energy for use in powering small, low-power, electronic devices. Low power applications are typically battery-powered. Wireless Sensor Network (WSN) is used in various application areas such as industrial, building, utilities, home, marine, habitat, traffic, animal, etc. With decrease in the size and cost of these systems, the use of wireless sensor nodes becomes widespread in process monitoring, natural environmental monitoring, security and surveillance [Gilbert and Balouchi, 2008, Stojmenovic, 2005]. WSNs provide important impact on many parts of human life, such as good understanding of human and animal behavior, natural and engineering systems [Raty, 2010, Kausar et al., 2014]. Energy harvesting has attracted much interest in the research community because of its potential use as a power supply in WSN to replace and overcome the limitations of batteries. There are several reasons why energy harvesting can be considered as an alternative to a battery.

- To harvest and use wasted energy.
- To remove the maintenance costs and time necessary for battery replacement.
- To overcome the problems related to the life-span of some device which is limited by the life-span of battery.
- To reduce the overall size of some electronic devices.
- Reduce environmental impact.
- Enable a sensor to grab its own power by harvesting energy from the ambiance.

In a WWTP, huge amount of energy in organic matters are available. This energy could be harvested by MFC's technology. Energy requirement for water treatment is usually given as a function of the global removal efficiency (Fig. 1.7). The global removal efficiency for WWTP is an indicator of the performance of the wastewater treatment plant. From the other hand, it was found that the power density of MFCs is about 1 kW/m^3 [Fan et al., 2007]. In this context, WWTP could be self-powered by the energy harvested from a large-scale MFCs. A stack of some MFCs is also able to supply a WSN.

The thesis focuses on management of the energy produced by a MFC or by a stack of MFCs, hydraulically coupled or isolated, for supplying autonomous sensors. It is divided in three parts.

1.8.1 Part 1: Modeling of MFC

Literature review in this part describes the operation of MFCs and links their electrical performances to bacterial mechanisms and the internal electrochemical reactions. The parameters which affect the performances of MFCs have been identified. The first step is to develop an analytical electrical model of MFCs based on the internal mechanisms. It presents the combination of static and dynamic mechanisms of MFC for different operating conditions. The results of modeling may lead to new design or configurations to improve energy production.

1.8.2 Part 2: Energy harvesting from one or a stack of MFCs

Powering an autonomous sensor from the energy harvested from MFC(s) required a power management unit (PMU) between the MFC(s) and the load. This PMU is normally composed around DC/DC converters. The low-voltage and low power of MFCs make the power management unit (front-end PMU) the most crucial part in the system. The section starts with a brief literature review on the low-voltage self-starting DC/DC converters and MPPT methods what leads to the design of a self-starting flyback converter, operating in a Discontinuous Conduction Mode (DCM). A MPPT algorithm is implanted in the converter, based on the impedance matching method. Different configurations (e.g. serial association, parallel association...) of MFC-powered systems are tested and compared. According to literature review, two voltage balancing circuits are also studied. These methods were applied and optimized for the first time on a serial stack of MFCs. An integrated voltage balancing circuit is designed, fabricated and tested with MFCs. The issue of the hydraulic coupling MFCs and its effect on the performance are analyzed for different operating conditions. This part introduces the concept of MFC-grid for powering off-the-grid applications.

1.8.3 Part 3: Field applications of MFC

One of the first applications could be the development of pilot-scale reactors at industrial locations where a high quality and reliable effluent is available. MFCs could be used for energy production and hydrogen production. In the section, MFCs are proved to be an alternative source of energy to batteries. Other applications are discussed in this part. The concept of an off-grid WSN powered by the energy harvested from MFCs is also presented.

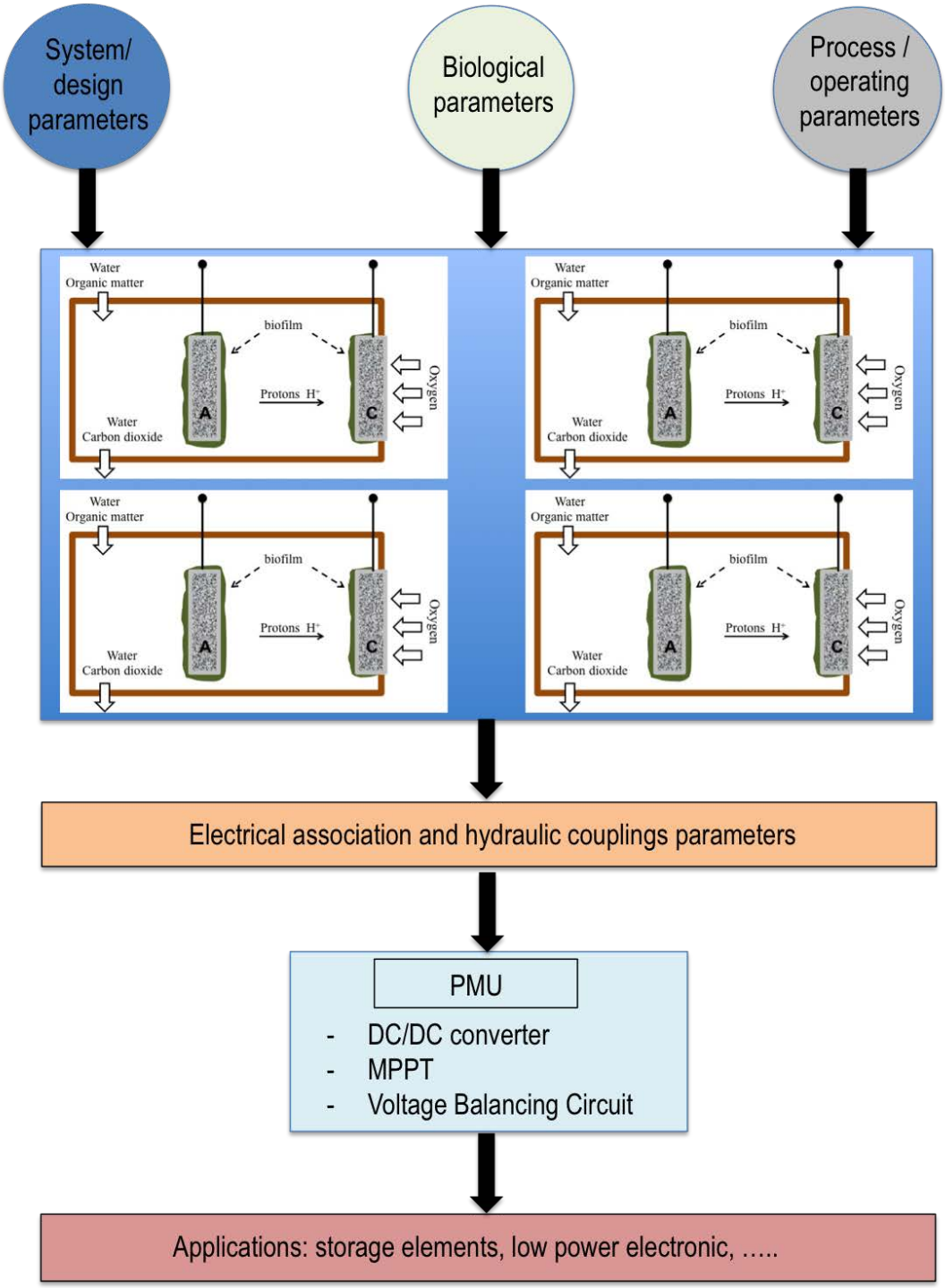

Figure 1.6: Research fields related to MFCs

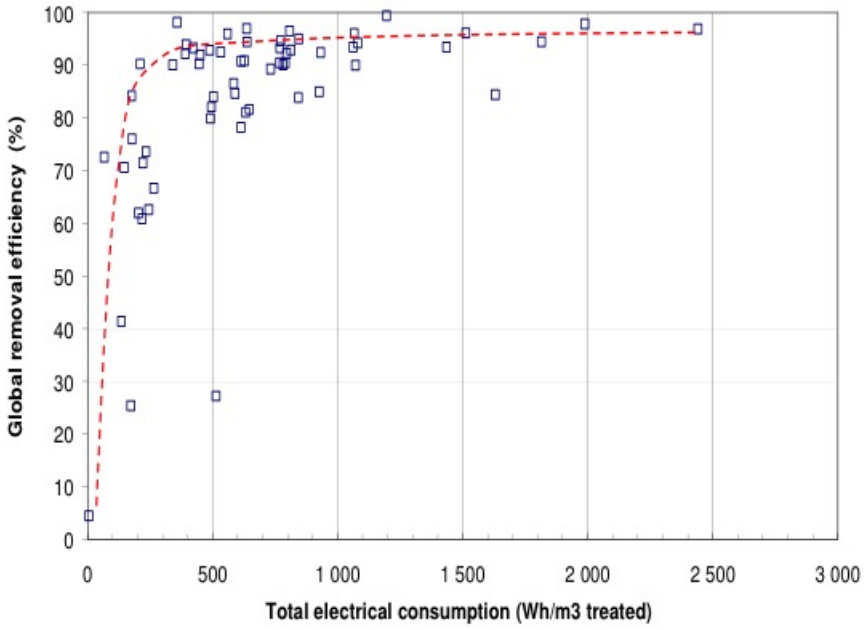

Figure 1.7: Evolution of the energy consumption with the global removal efficiency of WWTP [Amiel et al., 2011].

Part I

Microbial fuel cell as electricity generator

Chapter 2

Literature review

Contents

Microbial fuel cells (MFCs) have been used to produce electricity from different compounds, including acetate, lactate, and glucose. In this section, we will explain the principle of MFCs.

2.1 Microbial fuel cell principles

2.1.1 The energy metabolism of bacteria

All living organisms need energy and there are two main sources, chemical and light. Organisms can be classified regarding the kind of energy as either chemotrophs or phototrophs. Phototrophs are organisms that use photosynthesis to acquire energy. They use the energy from sunlight to convert carbon dioxide and water into organic materials to be utilized in cellular functions such as biosynthesis and respiration. The chemotrophs can be further divided into organochemotrophs which oxidize organic compounds and chemolithotrophs which oxidize inorganic compounds.

Electrons produced by the bacteria from the oxidation of substrates are transferred to the anode and flow to the cathode through the load. Electrons can be transferred to the anode by two main types of electron transfer. They are direct electron transfer (DET) and mediated electron transfer (MET) [Schröder, 2007]. In DET, the electrons are directly transferred from the microbial cell to the electrode via membrane-bound proteins, such as multiheme cytochromes, and/or via nanowires [Gorby and Fredrickson, 2006, Reguera et al., 2005]. In MET, electrons are transferred via an electrochemically

active compound, which could be a metabolite produced by microorganisms or an endogenous redox mediator [Hernandez and Newman, 2001]. If no exogenous mediators are added to the system, the MFC is classified as a “mediator less”. These types of electron transfer can be represented in Fig. 2.1 and 2.2. The fundamental task of the microbial cell is to electrochemically convert the contained chemical energy in a substrate (fuel) into a form that is accessible for electrochemical oxidation and thus for conversion into electric energy [Schröder, 2007].

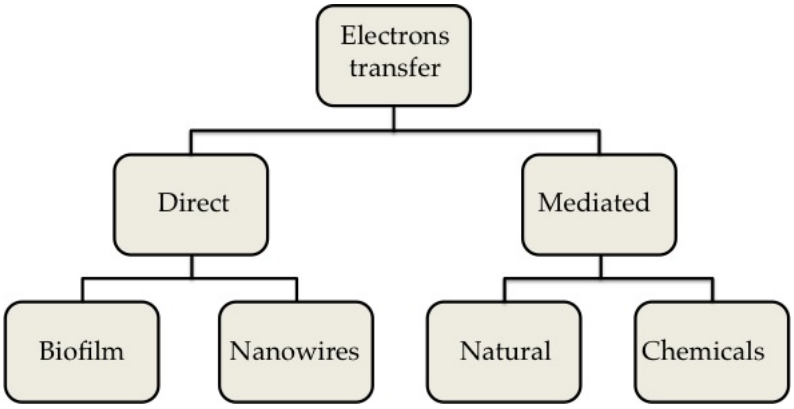

Figure 2.1: Electron transfer in microbial fuel cells

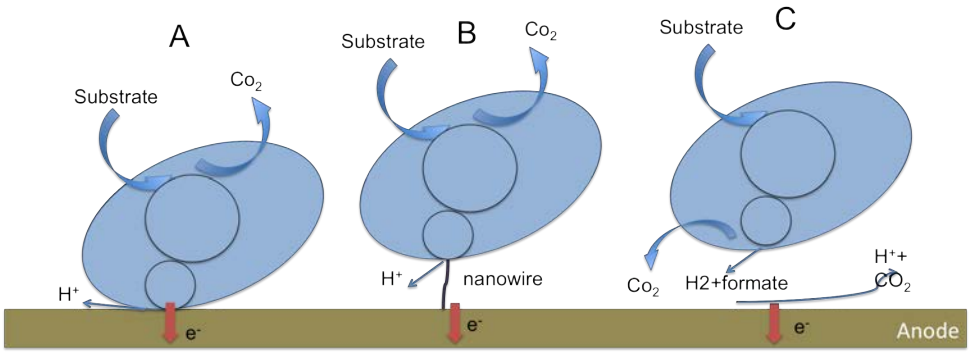

Figure 2.2: Illustration of the DET via (A) membrane bound cytochromes, (B) electronically conducting nanowires, (C) via oxidation of reduced fermentation products [Schröder, 2007].

2.1.2 Metabolism in MFC

Metabolisms of bacteria are discussed in [Aelterman et al., 2006a]. Chemotrophs bacteria are the most interesting. With their respiratory organisms, they oxidize chemical substances. In the presence of electron acceptor such as oxygen, this reaction releases energy. When the oxidation and reduction reactions in the respiratory mechanisms can be separated, we can harvest a part of the energy available from these reactions. MFC generally consists of an anode, a cathode and an electrolyte (which can be in a membrane

form in a double-chamber MFC). The anode and the cathode are electrically connected via an external circuit. In this design, the electrons generated in the oxidation reaction of the organic material near the anode are transferred by mechanisms of electron transfer to the anode. These electrons are then transferred through the external circuit to the cathode for corresponding reduction and the protons migrate to the cathode and combine with the electrons and the catholyte, such as oxygen, which is reduced at the cathode surface. Oxygen is mostly used as the terminal electron acceptor for the cathode reaction in MFCs, because of its high redox potential and abundance and sustainability in the air.

2.1.3 Energy mechanisms in a MFC

If the reaction is thermodynamically favorable in an MFC, electricity could be generated [Logan et al., 2006]. The reaction can be evaluated in terms of Gibbs free energy (G_{tot}) which is a measure of the maximal work that can be derived from the overall reaction [Bard et al., 1985]. Depending on the presence or absence of terminal electron acceptors, two major metabolic pathways can be distinguished: respiration in the presence of oxygen and fermentation in the absence of oxygen and exogenous oxidants. Aerobic respiration will occur with the highest energy gain when oxygen is available [Reimers CE, 2001, Tender, 2002]. Bacteria use inorganic and/ or organic compounds as terminal acceptors by an anaerobic respiration. The energy gain for the organisms in this case is limited by the low positive redox potentials of these oxidants and usually considerably lower compared to aerobic respiration. In fermentation, parts of the substrate serve as electron acceptor and become reduced, whilst other parts serve as electron donors and are oxidized. The energy gain by fermentation (2.1) will not exceed 7-8% of the energy gain by oxidation (2.2) [Thauer and Jungermann, 1977].

Fermentation of acetate:

$$CH_3COO^- + H^+ + 2H_2O \rightarrow 2CO_2 + 4H_2 \ \ (\Delta G^0 = -61\,kJ/mol) \tag{2.1}$$

Oxidation of acetate:

$$CH_3COO^- + H^+ + 2O_2 \rightarrow 2CO_2 + 2H_2O \ \ (\Delta G^0 = -854\,kJ/mol) \tag{2.2}$$

The theoretical energy available for the bacteria corresponds to the difference between the energy content of the reactants and the products as given in (2.3).

$$\Delta G_{tot} = nF(E_{RED} - E_{OX}) \tag{2.3}$$

Where n is the number of electrons involved in the reaction (mol), F is the constant of Faraday ($9.65*10^4$ C/mol), and E_{RED} and E_{OX} are the reduction and oxidation potentials respectively. A part of this energy, ΔG_{bio} is dissipated in the MFC due to the electrochemical and biological process. Therefore the total available energy of an electrochemical system significantly decreases and the available electrical energy could be given by 2.4.

$$\Delta G_{elec} = \Delta G_{tot} - \Delta G_{bio} \tag{2.4}$$

If the biological energy (ΔG_{bio}) becomes too large, the output electric energy will decrease. In a MFC, bacteria transfer electrons from the substrate at a low potential to the anode. Thus the energy gain for the bacteria is determined by the anode potential. To obtain a higher metabolic energy gain for the bacteria, a higher difference between the redox potential of the substrate and the anode potential is required. In (2.3), the variable n denotes the number of electrons transferred via electron transfer mechanisms. For acetate, the maximum number of electrons transferable is 8. In a microbial metabolism, only a limited number of electrons are transferable to the anode via a certain mechanism [Schröder, 2007, Logan et al., 2006].

2.2 Output voltage of a MFC

The oxidation of organic matter at the anode is coupled to a reduction reaction at the cathode. In MFC, a carbon source is oxidized under anaerobic conditions, using the anode as final electron acceptor. Electrons flow along the electrical circuit from the anode to the cathode. Produced protons are consumed by the reduction reaction at the cathode. In the case of the oxygen is used as electron acceptor at the cathode and acetate as the electron donor, the half reactions at the anode and cathode can be written as [Logan et al., 2006]:

Anode:

$$CH_3COO^- + 4H_2O \rightarrow 2HCO_3^- + 9H^+ + 8e^- \tag{2.5}$$

Cathode:

$$O_2 + 4H^+ + 4e^- \rightarrow 2H_2O \tag{2.6}$$

The maximum potential is the difference between the half reactions of the electron donor and acceptor under ideal conditions as expressed in (2.7).

$$E_{EMF} = E_{acceptor} - E_{donor} = E_{cathode} - E_{anode} \tag{2.7}$$

The theoretical potential of the electrode in a given typical condition is calculated using the Nernst equation and is given in (2.8)

$$E = E_0 + \left(\frac{RT}{nF}\right) ln\beta \tag{2.8}$$

Where E_0 is the standard free energy (at 298 K, 1 bar, 1 Mol, reported versus standard hydrogen electrode), R is the ideal gas constant (8.314 J/Kmol), T is the temperature (K), F is the Faraday constant, n is the number of moles of electrons transferred and β is the reaction ratio which is the ratio of the activities of the products divided by the reactants raised to their respective stoichiometric coefficient. The theoretical cell potential depends on the temperature and pH of solution [Hong Liu and Logan, 2005]. The theoretical potentials of the anode and the cathode are 0.187 V and 1.229 V respectively at standard conditions (298 K, [H+] =1 M). Using (2.8), we can calculate the theoretical anode and cathode potentials under specific conditions in MFC (with an acetate oxidizing anode ($HCO3^-$ = 5 mM, $CH3COO^-$ = 5 mM, pH = 7) and an oxygen reducing cathode (concentration of products and reactants: pO2 = 0.2, pH = 7) [Logan et al., 2006]. The theoretical anode potential will be –0.296 V and the theoretical cathode potential will be 0.805 V. The total cell potential of a MFC which uses the acetate as substrate and the oxygen as electron acceptor is therefore 0.805 – (–0.296)=1.101 V. This value cannot be achieved in practice due to various losses in the MFC. Voltage losses in bioelectrochemical systems can be divided into bacterial metabolic losses, electrode over-potentials and ohmic losses of the system. These losses will be discussed in the following sections.

2.2.1 Voltage drops

The electrochemical limitations on the performance of microbial fuel cells (MFCs) are due to the internal resistance (R_{int}), which is caused by different mechanisms including ohmic, activation, and mass transport losses [He et al., 2005, Rabaey et al., 2005b].

- Ohmic limitation is mostly due to the resistance of electrolytes and the various interconnections. The ohmic resistance is the resistance to the flow of ions in the electrolyte and to the flow of electrons through the electrode materials. This causes a voltage drop that is essentially proportional to current density. The ionic resistance is related to ion flow between the anode and the cathode. Electronic resistance is related to the conductivity of electrode materials and their connections. Optimizing the distance between the electrodes can reduce the ohmic resistance and improve MFC efficiency.

- Activation drop results at low current intensities from the large local potential difference necessary before allowing a reaction at the anode and cathode electrodes. This voltage drop is highly

non-linear. It can be reduced by improving electrode catalysts, increasing operating temperature slightly and increasing electrode surface area [Tiquia-Arashiro, 2014].

- Concentration or mass transport limitation is a resistance caused by delayed diffusion of reactants and products to and out of the reaction site and by the change in concentration of the reactants at the surface of the electrodes as the fuel is used. This mostly occurs at high current densities due to limited mass transfer of chemical species by diffusion to the electrode surface.

The Potential Efficiency (PE) is a unit representative of voltage drops. It is the fraction of voltage actually used as output voltage versus the theoretical voltage and it is given by (2.9).

$$PE = \frac{V_{OUT}}{\Delta E} \tag{2.9}$$

Where $\Delta E = E_{RED} - E_{OX}$

The potential efficiency varies over a wide range according to the design and the operating conditions. Very low value of PE of 2-6% was reported with glucose. Higher PEs were reported to 26–59% with acetate [Min and Logan, 2004].

2.2.2 Losses of electrons

In an ideal MFC, the anode is the unique electron acceptor available for the oxidation of the substrate. However, a fraction of electron may migrate to the cathode through the electrolyte or react with alternative electron acceptors like oxygen and non-organic oxidants, for example, to nitrate or sulfate or through fermentation and methanogenesis [Yu et al., 2012, Kim et al., 2011a]. The losses of electrons to other electron acceptors can result in a portion of the bacterial energy being sustained by non-electricity-generating processes. As long as the anode remains attractive enough for the bacteria due to its potential, alternative electron acceptors will not be stimulated. The potential of the anode should be kept as negative as possible to minimize the electrons which can be quenched by competitive electron acceptors. The Coulombic Efficiency (CE) is a unit representative of electron loss within MFC as defined by (2.10). It represents the percentage of electrons recovered from the organic matter (n_{eff}) versus the theoretical maximum number of electrons (n_{tot}) involved in the oxidation reaction.

$$CE = \frac{n_{eff}}{n_{total}} \tag{2.10}$$

The Coulombic Efficiency calculated for MFCs varies over a wide range. CEs from 0.7–8.1% were recorded in MFCs fed with wastewater, which contains fermentable substrates and alternative electron acceptors [He et al., 2005]. Higher CEs were reported to 12–28% with oxygen [Liu and Ramnarayanan, 2004, Pennsylvania, 2004] and 17–96% with ferricyanide [Rabaey et al., 2004, Rabaey et al., 2005a].

2.3 Parameters defining the performance of MFCs

Fig. 2.3 illustrates how the design of the MFC and the operating conditions affect power generation and sludge degradation through a complicated interrelated network. Apart from MFC design factors (configurations, materials, electron donor and acceptor determination), the operating conditions also play an important role in power generation and MFC performances. In order to achieve better performances, the modification of the electrode and the optimization of electrode distance, area, and roughness have to be carried out. In the anodic chamber, the enhancement of power generation and sludge degradation can be realized through the proper pretreatment of sludge, the improvement of mixing conditions and the optimization of dissolved oxygen (DO) concentration and air diffusion [Fang et al., 2010]. In the cathode chamber, the optimization of dissolved oxygen (DO) concentration, air diffusion and electrolyte type and concentration can also result in the enhancement of MFC performances [Wang et al., 2012]. The selection and cultivation of microorganisms with strong electricity generation ability is another kind of measure to improve power generation. The immobilization of bacteria on an electrode is also an attempt to improve the efficiency of a MFC [Yuan, 2011].

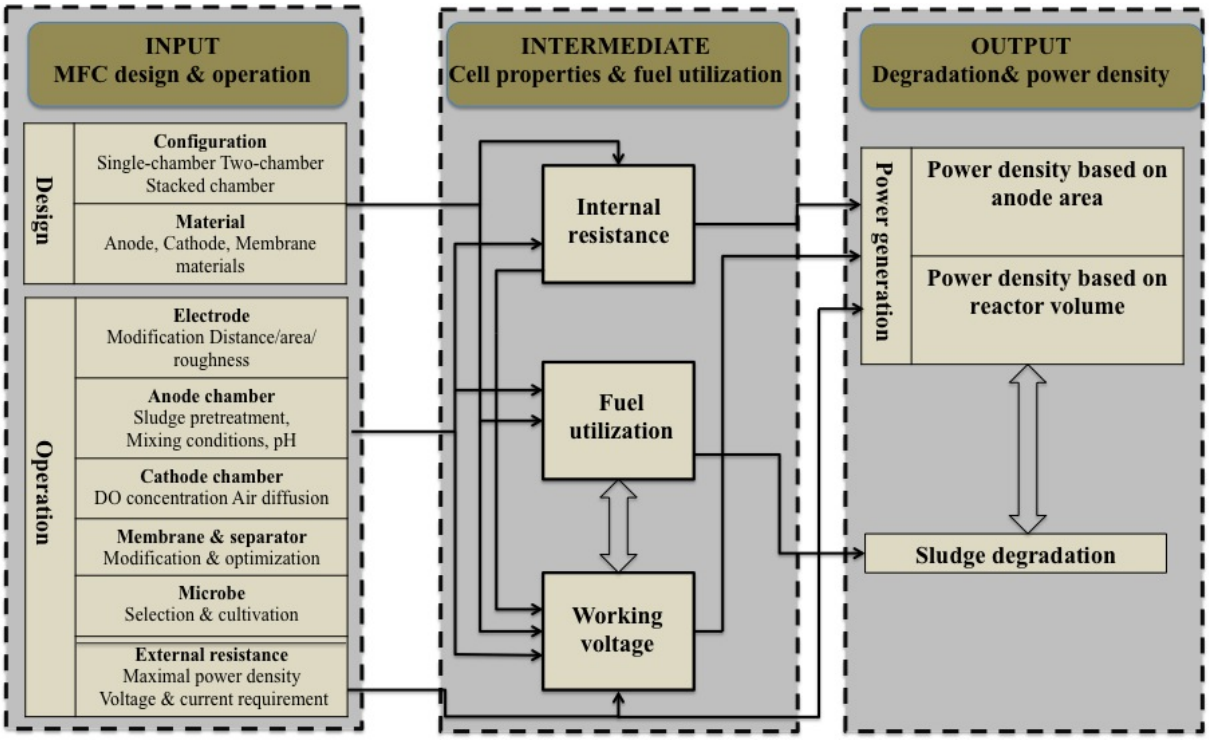

Figure 2.3: Interrelationships between operating conditions and MFC output power generation [Wang et al., 2012]

2.3.1 Open circuit voltage

Previous studies have shown that the Open Circuit Voltage (OCV or V_{oc}) depends on several parameters, including organic loading rate [Kim et al., 2010], cathode catalyst [HaoYu et al., 2007] and pH of the electrolyte [He et al., 2008]. The OCV is the difference of electrical potential between anode and cathode of an MFC in the absence of current. OCV can be measured between the anode and the cathode when no external load is connected and it typically does not exceed 1.101 V for acetate as electron donor and oxygen as electron acceptor. The difference between the measured cell voltage and the cell EMF is the sum of the over-potentials of the anode ($\triangle_a$), the cathode ($\triangle_c$) and the ohmic losses ($\triangle_{ohm}$) as given by (2.11).

$$V_{oc} = E_{EMF} - (\triangle_a + \triangle_c + \triangle_{ohm}) \tag{2.11}$$

2.3.2 Internal resistance

The maximum MFC voltage measured in open circuit is lower than the theoretical value although there is no current through the MFC. When a load is connected to the MFC, the MFC generates a current. The output voltage decreases due to the losses in the internal resistance. The internal resistance is an important factor to determine the output voltage. Many works concerned the minimization of this resistance based on its components (ohmic, activation and concentration resistance) [Larminie and Dicks, 2003, Hoogers, 2014]. Ohmic resistance can be reduced by checking thoroughly all contacts and increasing solution conductivity. Activation resistance can be reduced by increasing the electrode surface area and increasing the operating temperature which is tolerated by the bacteria. Concentration resistance can be limited by control of the current density.

2.3.3 Effect of temperature

Temperature has a large influence on the performances of a MFC because it changes the conductivity of the substrate and the microorganism activity of microbial community. The internal resistance of the MFC decreases by increasing temperature. That can be explained by the fact that ionic conductivity increases with temperature and therefore decreases the resistance [Gonzalez del Campo et al., 2013]. Increasing temperature results in a higher OCV and higher maximum power point. That can be explained by the following observation: the higher the temperature, the higher the microbial metabolism and the higher the performance. The optimum temperature for MFC is questionable because there are different electrogenic bacteria that have different appropriate temperature ranges. The temperature during the initial growth phase of biofilm must be favorable for these bacteria. Once the biofilm is formed, some microbial species are capable of adjusting their metabolism at different temperatures without a significant decrease in performances [Ahn and Logan, 2010, Martin et al., 2010].

2.3.4 Effect of pH

The optimal growth of bacteria requires a pH close to neutral between 6 and 9 [He et al., 2008]. The performances of MFC depend on the PH because it causes alterations in concentration of ions, biofilm formation, membrane potential and proton-motive force [Zhang et al., 2011, Oliveira et al., 2013]. In a dual chamber MFC, it was demonstrated that the MFC produce maximum current at the operating pH of 6.5 in the anode chamber [Jadhav and Ghangrekar, 2009]. Anodic pH has also a significant influence on the substrate degradation [Raghavulu et al., 2009].

In a one-chamber MFC, the optimal pH is between 8 and 10 with higher current generation. In this design, the pH value of the electrolyte affects both anodic and cathodic reactions. A high pH may inhibit the anodic bacterial activities but will be favorable to the cathodic reaction and therefore improve the overall performance of MFC [He et al., 2008, Puig et al., 2010].

2.3.5 Substrates used in MFCs

The substrate (or fuel) is an important biological factor affecting the performance and the electricity generation [Liu et al., 2009]. Different substrates have been used in MFCs ranging from pure compounds to complex mixtures of organic matter. Two of the most common substrates used in MFCs are *Acetate* and *Glucose*.

2.3.5.1 Acetate

In most of the MFC studies, acetate has been the chosen substrate for electricity generation [Min and Logan, 2004, Liu et al., 2005a]. Acetate is a simple substrate that is used as carbon source to induce electroactive bacteria [Bond et al., 2002]. It was reported that using acetate in a single-chamber MFC offers a maximum power density of 506 mW/m^2 @ 0.8 g/L[1], compared to 305 mW/m^2 @ 1 g/L produced with butyrate [Liu et al., 2005b].

2.3.5.2 Glucose

Glucose is also a commonly used substrate in MFCs. The energy conversion efficiency (ECE) of acetate and glucose as substrates in MFC was compared at 42% with acetate, but was only 3% with glucose [Lee et al., 2008]. For this reason, acetate will be used in our study as a reference substrate. Using complex mixtures of organic matter offers the possibility of enriching more diverse microbial communities, leading to better power generation [Pant et al., 2010].

[1] Power is normalized to the surface of the cathode. The technology of the anode and the cathode will define the reactor volume. There is no direct link between the surfacic density and the volumic density

2.3.5.3 Substrate concentration

Experimental data a in [Mathuriya and Sharma, 2010] indicated that the current generation decreases with the decrease in wastewater organic matter concentration. At low substrate concentration, the maximum power generation is proportionally linked to substrate concentration [Cheng et al., 2011]. This gives the ability to realize a biosensor that can measure the concentration [Ghoreyshi et al., 2011].

2.3.6 Influence of output load

The MFC performance will also depend on the value of the output load. The efficiency and the output voltage are not affected in the same way. Figure 2.4 shows the experimental efficiency as a function of the output load of the MFC. This suggests that the efficiency of the MFC is optimal for a given load value. The output resistance should be, therefore, adjusted in order to maximize the efficiency. The output voltage of the MFC increases with the load (Figure 2.4). However, when the load reaches high values, the output voltage begins to saturate.

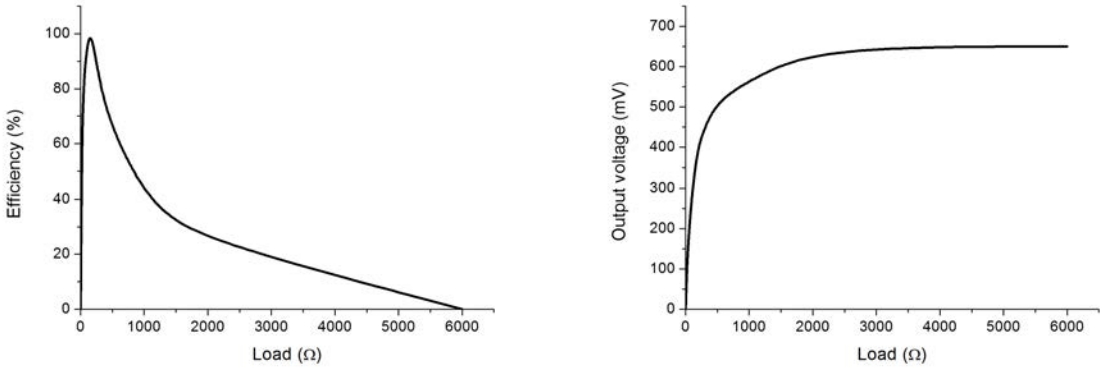

Figure 2.4: Typical efficiency and output voltage as a function of the output load

2.4 Materials of construction

2.4.1 Anode

Anodic materials must have a good electrical conductivity and low resistance. Anode must be fabricated with noncorrosive materials. The electrode material in the present MFC studies is carbon. Carbon anodes can be realized in many forms as graphite rod, carbon paper, graphite fiber brush, carbon cloth and carbon felt. The simplest carbon anodes used in MFCs are graphite rods due to their excellent electrical conductivity and relative low coast. In [Liu and Logan, 2004], eight graphite rod anodes were employed in an air-cathode MFC with a maximum power of 26 mW/m^2 of cathode area achieved using

sewage from a treatment plant as fuel. To maximize the anode surface and minimize electrode resistance, a carbon brush anode is used to obtain a maximum power density of 2400 mW/m^2 in an air-cathode MFC [Logan et al., 2007]. Carbon paper and carbon cloth were firstly used in hydrogen fuel cells. These anodes are later used in MFCs to reduce the distance between the two electrodes to minimize the internal resistance and improve the performances [Kim et al., 2007]. Some non-corrosive metal materials are tested and compared to carbon materials as stainless steel and titanium. Stainless steel plate was tested as electrode material for anodes and biocathode and the graphite anode appeared more efficient than the stainless steel anode [Dumas et al., 2007, Dumas et al., 2008]. In other studies, a stainless steel grid anode was reported with much higher current densities than plain graphite anode [Erable and Bergel, 2009]. In this study, carbon fiber brushes are used for the anode because it provides high surface, low cost and good performance based on results reported in literature [Logan et al., 2007].

2.4.2 Cathode

The cathode material greatly affects the power capacity of MFCs and its performances. A good cathode must have a high redox potential to capture protons. Most materials used at the anode have also been tested as the base materials of cathode: carbon clothes, stainless steel and graphite felt. To improve performances, Pt catalysts are usually used to increase the rate of oxygen reduction [Reimers CE, 2001, Liu and Logan, 2004]. However Pt is an expensive metal and this limits its practical application. Many researches have been made to decrease the costs of the MFC. It was found that the Pt coating can be kept as low as 0.1-2 mg/cm^2 [Cheng et al., 2006b]. Air–cathodes are the most commonly used configurations in lab-scale MFCs that require catalysts to generate higher power densities. In this case, cathodes are made of supporting conductive materials, such as carbon paper, carbon cloth, and platinum mesh, coated with a catalyst layer, Pt. Many efforts have been made to use air–cathodes without catalysts [Tran HT, 2010].

Table 2.1 compares the performances of the materials that are used in MFCs. A platinum-coated carbon paper (0.5 mg/cm^2 of Pt [Middaugh et al., 2006], Nafion, PTFE) is also chosen for the cathode because of its good performance.

Effect of Electrode Distance on Bioelectricity Production The electrode distance is a major limiting factor in MFC performance. The electrode distance affects the internal resistance of the MFC and therefore the power production. The trend to increase MFC performances with a decrease in electrode distance was observed in [Rismani-Yazdi et al., 2008, Jang et al., 2004, Sangeetha and Muthukumar, 2013, Kim et al., 2007, Cheng et al., 2006a, Hong Liu and Logan, 2005]. When electrons are generated in the anode section, average transport distance for a proton to travel from anode to the cathode is relatively long what leads to transport losses in the anode chamber. The distance between the anode and the cathode electrodes should be as close as possible to decrease the internal resistance [Sangeetha and Muthukumar, 2013, Jang et al., 2004]. However decreasing the distance may cause an electrical leak

Table 2.1: Electrode materials, configuration and power generation performance

Electrode	Materials	Effective area	Reactor configuration	Maximum power density	References
Anode	Carbon paper	22.5 cm^2	Two-bottle, air–cathode	600 mW/m^2 (a)	[Logan et al., 2007]
	Carbon mesh	7 cm^2	Single chamber cube air–cathode MFC	893 mW/m^2 (a)	[Wang X, 2009]
	Carbon brush	12 cm^2	Single chamber cube air–cathode MFC	2400 mW/m^2 (c)	[Logan et al., 2007]
	Stainless steel plate	0.12 cm^2	Artificial marine MFC	23 mW/m^2 (a)	[Dumas et al., 2007]
	Carbon clothes, Nafion, Pt	7 cm^2	Single chamber cube, air–cathode MFC	480 mW/m^2 (c)	[Cheng et al., 2006b]
Cathode	Stainless Steel Mesh, Nafion, Pt	7 cm^2	Single chamber cube, air–cathode MFC	1610 mW/m^2 (c)	[Long-long Zhang and Wölfle, 2010]
	Activated carbon fiber felt	36 cm^2	Cylindrical two chamber, air–cathode MFC	315 mW/m^2 (c)	[Deng et al., 2010]
	Carbon clothes, Pt	7 cm^2	Single chamber MFC	262 mW/m^2 (c)	[Liu and Ramnarayanan, 2004]

(a): power normalized to anode surface area, (c): power normalized to cathode surface area

and also decrease the performances [Cheng et al., 2006a]. In our case, a distance of 4 cm is chosen as a trade-off based on results reported in literature. Optimizing this distance is out-off the scope of the present work.

2.4.3 Membranes

In a two-chamber MFC design, the anode and the cathode are separated by a Proton Exchange Membrane (PEM). It allows proton transfer from the anode to the cathode and prevents oxygen diffusion in the anode compartment from the cathode compartment. Membrane capability for exchanging protons plays an important role on MFC performances. Nafion is the most popular PEM but it is still expensive and would be impractical for a large MFC systems. Ultrex CMI-7000 could be used as an alternative to Nafion [Rabaey et al., 2004]. For a long-term operation of MFC, biofilm can be formed on PEM. Fouling

can decrease proton transport from the anode to the cathode and increase the internal resistance of the system which decreases power production [Logan, 2008] and/or deteriorate MFC performance [Xu et al., 2012].

A membrane-less single-chamber MFC is used in this study to minimize the internal resistance, increase the power generation, cut cost and simplify reactor construction.

2.5 Electrical characteristics

Open circuit voltage, cell voltage and electrode potentials can be measured with a high impedance voltmeter connected in parallel with the circuit. Open circuit voltage and cell voltage are voltage differences between the anode and cathode while electrode potentials can only be determined against a suitable reference electrode. When the MFC is connected to a load, an electrical current flows through the load. The current is easily calculated using Ohm's law (I =V/R) for the measured cell voltage.

2.5.1 Polarization Curves

The term "polarization" is the change of MFC voltage (or electrode potential) from its equilibrium state due to a flow of current. A polarization curve or a static electrical characteristic curve represents the voltage (V) as a function of the current (I) or the current density. Polarization curve gives more details about the biochemical and electrochemical system. Polarization curves can be recorded for the cathode and/or the anode to give information on the performances of the individual electrodes and characterize their behavior, or it can be for the whole MFC to give information on the cell performance under specific operating conditions. There are several options for tracing the polarization curve

(a) Linear and cyclic sweep voltammetry (LSV and CV): in this method, the potential of the electrode (anode or cathode) is varied with a slow voltage scan rate (e.g. 1 mV s-1) and current is measured [Rabaey et al., 2004]. In the case where the scan goes in one direction only, the method is called linear sweep voltammetry (LSV). If the scan is continued in the reverse direction to come back to the initial potential, the method is called cyclic voltammetry (CV). An example of these measuring systems is potentiostat Ecochemie (Princeton Applied Research, USA). It is supplied by 4 electrodes consisting of electrodes (anode / cathode), a reference electrode, and a counter electrode. A two-electrode configuration is used to measure the internal resistance or the electrolyte conductivity. A three–electrode configuration with a reference electrode is most common for typical characterization to determine precisely the potential of the working electrodes [Logan et al., 2006].

(b) Galvanostatic discharge: the current is varied and the output voltage is measured [Bard and Faulkner, 1981].

(c) Frequency response analyzer: in this test, a sinusoidal signal with a variable frequency is applied on one electrode or the whole cell to measure electrode impedance, ohmic and internal impedance of the MFC.

(d) Connecting different loads to the MFC and measuring the currents and voltages, so-called resistorstat [Degrenne et al., 2013].

The simplest method to record the polarization curves, for the whole cell, is by using variable external loads between the anode and the cathode. The load should be changed periodically from open circuit to short circuit. The voltage is measured in pseudo-steady-state conditions and the current is to be calculated using Ohms' law. The performance of each electrode in the cell could be also studied by connecting the load between this electrode and a reference electrode. The nature of the MFC hinders the immediate response when the load is changed because the microorganisms require some time that are given to adjust to each new resistance value or some time for the biofilm to acclimate when resistances are changed. The establishment of the pseudo-steady state is still debated (immediate, seconds, minutes, hours), depending on the system (microbial communities, mechanisms of electrodes, substrate concentration) and the external resistance. For these reasons, it is difficult to record the genuine steady-state polarization curve. Moreover in a long–term polarization testing, the substrate concentration in the reactor, in discontinuous flow mode, will change due to substrate demand at the anode. The pseudo–steady state conditions are generally taken over several minutes. Longer time may change the microbial community and operating condition [Heilmann J, 2006,Logan et al., 2006]. From the other hand a fast sample rate leads to an overshoot phenomenon, i.e., back of the power density curve (after the peak power) towards lower current densities, rather than the expected higher current densities, which implies underperformance [Winfield et al., 2011,Zhu et al., 2013]. The optimal sample rates are to be discussed later.

Fig. 2.5 shows a typical static electrical characteristic of a MFC. When there is no load, at zero current, the cell voltage is the open circuit voltage (<1.1V), typically between 0.5V and 1V. The voltage curve starts with a large voltage drop at low current values due to the activation losses. By increasing the current, the voltage will fall more slowly, forming a linear drop with the current. The slope of the polarization curve in this region gives the internal resistance of the MFC, R_{int}. In linear region, the ohmic losses are dominant. At higher currents, the voltage falls rapidly due to the concentration losses.

2.5.2 Power Curves

When a MFC is connected to a load R_{ext}, the voltage cell V and the current I are fixed by the load. MFC performance is determined by the output power that is evaluated as (2.12)

$$P = VI = V^2/R_{ext} \tag{2.12}$$

This equation could also be written as (2.13)

$$P = (V_{oc}^2 R_{ext})/(R_{ext} + R_{int})^2 \tag{2.13}$$

with R_{int} is the internal resistance of MFC.

In order to compare electrical performance of different systems, the output power is normalized to anode or cathode surface area or to reactor volume, depending on application. To compare the performance of the anode or the cathode, power density (W/m^2) is calculated on the basis of the area of the cathode (A_c) or the anode (A_a) as (2.14).

$$P_{(a,c)} = V^2/(A_{(a,c)}R_{ext}) \tag{2.14}$$

The power may also be expressed as volumetric power (W/m^3) normalized to the total reactor volume υ as (2.15).

$$P_v = V^2/(\upsilon R_{ext}) \tag{2.15}$$

A power curve represents the output power (or power density) as a function of the MFC current (or current density). At open circuit voltage, there is no output power because there is no current. From this point onward, with current increasing, the power increases to a Maximum Power Point (MPP). From (2.13), we find that the MPP occurs when $R_{ext} = R_{int}$ and therefore it can be given by (2.16).

$$P_{max} = V_{oc}^2/4R_{int} \tag{2.16}$$

Beyond this point, the power drops due to the increase in losses to the point where no more power is produced at short circuit conditions.

The cell voltage and power are marginal or inadequate to supply typical low-power consuming applications. For example, low power microprocessors require circa 270 μA at 2.2 V, LEDs require over 20 mW and photodiodes require 33 mW. The power densities vary in a very wide range depending on the MFC technology, the design, the type of fuel, the operating conditions, etc. The highest output power density reported to date appears to be 4300 mW/m^2 of cathode surface [Rabaey et al., 2004]. In our lab-scale MFC, the output power density is 2500 mW/m^3. The standard power densities are encouraging but they should be enhanced to render MFC technology feasible for commercial applications.

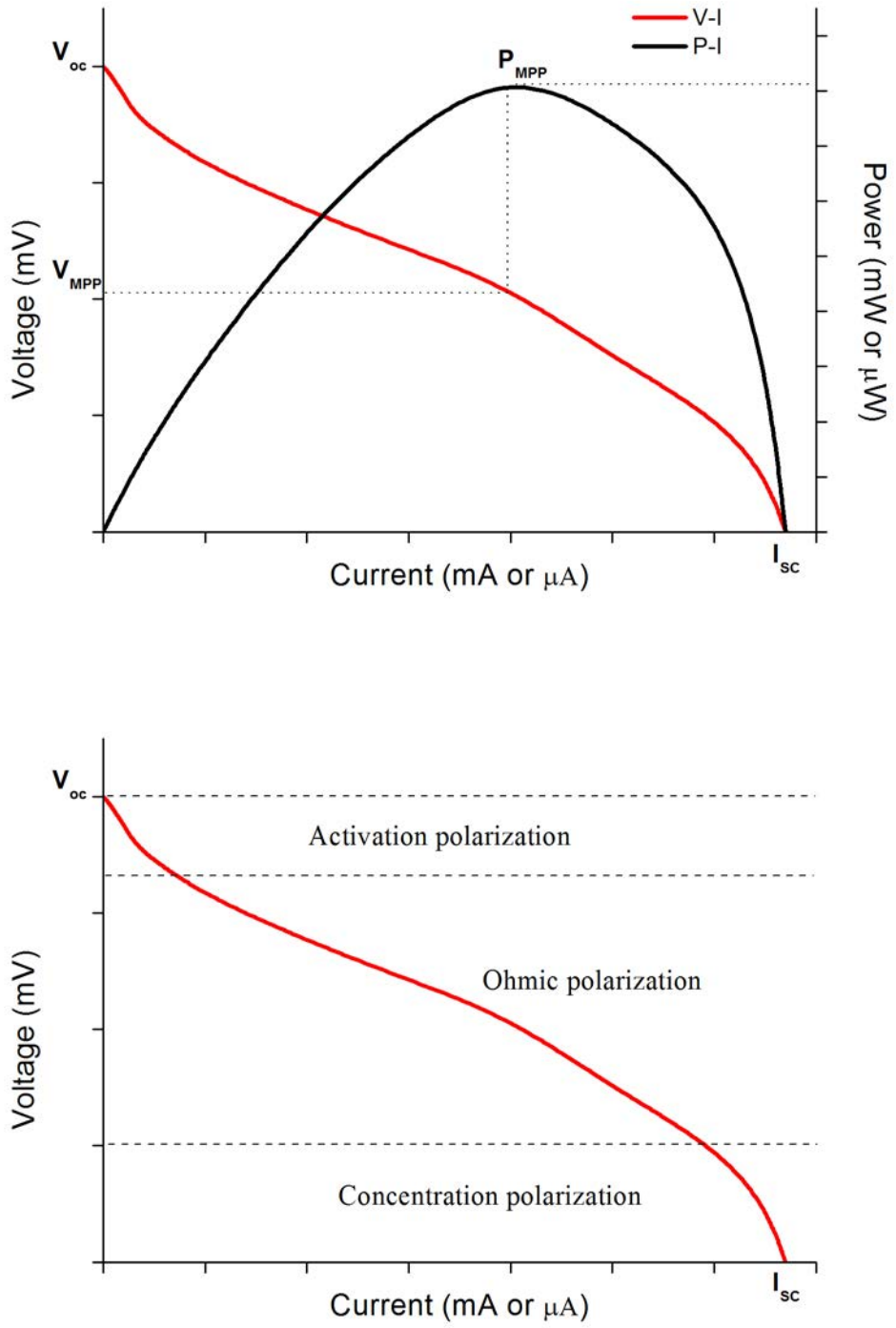

Figure 2.5: Typical static electrical characteristic of a MFC

Chapter 3

Electrical Model of Microbial Fuel Cells

Contents

3.1 Introduction

To be able to utilize microbial fuel cell in an effective way, analytical models are necessary so that the system behavior can be analyzed, tested, simulated by means of computer simulations in different conditions of operation and load. However since the microbial fuel cell is a multi-domain system involving simultaneously electrochemical and biological processes, mass and energy transfer, the development of a model is critical. While past results on MFCs have been based extensively on experimental studies, modeling and simulation remain scarcely developed. In the previous chapter, we discussed that the performances of MFC depend on many parameters such as the amount and type of bacteria, mass transfer phenomena, cathodic reactions, temperature and the efficiency of the proton transport. Modeling the effect of these parameters on the performances of a MFC may be substantial for developing the design and optimizing these parameters.

Several models of MFC have already been presented [Picioreanu et al., 2008, Oliveira et al., 2013, Picioreanu et al., 2007] with different approaches, dimension of study and areas of investigation. The majority of them, however, is able to simulate only the cell steady-state behavior, while the analysis of their performances in dynamic conditions is still important to render the rapid variation of electrochemical and electrical quantities. Some models are characterized by a high complexity [Ceraolo et al., 2003, Marcus et al., 2007, Picioreanu et al., 2007], with several partial differential equations and algebraic equations whose derivation is based on electrochemistry, biology and physics governing the phenomena taking place in the cell [Chávez-Ramírez et al., 2010]. This high complexity creates problems of simulation, parameter identifications.

A MFC model was proposed by Zhang and Halme [Zhang and Halme, 1995], but for an external mediator to transfer electrons which is not in use in modern MFCs. A dynamic, one-dimensional model for the biofilm, based on mass balance principles, was presented in [Torres et al., 2007]. The model describes that electrons from electron-donor oxidation and respiration are electrically conducted from a bacteria, through the biofilm matrix into the anode. An electrical model consists of two capacitances, representing the biofilm ($CPE_{biofilm}$) and the anode (CPE_{HL}), connected in parallel to their respective biofilm ($R_{biofilm}$), charge transfer ($R_{CT/P}$) resistances and mass transfer limitations (WDE) [Fradler et al., 2014] as shown in Fig. 3.1. A simplified model is used in [Yang et al., 2012]. No parameter identification or validation results were presented since the objective was to study a power management unit based on MFCs.

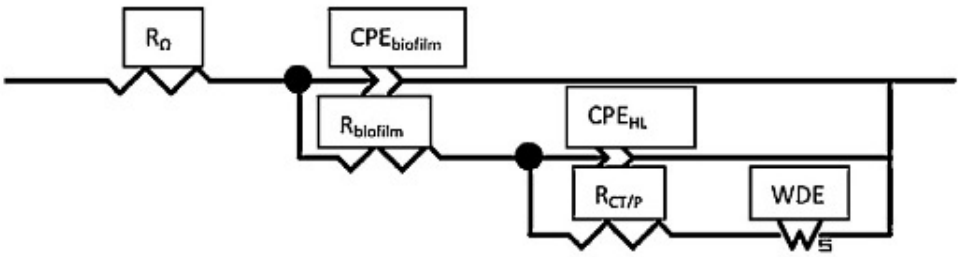

Figure 3.1: Equivalent circuit model of a MFC [Fradler et al., 2014].

A simple electrical model is presented in the following part.

3.2 Electrical characteristics

3.2.1 Construction of MFC

Based on literature, design parameters are chosen to optimize the performance and to reduce the cost. The lab-scale MFC is built using a carbon fiber brush anode and an air cathode. A PVC draining tube is used to form the reactor of 0.7 liter with 4 cm of distance between the electrodes. A cathode of 120 cm^2

of carbon cloth (30% Teflon treated, Fuel Cell Earth LLC, USA) is realized manually, using a paintbrush with 1.56 mg of black carbon and 0.5 mg of Platinum for every cm^2 of cathode surface area [Middaugh et al., 2006]. The cathode is connected to the electric cable with a titanium wire. The MFC is inoculated with wastewater from an industrial wastewater. MFC is then fed with 0.7 g of sodium acetate (1g of acetate/L, Sodium acetate: Sigma-Aldrich Chimie S.a.r.l, C2H3NaO2, 82.03 g/mol, PN 71183). MFC is then left for several days for the biofilm to develop. The objective is to study the MFC in steady-state and not during the biofilm development process. All the measurements are therefore achieved after stabilization. Fig. 3.2 shows a photo of the lab-scale MFC.

Figure 3.2: Photo of the lab-scale MFC

3.2.2 Static characteristics and the effect of sample rate

As mentioned previously, the evaluation of the pseudo-steady state in MFCs is an important parameter during a polarization sweep because it is the time given to microorganisms to adjust to each new resistance value. It has been found that low sample rates (t_c) are not convenient because they lead to an overestimation of the voltage and therefore the produced current/power [Watson and Logan, 2011,Logan, 2012]. This type of overestimation can be eliminated by using a very slow cyclic sweep voltammetry scan rate to stabilize current generation. Other problem may be addressed by the sample rate. It is called overshoot (i. e. the power curve doubles and comes back to lower current densities after the maximum power point). The overshoot is the result of an insufficient sample rate such that the microorganisms are not given enough time to adjust to the new resistance value. Mass transfer limitations and increasing the internal resistance are also suggested as a reason for this overshoot [Aelterman et al., 2006a, Winfield et al., 2011]. On the other hand, a large t_c will be critical because of substrate depletion, particularly in

batch mode systems. It is conventional that substrate concentrations should not be changed during the tests, because this would lead to different performance and non-comparable results [Ieropoulos et al., 2010]. A study of the sampling rates has shown that polarization sweep with different t_c (high t_c in the activation and the concentration zone and low t_c in the ohmic zone) could give more precise information about the performances [Ledezma et al., 2014].

To study the performance of MFCs at different time intervals (t_c), polarization and power curves are recorded for 2 sec, 1 min, 3 min and 10 min as shown in Fig. 3.3 and Fig. 3.4 for the same reactors and the same conditions. The voltage-current curves (polarization curves) were acquired by decreasing the load resistance from open-circuit to short circuit. The resistance values were set with an automated resistorstat tool, which performed sweeps of external resistor values (R_{ext}) ranging from 1MΩ to 4Ω (35 values), at controlled time intervals (t_c). The resulting voltage outputs were automatically measured by the resistorstat, calculating the output current (I) and the output power (P).

The experimental results show that the output power for a low sampling rate (2 sec) is 6.1 times higher than the measured power at t_c =10 min, what confirms the occurrence of overestimation at low sample rates. With a t_c =1 min, the overestimation decreases to 15% compared to t_c =10 min. In the case of t_c =3 min, no overestimation is noted before MPP. Beyond MPP, the output power is overestimated in the range of 1-2%. Therefore in our case, a t_c longer than 3 min is not necessary for the characterization of MFCs.

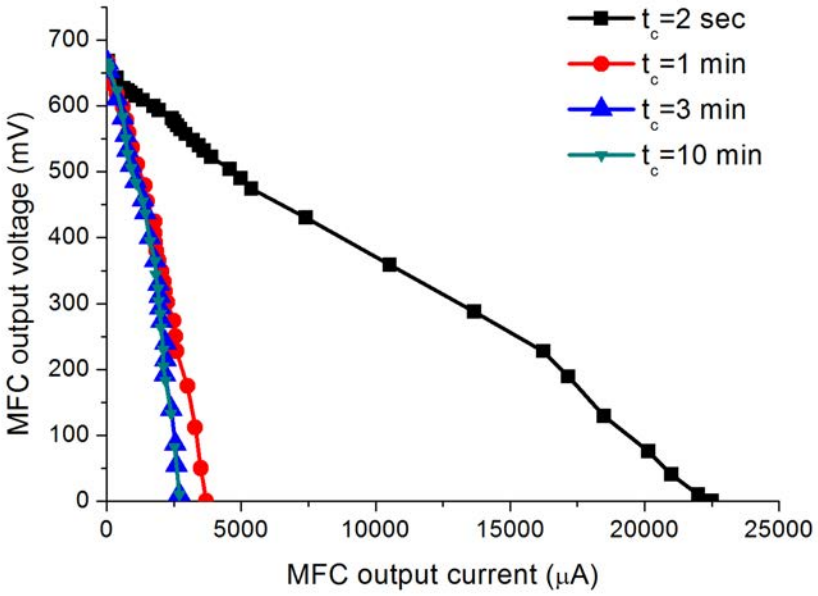

Figure 3.3: Polarization curves of the lab-scale MFC reactor for different sampling rates.

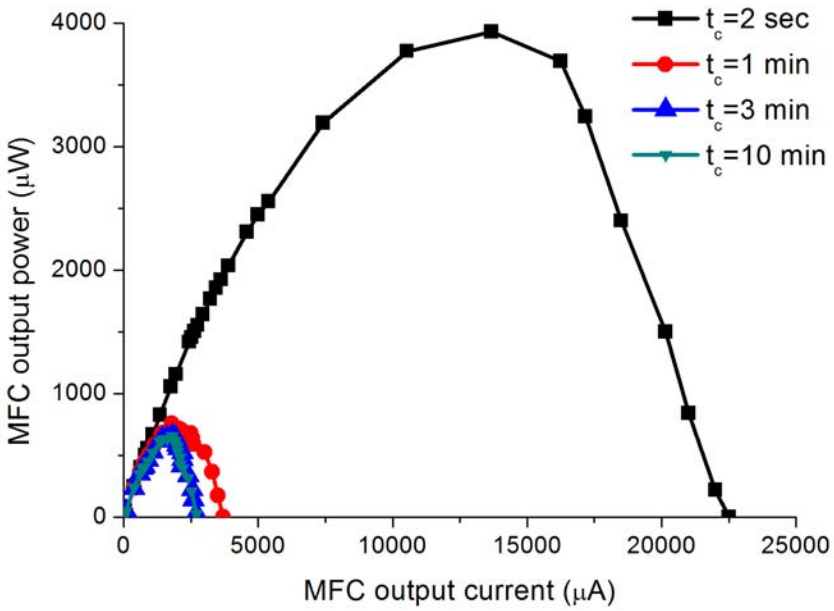

Figure 3.4: Power curves of the lab-scale MFC reactor for different sampling rates.

3.2.3 Dynamic characteristics

In the previous characteristics, the automated resistorstat is programmed to take the measurements at the end of the transient what hides the voltage evaluation during time t_c. To see the voltage evaluation during all the experiment time, two experiments were set up. In the first one, a classic polarization and power curves were recorded by changing the load resistance from open circuit to short circuit (25 values) at 3 min interval (Fig. 3.5-a). The second experiment is by changing the external resistance $R_{ext}(\Omega)$ in the same order at 3 min interval and 20 sec measurement interval (Fig. 3.5-b) in order to monitor the dynamic response of MFCs to changes in the load. The polarization curves for the two experiments are presented in Fig. 3.6. From Joule's law, the electrical power can be calculated for the different current values resulting in the power curve as shown in Fig. 3.7. These curves provide considerable information not only about the performance but also about the dynamic response of MFC when it is connected to a load. Similar spikes were also observed in other studies [Ledezma et al., 2014]. It was considered as an indicator of the power losses or overestimation. The results show a non-immediate response of MFC to the load changes (see Fig. 3.8). Applying a load of 450 Ω, the voltage does not reach the corresponding voltage immediately; it decreases across the same load until it stabilizes. The output power also decreased until it stabilizes. After stabilization, the load is changed to 342 Ω and so on.

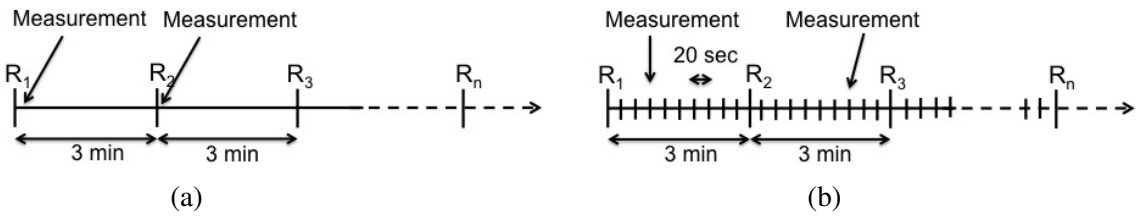

Figure 3.5: Sampling rate schedule during the two experiments

As expected, bacteria in MFC need a certain time to adjust to the new load value what means that the system suffers from some form of “time-delay”. Electrically that could be explained by a capacitive effect of MFC which creates a time delay or time-constant in the MFC operation.

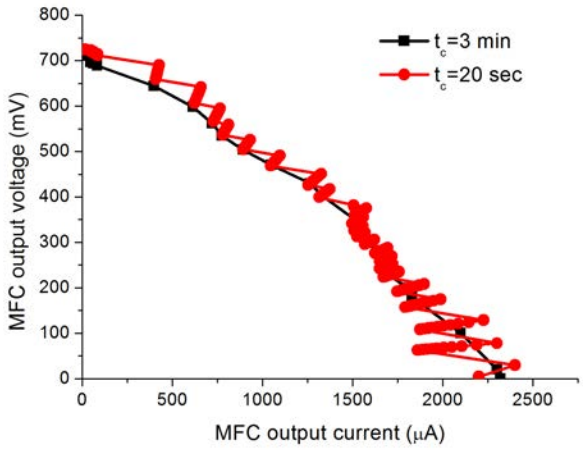

Figure 3.6: Polarization curve of MFC with 20 sec and 3 min sampling rate

3.3 Modeling the MFC

The EMF corresponds to the theoretical maximum voltage of a MFC. Such voltage is never achieved practically by MFCs because of voltage drops and current drops. The output voltage is therefore expressed as (3.1)

$$V = V_{OC} - \Delta V_{act} - \Delta V_{ohm} - \Delta V_{con} \tag{3.1}$$

- Where V_{oc} is the theoretical, reversible, open circuit voltage.

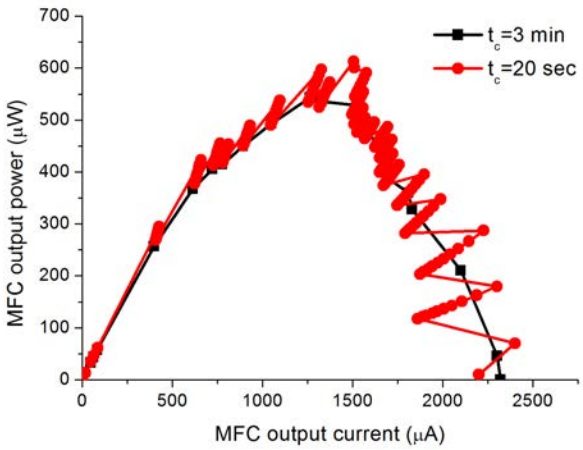

Figure 3.7: Power curve of MFC with 20 sec and 3 min sampling rate

- ΔV_{ohm} is the ohmic drop. The value of the ohmic voltage drop is simply proportional to the current (3.2)

$$\Delta V_{ohm} = R_{ohm} I \tag{3.2}$$

where I is the current or the current density given in A or mA.cm^{-2}, R_{ohm} is the ohmic resistance (in Ω or kΩ.cm^2).

- ΔV_{act} is the activation voltage drop and given by the so-called Tafel equation (3.3):

$$\Delta V_{act} = B ln(I) \tag{3.3}$$

The expression of the activation losses is valid when I>1A which is not a valid assumption in the case of MFCs. For currents below 1A, 3.3 can be modified by an almost equivalent expression [Degrenne et al., 2012b]. The activation voltage drop is modified as (3.4):

$$\triangle V_{act} = B \ln(\frac{I}{C} + 1) \tag{3.4}$$

Where B and C are constants depending on the electrode and cell conditions.

- ΔV_{con} is the mass transport or concentration voltage drop and given by Nernst equation (3.5):

$$\triangle V_{con} = D \exp(E.I) \tag{3.5}$$

where D and E are constants to be determined.

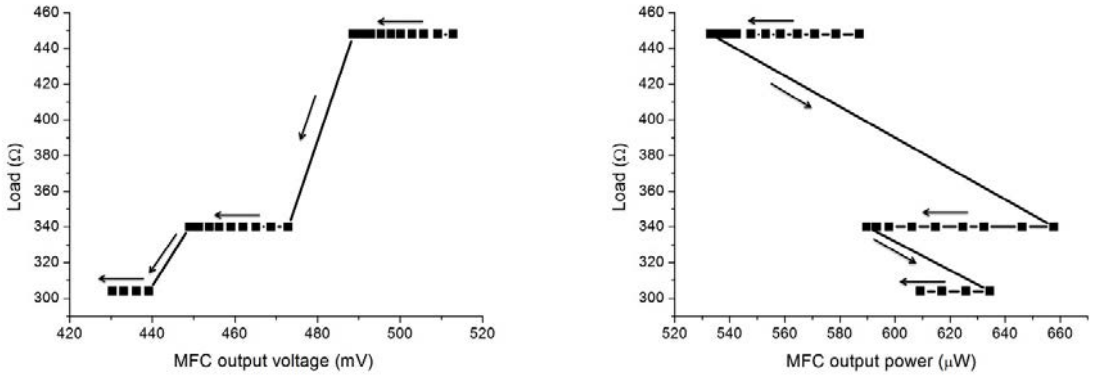

Figure 3.8: Evaluation of the voltage and the power of the MFC with 20 sec sampling rate, zoom on a part of the curves in Fig. 3.6 and 3.7.

The equation for the operating voltage of an MFC at a current I can be written as (3.6):

$$V = V_{OC} - B\ln(\frac{I}{C}+1) - R_{ohm}I - D\exp(E.I) \tag{3.6}$$

This equation defines the analytical expression of a polarization curve with 6 parameters to be identified. The open circuit voltage (V_{oc}) is usually between 0.5V and 1V and always smaller than EMF. It can be measured by the resistorstat or by a high impedance voltmeter and it was obtained 0.72V for the lab-scale MFC (see Fig. 3.6). The other 5 parameters are determined through fitting of the experimental polarization curve with the 5-parameter equations (Prism software®). This fitting is simple to evaluate using a spreadsheet (such as EXCEL), or programs such as MATLAB. These parameters (R_{ohm}, B, C, D and E) are determined here using Prism software. The equation of the output voltage can be rewritten as (3.7) for the lab-scale reactor at 1 g/L of acetate.

$$V = 0.72 - 177.I - 0.01\ln(\frac{I}{0.000183}+1) - 0.0114\exp(1403.I) \tag{3.7}$$

In terms of electrical equivalent circuit, the above analytical equations can be represented by an ideal voltage source (open circuit voltage of the MFC) connected to a number of electrical components for the different voltage losses. Considering that the ohmic drop is proportional to the current, it can be represented by a constant resistance equal to the ohmic resistance of the MFC (the resistance of electrolytes and the various interconnections). The other drops are non-linear and are represented with variable resistances as shown in Fig. 3.10-a. The comparison between the analytical model and the experimental curve is presented in Fig. 3.9. These results prove that the model is valid in steady state. The effect of the operating conditions on these parameters will be studied later.

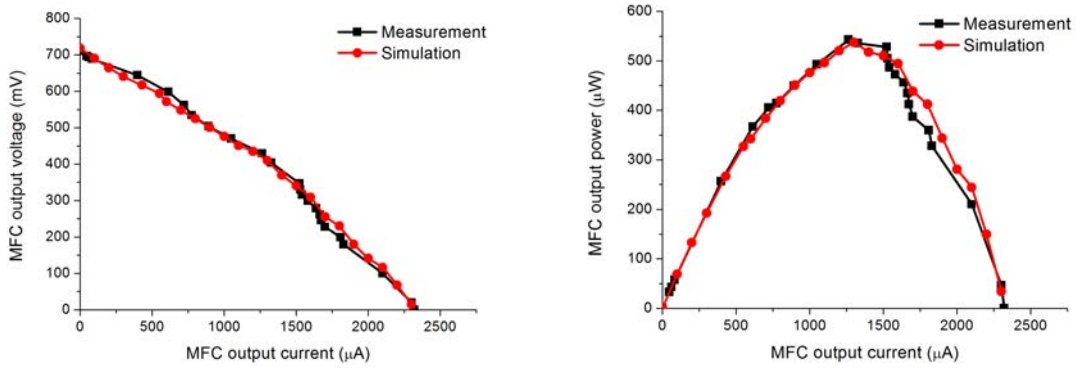

Figure 3.9: Experimental measurement and evaluation of the analytical model for a lab-scale reactor with 3 min sampling rate

Measurements on MFCs show non-immediate reaction caused by the internal mechanisms (i.e. activation and concentration). The interface between each electrode and its surrounding electrolyte forms a capacitor. The combination of static and dynamic mechanisms can be integrated in the electrical model: the effects of both concentration and activation overvoltages can be modeled by variable capacitors connected in parallel with the variable resistances as in Fig. 3.10-b. MATLAB® is used to evaluate the value of the capacitors and their relations to current and voltage.

Considering that the concentration drop occurs at high current densities where the MFC has a limited performance, the capacitive effect of concentration drop is almost negligible compared to the activation drop in the operation range of MFCs. The electrical model therefore can be simplified as shown in Fig. 3.10-c. The resulting capacitor is considered as the MFC equivalent capacitor. This approximation has no effect on the operation of MFC in steady-state but it will create perturbations in the dynamic operation at high current.

3.3.1 Analysis of voltage drops

When the MFC is connected to an external resistance R_{ext}, Ohm's law gives the proportionality between the microbial fuel cell output voltage V and the current I through the resistor.

$$V = R_{ext} I \tag{3.8}$$

It is simple to calculate the various voltage drops that affect the ideal output voltage from a 3 min sampling rate polarization curve sample rates. The activation drop (3.4) is not important compared to the other losses. The concentration drops (3.5) increase exponentially with the current and becomes very important at high current densities due to the limited mass transfer of chemical species by diffusion to

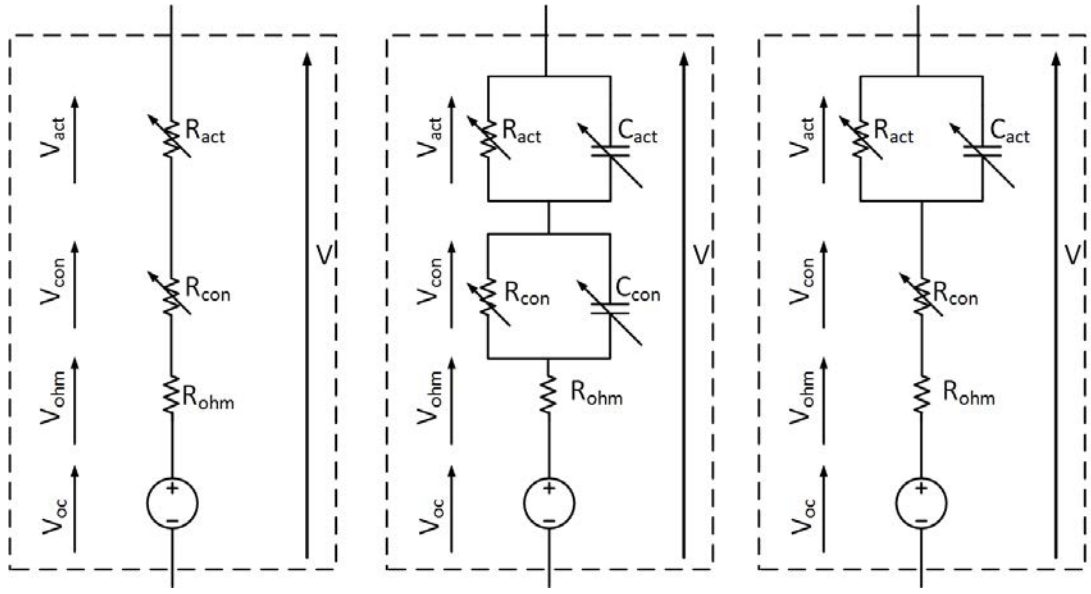

Figure 3.10: Electrical equivalent circuits for a MFC

the electrode surface. Activation, concentration and the total internal resistances are calculated using (3.9), (3.10) and (3.11) as illustrated in Fig. 3.12. The results show that the internal resistance increases at higher current densities due to the limited mass transfer.

$$R_{act} = \frac{\Delta V_{act}}{I} \tag{3.9}$$

$$R_{con} = \frac{\Delta V_{con}}{I} \tag{3.10}$$

$$R_{int} = R_{ohm} + R_{act} + R_{con} \tag{3.11}$$

The concentration drop and ohmic drop are calculated from the polarization curve with 20 sec sampling rate using Nernst and ohm laws (3.7). The activation drop can then be calculated by Kirchhoff laws. Fig. 3.13 shows the different types of voltage drop as a function of the MFC current. The perturbations at high current densities are due to the neglect of the concentration capacitor and may be due to other unknown parameters. Fig. 3.14 shows the evolution of the different impedances of the MFC model. A comparison between the voltage drops in two experiences (3 min and 20 sec sampling rate) shows that

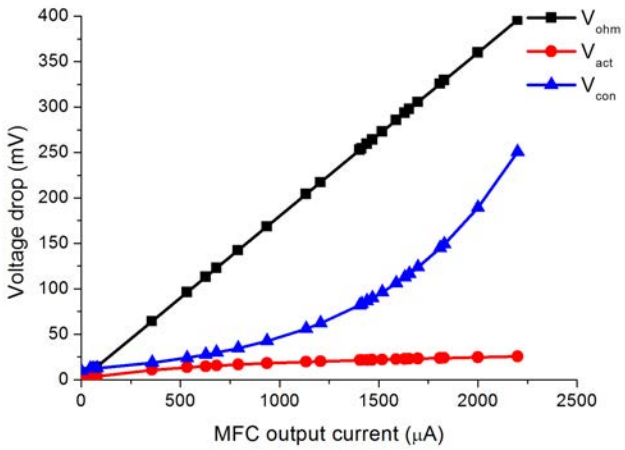

Figure 3.11: The activation, ohmic and concentration voltage drops from the polarization curve with 3min sampling rate

the concentration and ohm drops are almost the same. Therefore the change in the output voltage in this experience can be explained by the apparition of the activation capacitive effect. Comparing Fig. 3.12 and Fig. 3.14 gives that the activation capacitor is a non-linear capacitor as the activation resistance. We can determine this capacitor as a function of the output voltage (Fig. 3.15). The value of the capacitor depends on electrode polarization. The results show that the relatively high surface area provided by the electrodes with an electrochemically active biofilm, exhibits relatively high capacitive behavior in the reactor. It can be estimated that the specific capacitance is approximately 30 mF/L, at MPPT, based on reactor liquid volume or 166 $\mu F/cm^2$ based on the cathode surface. This capacitor is equivalent to two capacitors: i) the double layer capacitance of the biofilm and ii) the Helmholtz layer capacitance. Between an electrode and the electrolyte, there is a complex electrical structure known as the electrical double layer. This layer stores charges electrostatically at the electrode/electrolyte interface. The amount of electric charges stored in this capacitance is linearly proportional to the voltage and depends on the electrode surface. The value of the double layer capacitance depends on various factors such as the electrode polarization, the ionic concentration, temperature, the type of ions, oxide layers, the roughness of the electrode, the electrode material and its specific surface area, etc. The value of the capacitance found in literature is in the range from 30 to 200 $\mu F/cm^2$ [Fradler et al., 2014]. In [Fradler et al., 2014], an Electrochemical Impedance Spectroscopy (EIS) showed that the Helmholtz layer presents a capacitance of more than ten times the one of the biofilm. Another study showed that the double layer capacitance is 100 times larger that the capacitance of the biofilm [Ter Heijne et al., 2011]. The calculated capacitor could be therefore considered as the representation of only the double layer capacitance.

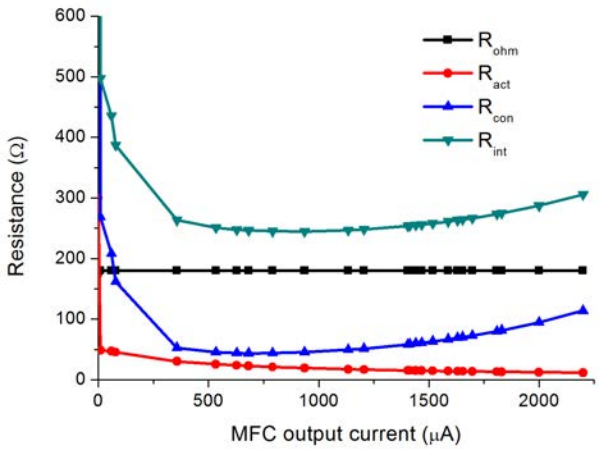

Figure 3.12: Evolution of the different impedances of the MFC model from the polarization curve with 3 min sampling rate

3.4 Validation of the model

The model developed using Tafel, Ohm and Nernst expressions proved to model properly the static electrical characteristics of a MFC. Adding capacitors in parallel with the resistances as shown in Fig. 3.10 represents the combination of static and dynamic mechanisms. The model is validated for different values of sample rate. Comparison between results of simulation and experiment for the polarization and the power curves are given in Fig. 3.16 and Fig. 3.17 for 20 sec sample rate. At high current densities, the model does not provide an accurate response. This is because of the neglect of the concentration capacitor. So far this is not a critical issue because MPP is situated at lower current densities and the model offers a proper evaluation. The model was also validated on a serial stack of MFCs with voltage balancing circuits [Khaled et al., 2015].

3.5 Analysis of losses

When the MFC is connected to an external resistance, Joule's law gives access to the losses through each representative resistor in the model ((3.12), (3.13) and (3.14)). The calculation shows that the losses in the ohmic resistor are the most significant ones. Decreasing the load increases the concentration losses that become higher than the activation losses. For example, at MPP, the activation losses are 38 µW, the ohmic losses 377 µW and concentration losses 119 µW. The sum of these losses represents 534 µW. Fig. 3.18 shows the experimental breakdown of losses at 20 sec sampling rates. It is remarkable that ohmic and concentration losses are almost the same for 3 min and 20 sec sampling rate respectively. The

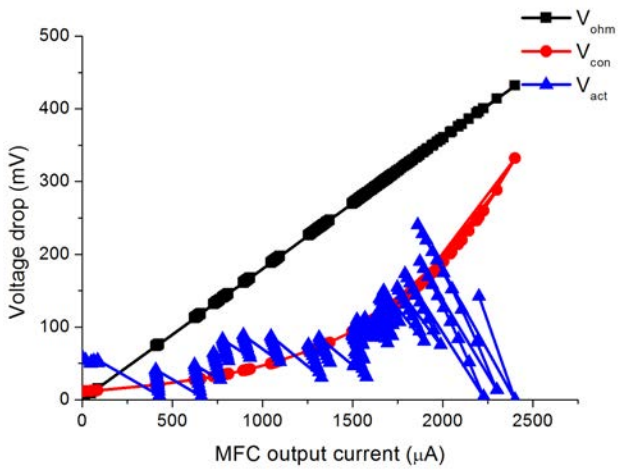

Figure 3.13: Activation, ohmic and concentration voltage drops with 20 sec sampling rate

changes in the activation losses can be explained by the activation capacitor which causes changes in the current.

$$P_{ohm} = \Delta V_{ohm} I = R_{ohm} I^2 \tag{3.12}$$

$$P_{con} = \Delta V_{con} I = R_{con} I^2 \tag{3.13}$$

$$P_{act} = \Delta V_{act} I = R_{act} I^2 \tag{3.14}$$

The power produced by bacteria (P_{TOT}) will not be equal to the output power due to electrode over-potentials (activation, concentration and ohmic). This energy could be written as (3.15): the sum of total internal losses (P_{losses}) (3.16) and the output power, P_{out} as shown in Fig. 3.19. Increasing the current, the output power and the total losses increase. The two curves intersect at the point of maximum power. At the intersection points, the output power equals the internal losses what confirms that the internal resistance equals the load resistor. That leads to the following conclusion: to obtain maximum external

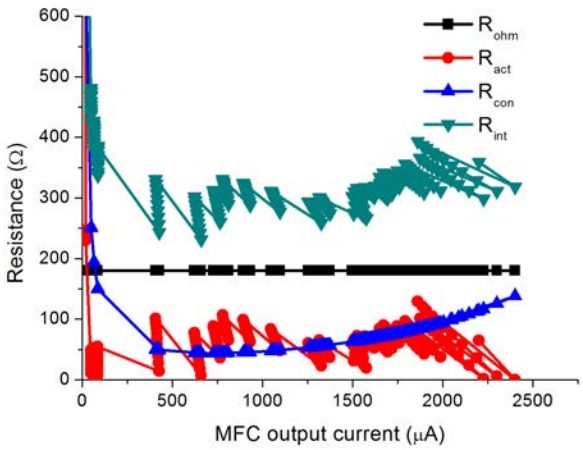

Figure 3.14: Evolution of the different impedances of the MFC model with 20 sec sampling rate

power from an MFC, the resistance of the load must be equal to the internal resistance of the MFC (Jacobi's law) [Thompson and Phillips, 2009] as shown in Fig. 3.20.

$$P_{tot} = P_{losses} + P_{out} \tag{3.15}$$

$$P_{losses} = P_{ohm} + P_{con} + P_{act} \tag{3.16}$$

3.6 Substrate concentration

Acetate and glucose, as the most common substrates, with different concentrations have been studied by many researchers [Lee et al., 2008, Cheng et al., 2011, Liu et al., 2005b]. But it is difficult from literature to compare MFCs performances, due to different operating conditions such as surface area, type of electrodes and different microorganisms.

To study the influence of substrate concentration on the performance of the MFC and its effect on the model parameters, MFCs were studied for different concentration. Fig. 3.21 presents the experimental electrical characteristics of the MFC for five values of concentration (2, 1, 0.75, 0.5, 0.25) g/L of acetate. Increasing the concentration from 0.25 g/L to 1 g/L increases the output power. The results show a limiting current with values of 878 µA for 0.25 g/L, 1700 µA for 0.5 g/L, 2200 µA for 0.75 g/L and 2320 µA for 1 g/L. Output power curves also responded to the increase in concentration from 0.25 to 1 g/L and maximum values are obtained at 162 µW, 323 µW, 419 µW and 470 µW for 0.25, 0.5, 0.75 and 1 g/L

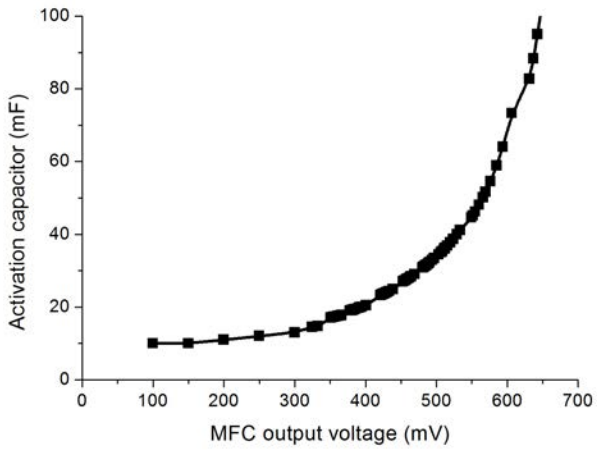

Figure 3.15: Evolution of the activation equivalent capacitor

respectively. Increasing the concentration to 2 g/L decreases the output power to 348 µW. Most of the acetate remains unconsumed at high concentrations. Tacking the case of 1 g/L as a reference, the output powers are 34.4%, 68.7%, 89% and 74% of the reference power for 0.25, 0.5, 0.75, 2 g/L of acetate respectively.

For each concentration, activation, ohmic and concentration resistances are analyzed using the electrical model in Fig. 3.10. Decreasing the concentration from 1 to 0.25 g/L, the ohmic and the concentration drop increase while the activation drop decreases as a consequence of decreasing the microbial activities as shown in Fig. 3.22. The total internal resistances are 255, 273, 330 and 633 Ω for 1, 0.75, 0.5 and 0.25 g/L respectively. Increasing the concentration above 1 g/L will decrease MPP. The main reason of the reverse relationship of power and substrate concentration is that high concentration of substrate would inhibit the bacteria activities [Shen and Wang, 1994]. In addition, it increases the concentration resistance and most of the acetate remains unconsumed at high concentrations. The results reveal that the optimum concentration with the highest electrical performances is near 1 g/L of acetate. These results are true for all types of MFCs i.e. at specific concentration, the MFC has an optimal performance. Higher or lower concentration will negatively affect the performances.

In batch mode, the concentration of acetate will decrease naturally. That means, during operation, the internal resistance of the MFC increases what decreases the performances unless the load is modified accordingly in a kind of feedback action.

3.7 Effect of temperature

Temperature is an important factor on the performance of MFCs. [Hong Liu and Logan, 2005] has reported only a slight reduction in power density (9%) when the temperature was reduced from 32 to

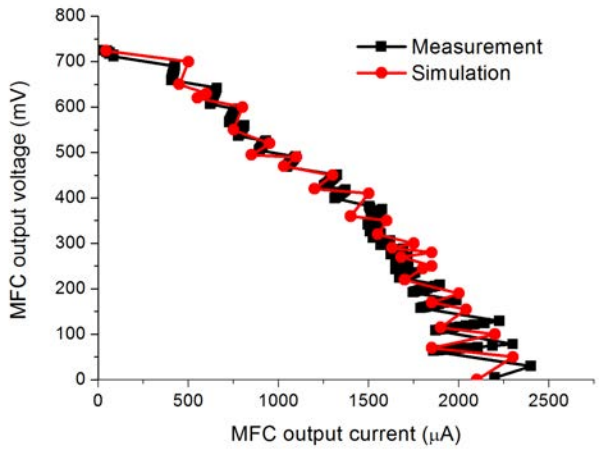

Figure 3.16: Comparison between the simulation results and experimental polarization curves with 20 sec sampling rate

20°C. [Ahn and Logan, 2010] has studied the MFC performance at ambient (23 ± 3 °C) and mesophilic temperatures (30 ± 1 °C) and demonstrated that temperature effects are dependent on the substrate, and that temperature changes are important for complex substrates such as domestic wastewater. Recently [Larrosa-Guerrero et al., 2010] have reported the performance of single and double chamber MFCs tested in batch mode at different operating temperatures ranging from 4 to 35°C. Temperature plays a crucial factor on the biological activity and electricity production.

To analyze the influence of temperature on the behavior of MFCs, the effect was studied by changing the operation temperature in a controlled temperature chamber ranging between 15°C and 40°C. Results are illustrated in Fig. 3.24. Power generation by MFCs was significantly affected by ambient temperature. The results show a limited current with values of 1525 µA for 15°C, 1910 µA for 20°C, 3200 µA for 30°C and 3200 µA for 40°C respectively. Output power curves also responded to the increase in temperature, as expected, and maximum values are 485 µW, 490 µW 607 µW and 812 µW for 15°C, 20°C, 30°C and 40°C respectively. Increasing the performance of MFCs as a function of the temperature can be explained by improving the biological activity which will contribute to lower the internal resistance of the cells. By increasing the reaction temperature, the thermal energy available in the system is increased, which makes reactants obtain enough energy to reach activated state. Temperature increase is also propitious to anaerobic organisms, which has a better electricity production environment.

The internal losses (ohmic, activation and concentration) are evaluated using the electrical model. Fig. 3.25 presents the ohmic, activation and concentration voltage drops for 15°C, 20°C, 30°C and 40°C. The ohmic resistance is almost constant with the change in ambient temperature from 15°C to 40°C what is not enough to change the conductivity of the substrate. Activation resistance increases slightly with higher temperature. The effect of temperature on the concentration resistance is the most important. The

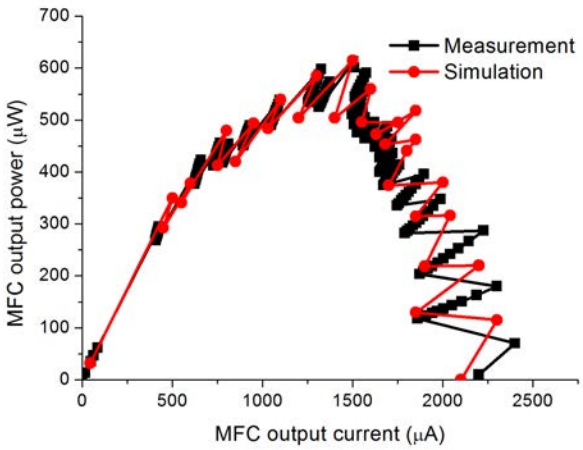

Figure 3.17: Comparison between the simulation results and experimental power curves with 20 sec sampling rate

concentration resistance is about 3 Ω at 40°C compared to 114 Ω at MPP at 20°C. The results can be explained by an increase in the bacterial activities with the temperature which increases the speed of compounds to the surface of the anode and improves the mass transfer.

3.8 Conclusion

In this chapter, an electrical model of MFCs is presented: it is developed analytically based on the internal mechanisms of MFCs. The combination of static and dynamic mechanisms is represented as an equivalent electrical model for readability. The MFC internal resistance is modeled as a combination of anodic resistance, cathodic resistance, and ohmic resistance, while the anodic and cathodic resistances are current-dependent. There is a capacitance at the interface between the electrode and its surrounding electrolyte/substrate when the charges in the electrode are separated from those in the electrolyte.

The parameters of this model were identified from measurements through fitting of experimental polarization curve. The model was tested and proved to fit adequately with a large number of experimental results. It was validated in static and dynamic states. The model permits to get better insight on the metabolism in MFCs. The different internal resistances, voltage drops and losses in MFC are evaluated what is useful to improve the performances. This model is shown to be sensitive to parameters such as temperature and substrate concentration. This study gives a more precise and more realistic model than what covers literature. This model is a prerequisite to the design of harvesting electrical circuits because it can be used simply in electrical simulation software.

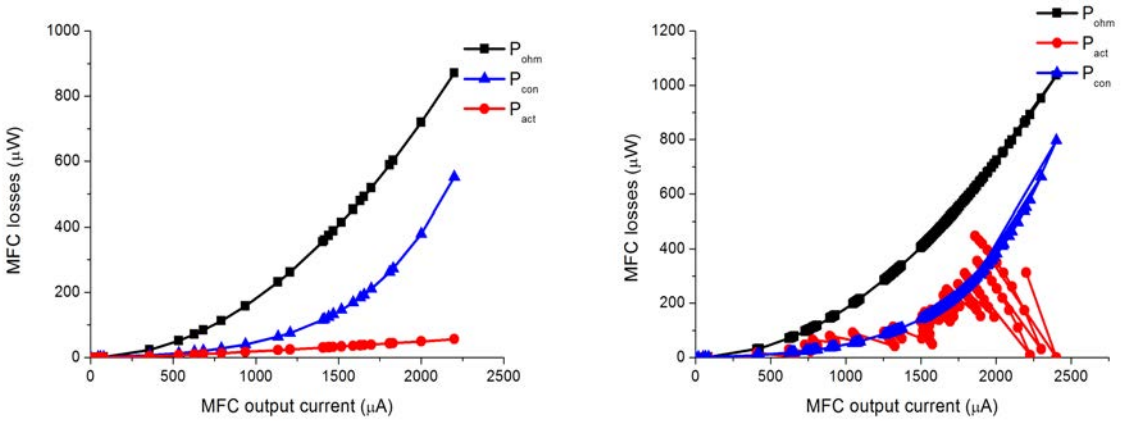

Figure 3.18: Breakdown of losses in the MFC with 3 min (left) and 20 sec (right) sampling rate

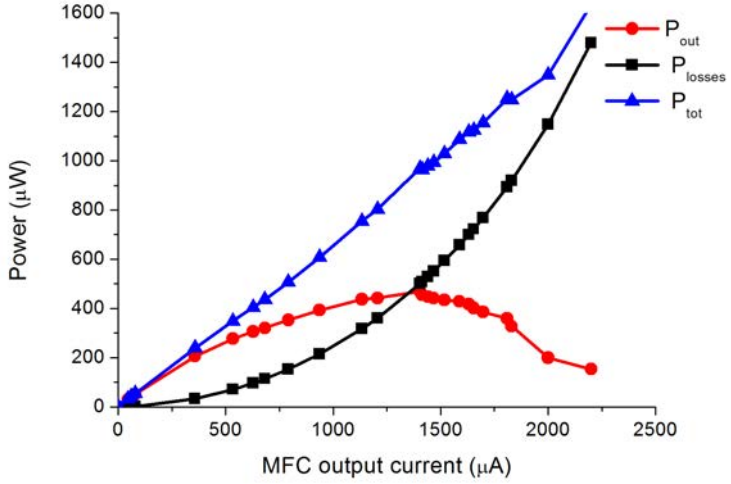

Figure 3.19: Breakdown of all power contribution in a lab-scale reactor with 3 min sampling rate

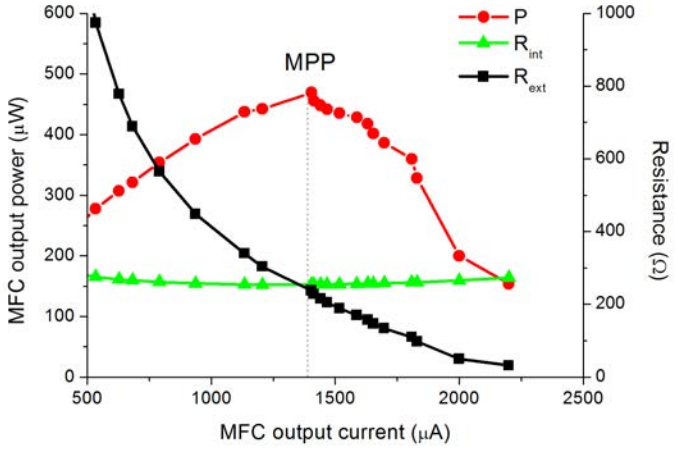

Figure 3.20: Internal resistance (R_{int}), load (R_{ext}) and output power as a function of the current (lab-scale reactor, 3 min sampling rate)

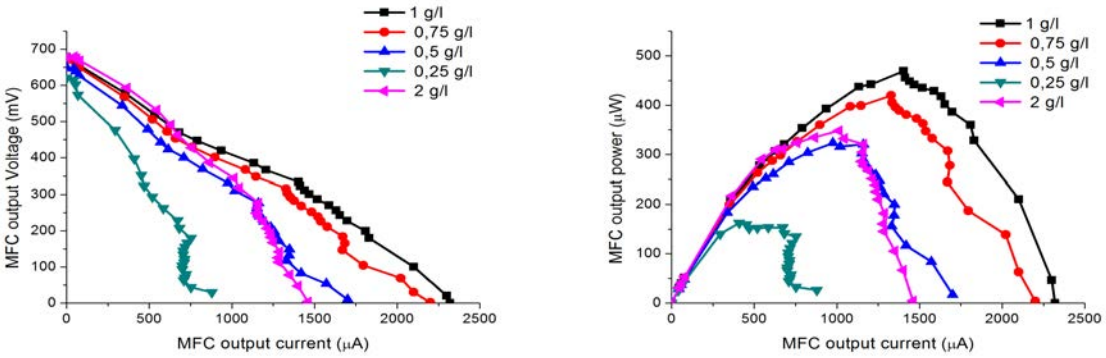

Figure 3.21: Experimental polarization and power curves of MFC for different values of concentration of acetate (3 min sampling rate)

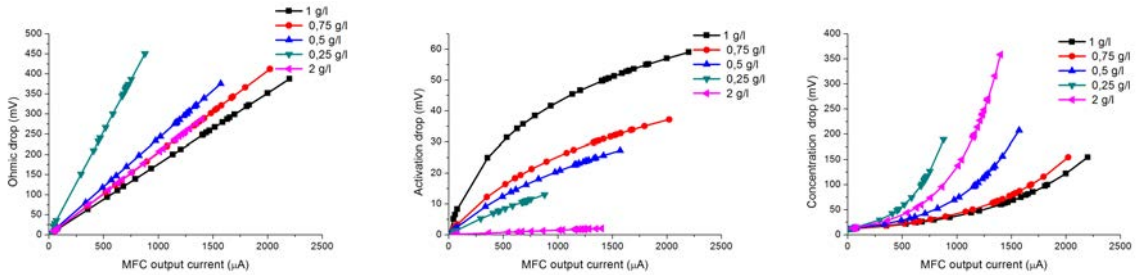

(a) (b) (c)

Figure 3.22: Different voltage drops for different values of concentration of acetate in a lab-scale reactor

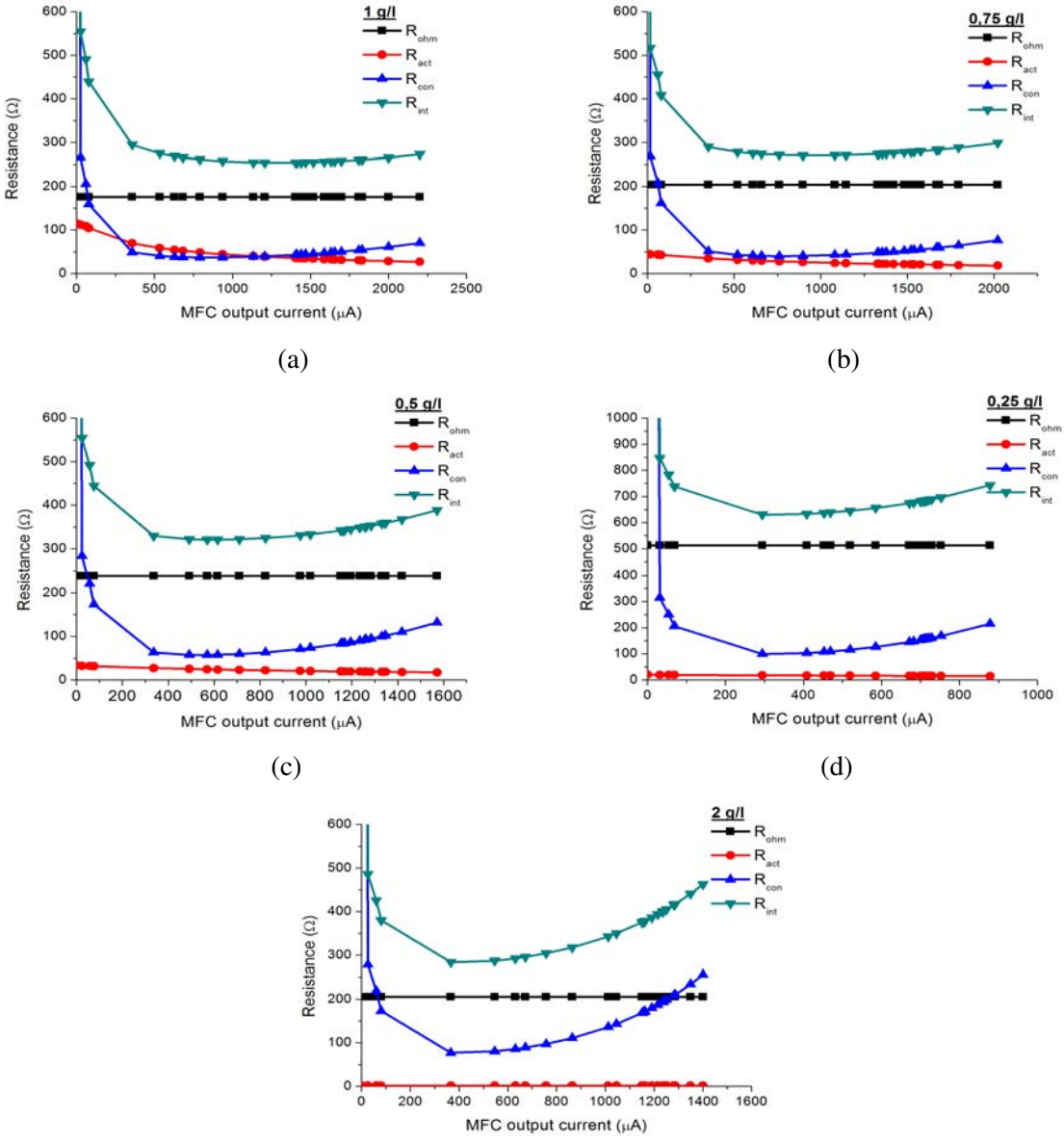

Figure 3.23: Evaluated different resistances for different values of concentration of acetate in a lab-scale reactor

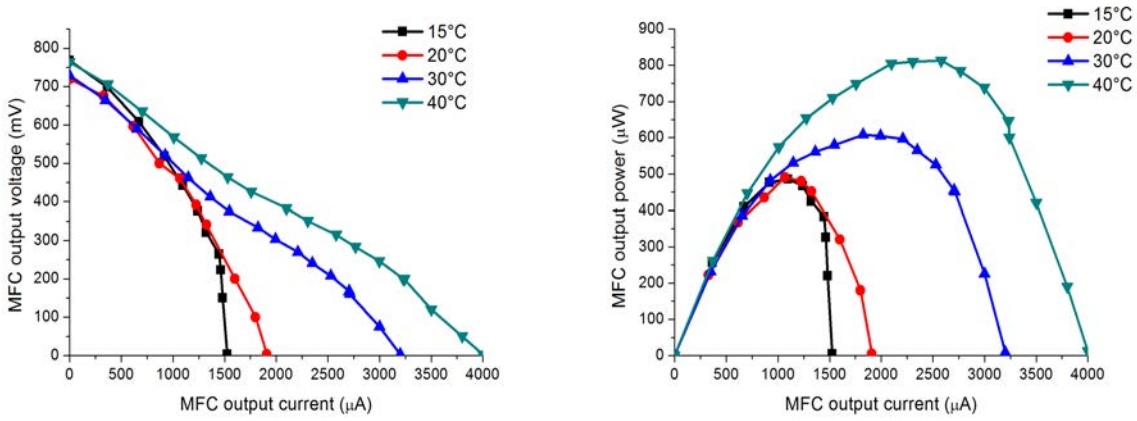

Figure 3.24: Experimental polarization and power curves for different values of ambient temperature (3 min sampling rate)

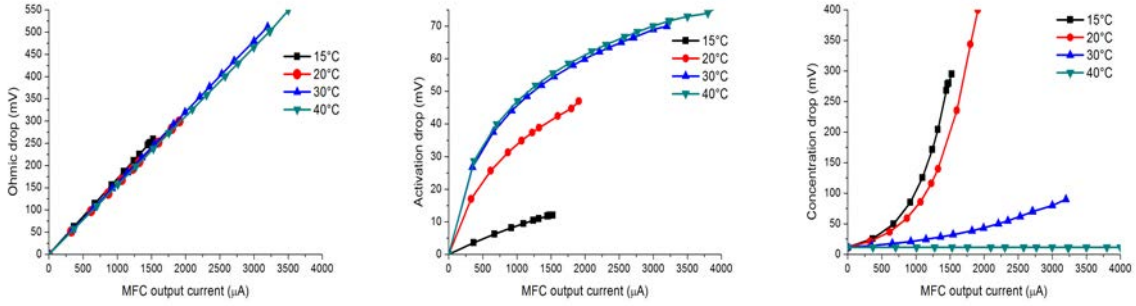

(a) (b) (c)

Figure 3.25: Different voltage drops for different ambient temperature

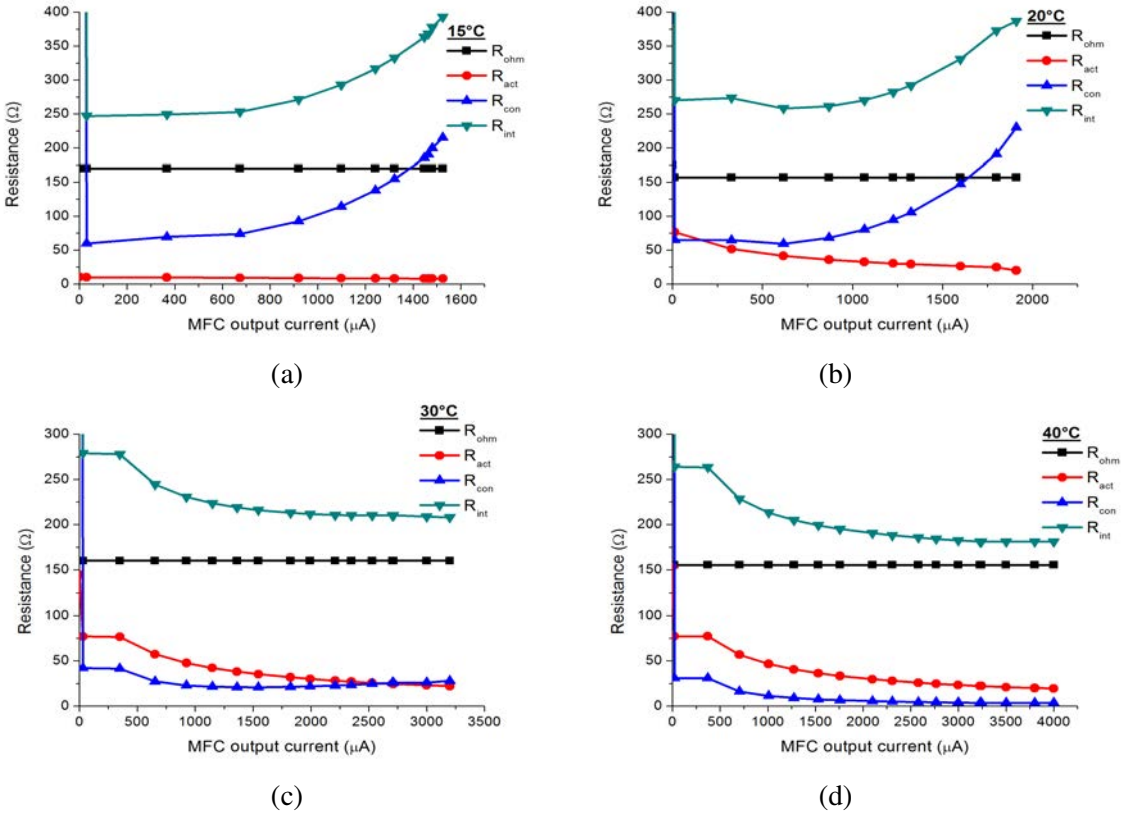

Figure 3.26: Evaluated resistances for different values of ambient temperature

Part II

Energy harvesting from microbial fuel cells

Chapter 4

Literature review

Contents

Harvesting energy from ambient source is an effective solution for powering low power applications. Electrical characteristics for these sources introduce constraints on the power management system. The low voltage and low power inhibit the use of standard topologies since the threshold voltage of standard CMOS transistors is generally between 0.5 V and some volts in CMOS technology. A start-up sub-circuit is therefore required. A specific sub-circuit is also required to control the operation of MFCs for MPPT.

4.1 Start-up techniques

4.1.1 Start-up with external source

When the input voltage is very low, the start-up problem can be solved by using an external source, such as a rechargeable battery. In literature, a micro-battery was used to start-up and to regulate the output voltage of a boost converter in [T. Paing and Popovic, 2008] as shown in Fig. 4.1. A pre-charged capacitor or super-capacitor overcomes the battery-related limitations. However this solution is not very common in literature because of the leakage current of the capacitors and super-capacitors. Besides voltage of this capacitor should be monitored continuously and recharge adequately it if the voltage decreases below the operation voltage. In term of autonomy, these systems could not operate without the external source.

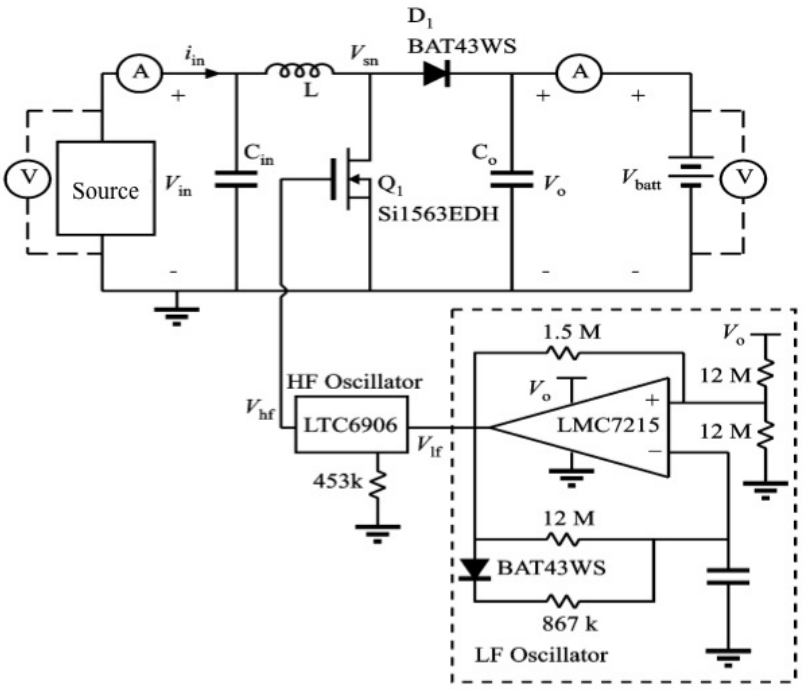

Figure 4.1: Start-up circuit with a micro-battery (V_0) [T. Paing and Popovic, 2008]

4.1.2 Self-starting methods

Many self-starting methods have been studied. A mechanical switch was used at the start-up for charging a capacitor from a mechanical vibration source [Ramadass and Chandrakasan, 2011]. In switched-based transformer, so-called "Armstrong oscillator", thanks to the advantageous turn ratio of the coupled converter, these converters can start-up at very low input voltages. The transformer primary is generally controlled by a JFET for normally-on feature. The voltage at the secondary of the transformer is alternative. A diode must be used to rectify the alternative voltage at the secondary of the transformer to obtain the negative output voltage to control the JFET, what makes this circuit unpractical for most applications. The converter was tested for RF energy harvesting and the efficiency is about 30% [Adami, 2013]. The circuit is presented in Fig. 4.2-a. The same circuit was optimized also for energy harvesting from MFCs, the efficiency was 60% [Adami et al., 2011]. A third winding could be added to solve the problem of the negative output voltage and obtain a positive one [Adami et al., 2011] as shown in Fig. 4.2-b. In [Damaschke, 1997, Adami et al., 2011], two transformers were used in the converter. One transformer behaves to the main converter. The other transformer 1:45:65 is used to start-up at 300 mV as shown in Fig. 4.3. Although the circuit is complex and have a large number of inductive components, the maximum overall efficiency is 76 % [Damaschke, 1997].

Coupling the Armstrong oscillator to start-up a flyback or a boost converter is also possible. That gives the possibility to merge these two transformers in one transformer to be used for start-up and also

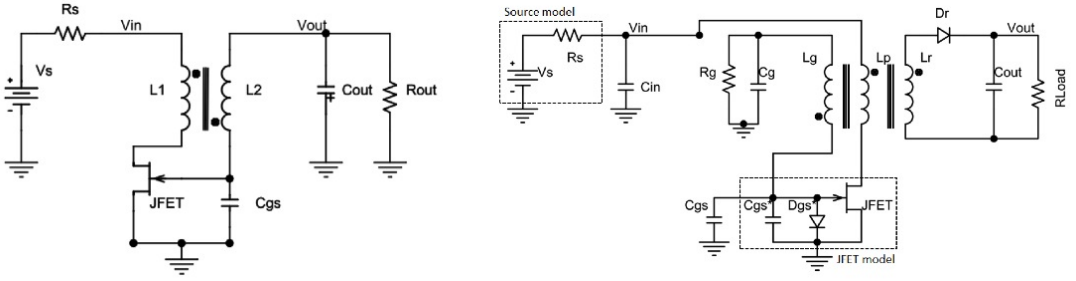

(a) (b)

Figure 4.2: Transformer-based start-up circuit with two windings transformer (left) and with three windings transformer (right) [Adami et al., 2011]

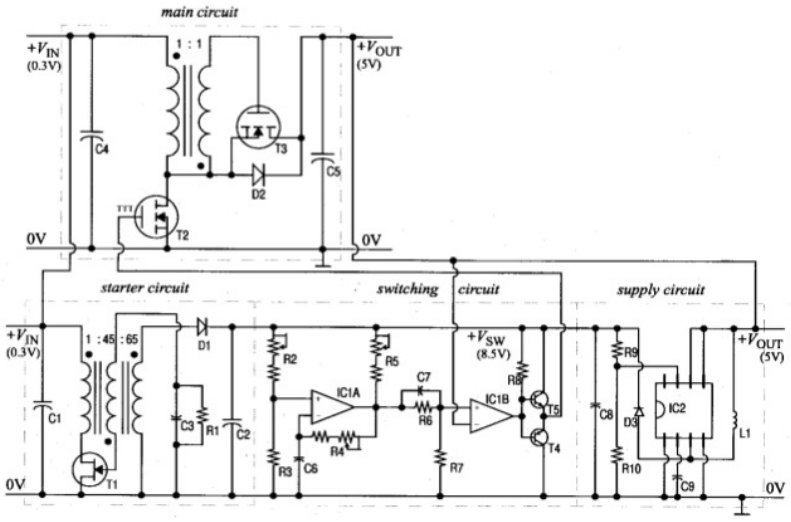

Figure 4.3: Circuit diagram of the low input voltage converter for thermoelectric generator proposed in [Damaschke, 1997].

for the main converter [Mateu et al., 2007]. In [Degrenne, 2012, Degrenne et al., 2012a], the Armstrong oscillator is coupled to a boost converter for energy harvesting from MFCs. The primary inductance of the Armstrong oscillator was merged with the inductance of the boost converter as shown in Fig. 4.4. The circuit is able to start-up at low input voltage near 140 mV.

There are three commercially available converters based on switched transformer dedicated to energy harvesting:

- Fraunhofer ME-PMA2: It is a flyback converter type. It uses a switched transformer. The secondary winding is only needed for controlling the switching transistors. The converter employs a low-voltage self- oscillating boost converter to start-up at 20 mV. The efficiency reaches 90% for 500 mV of input voltage. The consumption of this converter is nevertheless high (10 milliampere).

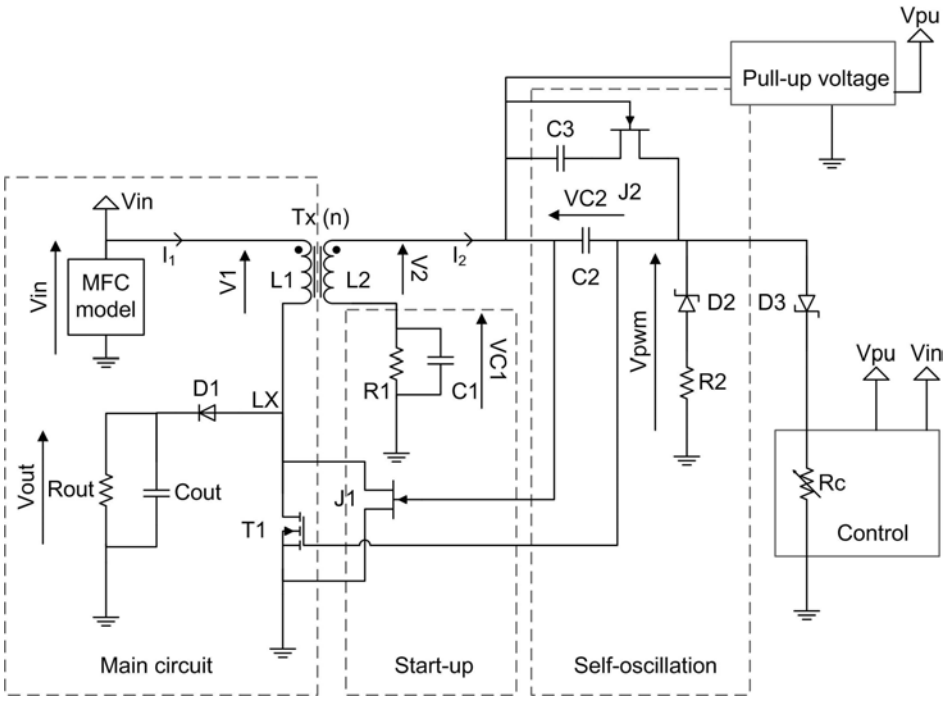

Figure 4.4: Schematic of the boost converter with a start-up sub-circuit [Degrenne et al., 2012a,Degrenne, 2012]

- EnOcean ECT310: This converter is designed for energy harvesting from thermoelectric generators (TEGs) which have input source impedances < 2 Ω. The start-up voltage is as low as 20 mV with 30% efficiency. The circuit has a voltage output ranging from 3 to 5 V.

- Linear technology LTC3108 and LTC3109: The converter, in Fig. 4.5, uses a small external step-up transformer with high turn ratio (1:100) associated with a charge pump to operate at input voltages as low as 20 mV. This circuit has a selectable output voltage of 2.35, 3.3, 4.1 or 5 V. It has a regulated 2.2V output for powering low power microprocessors. LTC3109 is similar to LTC3108 but it enables energy harvesting from TEGs regardless of polarity. In both converters, a storage capacitor can be connected with the converter to provide power when the source is unavailable.

In [Grgić et al., 2009], a half-wave rectifier was used at the secondary of the transformer to rectify the alternative output voltage. The converter was realized by seven cascaded print transformers. The converter has a very low start-up voltage of about 6 mV but an efficiency of 18%.

4.2 Maximum Power Point Tracking (MPPT)

In any energy harvesting system from low-power transducers (photovoltaic, thermoelectric generators, fuel cells, ...), the system should be able to extract as much energy as possible from the source. Systems

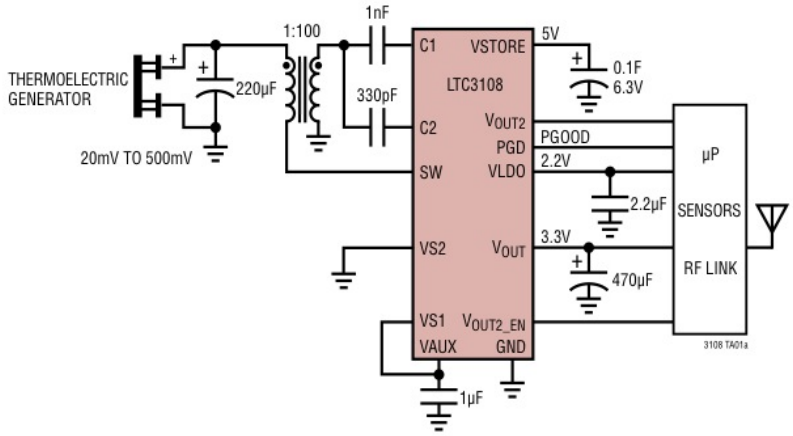

Figure 4.5: LTC3108 converter

have to operate at their maximum power point (MPP). However a MPP varies with the operating conditions. The operation of photovoltaic, for example, varies with insolation, temperature and other effects. On the power curve of the source (power–voltage), there exists only one point between the open circuit and the short circuit, called maximum power point (MPP) where power is maximum. This point varies with the operating condition and should be determined for all expected operating conditions.

A power converter, DC/DC (buck/boost/buck– boost) converter as shown in Fig 4.6 is used between the source and the load to achieve MPPT. These systems use many algorithms to ensure that the transducer always operates at its MPP. These algorithms are called MPPT techniques. A digital controller is generally used to control the converter. A number of MPPT methods have been reported in literature. These methods vary in complexity, cost, required sensors, convergence speed and implementation hardware. These methods can be classified into three groups: indirect (Offline), direct (Online) and other techniques. In the next section, the main MPPT methods will be recalled.

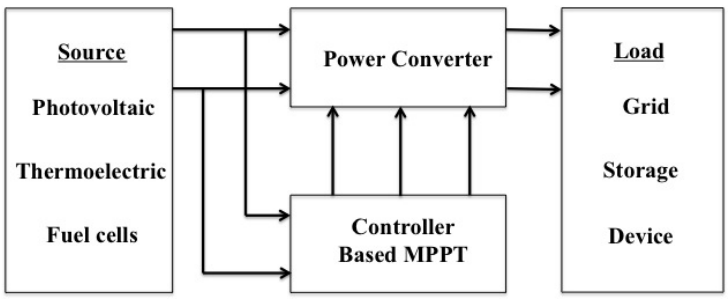

Figure 4.6: Block diagram of MPPT controller for energy harvesting systems

4.2.1 Indirect control techniques

4.2.1.1 Open circuit voltage and short circuit current based MPPT

This method is firstly used to control MPP for solar systems [Kobayashi et al., 2006]. The maximum power point voltage, V_{MPP}, and open circuit voltage, V_{OC}, have a linear dependence defined by (4.1) for different solar radiation and operating temperatures. The maximum power point current, I_{MPP}, and short circuit current, I_{SC}, have also a linear dependence defined by (4.2).

$$V_{MPP} = K_V V_{OC} \tag{4.1}$$

$$I_{MPP} = K_I I_{SC} \tag{4.2}$$

For photovoltaic, for example, the factor k_V has been reported to be between 0.7 and 0.95 and k_I is between 0.7 and 0.9 [Veerachary Mummadi and Uezato, 2002].

In this method, the algorithm is implanted in a microcontroller to drive the converter. The control is achieving by continuously tacking samples of short circuit current or open circuit voltage, computing of maximum current or maximum voltage and adjusting the duty cycle of the converter. The maximum current or maximum voltage is to be calculated by these methods, no derivatives are required. The main drawback of these methods is the losses during sampling.

4.2.1.2 Impedance matching

The first time that the maximum power transfer theorem was published is around 1840. This theorem, also known as “Jacobi’s law” states that the maximum extracted power from a source with a finite internal resistance occurs when the resistance of the load equals the resistance of the source, also called impedance matching as presented in Fig. 4.7. This method was used to MPPT for different type of source. Application of this method with photovoltaic was presented in [Longlong Zhang and Wölfle, 2010]. A variable inductor based on a sloped air-gap (SAG) was used to control the internal resistance of a buck converter. In [Win et al., 2011, Nagayoshi and Kajikawa, 2007], the impedance matching MPPT circuit is used in a buck-boost converter for thermoelectric energy harvester system. A constant or variable duty cycle could be used for resistance adapting. This method is also used with a flyback converter for RF energy harvesting [Adami et al., 2011]. A constant frequency and duty cycle are used to achieve the maximum power transfer theorem. This method could be implanted in a DC/DC converter to adapt the internal resistance of the converter with the internal resistance of the source by changing the duty cycle or the frequency to track the MPP of the source.

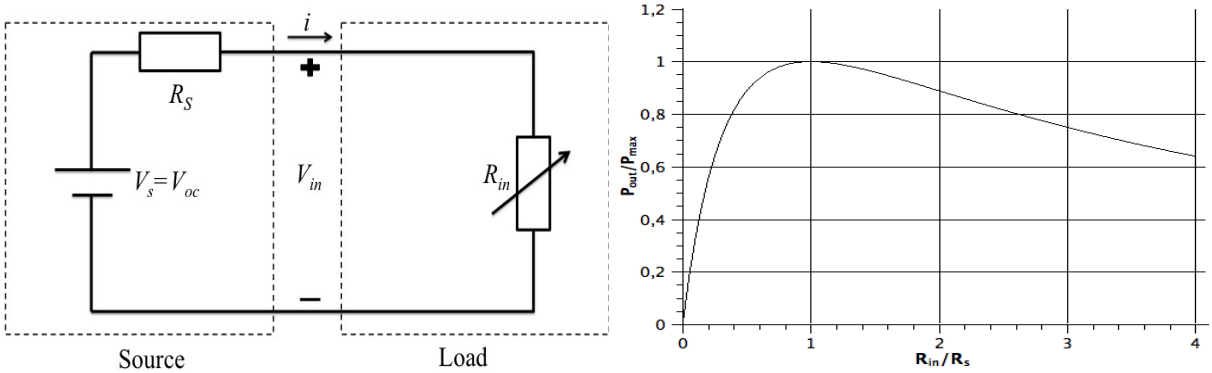

Figure 4.7: Principle of impedance matching MPPT method

4.2.1.3 Look-up table method

In this method, the characteristics of the source are studied and relevant values are stored for different possible conditions in a look-up table. The output power is to be measured and compared with stored values. If large amount of data is stored, a large memory is required and therefore the speed of tracking is affected [Esram and Chapman, 2007].

4.2.1.4 Curve- fitting-based MPPT

A mathematical model and equations describing the output characteristics are required in this technique. The maximum output power is calculated by this model and compared with the measured output power. One complexity of this method is to find a validated model of the source tacking into account all the operating conditions.

4.2.2 Direct control techniques

4.2.2.1 The perturb and observe method (P&O)

Perturb & Observe (P&O) algorithm creates an external or internal perturbation in the operation and compares the output power with that of the previous recorded power [Wasynczuk, 1983, Chung and Ho, 2003]. A perturbation in the duty ratio of the power converter or in the operating voltage can change the output power. P&O algorithm senses the source output voltage and current periodically and calculates the output power.

From Fig. 4.8, it can be seen that incrementing the voltage increases the power when operating on the left of the MPP and duty cycle is to be increased to increase the voltage so as to reach MPP. If the decrementing voltage decreases the power when operating on the left of the MPP and duty cycle is also to be increased to reach MPP. If there is an increase in power, the subsequent perturbation should be kept in the same direction to reach the MPP, but if the power decreases, the direction of perturbation should

be reversed. When the MPP is reached, the algorithm oscillates around the peak point. This algorithm is summarized in Table 4.1.

The perturbation step size should be chosen carefully. A smaller size slows down the MPPT. If large steps are chosen, it will decrease efficiency. A proposed solution is to have a variable perturbation size that gets smaller towards the MPP [Kasa and Iwamoto, 2000, Xiao and Dunford, 2004, Femia and Vitelli, 2005]. Two sensors are usually required to measure the output current and voltage. One sensor only could be used for the voltage and the current could be estimated [Kasa and Iwamoto, 2000].

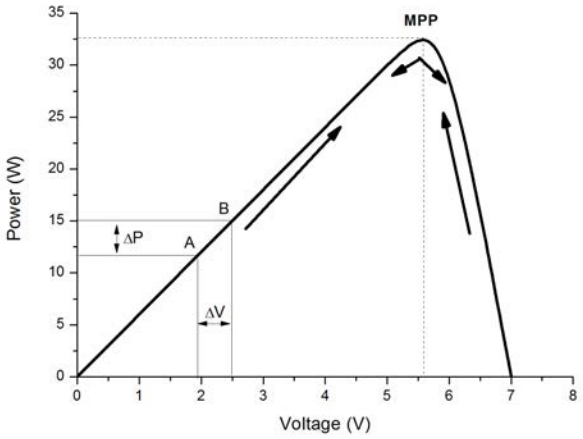

Figure 4.8: Typical Power versus Voltage for Perturb and Observe Algorithm

Table 4.1: Summary of P&O algorithm

Perturb.	Change in V	Change in P	Operating location	Next perturb.
positive	$\Delta V > 0$	$\Delta P > 0$	Left of MPP	Positive
Negative	$\Delta V < 0$	$\Delta P > 0$	Right of MPP	Negative
Positive	$\Delta V > 0$	$\Delta P < 0$	Right of MPP	Negative
Negative	$\Delta V < 0$	$\Delta P < 0$	Left of MPP	Positive

4.2.2.2 Incremental conductance (IC)

The incremental conductance method is based on the fact that the slope of the power curve is zero at the MPP, positive on the left of the MPP, and negative on the right of the MPP [Vikrant.A.Chaudhari, 2005]. This algorithm has advantages over P&O in that it can determine when the MPPT has reached the MPP and stops the oscillation. This method is too complex to implement compared P&O.

Many other methods could be used to control the MPP. MPPT methods use the load parameters to control the operation by maximizing the output voltage or the output current instead of tracking the MPP of the source.

4.3 Maximum power point control for MFC

The nature of the source determines the method of MPPT. As seen from literature review, some of these methods need sensors to measure the voltage and/or the current. Others need a large memory capacity to achieve the MPPT. Three MPPT algorithms are commonly used with solar system, thermoelectric and ambient RF, namely Perturb & Observe (P&O) method, incremental conductance method and approaches using the source characteristics such as impedance matching and fraction of open circuit voltage tracking. P&O and IC designs utilize feedback sensors and digital computation adding to the power losses. Losses in these circuits render them unsuitable for low power harvesters. As a consequence, P&O and IC MPPT algorithms are not considered for implementation in low power energy harvesting system. Fraction of open circuit voltage tracking method is tested in [Degrenne et al., 2012a] for energy harvesting from MFCs. Implantation of this method in a boost converter to control the MPP was also studied. The open circuit voltage of MFC was considered as a constant value of 0.6 V. With the non-uniformities of MFCs, the circuit could be adjusted manually to track the MPP. A self-oscillation circuit is used to drive the switch what renders difficult to control the switching frequency.

Under the same operating conditions, the output power of the MFC can be varied by changing the load resistance. As a result, the load resistance should be modified to be adapted to the internal resistance of the MFC. In the case where the MFC is connected with a converter, the input resistance of the converter should be modified by tuning the switching frequency and/or the duty-cycle. Tacking into account the non-uniformities in characteristics of MFCs, the converter should be adapted to deal with. Impedance matching MPPT method is tested and implemented in a flyback converter in Chapter 6.

4.4 Conclusion

In this chapter, the need of an autonomous system is presented. Several starting-up methods are presented. Some of them use an external source to start-up which is not practical for energy harvesting. Using some self starting-up methods, such as an Armstrong oscillator, the start-up is possible with very low voltages. In any energy harvesting system, the output power changes with the load. A MPPT is necessary to extract the maximum available power from the source. Only some MPPT algorithms in literature may be implemented in low power harvesters. Impedance matching MPPT method is based on the load resistance adaptation or the internal resistance tuning of the converter and could be easily implemented for energy harvesting from MFC.

Chapter 5

DC-DC converters

Contents

The characteristics of MFCs as an energy source pose constraints on converter design. The output voltage is lower than the threshold voltage of standard available MOSFETs and JFETs. The low output voltage of MFCs requires a high step- up converter to increase the voltage to the supply voltage of applications. A large number of dc-dc converter circuits are known to increase or decrease the magnitude of the dc voltage and/or invert its polarity. In our applications, the step-up converters are more interesting.

5.1 Converter topologies

Switched-capacitor converters are generally considered when a low power is to be stepped-up. Unfortunately it is not wise to short-circuit the MFC with a large capacitor at zero voltage initial condition. A large inductance is more suited to limit the switch current. Our study is limited to magnetic DC/DC converters.

5.1.1 Boost converter

The schematic in Fig. 5.1 shows the basic step-up boost converter. The input current for a boost converter is continuous, or non-pulsating, because the diode (D) conducts only during a portion of the switching cycle. The output capacitor supplies the entire load current for the rest of the switching cycle. Fig. 5.2 presents the switching operation of a boost converter during one cycle. During the first phase, the switch M is on and the voltage applied to the inductor nearly equals the input voltage. During the second phase,

the switch M is off and the voltage applied to the inductor equals $V_{in} - V_{out}$. The total voltage applied on the inductor over one cycle is given by (5.1) in continuous conduction mode.

$$\int_0^T V_L(t)dt = V_{in}dT + (V_{in} - V_{out})(1-d)T \tag{5.1}$$

where d is the duty cycle.

By setting this equation equal to zero, the output voltage of a boost converter is given by (5.2).

$$V_{out} = \frac{1}{1-d}V_{in} \tag{5.2}$$

Two modes of operation in a boost converter are continuous or discontinuous inductor current mode. In continuous conduction mode (CCM), current flows continuously in the inductor during the entire switching cycle in steady-state operation. In discontinuous conduction mode (DCM), inductor current is zero for a portion of the switching cycle. It starts at zero, reaches peak value, and returns to zero during each switching cycle.

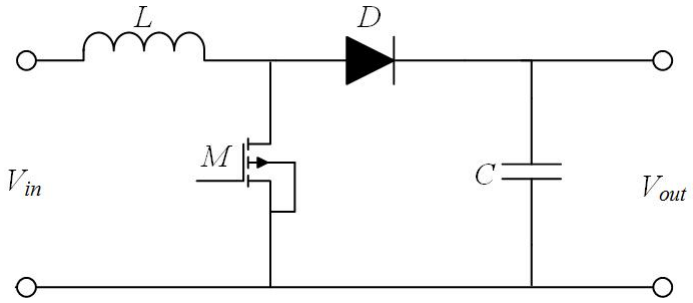

Figure 5.1: Boost converter circuit

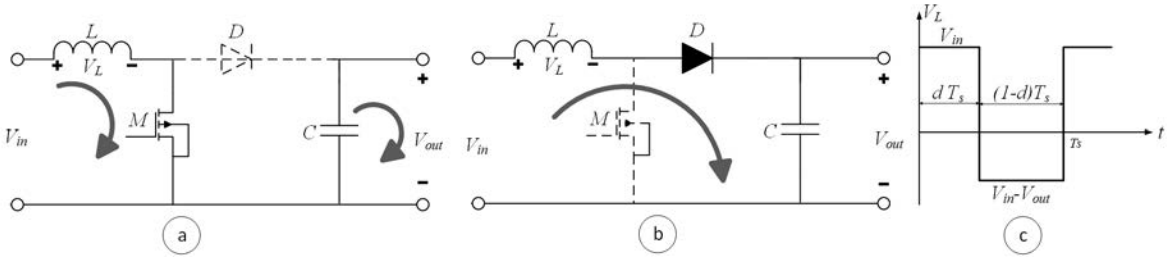

Figure 5.2: Typical switching operation of a boost converter. (a) Shows the circuit during the first phase, (b) shows the circuit during the second phase and (C) shows the voltage across the inductor.

5.1.2 Buck-boost converter

Buck-boost converter, in Fig. 5.3, has an output voltage magnitude that is either larger than or less than the input voltage magnitude. The output voltage is given by (5.3) in CCM.

$$V_{out} = -\frac{d}{1-d}V_{in} \tag{5.3}$$

From (5.3), it can be seen that the output voltage is always negative and its absolute value increases with d. This converter is either step-up converter (boost) or step-down converter (buck).

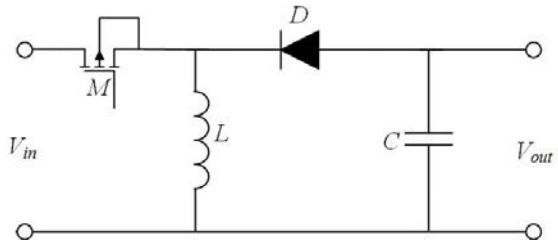

Figure 5.3: Buck-boost converter circuit

5.1.3 Cuk converter

The CUK converter uses capacitive energy transfer between input and output as shown in Fig. 5.4. It is a boost converter coupled with a buck converter by a capacitor. It could be a step-up or a step-down converter since the output voltage is the same as in the buck-boost converter.

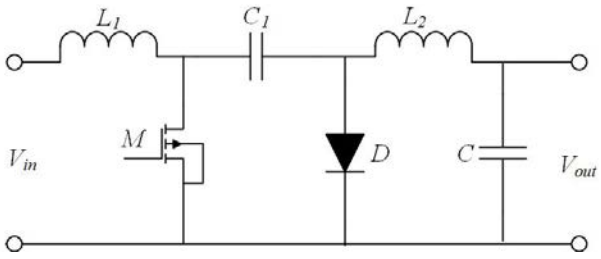

Figure 5.4: Cuk converter circuit

5.1.4 Sepic converter

The Single-ended primary-inductor converter SEPIC converter, presented in Fig. 5.5, uses a series capacitor to couple energy from the input to the output. It is operated like a traditional buck-boost converter,

but has advantages of having non-inverted output. It can either step-up or step-down the output voltage magnitude. The output voltage is given by (5.4).

$$V_{out} = \frac{d}{1-d} V_{in} \tag{5.4}$$

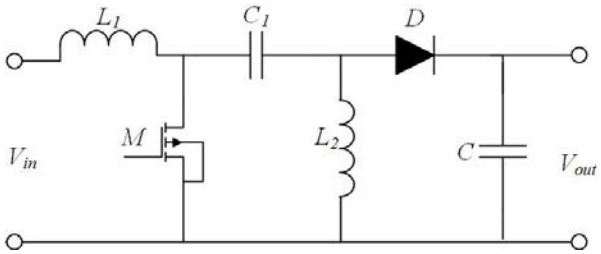

Figure 5.5: Sepic converter circuit

5.1.5 Isolated DC-DC converters

Transformer-based converters provide galvanic isolation between the input and the output. In many DC-DC applications, multiple outputs may be required. The output isolation may need to be implemented to provide either a simple isolated output power source, or to generate different voltage rails depending on the application. Since the output is isolated from the input, the choice of reference voltage for the output side can be arbitrary. In addition, it may be required to meet safety standards. The transformer-based converter provides the ability to control the internal impedance of the converter for MPPT by impedance matching. Fig. 5.6 shows the standard isolated configurations. The full- bridge, half-bridge and forward converters are isolated versions of the buck converter. The flyback converter is an isolated buck-boost converter. The full- bridge, half-bridge and forward converters are so complex and usually used at high power levels.

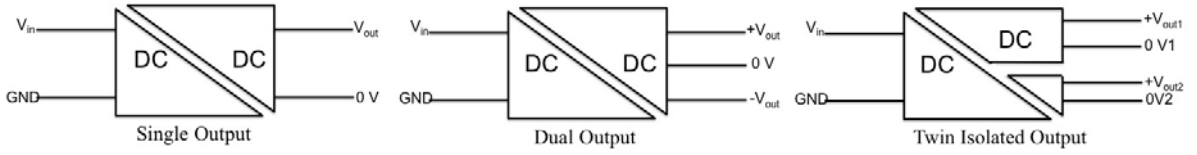

Figure 5.6: Standard isolated configurations

5.2 Flyback converter

The flyback converter is the most interesting converter for low power applications [Picard, 2010]. The output power of the flyback circuit may vary from less than 1 milliwatt to 100 watts. The input voltage can vary over wide range of input voltage. The main advantage is that the output voltage is isolated from the input main supply by coupled inductors. This converter therefore can offer single or multiple output voltages. Its best features are low system cost, simplicity, and relative ease of implementation. The flyback converter is based on the buck-boost converter where the input and the output are isolated by a two-winding magnetic device. Figure 5.7 presents the development of the buck-boost converter to create a flyback converter.

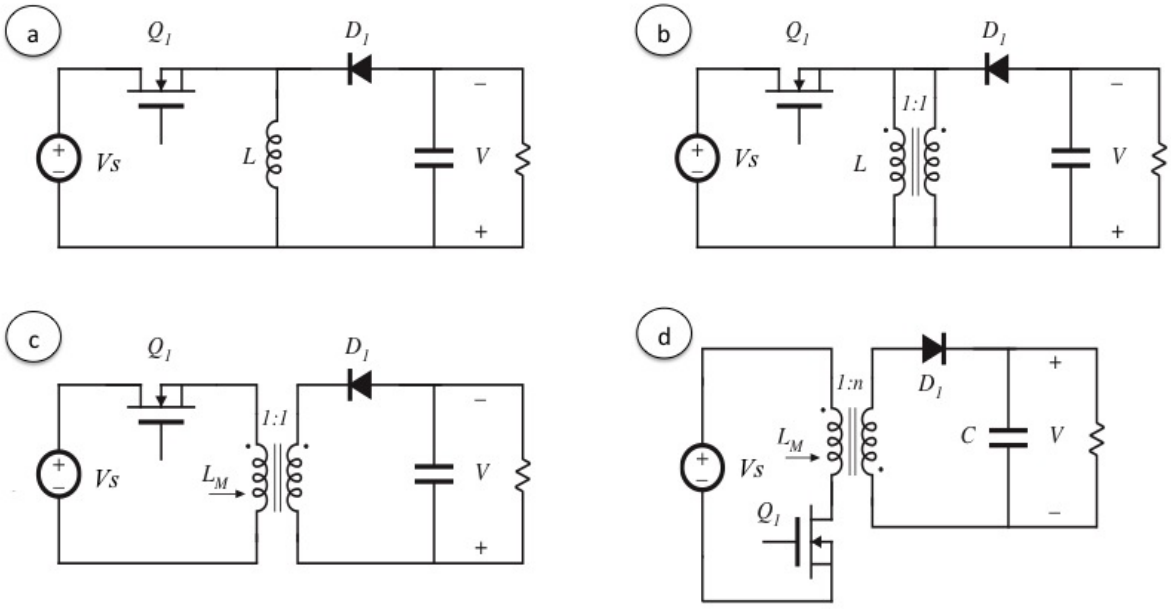

Figure 5.7: Derivation of the flyback converter: (a) buck-boost converter, (b) inductor L is divided into two parallel inductors, (c) inductors are isolated, leading to the flyback converter with a 1:1 turns ratio and negative output voltage, (d) with a 1:n turns ratio and positive output voltage [Taylor, 2004].

The flyback converter requires a single controllable fast switch like a MOSFET. Primary and secondary inductors of the transformer should have a good coupling so that they are linked by nearly the same magnetic flux. The two-winding inductors could be represented as a transformer, so-called “flyback transformer”, although it works differently from a traditional transformer. In a traditional transformer current flow simultaneously in primary and secondary windings which is not the case in the flyback transformer. Secondary voltage is rectified and filtered using just a diode and a capacitor.

5.2.1 Principle of Operation

Figure 5.8 presents the topology of the flyback converter and the equivalent circuit during the operation phases.

Phase1: The switch is on and the input voltage is applied to the primary inductor. The primary current rises linearly until it arrives to the maximal value at the end of T_{on} as given by (5.5). The diode at this time is reverse-biased (off) due to the induced voltage in the secondary. The voltage drop at the terminals of the diode is equal to $-(nV_{in}+V_{out})$. Consequently, there is no current in the secondary windings.

$$i_p(t) = \frac{V_{in}}{L_p}t \tag{5.5}$$

Phase2: When the switch is turned off, the primary current falls down and the voltage polarities across the windings reverse what makes the diode in the secondary circuit forward-biased. The secondary winding starts charging the output capacitor and supplying the load by transferring magnetic field energy into electricity at the output (V_d+V_{out}). The secondary current decreases linearly from the maximum value I_{s-max} (see (5.6)). The off-period of the switch determines the operation mode of converter. In discontinuous conduction mode DCM, the off period is sufficiently large for the secondary current to decays to zero. From the other hand if the next cycle starts before the secondary current goes to zero, the converter is then under continuous conduction mode of operation CCM.

$$i_s(t) = -\frac{V_{out}}{L_s}t + I_{s-max} \tag{5.6}$$

Phase3: This mode occurs only in DCM after complete transfer of the energy of magnetic field to the output. The diode stops conducting and the output capacitor continues to supply voltage to the load. Fig. 5.9 shows flyback circuit waveforms under CCM and DCM.

- Continuous conduction mode: the energy stored in the transformer is not completely transferred to the secondary; that is, the Flyback current does not reach zero before the next switching cycle.

The output voltage of the flyback in CCM is function of the duty cycle and the turn-ratio and is given by (5.7).

$$V_{out} = n\frac{d}{1-d}V_{in} \tag{5.7}$$

The input impedance of the flyback for a load R_L is given by (5.8).

$$R_{in} = n^2\left(\frac{d}{1-d}\right)^2 R_L \tag{5.8}$$

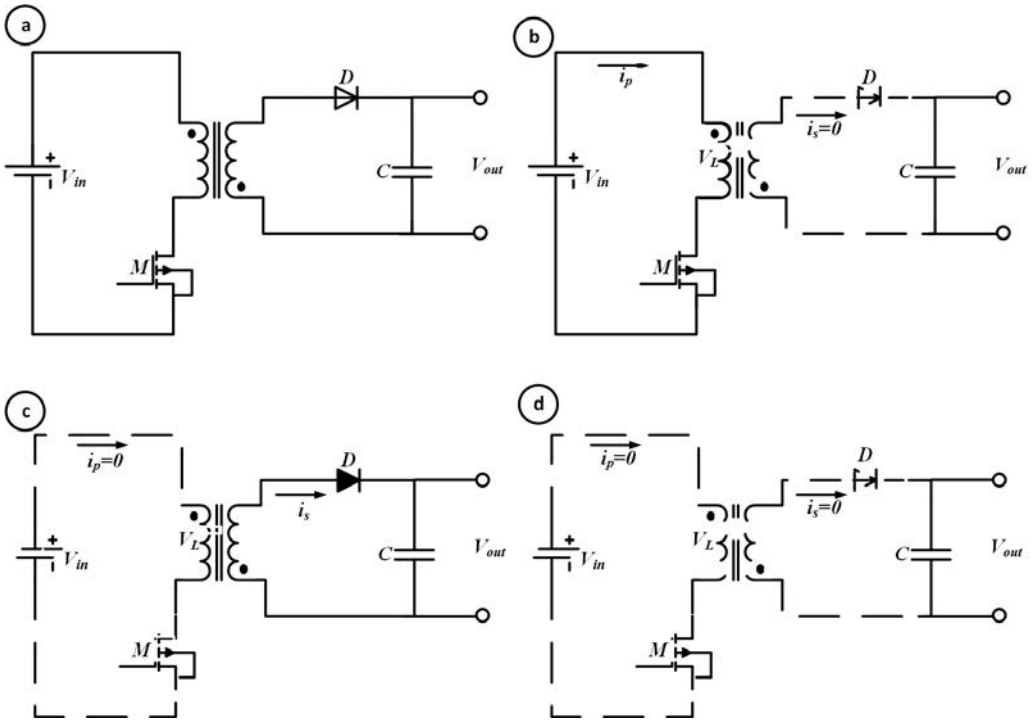

Figure 5.8: Flyback converter (a), equivalent circuit in phase 1 (b), equivalent circuit in phase 2 (c), equivalent circuit in phase 3 (d)

- Discontinuous conduction mode: all the energy stored in the core is delivered to the secondary during the turn-off phase (Flyback period), and the secondary current falls back to zero before the switch turns-on again.

The output voltage of the flyback for a load R_L is given by (5.9).

$$V_{out} = \frac{1}{2}\sqrt{\frac{R_L}{R_s}}V_{in} \tag{5.9}$$

Where R_s is the internal resistance of the source.

The input impedance of the flyback can be calculated tacking into account the ratio between the input voltage and the average value of the primary current which could be calculated by (5.10). The input impedance (R_{in}) is given by (5.11).

$$i_{p-AVG} = \frac{1}{T_s}\int_0^{dT_s}\frac{V_{in}}{L_p}tdt = \frac{V_{in}d^2}{2L_pf} \tag{5.10}$$

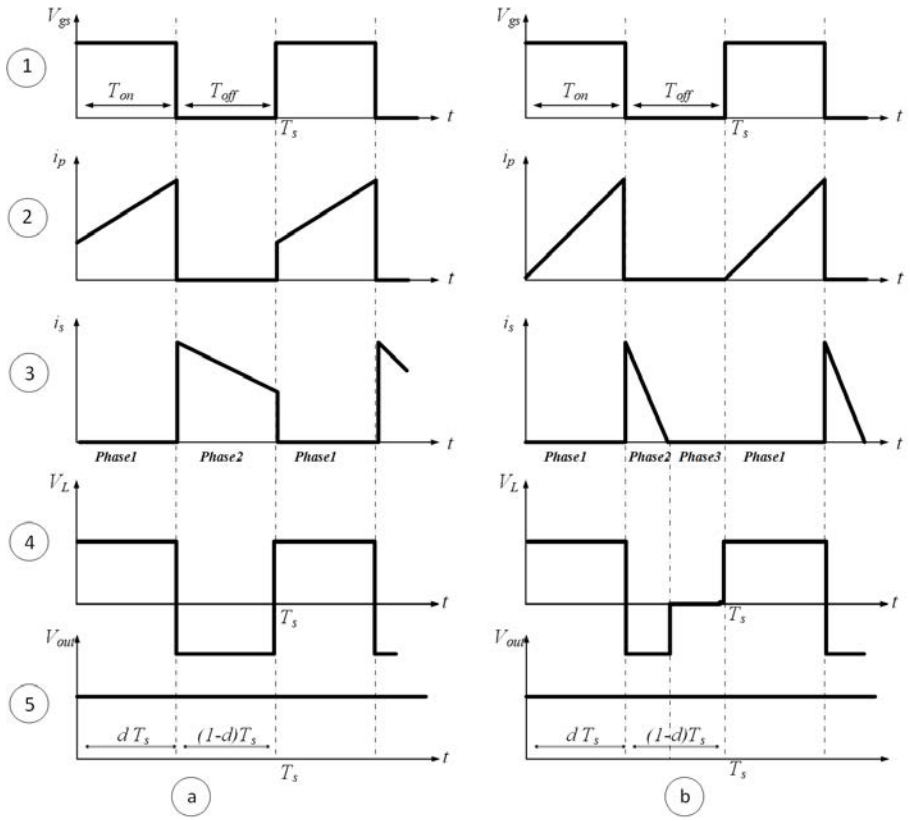

Figure 5.9: Flyback circuit waveforms under continuous conduction mode (a) and discontinuous conduction mode (b), (1) shows the control voltage of MOSFET switch, (2) shows the primary current, (3) shows the secondary current, (4) shows the inductor voltage on the primary side of the transformer and (5) shows the converter output voltage.

where f is the switching frequency, L_p is the primary inductance, d is the duty cycle and V_{in} is the input voltage of the converter.

$$R_{in} = \frac{V_{in}}{i_{p-AVG}} = \frac{2L_p f}{d^2} \tag{5.11}$$

For low output current and power levels, the flyback is in DCM usually the preferred operating mode, due to its simpler control loop implementation, fast transient response and lower turn-on losses [Picard, 2010]. The DCM characteristics of the flyback converter are very attractive for impedance matching. The output voltage of flyback in DCM is independent of the turn-ratio n. The input resistance is linear with the inductance of the inductor L_p and controllable by the frequency f and the duty cycle d. The input resistance is also independent of the load resistance R_L and the turns ratio n. That gives, by control of the duty ratio or the frequency, an excellent tool for impedance matching and to control the maximum power

transfer. In fact a buck-boost converter in DCM operation provides almost the same characteristics. The advantage of flyback in comparison with a buck-boost converter is still the galvanic isolation between the input and output. Additionally very few components are needed to build a flyback converter (only one switching device, one diode and one transformer are required).

5.3 Conclusion

This short chapter discusses the structures of acceptable DC/DC converter to be connected to the MFC. The flyback architecture in DCM operation is preferred and detailed in the next chapter.

Chapter 6

Autonomous flyback converter for MFCs

Contents

In this section, the design and fabrication of the flyback circuit under DCM operation for harvesting energy from MFCs will be presented. This will include the circuit design, component selection and tests of the operation.

6.1 Specifications

The converter design was based on the electrical characteristics of MFCs. The circuit should start and operate at low voltages about 0.3 V. The step-up ratio should be high to reach sufficient output voltages to supply applications. Because MFCs are strongly non-uniform generators and to give the possibility to operate with a stack of serially-connected generators, the converter should operate over a wide range of input power with a minimum power level of 300 µW. Efficiency has to be maximized. As shown previously, the maximum power point for MFCs occurs at voltages almost equal to 50% of the open circuit voltage (see I). The designed converter should deal efficiently with the non-uniformities between MFCs and should be able to track the MPP for these different MFCs.

6.2 Design

The flyback converter is divided into sub-circuits. This provides a straightforward way to design and analyze the circuit. The sub-circuits of the flyback converter are the main circuit of the converter, start-up circuit, switching circuit, and the feedback as shown in Fig. 6.1. The main circuit is the same as the one studied in Fig. 5.8. MFCs require an auxiliary circuit for powering the controller in the switching circuit. A feedback circuit is provided for MPPT.

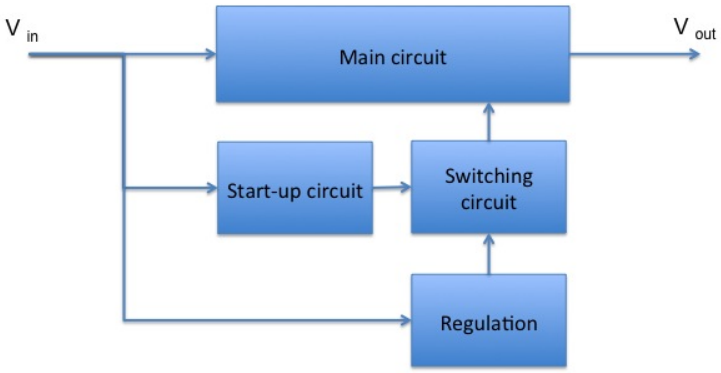

Figure 6.1: Diagram of the main sub-circuits in the flyback converter.

6.2.1 Start-up circuit

The input voltage of the start-up circuit is the principal input voltage while an output voltage of 1.5 V minimum is required for the switch. A step-up circuit is required for charging a start-up capacitor. A commercially charge pump IC, S-882Z, is selected. The start-up voltage of the charge pump is about 300 mV which is compatible with the source specifications. When the input voltage is equal or higher than the start-up voltage, the charge pump starts operation and the start-up capacitor C_p is gradually charged (phase-1). Although the voltage of this capacitor increases gradually, the output voltage of the charge pump is still null. As soon as the voltage of the capacitor C_p reaches the minimum level of 2.4 V, it starts transferring the energy to charge the capacitor C_c (phase-2). The discharge stops when the voltage across the capacitor C_p declines to the level of the discharge stop voltage (1.8 V) (phase-3, 4). Fig. 6.2 explains the operation diagram of the charge pump S-882Z. Values of the capacitors are to be selected carefully because they have to store the required energy for switching but high capacitors C_p and C_c cause a long start-up time.

6.2.2 Switching circuit and regulation

The switching circuit is composed of an oscillator and the gate of a switch. The role of the oscillator is to drive the switch by producing a square control waves with a controllable frequency and duty cycle.

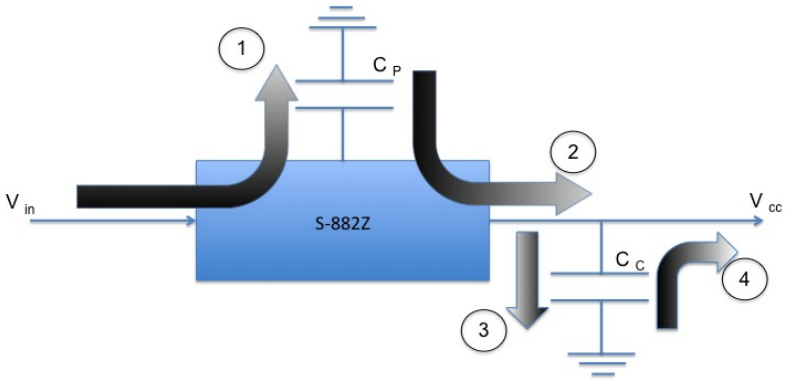

Figure 6.2: Operation diagram of the charge pump S-882Z

The choice of this controller has to be based on minimization of the power consumption. The power consumption of the oscillator is usually a function of the supply voltage Vcc and the frequency f. For example, at 25 kHz the supply currents are 1 and 7 μA at supply voltages of 1 and 3 V which results in 1 and 21 μW, respectively for the TS3001. At 5 kHz, the power decreases to 0.7 and 14 μW at supply voltages of 1 and 3 V, respectively. However the supply voltage and the frequency are not independent values. The output voltage of the oscillator drives the gate of the switch and the frequency controls the internal impedance of the converter. The power consumption of the oscillator also depends on the power consumption by the gate of the switch required to charge and discharge the capacitor (C_{oss}) between the drain and the source. This power can be evaluated by (6.1).

$$P_{sw-Coss} = \frac{1}{2} C_{oss} V_{drain}^2 f \tag{6.1}$$

The power consumption of the oscillator TS3001 from Touchstone Semiconductor, the low level of supply voltage and the easiness to control the frequency make it a very good candidate among the commercially-available oscillator. Usually the oscillator requires a supply voltage higher than 1 V, such as LTC6906 which requires a 2.7V to 3.6V, which is not available in our source. In our design, the oscillator is supplied from the output of the charge pump. The TS3001 can run with a voltage as low as 1 V which is suitable for the charge pump with very low power consumption (1 V/1 μW at 25 kHz). Figure 6.3 presents the oscillator current. One solution was studied to improve the performance of the converter by using the charge pump only at the start-up. After the start-up, there is an output voltage that can be used to power the controller. The main advantage of this solution is to eliminate the charge pump after the start-up. The drawback is that the output voltage is not controlled. In an open circuit, for example, the output voltage is too high and it exceeds the nominal voltage of the controller. A solution was proposed in [Wu et al., 2012] using diodes to adapt the output voltage to the nominal voltage of the controller. The power losses in the diode resistances and the required switching circuit are very important. If the output

voltage is lower than the nominal voltage of the controller, the output voltage will not be able to supply the controller. An additional circuit is required to regulate the oscillator supply voltage. The oscillator is therefore supplied from the output of the charge pump all the time of operation. The output frequency can be controlled from 10 kHz to 110 kHz by modified the resistance connected with the pin *Rset* from 1 MΩ to10 MΩ as shown on Fig. 6.4. The frequency will be controlled by the input voltage, Vin. *Rset* box is a digital potentiometer architecture consisted of resistor array controlled by MOSFETs ALD110902. Function of the input voltage, the resistance *Rset* will be controlled to produce the desired frequency. One modification on the input voltage will change *Rset* resistance by switching on or switching off one or more MOSFETs. That will create a new frequency to modify the converter input resistance to extract the maximum power of the source (impedance matching).

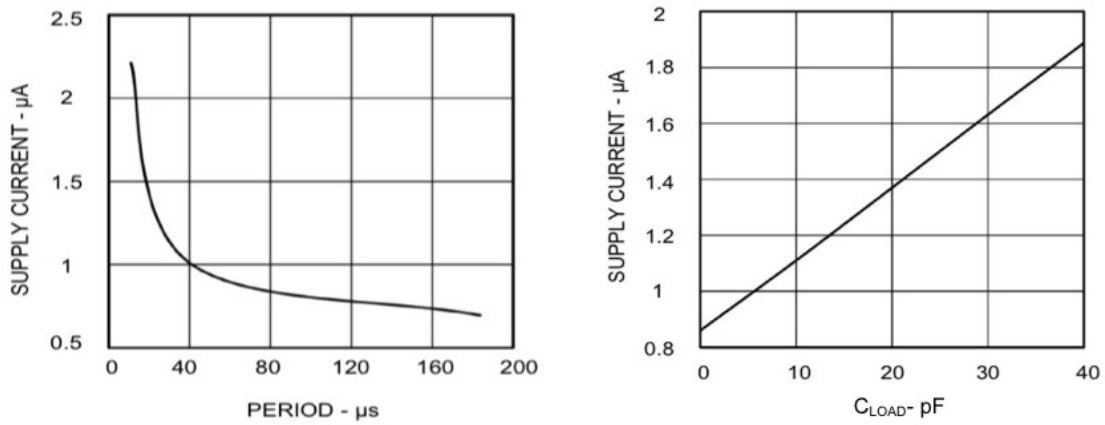

Figure 6.3: Supply current of controller TS3001 vs the period (left) and vs the load capacitor (right) (data from datasheet [Silicon.labs, 2014])

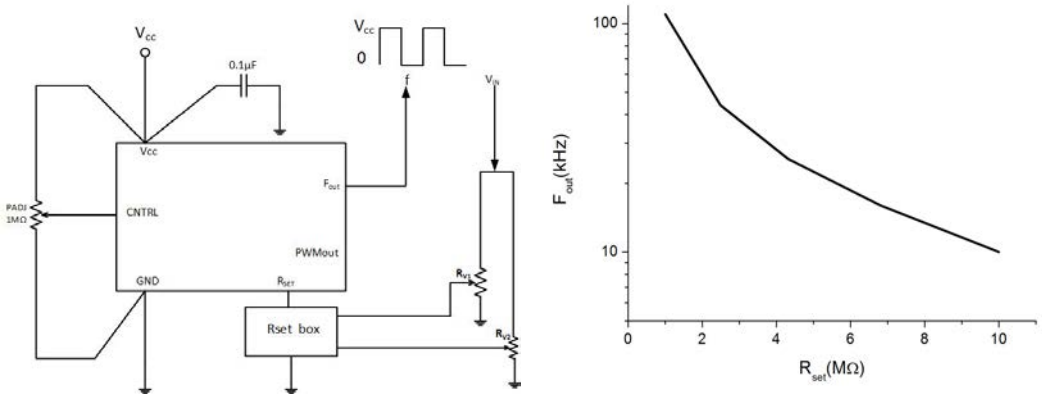

Figure 6.4: Circuit of TS3001 oscillator (left) and characteristic of output frequency (right) (data from datasheet [Silicon.labs, 2014])

6.2.3 The main circuit

The main circuit is a modified Flyback converter with two coupled inductors. A discontinuous conduction mode (DCM) with a variable frequency is chosen for the control of maximum power point (MPPT) adapting the internal resistance of the converter (impedance matching). The flyback converter is detailed in Fig. 6.5.

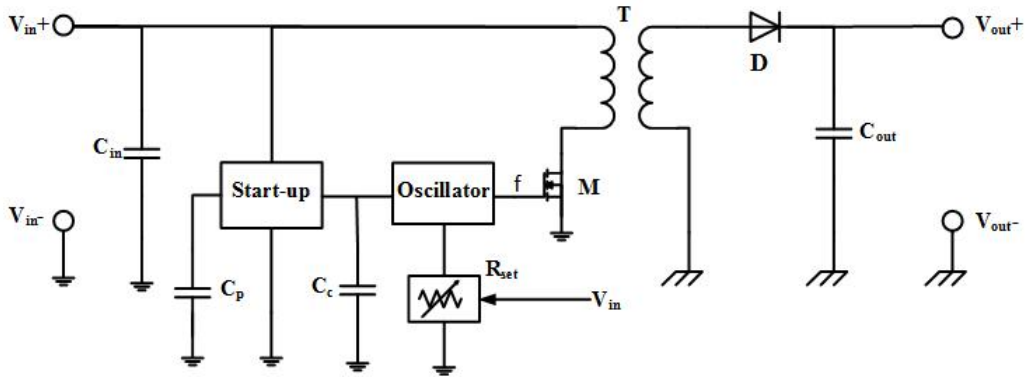

Figure 6.5: Schematic of the flyback converter.

6.2.3.1 Selection of main switch

The gate of the switch is driven by the controller output voltage, V_{CC}. The threshold voltage of the switch has to be between 1 and 2 V. Moreover there are 2 types of losses in the switch: conduction losses and switching losses. Conduction losses are caused by the internal drain-source resistance of the switch $R_{DS}(on)$ when it's crossed by the on-state current. Drain-source capacitance or the output capacitance (C_{oss}) creates switching losses in all MOSFETs. The energy stored in C_{oss} , in each cycle, is dissipated in the MOSFET. These losses are proportional to the values of the parasitic capacitances and the switching frequency (see (6.1)). To minimize the total losses in the switch, the frequency f, the resistance $R_{DS}(on)$, drain-source capacitance (C_{oss}) should all be minimized. Another type of losses occurs during the turn-off, so-called crossover losses. It's well known that a faster transition, i.e. a short turn-off fall-time, results in lower crossover losses [Pi Changming and Wenhong, 2010]. Taking in account all these considerations, the MOSFET FDV301N appears as a good candidate for the flyback converter. It has a low Gate Threshold Voltage ($V_{GS}(th) \approx 1V$) and is suitable to be controlled by the selected oscillator TS3001. It has an acceptable $R_{DS}(on)$, very low turn-off fall-time and very low drain-source capacitance (C_{oss}). Table 6.1 presents the main specifications of MOSFET FDV301N.

Table 6.1: Specifications of MOSFET FDV301N

	Description	Value	Unit
$R_{DS}(on)$	Static drain-source on-resistance at V_{GS}=2 V	6.5	Ω
$V_{GS}(th)$	Gate threshold voltage	1.06	V
Q_g	Total gate charge at V_{GS}=2 V	200	pC
C_g	Grille capacitance	200	pF
C_{oss}	Output capacitance	10	pF
t_{off}	Turn-off fall-time	3.5	ns

The internal resistance of the flyback converter in DCM is independent of the input or output voltage and depends only to the primary inductance, the switching frequency and the duty cycle. From (5.11), the internal resistance of the flyback could be given by (6.2).

$$R_{in} = \frac{2L_m f}{d^2} \tag{6.2}$$

To ensure the operation in DCM of the flyback converter over a wide range of input voltage and to simplify the control, the duty cycle was fixed to be d=0.5 [T. Paing and Popovic, 2008]. That also reduces the consumption of the control circuit because enabling the PWM engine increases the TS3001 operating supply current from 5 to 10 times. For a designed converter, the primary inductance is constant. Therefore the converter internal resistance could vary only in function of frequency. Experimental tests show that the internal resistance of the lab-scale varies between R_{min}=100 and R_{max}=300 Ω. Taking into account (6.2), the relation between the frequency and the primary inductor can be illustrated in Fig. 6.6.

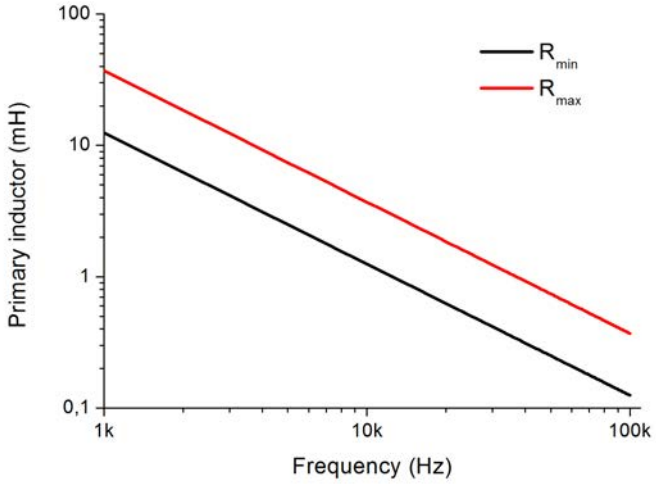

Figure 6.6: Primary inductor of the flyback transformer vs the frequency

To determine the optimal switching frequency, the circuit was simulated using a simple model consisted of a voltage source and a serial resistance for R_{min} and R_{max}. Taking in account all the losses produced by the main circuit and the control circuit, the maximum global efficiency was plotted against the switching frequency f as shown in Fig. 6.7. The simulated maximum efficiency for low frequency is low because the switching speed is not enough to extract all the available energy. For high frequency, the losses in the circuit are more important. The efficiency therefore is low. The optimal efficiency occurs near a frequency of 10 kHz for the case of minimum resistance and of 28 kHz for the case of maximum resistance. Moreover there is an inverse relationship between the size of the transformer and its frequency of operation. Taking for example a frequency of 1 kHz, the primary inductance is about 10 times larger than in the case of 10 kHz (Fig. 6.6). The size of the transformer is approximately 3 times bigger than in the case of 10 kHz. On the other hand, the high frequency permits the use of a much smaller transformer. However, losses increase at high frequency due to hysteresis and due to the eddy currents circulating in the magnetic core of transformer.

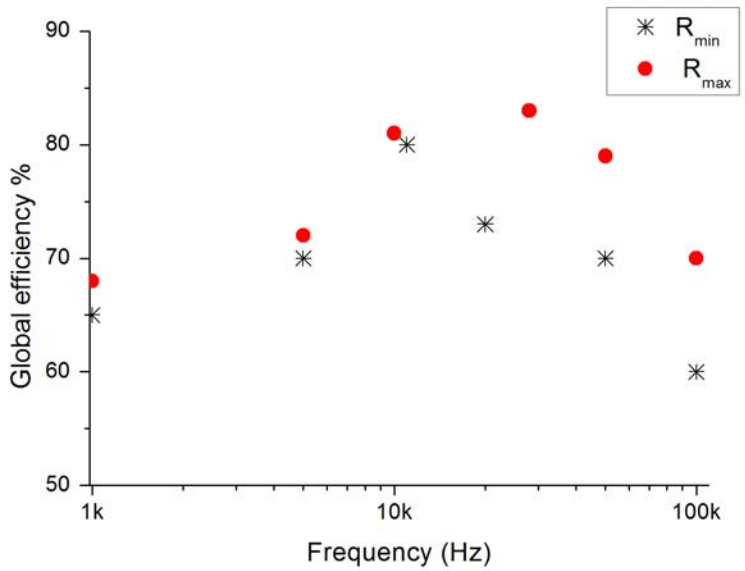

Figure 6.7: Simulated efficiency of the converter as a function of the switching frequency

6.2.3.2 Design of two coupled inductances

In a flyback converter designed to operate in discontinuous conduction mode, the required inductance value is reasonable and the inductor size may be smaller than in a flyback converter designed to operate in a continuous mode. That is because the output voltage in DCM flyback converter is independent of the turn-ratio n. In order to minimize the size of the transformer and the secondary resistance, the turn-ratio can be taken to $n = 1$. As previously discussed, the optimal efficiency occurs around a frequency of

10 kHz to 28 kHz for the case of R_{min} and R_{max} respectively. From Fig. 6.6, the corresponding value of the primary inductance is $l_m = 1.25mH$ for R_{min} and R_{max}. Several methods are in common use for calculating the number of turns, N, depending on the circuit magnetic. Whether the gap is discrete or distributed, the effective permeability can be used for calculating the number of turns using (6.3) and Table 6.2. The entirely core can be presented as an equivalent to a solid homogeneous core made of an "imaginary" material with permeability μ_r. This method is useful for distributed gap cores, where the gap cannot be physically measured [Instruments, 2001].

$$N^2 = \frac{L_m l_e}{\mu_r \, \mu_0 \, A_e 10^{-2}} \tag{6.3}$$

Table 6.2: Parameters of eq. 6.3

Symbol	Description
N	Number of turns
L_m(H)	Primary inductance
l_e (cm)	Effective path length
μ_r	Relative permeability
μ_0	Permeability
A_e (cm^2)	Effective cross-sectional area

For the pre-gapped ferrite cores or distributed-gap powdered metal cores, there is a convenient method for calculating inductance or the number of turns by using the inductance factor A_L defined by (6.4). It is a manufacturing constant expressed in $nH/turn^2$ or as abbreviation in some data-sheets in nH.

$$A_L = L/N^2 \tag{6.4}$$

To minimize the number of turns that will lead to minimize the size of transformer and then the losses, the selected cores should have an important inductance factor. The selected core is a ferrite ring toroid core, from Fair-Rite Products Corp, that has the characteristics in Fig. 6.8.

Symbol	Description	Value	Unit
$\sum l/A$	Core constant	10.4	cm^{-1}
l_e	Effective path length	3.12	cm
μ_r	Relative permeability at 10kHz	2000	
A_e	Effective cross-sectional area	0.299	cm^2
V_e	Effective core volume	0.93	cm^3
A_L	Inductance factor	2775	nH
B_{sat}	Saturation induction	500	mT
F_b	Frequency band	100-150	kHz
A	Internal diameter	12.7	mm
B	External diameter	7.9	mm
C	Thickness	12.7	mm

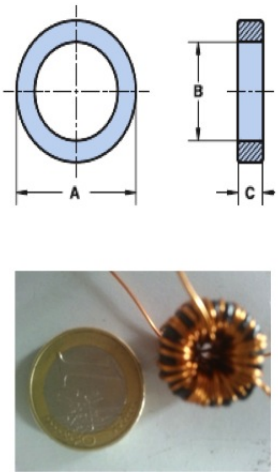

Figure 6.8: Characteristics of selected core

From (6.4) and the inductance factor of the core, the number of turns of the primary inductor, N_{pri}, can be calculated and is equal to 21 turns. Considering $n = 1$, the number of turns of secondary inductor, N_{sec}, is equal to 21 turns. The primary and secondary turns are carried out in 0.56 mm copper wire to minimize the ohmic resistance of the transformer. Table 6.3 gives the specifications of the designed flyback transformer.

Table 6.3: Specifications of designed transformer

	Symbol	Description	Value
primary inductor	N_{pri}	Primary turns	21
	L_{pri}	Primary Inductance	1.25 mH
	R_{pri}	Primary Resistance	1.2 Ω
Secondary inductor	N_{sec}	Secondary turns	21
	L_{sec}	Secondary Inductance	1.25 mH
	R_{sec}	Secondary Resistance	1.2 Ω

6.2.3.3 The diode

The diode allows the current at defined voltage to flow from the secondary inductor to be stored in the capacitor. It also prevents the current flow in the reverse direction. In DCM, there is no diode reverse recovery losses in the rectifier. The low level of voltage requires a diode with a low threshold voltage (V_d), low $R_{DS(}ON)$ and low diode capacitance to limit the conduction and commutation losses. Diode losses by conduction can be given by (6.5).

$$P_{cnd-d} = V_d i_{d-avg} \tag{6.5}$$

where i_{d-avg} is the average value of the secondary current.
Diode capacitance (C_j) causes also commutation losses and can be evaluated by (6.6).

$$P_{sw-d} = \frac{1}{2} C_j (nV_{in} + V_{out}) f \tag{6.6}$$

Many diodes were tested for this circuit. Two of them, BAT54 and HSMS-282, had almost the same performance. A schottky diode BAT54 was selected because it presented the lowest losses. Table 6.4 depicts main diodes parameters.

Table 6.4: Specifications of BAT54 and HSMS-282 diodes

	Symbol	Description	Value
BAT54	V_d	Forward voltage	240 mV
	$R_{DS}(on)$	On-resistance	2 Ω
	C_j	Junction Capacitance	10 pF
HSMS-282	V_d	Forward voltage	200 mV
	$R_{DS}(on)$	On-resistance	10 Ω
	C_j	Junction Capacitance	0.7 pF

6.3 Result and discussion

The flyback converter was fabricated as the schematic in Fig. 6.5. Table 6.5 resumes the components used in the converter.

Table 6.5: Components of Flyback converter

Symbol	Description	Parameters
C_{out}	Input capacitor	100 µF
C_{in}	Output capacitor	100 µF
D	Diode	BAT54
M	MOSFET	FDV301N
C_p	Start-up capacitor	10 µF
C_c	Start-up capacitor	20 µF
T	Flyback transformer	described in Tab. 6.3

6.3.1 Test of the flyback converter with an emulator of the microbial fuel cell

The firstly converter was tested with a simple emulator of microbial fuel cell in open circuit voltage and for a load of 50 kΩ. The maximum power delivered by this emulator is 793 µW. Fig 6.9 presents the control frequency (CH1), the output voltage (CH2), the voltage of Cc capacitor (CH3) and the voltage of Cp capacitor (CH4) in open circuit. Since the input voltage is higher than the start-up voltage of the

charge pump, it starts-up and the voltage of the capacitor Cp raises. When it becomes 2.4 V, the capacitor Cp starts to discharge into the capacitor Cc. When the voltage of Cc reaches to 1 V, the oscillator starts to drive the MOSFET and the output voltage starts to rise. The output voltage in open circuit is 19.5 V. The converter is tested also for a load of 50 kΩ as shown in Fig. 6.10. The output voltage was 5.3 V. The ratio of the maximum achieved power is 70.8 %. The input current was measured and is equal to 2550 µA. The efficiency calculated as the relation between the output power and the input power 73.3 %. The extracted power therefore is equal to 96.5% of maximum available power. The curve of the efficiency as a function of the load was plotted in Fig. 6.11.

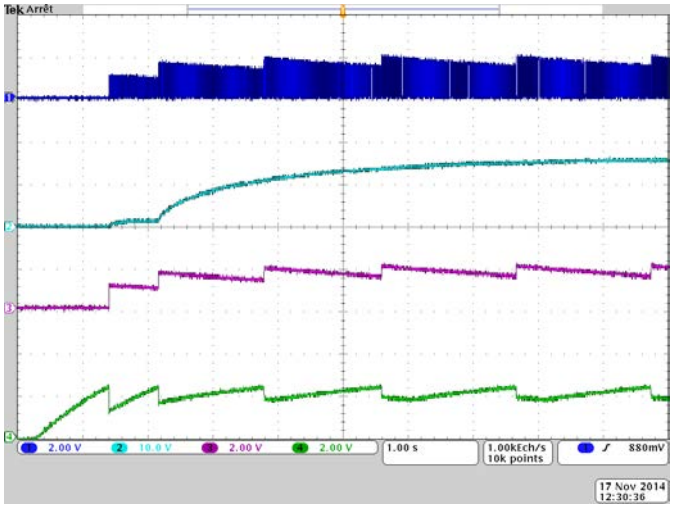

Figure 6.9: Control frequency (CH1), output voltage (CH2), voltage of Cc capacitor (CH3) and voltage of Cp capacitor (CH4) in open circuit

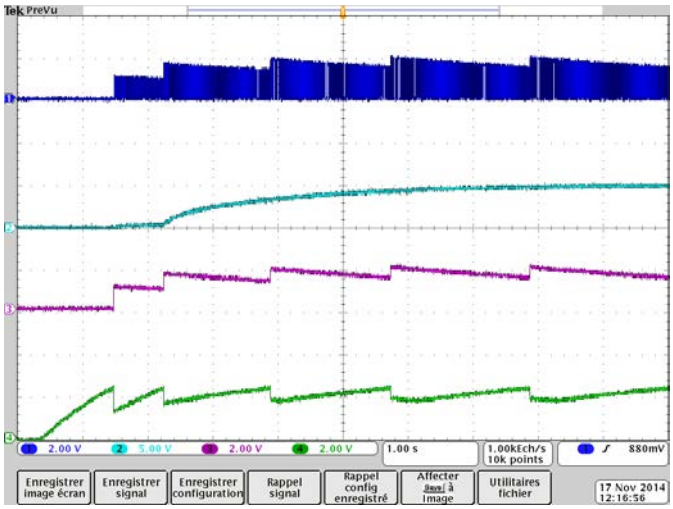

Figure 6.10: Control frequency (CH1), output voltage (CH2), voltage of Cc capacitor (CH3) and voltage of Cp capacitor (CH4) for a load of 50 kΩ

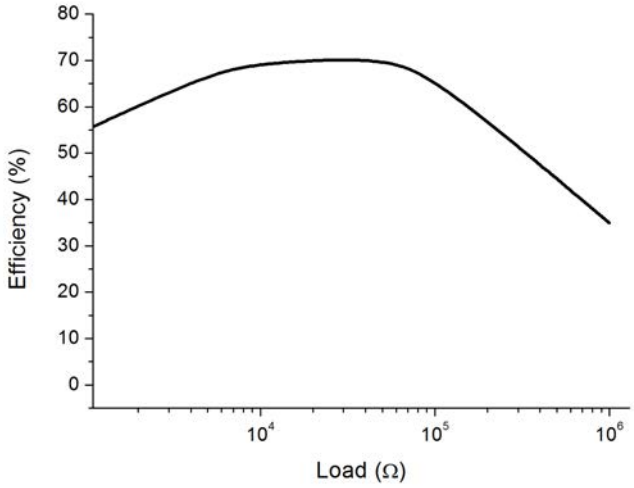

Figure 6.11: Measured efficiency of the flyback converter as a function of the load

The output voltage is tested as a function of the input voltage, for two loads 1 MΩ and 10 kΩ as shown in Fig. 6.12. The start-up voltage of the converter is about 320 mV. This voltage is limited by the start-up voltage of the charge pump. Using an external source to supply the controller, the start-up voltage decreases to 135 mV. The start-up required power is about 214 μW.

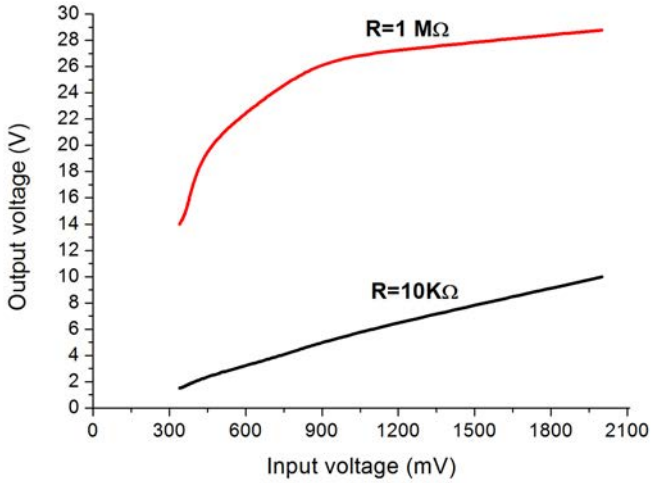

Figure 6.12: Measured output voltage as a function of the input voltage for two loads 1 MΩ and 10 kΩ

6.3.2 Input Impedance

To maximize the extracted power of the generator, the internal impedance of the flyback should be equal to the internal resistance of the generator. In our design, the start-up circuit (charge pump) is connected in parallel with the main circuit which may change the input impedance of the converter. To verify the effect of this connection, the impedance of converter was studied as a function of the frequency in two cases. The input impedance when the start-up circuit is connected with the main converter is shown in Fig. 6.5. Secondly, the start-up circuit was disconnected and powered by an external source. In the two cases, the input impedances were calculated dividing the average input voltage and the average input current. The input impedances in the two cases were plotted in Fig.6.13. The impedance variations are almost similar for the two cases since the charge pump presents a resistance of almost 20 times higher than the input resistance of the main circuit, so it can be neglected.

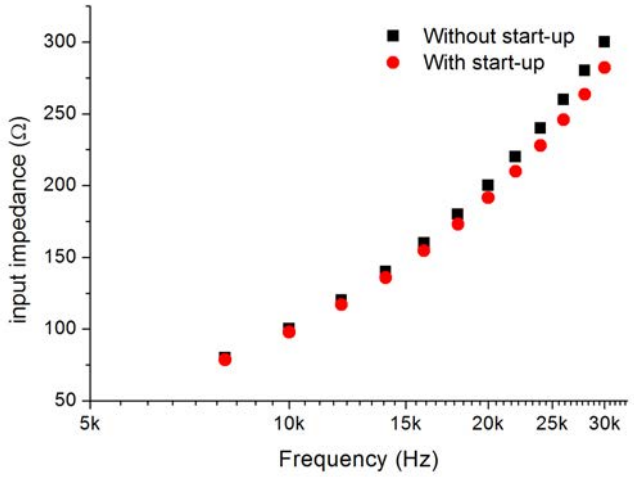

Figure 6.13: Input impedance of converter vs the switching frequency with and without the start-up circuit

To study the performance of the MPPT, the converter was tested with many models of microbial fuel cells with a different range of open circuit voltage and internal resistance. The switching frequency was monitored for each model. The input voltage was equal to (50± 5)% of the open circuit. Fig. 6.14 presents the change in switching frequency as a function of the source voltage.

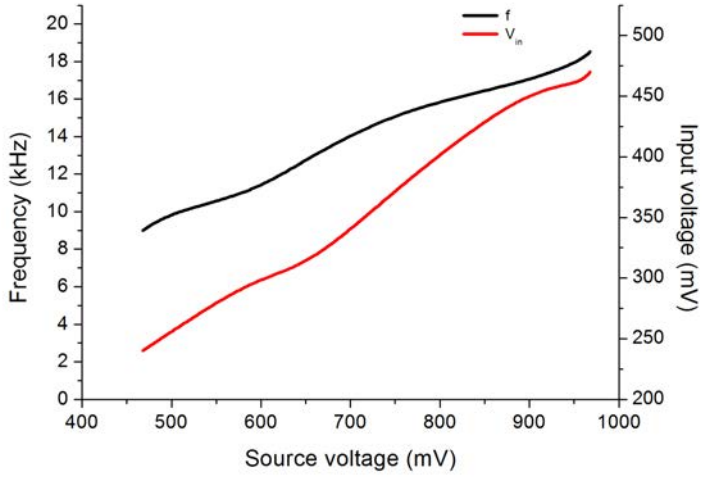

Figure 6.14: Change in switching frequency as a function of the source output voltage

6.3.3 Test of the flyback converter with a MFC

The converter was also tested with a MFC. The static characteristics of the MFC are presented in Fig. 6.15. The open circuit voltage is 580 mV. The maximum power of the MFC is 755 μW. The maximum power point occurs at 300 mV, i.e. 50% of the open circuit voltage of the MFC. The output voltage and the output power were plotted as a function of the output current in Fig. 6.16. The open circuit voltage is about 20 V and the voltage at MPP is 6.4 V for a load of 76 kΩ. The maximum output power is 538 μW. The maximum efficiency is 71.2 %.

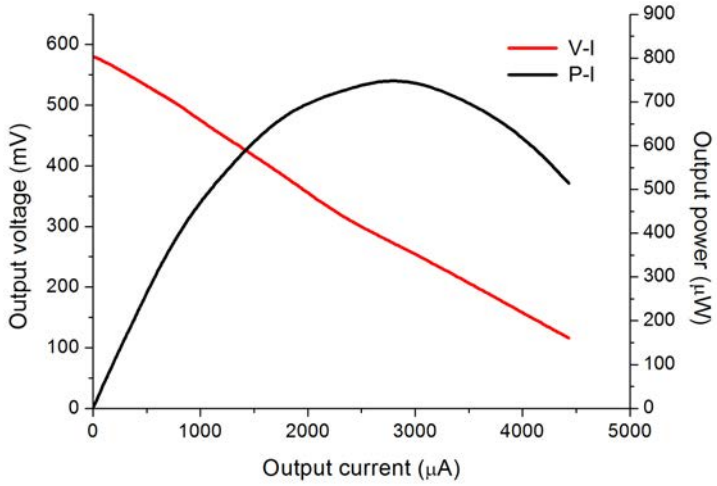

Figure 6.15: Measured characteristics static of the MFC

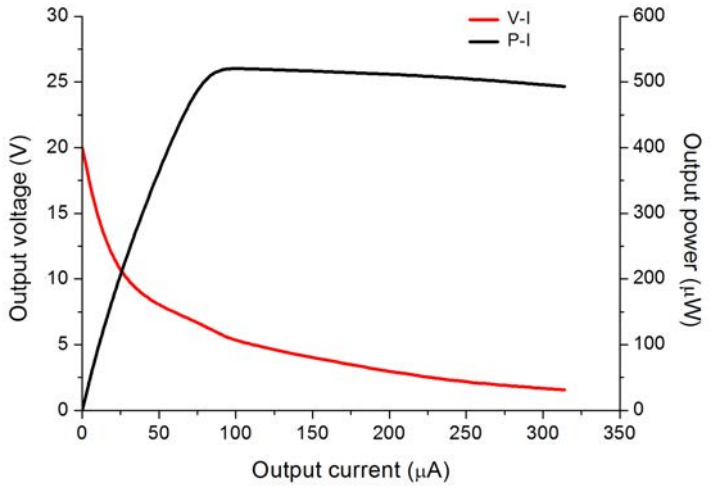

Figure 6.16: Experimental output voltage and output power of the flyback converter powered by the MFC

The flyback was also tested with two other MFCs and the efficiency was 72.8% and 72.3%.

6.3.4 Breakdown of losses

Losses in the flyback converter are evaluated by using the analytical equations given before. Table 6.6 shows the repartitions of these losses in all flyback components. There are three types of losses in the MOSFET. They are conduction losses presented by the ohmic resistance of the drain source of the MOSFET, switching losses dissipated by charging and discharging the capacitor C_{oss} and crossover losses which occur during the turn-off of MOSFET. The most important losses occur in the MOSFET switch by conduction although its low $R_{DS}(on)$. The diode at the output of the flyback presents also conduction and switching losses. The resistances of primary and secondary coils of the flyback transformer dissipate power. In the control circuit, the losses are the sum of the power consumption of the control circuit presented by the average current $i_{ctrl-avg}$ when the controller is unloaded and the losses in the gate of the MOSFET presented by the input capacitor (C_{gin}). The start-up circuit consumed a current $i_{start-avg}$, the power losses can be calculated as the product of the input voltage by the average start-up current when the charge pump is unloaded. Figure 6.17 represents the distribution of these losses in the flyback converter. The most important losses occur in the MOSFET switch by conduction (128 µW), although its low $R_{DS}(on)$. The total losses in the circuit are about 220 µW.

Table 6.6: Losses in the Flyback converter

Component	Losses	Description	Expression	Value µW
MOSFET	$P_{cnd-Mos}$	Conduction	$R_{DS}(on)\frac{V_s^2}{3dR_s^2}$	128
	$P_{sw-toff}$	Crossover losses	$\frac{1}{2}t_f(\frac{V_s}{2}+\frac{V_{out}}{m})\frac{V_s}{dR_s}f$	1.28
	$P_{sw-Coss}$	Sw. Out. Capacitor	$\frac{1}{2}C_{oss}(\frac{V_s}{2}+\frac{V_{out}}{m})^2 f$	2.23
DIODE	P_{cnd-d}	Conduction	$\frac{V_d V_s^2}{4V_{out}R_s}$	24.7
	P_{sw-Cj}	Junction Capacitor	$\frac{1}{2}C_j(m\frac{V_s}{2}+V_{out})^2 f$	0.15
INDUCTANCES	$P_{cnd-ind}$	Conduction	$(R_{pri}+R_{sec}\frac{V_s}{2mV_{out}})\frac{V_s^2}{3dR_s^2}$	23
CONTROL	P_{Driv}	Driver	$Q_g V_g f = C_{gin}V_g^2 f$	6
	P_{ctrl}	Controller	$V_g i_{ctrl-avg}$	2
	P_{reg}	Regulation		2.5
START-UP CIRCUIT	P_{start}	Start-up	$V_{in}i_{start-avg}$	30.1
TOTAL LOSSES	P_{tot}	—	$\sum losses$	219.96

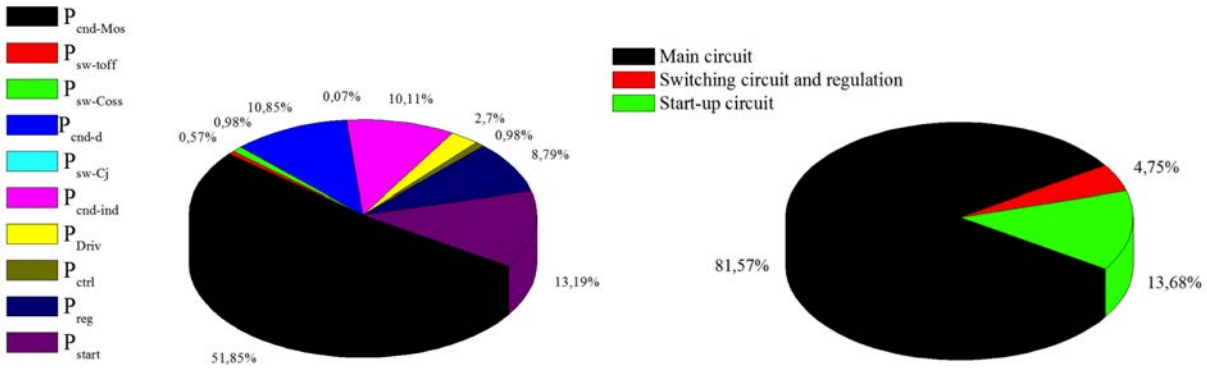

Figure 6.17: Distribution of losses in the flyback converter

6.4 Conclusion

In this chapter, an autonomous flyback converter for energy harvesting from microbial fuel cells was designed and fabricated. Discontinuous conduction mode operation of the flyback permits to control the MPP operation by impedance matching. The circuit was optimized to minimize the losses and maximize the efficiency. A 0.3 V charge pump was used to continuously supply the controller. The flyback converter was tested with a model of MFC to monitor the operation. The operation of MPPT occurs by changing the switching frequency as a function of the source voltage. The flyback can start-up at low voltage, around 300 mV. The flyback converter was then tested with a 580 mV open circuit voltage and 755 μW maximum power MFC. The output open circuit voltage was about 20 V and the voltage at MPP was 6.4 V for a load of 76 kΩ. The maximum efficiency was 71.2 %. The converter will be tested with a stack of MFCs in chapter 8.

Chapter 7

Energy harvesting from a stack of microbial fuel cells

Contents

7.1 Introduction

Like the other type of energy harvesters and batteries, the energy produced by MFCs can be collected to build a mini-generator able to power the desired application. In wastewater treatment plant, a large amount of organic matter is naturally existent. The volumetric energy produced by an elementary MFC is limited. It was found that connecting multiple small-size MFCs together is more efficient than increasing the size of an individual cell [Ieropoulos et al., 2008]. One way to harvest the maximum of the available energy in wastewater treatment plant WWTP is to build a stack of a large number of MFCs. The volume of the stack can be implemented at various scales according to the available source of organic matter. As

an example, in the case of a wastewater treatment plant, they can be thousands or even ten of thousands of individual MFCs. These MFCs could be serially and/or parallely connected to improve the voltage and/or the current. In the two cases, the output power for each MFC will be added to the stack. The consumption of the energy will be local to supply the local off-the-grid applications (monitoring system, pumps, lighting, control.....), according to the generator capacity. In this case, each load requires different supply specifications. The stack could be divided in many sub-stacks. Each sub-stack is sized corresponding to its consumer. A number of power management units equal to the number of consumer is required. The harvested energy is preferred to be previously stored in capacitors or supercapacitors before suppling the application. For the low power applications (screen, wireless communication module, sensor), an ultra-low power management unit is necessary to step-up the voltage.

The performance of the MFC-stack is impacted by many issues. These problems can be divided according to the type of electrical connection of MFCs in the stack. In a stack of serially-connected MFCs, the effect of non-uniformities of the stacked MFCs could negatively affect the global efficiency. A stack of 6 MFCs was tested in [Aelterman et al., 2006b]. At high current densities, the individual voltages MFCs diverging and some of them had negative voltages. This phenomenon was discussed as "voltage reversal". In this case, the MFCs subject to voltage reversals absorb the electrical energy produced by the other MFCs instead of produce it. When voltage reversal occurred in stacked MFCs, problems are incurred in terms of high-voltage production and the lifetime of an MFC [Gurung et al., 2012]. The voltage reversal phenomenon can be explained by either a lack of fuel supply, insufficient catalytic substrate conversion in the MFC, non-uniform design, difference in bacterial activities and community [Choi and Chae, 2011, Aelterman et al., 2006b]. Limitations in the anode chamber have been discussed to be a cause of voltage reversal [Gurung et al., 2012]. The internal resistance effect was also suggested and discussed in several literature reports [Greenman et al., 2011, An et al., 2015]. However, the internal resistance includes variables such as charge-transfer resistance and mass-transfer resistance what makes it difficult to explain. To overcome the voltage reversal phenomenon, it was proposed to control the substrate concentration. However, the control of organic concentration is not practical and not easy to achieve in an environmental plant [An et al., 2015]. In literature, many reports have presented a stack of MFCs without voltage reversal by using converters and maximum power point tracking (MPPT) algorithms. In [Kim and Kim, 2011], a capacitive converter was presented to step-up the voltage and prevents the voltage reversal. The MFCs were connected in parallel with supercapacitors in a first approach. The supercapacitors are serially connected with the load in the second phase to step-up the voltage. The system contains many supercapacitors and a control system and many switches what makes it complex and expensive. The issue of voltage reversal was also studied with solar cells, battery and supercapacitor. Many circuits were used to prevent the voltage reversal and protect the equipments [Vighetti et al., 2010, Kim et al., 2011b]. These methods are commonly used with solar cells. The efficiency of these circuits is limited and not adapted to low power generators like MFCs.

Non-uniformities were also compensated with electronic circuits that enable voltage equalizing [Vighetti et al., 2010, Daowd et al., 2011].

In the case where MFCs are hydraulically connected, another phenomena appeared leading to more losses and result in poor stack efficiency. This phenomenon was firstly discovered in hydrogen fuel cell stacks (planar array configuration). It was noted that the open circuit voltage and current behavior of such a series connected cells is lower than would be predicted from the hydraulically isolated cells. A parasitic current is generated between serially connected anodes and cathodes of two unit cells and decreases the efficiency of the stack [O'Hayre et al., 2003].

In a stack of parallely connected MFCs, all MFCs in the stack have the same voltage while the individual currents are added. The output voltage in this case is still smaller than the threshold voltage of CMOS technologies what impacts the design of the power management unit and decreases the efficiency.

Application of voltage balancing circuits on MFCs will be studied in this chapter while the problem of hydraulically connected MFCs will be treated in chapter 8.

7.2 Voltage balancing circuit

Many circuits in literature are proposed to equalize the voltage of unbalanced sources connected in series. They are firstly used with battery to prolong the battery life cycle and avoid damages to the cells. One inefficient cell in the stack limits the operation of the whole stack and therefore cell balancing methods are introduced. With cell balancing methods the cell voltage in a stack can be equalized and the global performance can be improved. There are basically two methods of charge balancing: passive and active cell balancing.

7.2.1 Passive cell balancing

The circuit senses voltage across cells and try to equalize the cells by extracting energy from the maximally charged ones and dissipating it in shunts or resistors [Asumadu et al., 2005] as shown in Fig. 7.1, or selectively removing imbalanced cells from the battery pack [Shibata et al., 2001] as shown in Fig. 7.2. Hence with passive balancing, a stack is equalized by discharging the cells until all cell voltages equal the lowest one. Passive balancing is very slow and the excess energy during balancing is dissipated as heat. They have therefore a poor global efficiency which is not suitable for low power sources like MFCs.

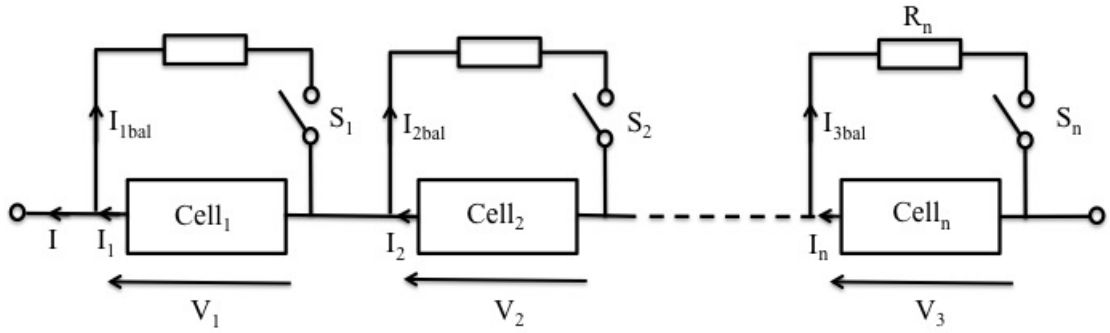

Figure 7.1: Serial stack with passive balancing circuit (shunting) [Asumadu et al., 2005]

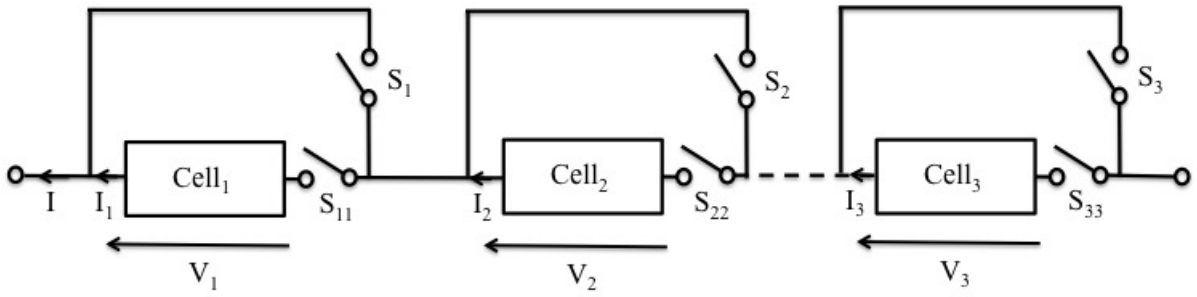

Figure 7.2: Serial stack with passive balancing circuit (complete disconnection) [Shibata et al., 2001]

7.2.2 Active cell balancing

Energy transfer between cells in the stack is called active cell balancing. In these methods, energy is transferred from a cell or a stack to a short-term energy storage and then to the other cells or the stack. The temporal energy storage can either be a capacitor or an inductor and the circuits are thus called capacitive balancing and inductive balancing circuits. Therefore, a weak cell can be supported by the energy from the other cells in the stack.

7.2.2.1 Capacitive balancing

Capacitive cell balancing utilizes capacitor(s) as external energy storage for shuttling the energy between the cells to achieve the balancing. The capacitor is connected to an energetic cell voltage and over a system of switches it is connected to a less energetic cell voltage and discharged to a weak voltage value. The capacitor shuttling can be categorized into two modes: the basic switched-capacitor and single switched-capacitor. In basic switched-capacitor, one capacitor is used for every two adjacent cells (charge shuttling as shown in Fig. 7.3). Energy can only be transferred between two adjacent battery cells. If the strongest cell is (electrically) far away from the weakest one, the energy has to be transferred through the whole stack to achieve the balancing [Cao et al., 2008, Pascual, 1998, West and Krein, 2000].

It requires n-1 capacitors and 2n switches to balance n cells. Its control strategy is simple because it has only two states. In addition, it does not need intelligent control.

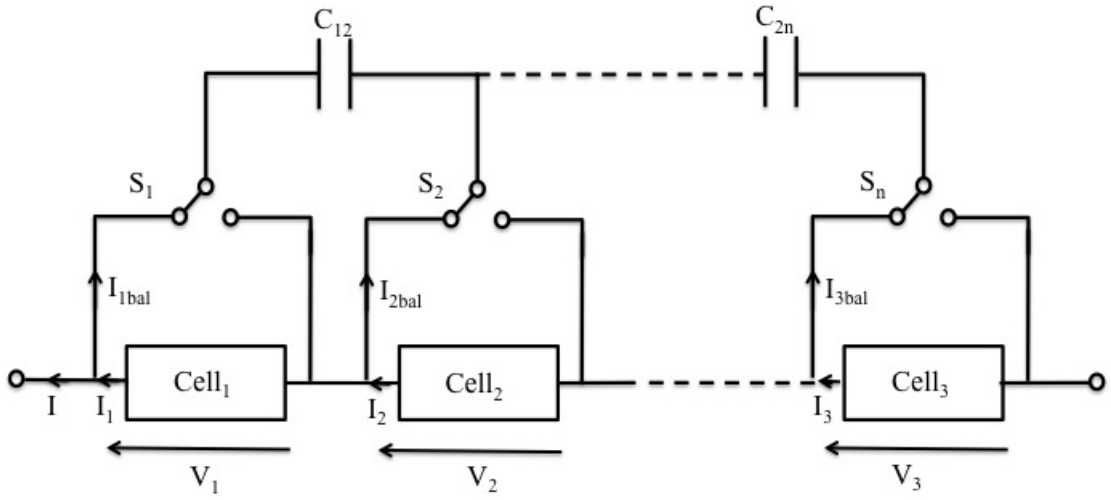

Figure 7.3: Switched-capacitor cell balancing topology.

One capacitor can be used for the whole stack (flying capacitor as shown in Fig. 7.4) [Speltino et al., 2010, Cao et al., 2008]. An intelligent control of this circuit, the energy can be transferred between the strongest and the weakest cells directly. It requires one capacitor and 2n switches to balance n cells. The disadvantage of the one switched-capacitor topology for batteries is the relatively long equalization time. More advanced control strategies are used to speed-up the balancing as the circuit presented in Fig. 7.5 [Baughman and Ferdowsi, 2008].

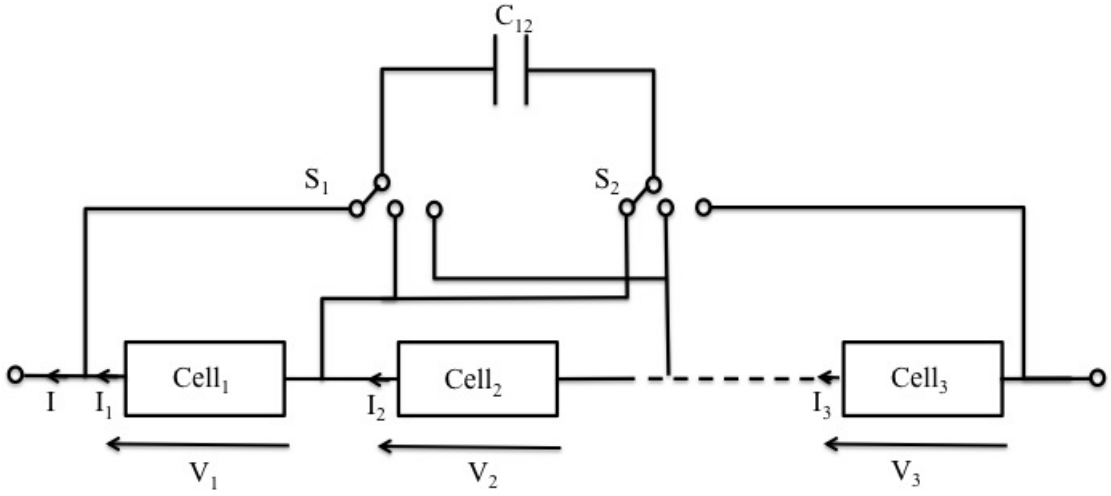

Figure 7.4: Single switched-capacitor balancing topology

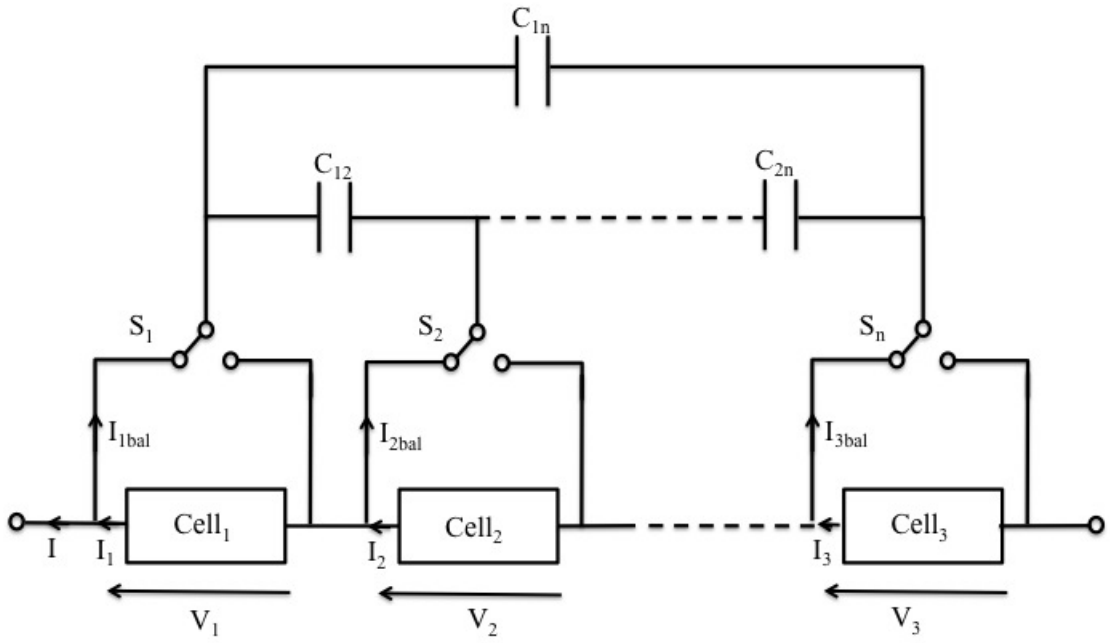

Figure 7.5: Switched-capacitor balancing topology

7.2.2.2 Inductive balancing

Inductive balancing circuits use inductor(s) or transformers to transfer energy from a cell or group of cells to another cells. One inductor could be used for transferring energy between the whole stack. The control system senses the voltage of the cells in the stack and selects the two cells which will be used for energy transferring to achieve the balancing [Park et al., 2007].

A multi-inductor system uses n-1 inductor(s) for balancing n cells (see Fig. 7.6) and the controller senses the voltage difference of the two neighboring cells, then applying a PWM to firstly switch on the higher cell. In a long string stack, this method takes a long time for transferring the energy from the first cell to the last one. Single-inductor has less equalization time than the multi-inductor topology [Moo et al., 2003].

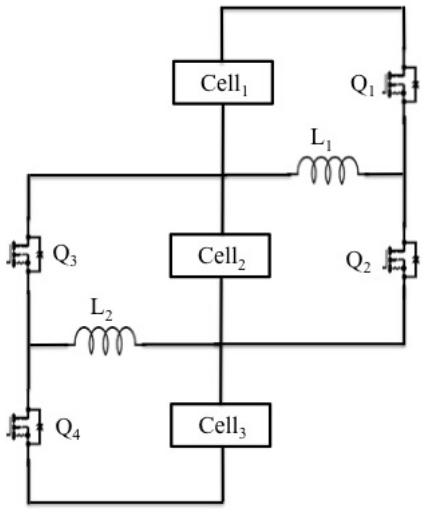

Figure 7.6: Multi-inductor balancing topology [Moo et al., 2003]

Single windings and multi-windings transformers are used also to achieve the balancing in two techniques. "Pack-to-cell topology" is based on transferring the energy from the whole stack through the switching transformer to the weak cell(s) using the corresponding switch(s). The second technique "cell-to-pack topology" is based on transferring the energy from the energetic cell(s) through the transformer into the stack [Cao et al., 2008, Cadar et al., 2010, Imtiaz and Khan, 2011, Einhorn et al., 2011].

All these circuits are quite complicated because they require an intelligent control circuit including processors, sensors as well as PWM oscillators. Another drawback is the number of required inductors which create additional losses. These circuits are expensive, not efficient and thus not adapted to low-power sources like MFCs.

7.2.2.3 Balancing methods based on DC/DC converters

Cûk, Buck or/and Boost, Flyback, Ramp, full-bridge and quasi-resonant converters are used for cell balancing. Cûk converter was tested in [Lee, 2005]. A stack of n cells required (n−1) individual cell equalizers of two inductors, two switches and one capacitor for each one. The drawback of the Cûk converter for balancing is a relatively long equalization time and complexity control. A step down (Buck), step-up (Boost) and Buck-Boost energy converters could be used to achieve the balancing [Moo, 2010]. An accurate cells voltage sensing as well as an intelligent controller are needed for the converters operation what makes them relatively expensive and complex [Daowd et al., 2011]. Flyback converters in isolated structure are easy to implement for large number of cells but they suffer from high magnetic losses [Chakraborty, 2004]. Energy transfer between cells with converters requires a bidirectional DC/DC converter for every two adjacent battery cells which means (n-1) converters for a stack of n cells as shown in Fig. 7.7 [Wen et al., 2009, Nishijima et al., 2000]. The balancing can be achieved by switching one bidirectional DC/DC converter to transfer charge either from one cell to the whole stack

or from the whole stack to a single cell [Shin et al., 2010, Bonfiglio and Roessler, 2009]. Unfortunately, all energy converter have a very complex control as well as a high cost and thus they doesn't suitable for energy harvesting.

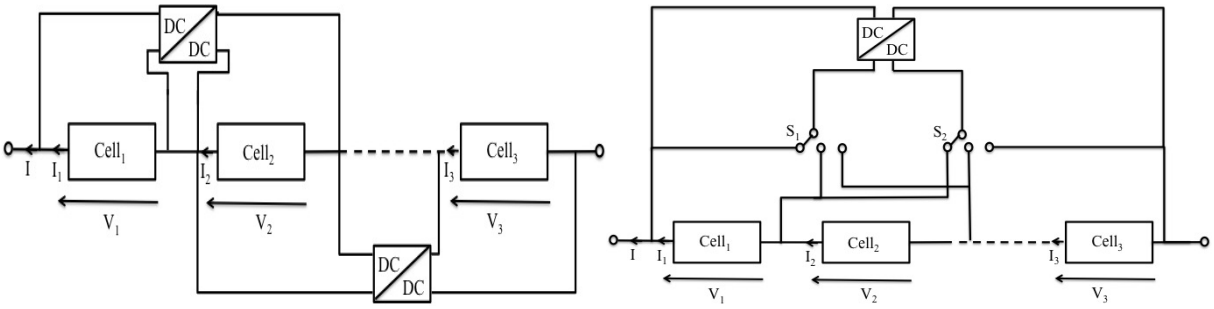

Figure 7.7: Balancing with one DC/DC converter for every two adjacent cells (left) and with one switched DC/DC converter for the whole stack (right) [Shin et al., 2010, Bonfiglio and Roessler, 2009].

7.3 Voltage balancing circuit for a serial stack of MFCs

A comparison of different voltage cell balancing topologies can be found in [Daowd et al., 2011]. Table 7.1 summarizes the control complexity, the cost, the performance of these circuits, the advantages and the disadvantages. The specifications of MFCs and low power generators limit the application of these circuits. MFCs required a low complexity, simple control, low cost and high efficiency voltage balancing circuits. Switched-capacitor methods require only 2n switches, n capacitor and one oscillator. Switched-capacitor is the simplest method due to no bulky magnetic components such as multiple winding transformers. Moreover, closed-loop and sensing are not required. They offer therefore good perspectives for a serial stack of MFCs. Application of switched-capacitor voltage balancing circuit on MFCs was studied theoretically and validated in simulation in [Degrenne, 2012]. No experimental data was shown. In the next section, a practical application of this method will be presented. Another method was proposed in [Degrenne, 2012], called "switched-MFCs", based on using the internal capacitor of MFCs to achieve the balancing. This method was also presented and simulated but no experimental results were shown. The circuit was tested with MFCs. A modified switched-MFCs is also tested experimentally in the following sections.

Table 7.1: Comparison of Different Cell Balancing Topologies

Circuit	Complexity	Cost	Efficiency	Comment
Shunting Resistor	Simple	Low	Satisfactory	Relatively high energy losses in the resistors
Complete disconnection	Medium	Medium	Low	Additional losses in the serial switches with cells
Switched-Capacitor	Simple	Low	Excellent	No need for closed loop control or intelligent control
Single Inductor	Complex	High	Good	Fast equalization speed with a stack high number of cells
Multi Inductor	Complex	High	Medium	Needs accurate voltage sensing
Single Winding Transformer	Complex	High	Good	No flexibility to add new cells
Multi Winding Transformer	Complex	High	Medium	No flexibility to add new cells, high magnetic losses
Converters	Complex	High	Medium	Intelligent control needed, high number of components

7.4 Switched-capacitor method

Switched-capacitor, also known as “Shuttling capacitors cell balancing” basically utilizes external capacitors as external energy storage elements for “shuttling” the energy between the cells so as to achieve the cells’ voltage balancing.

The switched-capacitor (SC) scheme for a stack of 2 MFCs is illustrated in Fig. 7.8. It requires one capacitor, one oscillator and four bi-directional switches for balancing the two cells. The SC control strategy is very simple because it has only two states, shuttling between the whole cells sequentially, moving the switches frequently from the upper position to the lower position and again to the upper one. Assuming that MFC_1 is the strong MFC, the voltage of MFC_1 is therefore higher than the one of MFC_2. As shown in chapter 3, the internal capacitor of MFCs is ranged between 200 and 600 mF (identification of the electrical model). The balancing capacitor is assumed to be significantly lower than the internal capacitances of the MFCs. The voltage across a MFC is considered constant during a switching period.

In the first phase, the external capacitor C_b is connected in parallel with MFC_1 and the capacitor will charge. Assuming that the capacitor in non pre-charged, the voltage across the capacitor during this phase is given by (7.1). In the second phase, the external capacitor is connected in parallel with MFC_2 and the capacitor will discharge. The voltage across the capacitor at the end of this phase is given by

(7.2). The voltage across the capacitor at the end of phase 1 is given by (7.3), where $\tau = 2R_{SW}C_b$: R_{SW} is the switch resistance.

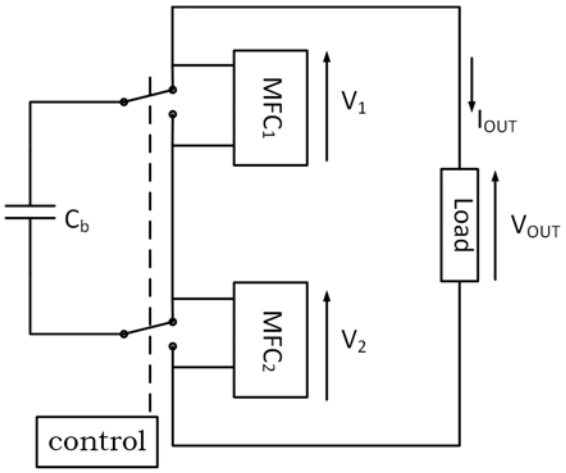

Figure 7.8: Switched-capacitor balancing circuit for MFCs

$$V_{Cb1} = V_1(1 - \exp(-t/\tau)) \tag{7.1}$$

$$V_{Cb2} = V_2 + (V_{Cb1} - V_2)\exp(-t/\tau) \tag{7.2}$$

$$V_{Cb1} = V_1 + (V_{cb2} - V_1)\exp(-t/\tau) \tag{7.3}$$

Because the capacitor C_b is repeatedly connected in parallel to the strong cell and weak cell with the same duty cycle, the voltage of capacitor C_b is then the average voltage of the two cells:

$$< V_{Cb} >= (V_1 + V_2)/2 \tag{7.4}$$

Circuit equations (see Fig.7.9) for 50% duty cycle in open circuit condition come as:

$$\begin{bmatrix} V_1 - V_C \\ 0 \end{bmatrix} = \begin{bmatrix} (V_1 - V_2)/2 \\ 0 \end{bmatrix} = \begin{bmatrix} 2R_{sw} + R_1 & 0 \\ 0 & 0 \end{bmatrix} \begin{bmatrix} i_{1A} \\ i_{2A} \end{bmatrix} \tag{7.5}$$

$$\begin{bmatrix} 0 \\ V_2 - V_C \end{bmatrix} = \begin{bmatrix} 0 \\ -(V_1 - V_2)/2 \end{bmatrix} = \begin{bmatrix} 0 & 0 \\ 0 & 2R_{sw} + R_2 \end{bmatrix} \begin{bmatrix} i_{1B} \\ i_{2B} \end{bmatrix} \tag{7.6}$$

From (7.5) and (7.6), the expression of total current through each MFC can be inferred as (7.7).

$$\begin{bmatrix} I_1 \\ I_2 \end{bmatrix} = \begin{bmatrix} i_{1A} \\ i_{2A} \end{bmatrix} + \begin{bmatrix} i_{1B} \\ i_{2B} \end{bmatrix} = \begin{bmatrix} \frac{V_1 - V_2}{2(2R_{sw} + R_1)} \\ -\frac{V_1 - V_2}{2(2R_{sw} + R_2)} \end{bmatrix} \tag{7.7}$$

With:

$$V_1 = V_{OC1} - R_1 I_1 \tag{7.8}$$

$$V_2 = V_{OC2} - R_2 I_2 \tag{7.9}$$

where V_{OC1} and V_{OC2} are the open circuit voltage of MFC_1 and MFC_2 respectively, R_1 and R_2 are the internal resistance of MFC_1 and MFC_2 respectively.

Finally the output voltage of the stack is:

$$V_1 + V_2 = V_{OUT} \tag{7.10}$$

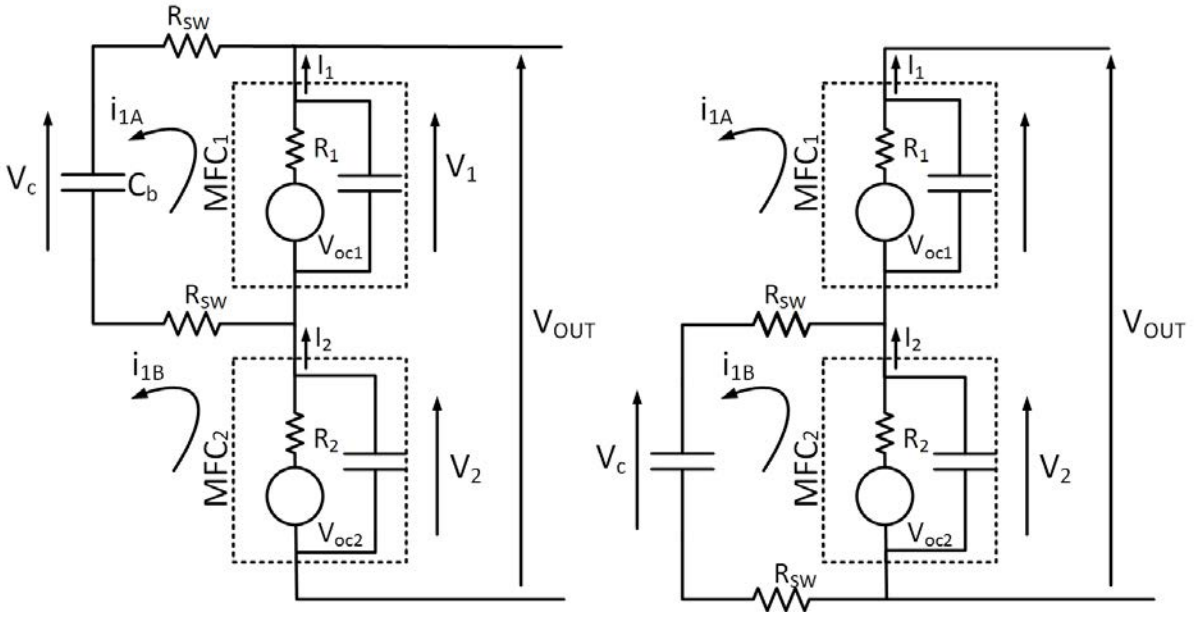

Figure 7.9: Equivalent circuit for the balancing scheme in Fig. 7.8

Loss analysis

The circuit of switched-capacitor suffers from four types of losses: a) conduction losses in the switches, b) losses in the internal resistances R_1 and R_2, c) switching losses in the shuttling switches and d) losses in the balancing capacitor.

Conduction losses in the shuttling switches are caused by the resistance of the switches R_{SW} given by the expression in (7.11) with an extension to n switches to balance n MFCs with (n-1) capacitors.

$$P_{con} = nR_{SW} < I_{SW} >^2 \tag{7.11}$$

The internal losses in MFCs are caused by the internal resistance of the connected MFCs. These losses exist even in the case where there is no balancing circuit.

These two losses are already token into account in the expressions of I_1 and I_2 , as shown in the previous section.

Switching losses are proportional to the switching frequency. These losses can be evaluated for one switch by (7.12). Where C_{oss} is the output capacitor and V_{ds} is the drain-source voltage. The total switching losses in a circuit of n MFCs are given by (7.13).

$$P_{sw} = \frac{1}{2} C_{oss} V_{ds}^2 f \tag{7.12}$$

$$P_{sw} = n C_{oss} V_{ds}^2 f \tag{7.13}$$

The power dissipated in the balancing capacitor can be neglected.

Breakdown of losses will be discussed later with a comparison of two balancing scheme.

7.5 Switched-MFCs

The electrical model of MFCs presented in chapter 3 includes a capacitor. This capacitor can achieve the same goal as the balancing capacitor in the SC circuit. The switched-MFC circuit supposes that MFCs are connected in series and in parallel alternatively at frequency f. In [Degrenne, 2012], the circuit was studied as follows: during phase 1 of operation, MFCs are serially connected to the load and they are crossed by the same current. In phase 2 of operation, the MFCs are connected in parallel and disconnected of the load as shown in Fig. 7.10. In this configuration the output voltage is ranging between zero (when the load is disconnected - phase 2) and the sum of MFCs' voltages (when the load is connected - phase 1). It requires 4 switches for a stack of 2 MFCs. Losses in this circuit are too significant and the efficiency will not exceed 70%. To increase this efficiency, the load is connected during the second phase (see 7.11). Indeed in this way the voltage and so the output power is not null during phase 2 what should improve the global efficiency. The output voltage is therefore ranging between the sum of MFCs' voltages when the MFCs are connected in series (phase 1, switch Sw_2 is closed) and the common voltage when the MFCs are connected in parallel (phase 2, switches Sw_1 and Sw_3 are closed). Moreover, this configuration requires only 3 switches instead of 4 what helps improving the performance. Balancing n MFCs using the switched-MFC method requires 3(n − 1) switches compared to [3(n − 1) + 1] switches for the primary method.

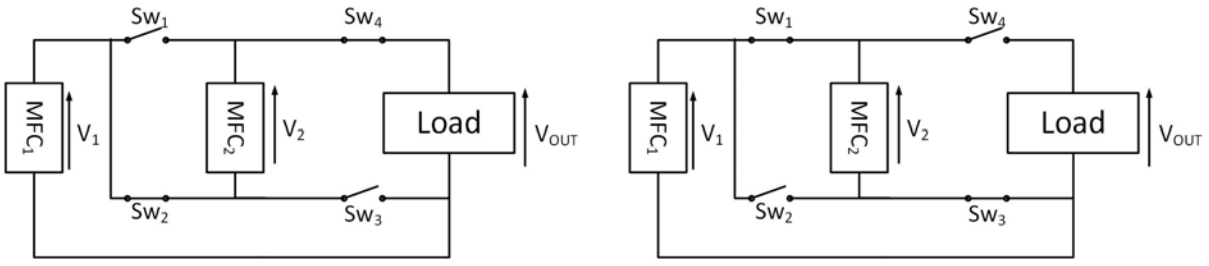

Figure 7.10: Switched-MFC balancing topology

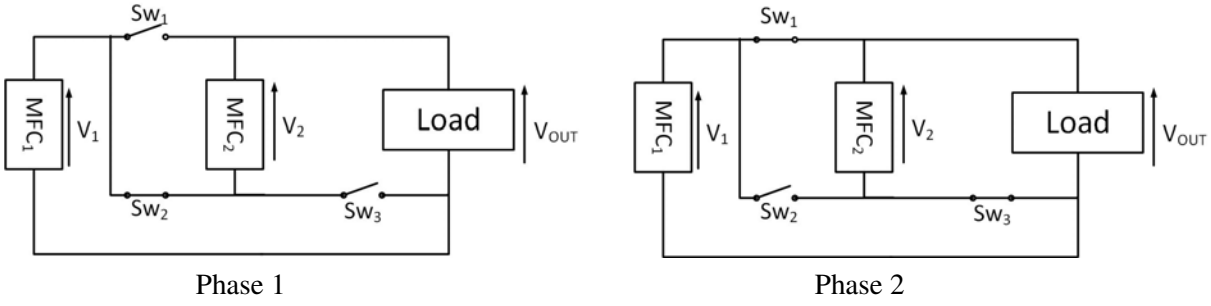

Figure 7.11: Modified switched-MFC balancing topology

Losses' analysis

In phase1, the switches are crossed by the output current while in phase2, they are crossed by the MFCs current. Conduction losses in phase1 are therefore higher than in phase2. The total conduction losses can be expressed as (7.14).

$$P_{con} = \sum_{k=1}^{2(n-1)} (R_{SW} {I_K}^2) \tag{7.14}$$

Switching losses in a circuit of n MFCs are given by (7.15).

$$P_{sw} = \frac{3}{2}(n-1) C_{oss} V_{ds}^2 f \tag{7.15}$$

7.6 Performance analysis

The performance of the two balancing schemes will be studied in this section. Two MFCs were characterized and tested in a serial stack without balancing circuit, then with switched-capacitor circuit and with switched-MFC circuit. Figure 7.12 presents polarization and power curves for the 2 non-uniform

MFCs. There is a notable difference between the two characteristics of MFCs: 0.98 V and 0.693 V in open circuit and 1715 µW and 540 µW output power at MPP respectively. The efficiency in this part is defined as the ratio of the maximum achieved power (P_{Out}) is the output power for the associated MFCs and the sum of MPPs for individual MFCs ($\sum P_{Mpp}$) (7.16).

$$\eta = P_{Out} / \sum P_{MPP} * 100 \tag{7.16}$$

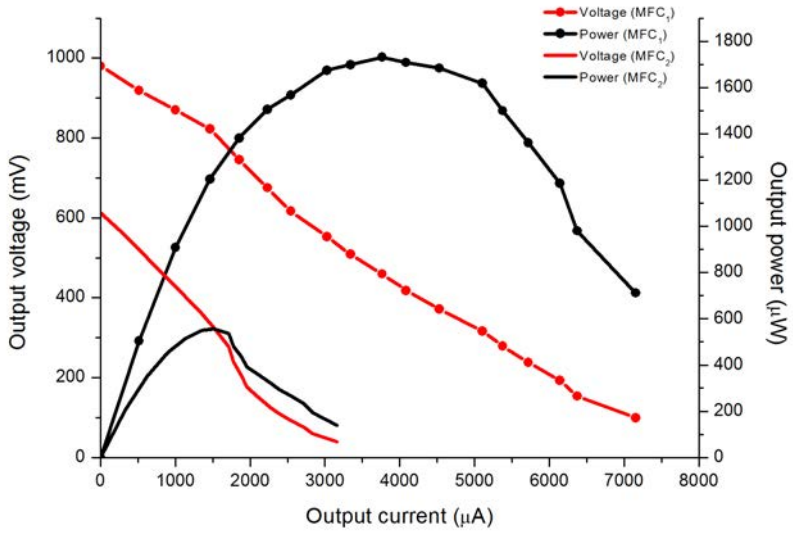

Figure 7.12: Experimental polarization and power curves for lab-scale reactors MFC_1 and MFC_2 (3 min sampling rate)

7.6.1 A stack of 2 MFCs without balancing circuit

The V-I and P-I polarization curves for the stack are given in Fig. 7.13. At the maximum power point, the voltage of each MFC is different, leading to a non-optimal operating point when they are connected in series. For high values of current, the voltages of MFC_1, V_1, and MFC_2, V_2, drift apart, eventually leading to a negative value of V_2 (the weak MFC) as shown in Fig. 7.13-a. This phenomenon was discussed as "voltage reversal". The ratio of maximum achieved power in this association is about 75%.

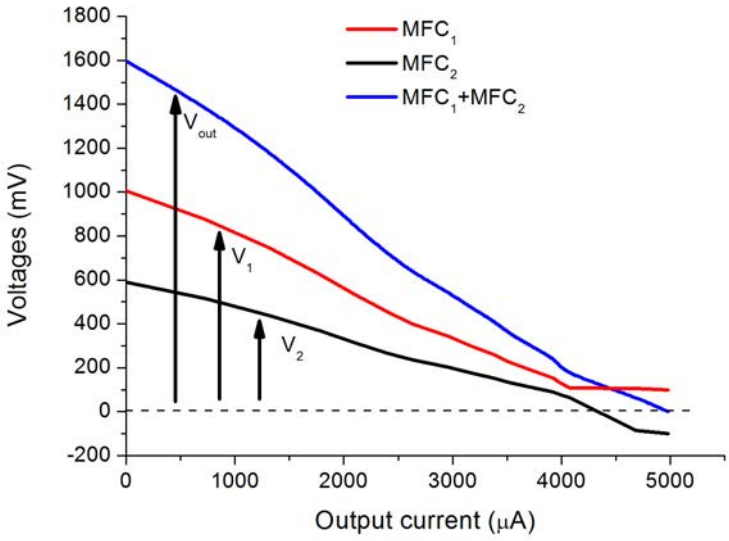

(a)

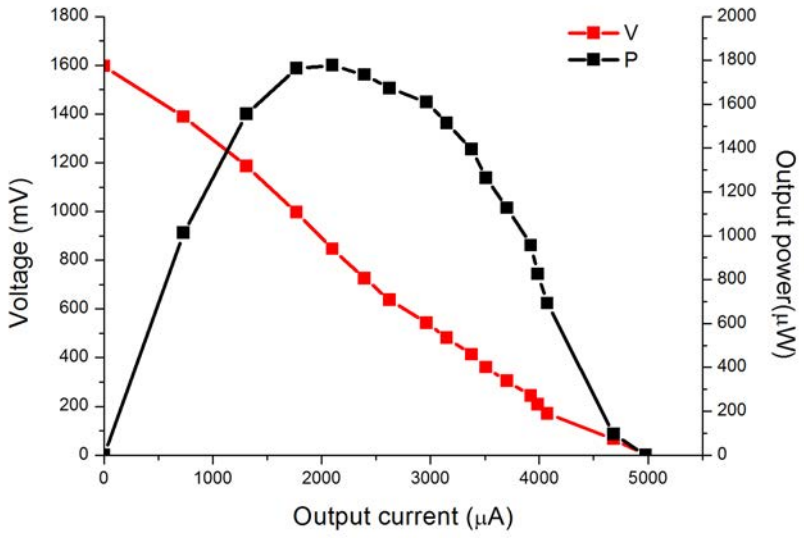

(b)

Figure 7.13: Experimental polarization and power curves for the stack of MFCs (3 min sampling rate)

7.6.2 Switched-Capacitor balancing circuit

The application of the switched-capacitor scheme on MFCs was simulated using SABER®, to optimize the switching frequency f and the capacitor C_b value. The simulated efficiency of the association is plotted in Fig. 7.14. At low switching frequency, the circuit is not useful and voltages are not balanced.

A switched-capacitor circuit behaves like a resistance of decreasing value when the switching frequency increases. The ratio of maximum achieved power for f =1 Hz is around 75 % (similar to the case of no balancing scheme). Increasing the switching frequency to 100 Hz begins to degrade fast the efficiency. At this low frequency, connecting an external and large capacitor to a MFC interacts with its internal operation. It changes the operating point of the MFC to a non-optimal point (61.2 % of the maximum power for MFC_1 and 87 % for MFC_2). The switches produce higher switching losses but not in a detrimental value. However it leads to a decrease in the total efficiency. At 100 Hz switching frequency, the switches are crossed by relatively high currents (3 mA for a load of 350 Ω) what leads to significant conduction losses (about 20 µW). At higher switching frequency, a lower value of current crosses the switches (500 µA) hence lower conduction losses. In this case balancing the voltage of MFCs becomes more efficient and the positive action of balancing operation is larger than the impact of total losses in switches. The ratio of maximum achieved power increases to 90% for a frequency above 10 kHz (as calculated according to (7.16)). MFC_1 offers 97.8% of its maximum power while MFC_2 offers 85 % of its maximum power.

The application of SC circuits is studied experimentally using 0.45-Ω QUAD SPDT ANALOG low consumption switches (0.5 µW) and a TS3001 Oscillator (2 µW). The total losses in the circuit in this case are about 124 µW. Figure 7.15 shows V-I and P-I curves for the associated MFCs with the SC balancing circuit at 10 kHz and with a capacitor of 500 µF. The ratio of maximum achieved power reaches 90% for f=10 kHz (close to the simulation values). The unbalanced stack of MFCs features originally 75% of efficiency. The interest of the voltage balancing is also demonstrated.

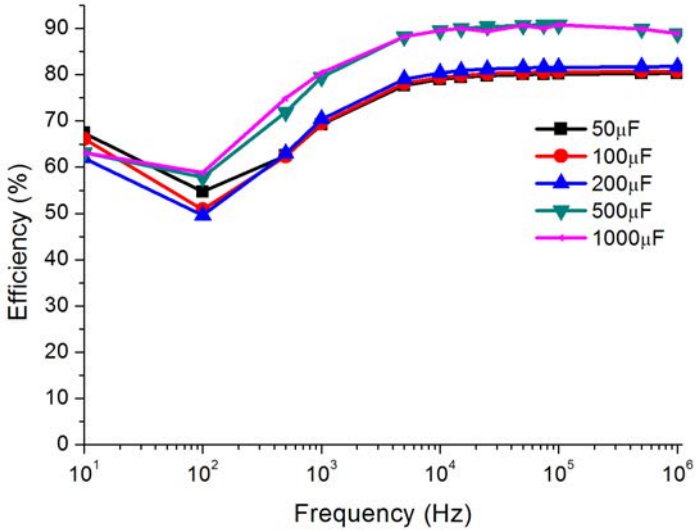

Figure 7.14: Simulated ratio of maximum achieved power of the stack vs the switching frequency for different values of balancing capacitor C_b

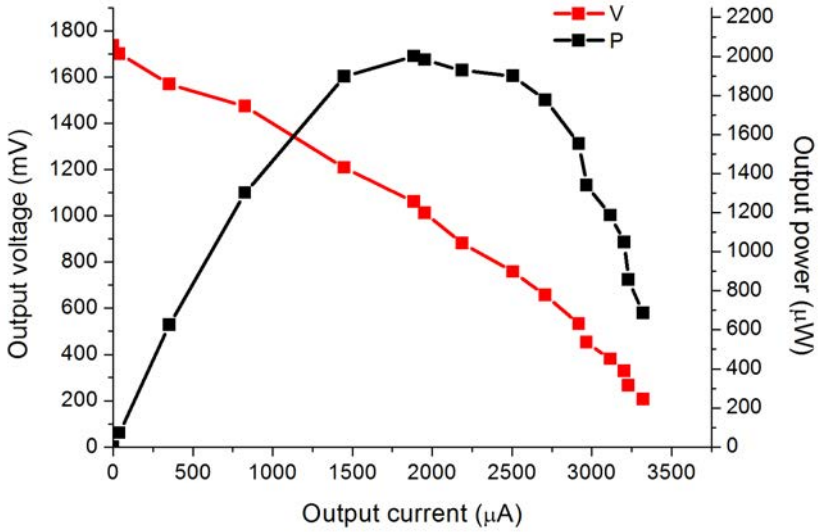

Figure 7.15: Experimental polarization and power curves with the SC balancing circuit (10 kHz, 500 μF, 3 min sampling rate)

7.6.3 Switched-MFC balancing circuit

The circuit is fabricated using dual single-pole/double-throw (SPDT) analog switch ISL54050 and a TS3001 oscillator. The low ON-resistance of the switches (0.3 Ω) helps minimizing switching losses. The ratio of maximum achieved power of the association according to the switching frequency was optimized using simulation. At low switching frequency, the circuit is not useful and voltages are not balanced. The ratio of maximum achieved power for f_s =1 Hz is around 10 %. The value increases with switching frequency and reaches up to 83% for 10 kHz as plotted in Fig. 7.16. Beyond this frequency the performance decreases again because of the switching losses that become more important. Figure 7.17 shows V-I and P-I polarization curves at 10 kHz.

In this scheme, the switches are crossed by the MFCs' currents (4 mA) what leads to higher losses than the SC scheme where the switches are only crossed by the balancing current that is quite low compared to MFCs current.

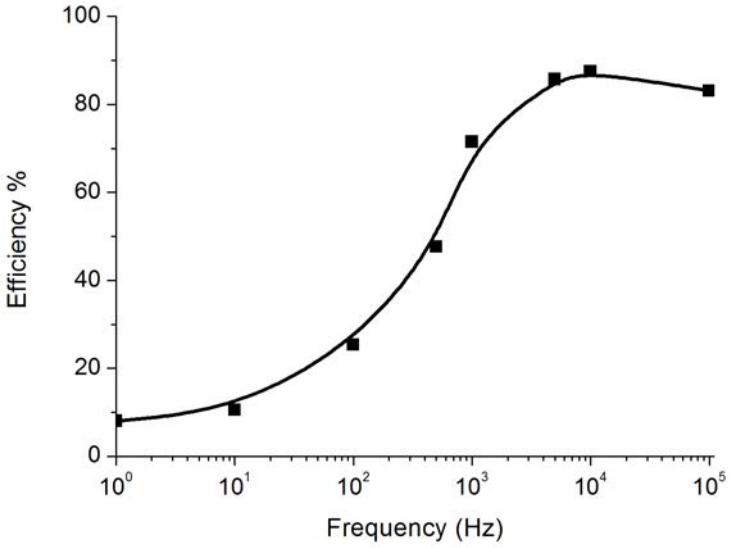

Figure 7.16: Simulated ratio of maximum achieved power vs the switching frequency with the switched-MFC balancing circuit

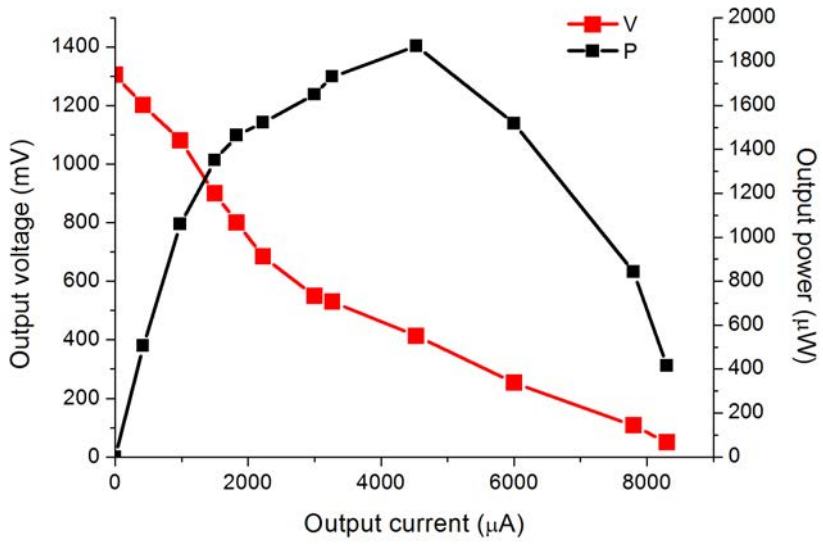

Figure 7.17: Experimental polarization and power curves with the Switched-MFC balancing circuit (10 kHz, 3 min sampling rate)

Table 7.2 summarizes results for a 2-stage voltage balancing circuit. The switched-capacitor circuit is mostly efficient voltage balancing circuit. The ratio of maximum achieved power reaches 90% for

f_s=10 kHz at MPP. It has a gain of +14.6% with respect to MFCs' association without balancing. This circuit offers a low-cost, low-power discrete implementation for MFCs.

Table 7.2: Table of results for the series-associated MFCs with or without balancing circuits

	V_{oc} (mV)	MPP (μW)	η%
Optimum association (theoretical)	1673	2255.9	100
Natural association	1610.5	1735.2	75.9
With SC balancing circuit	1715	2041.2	90.5
With S-MFC balancing scheme	1305	1876.9	83.2

7.7 Generalization to a n-stage switched-capacitor voltage balancing circuit

From the above discussion on a stack of two-stage MFCs, the switched-capacitor circuit is the most adapted voltage balancing circuit. To generalize the study to a stack of n MFCs, the circuit was simulated for different number of non-uniform MFCs with different degrees of dispersion as shown in Table 7.3. The analysis gives the following results:

- The global efficiency is not affected by the order of cells in the stack because the balancing over pairs of MFCs propagates the process over the full stack until convergence to the steady-state.
- A switching frequency about 10 kHz is suitable for all the configuration.
- The efficiency decreases with wideness of dispersion level among MFCs.
- Applying the switched-capacitor circuit on a stack of uniform MFCs is acceptable for energy harvesting to simplify the control system.

Table 7.3: Efficiency of balancing for different level of dispersion in MFCs (1: MFC with MPPT at 200μW, 2: MFC with MPPT at 500μW, 3: MFC with MPPT at 1000μW)

Stack	η%
1, 1, 1, 1, 1	98.77
2, 2, 2, 2, 2, 2	98.75
1, 2, 1, 2, 1, 2	93.5
1, 1, 1, 2, 2, 2	93.5
1, 3, 1, 3, 1, 3	90.4
1, 1, 1, 3, 3, 3	90.4
3, 2, 3, 2, 3, 2	94.1
3, 2, 1, 3, 2, 3, 1, 2	93.8
1, 1, 1, 1, 1, 1, 1, 2	98.6
3, 3, 3, 3, 3, 3, 3, 3	99.28

Increasing the number of such strong MFCs in the stack, enables to attain characteristics of photovoltaic (V_{oc}=40 V) but without the problem of illumination. At this point, all considerations of energy management about photovoltaic panel can be applied to the MFC stack.

7.8 Towards an integrated voltage balancing circuit

The studied circuits are manufactured using discrete of-the-shelf components, resulting in high complexity. As a possible way to overcome these possible limitations, an integrated approach to design and manufacture this system can improve performance, reliability and cost effectiveness. The integration of power electronic systems reduces design and implementation time cycles and improves usage of space. The integration eliminates interconnection problems in the system which ultimately improves system reliability and reduces cost if not losses. For these reasons, the SC balancing circuit is studied for integration. The circuit is designed to manage a stack of 5 MFCs [1]. The output voltage of a serial stack of 5 MFCs can reach the required voltage to auto-supply the circuit. CMOS transistors (Complementary Metal Oxide Semiconductor) technology is suitable to realize low-cost, low-power circuits. The technology HCMOS9GP 130 nm was selected for availability and pertinence to the context. In order to test performance of the circuit with a different number of MFCs, a logical input selects the number of MFCs in the stack as shown in Table 7.4. HCMOS9 is limited in voltage capability to 2.5 V, hence the choice of 5 MFCs with the targeted voltage near 2.5V. Ten MOSFETs (5 NMOS and 5 PMOS) are integrated as shown in Fig. 7.18. The circuit is realized with 18 pins of input/output and 4*4 mm TQFP32 (Thin Quad Flat Pack) package. A PCB was then realized with external capacitors because 500 µF is out of possible integration as shown in Fig. 7.19. The circuit was simulated and the simulated efficiency indicated 93.7% of ratio of maximum achieved power for 5 MFCs of dispersion level (1, 2, 3, 2, 1) to Table 7.3. The circuit is tested but it is noted that the oscillator was not able to start. This is due to a design default or issue of start-up conditions. Investigation is on-going. A bare die of the chip will be directly bounded on a PCB to bypass the oscillator output (“pulse” pad) to verify our primary assumption.

Table 7.4: Configuration of the logic input to control the number of MFCs in the stack

P_0	P_1	Number of MFCs
1	1	2
0	1	3
1	0	4
0	0	5

[1] This section was realized with the help of Guillaume Vine, temporary engineer at Ampère-lab.

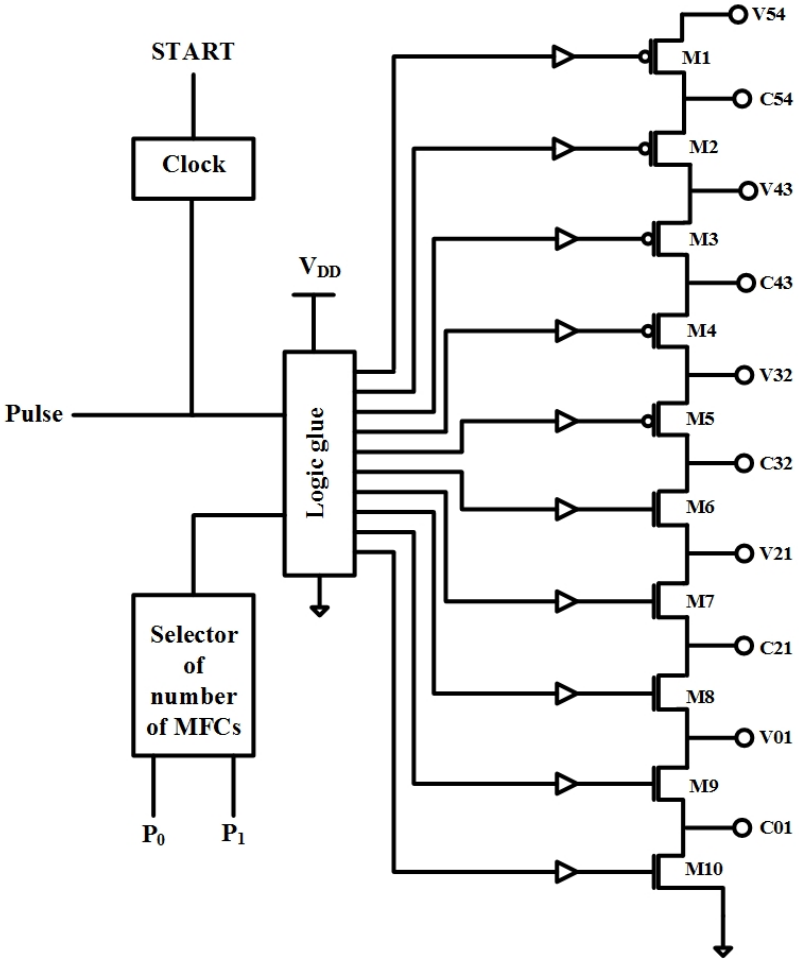

Figure 7.18: Schematic of the integrated SC voltage balancing circuit

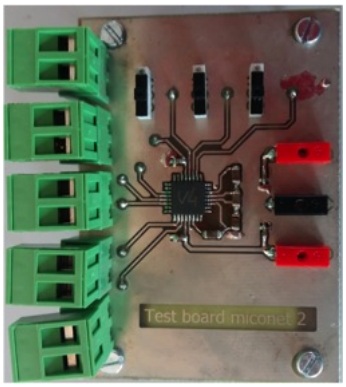

Figure 7.19: Test board of the integrated circuit

7.9 Configuration of a MFC-powered system

To supply a practical application from the energy harvested from MFCs, a stack of MFCs is required to cover the energy demand. A DC/DC converter is required to step-up (adapt) the voltage and control the operation of MFCs. In order to step-up the voltage of MFCs with highest efficiency, many topologies are possible. In the following part, we study the possible power delivery topologies to supply an application from a stack of two MFCs. Figure 7.20 shows the studied cases. The converter in this part is the flyback converter studied in chapter 6.

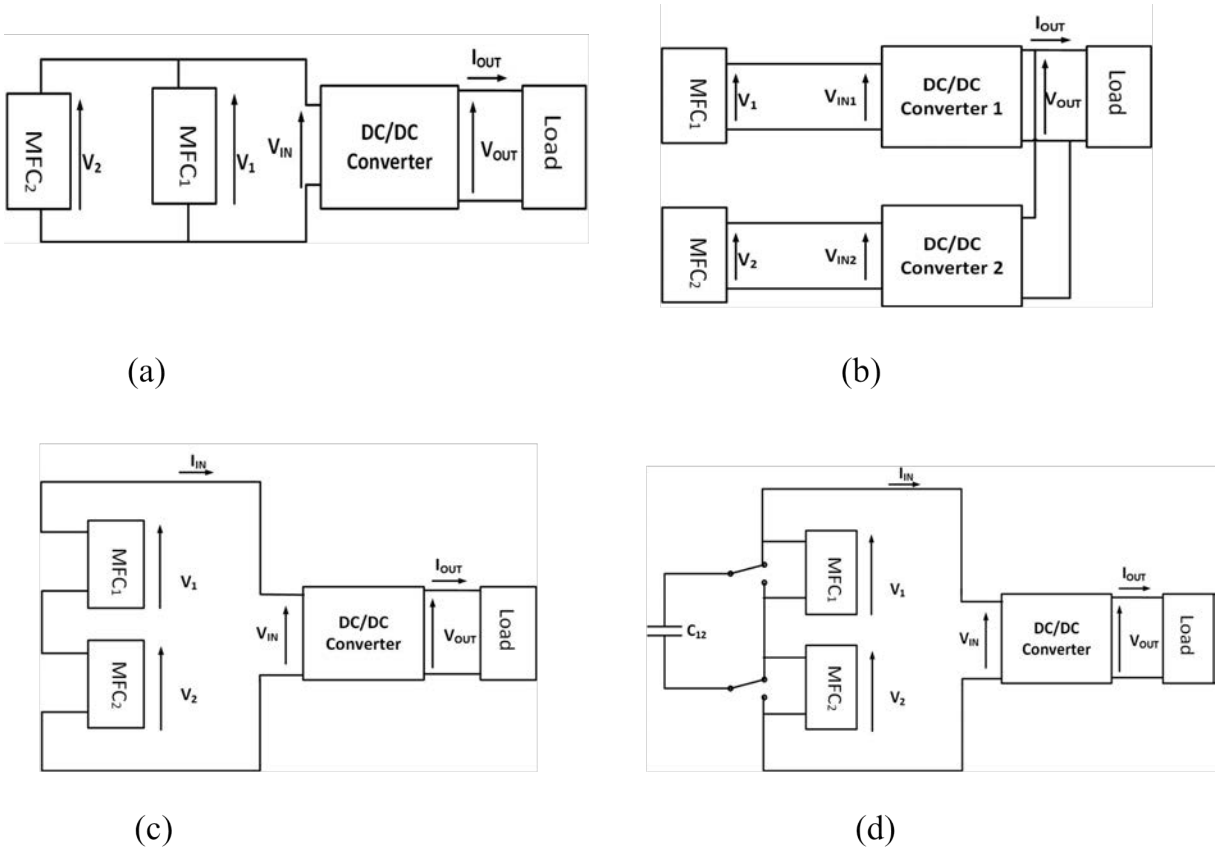

Figure 7.20: Parallel association of non-identical MFCs with one flyback converter (a), MFC individually connected to a flyback converter and the converter outputs connected in parallel (b), MFCs connected in series with the flyback converter (c) and MFCs serially connected with the flyback converter and switched-capacitor voltage balancing circuit (d)

7.9.1 A parallel stack of 2 MFCs with the flyback converter

The association of the MFCs in parallel takes over the issue of voltage reversal. The MFCs in this case have the same voltage. The main drawback in this case is the low input voltage of the flyback. At MPPT the measured input voltage is 497 mV. The operation of the converter is not efficient 68.5 % (efficiency calculated as the relation between the output power and the input power). The ratio of maximum achieved power is 63.8% at MPPT as shown in Fig. 7.21. The losses in the converter are 703 µW what are higher than the maximum power of MFC_2.

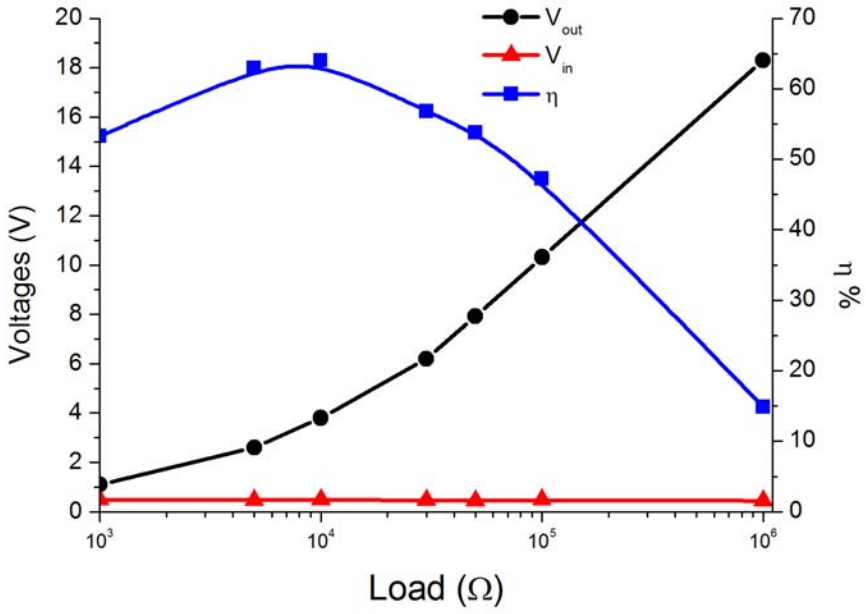

Figure 7.21: Experimental input voltage (V_{in}), output voltage (V_{out}) of the converter and the percent of maximum power achieved in the case of a parallel stack with the flyback converter

7.9.2 Individual MFCs

Regardless of economic considerations, using a flyback converter with each MFC has been studied (Fig. 7.20.b). The serial association of output of converter is not possible because of the different output voltages caused by non-uniformities of MFCs. The input voltage of converter 1 (connected to the strongest MFC, MFC_1) at MPPT is 508 mV and it has an efficiency of 75.1% while the converter 2 has an efficiency of 47%. The ratio of maximum achieved power is 50.47% at MPPT.

7.9.3 A serial stack with one converter

The third configuration is a natural serial association of 2 MFCs with one flyback converter as shown in Fig. 7.20.c. The measured output voltage is about 15 V at open circuit and 3.7 V at MPPT. The input voltage is 788 mV. The ratio of maximum achieved power achieved is 66.4% at MPPT as shown in Fig. 7.22. MFC_1 operates at 69% of MPP against 58% for MFC_2.

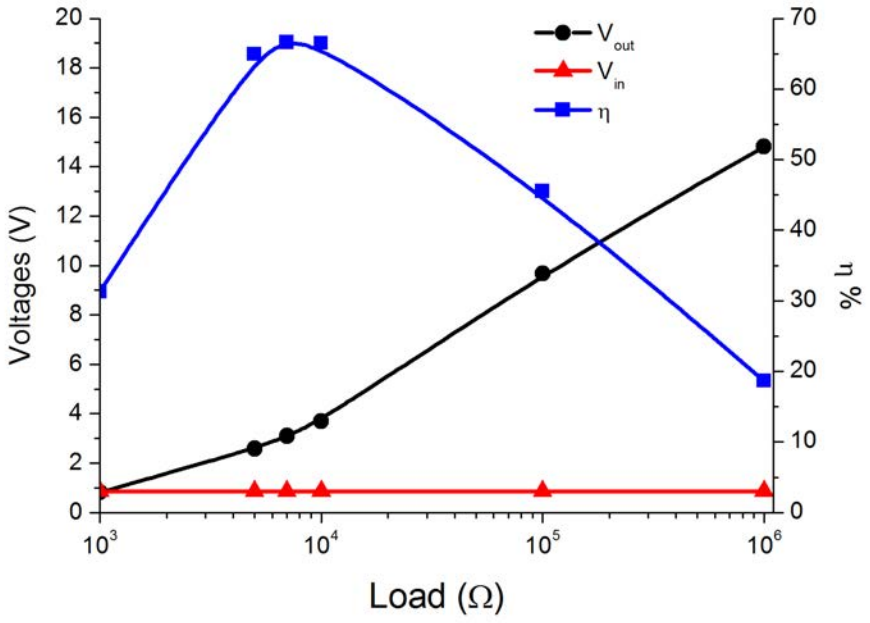

Figure 7.22: Experimental input and output voltage of the converter and the ratio of maximum achieved power in the case of a natural serial stack with one flyback converter

7.9.4 A balanced serial stack with one converter

The application of voltage balancing circuit on a serial stack of non-uniform MFCs proved an efficient operation. The switched-capacitor circuit was demonstrated previously as the best candidate. The application of this circuit to the stack increases the ratio of maximum achieved power to 87% at MPPT. The measured output voltage of the flyback in this case is 17 V open circuit and 4.2 V at MPPT as shown in Fig. 7.23. MFC_1 operates at 95% of MPP and 98% for MFC_2. The input voltage is 805 mV which is almost equal to 50% from the open circuit voltage of the stack. That proves the operation of converter at MPP. The efficiency of the converter alone is 83.7%. The efficiency of total power management unit is 80.1%.

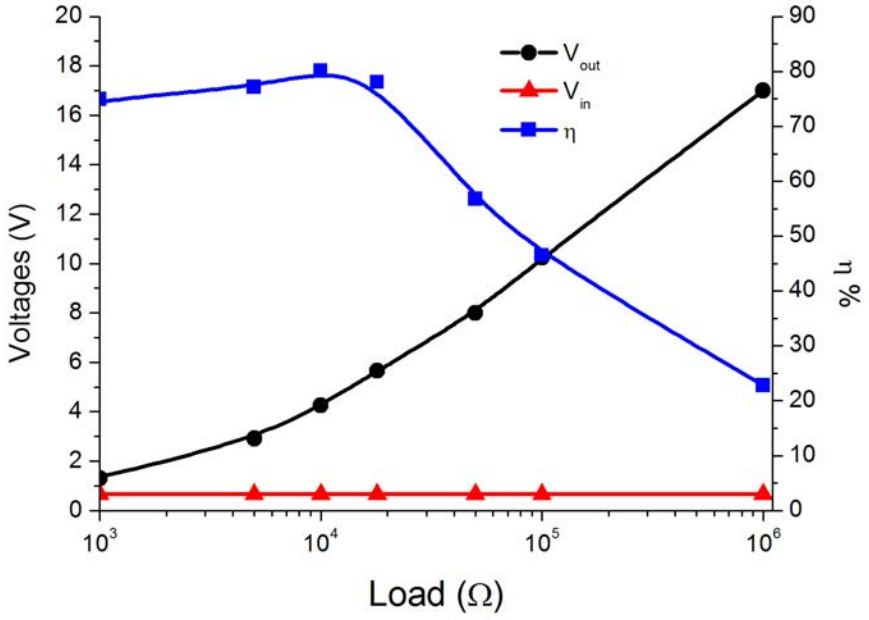

Figure 7.23: Experimental input and output voltage of the converter and the ratio of maximum achieved power in the case of balanced serial stack with one flyback converter

7.10 Conclusion

To associate a number of MFCs, many scenarios were studied and compared on a stack of 2 MFCs. The parallel association does not have a good efficiency because of the low voltage of the stack. The efficiency of the serial association of MFCs with the flyback converter is limited by the non-uniformities of the characteristics of MFCs. A power management unit includes a voltage balancing circuit and the flyback converter offers the most efficient configuration. The dispersion of MFC performances is one issue that will decrease the efficiency of a serial association compared to individual performances of MFCs. A circuit that enables voltage balancing across serially-associated MFCs is required. Balancing voltage across all MFCs in the stack achieves a higher operating voltage and therefore better performances. Two balancing methods were studied and tested with MFCs. The switched-capacitor circuit transfers energy from the strongest to the weakest MFCs. Switched-MFCs use their internal capacitor to equilibrate the voltages. Both circuits are able to prevent the voltage reversal effect. The switched-capacitor circuit is good candidate. This voltage-balancing circuit offers a low-cost effective solution to increase the energy generation of MFCs.

Chapter 8

Hydraulically connected microbial fuel cells

Contents

8.1 Introduction

The first researches on MFCs were based on batch systems. Each cell was fabricated to have a closed reactor. There is no hydraulic connection between cells. Fed batch system may not be suitable for continuous power generation. Considering wastewater treatment systems operate in a continuous mode, there should be no hesitation in using serial stacks under continuous flow within the stacks. Moreover, it has been demonstrated that a serial stack of MFCs under continuous flow are capable of larger treatment capacity than a parallel stack of the same cells [Pinto et al., 2010]. The integration of water treatment with electricity generation, in wastewater treatment plant, is of particular advantage that can encourage MFCs to find their first commercial application [Liu and Logan, 2004, Pinto et al., 2010]. In these configurations, air-cathode-MFCs could be placed on the circulation pipe or may be replacing the pipe other structures as the one presented in [Liu and Logan, 2004]. In environmental MFCs, such as sediment-based benthic MFCs or BMFCs, MFCs are planted undersea to generate electrical current from the natural redox gradients that commonly occur across the sediment-water interface. In general, a BMFC consists of a circuit in which inert but electrically conductive electrodes are placed in an anoxic

zone (the anode) and an oxic zone (cathode) as shown in Fig. 8.1. In this case, there is no way to operate the MFCs in batch-mode what gives the importance to study the effect of the fluidic connection on the performance of the MFCs.

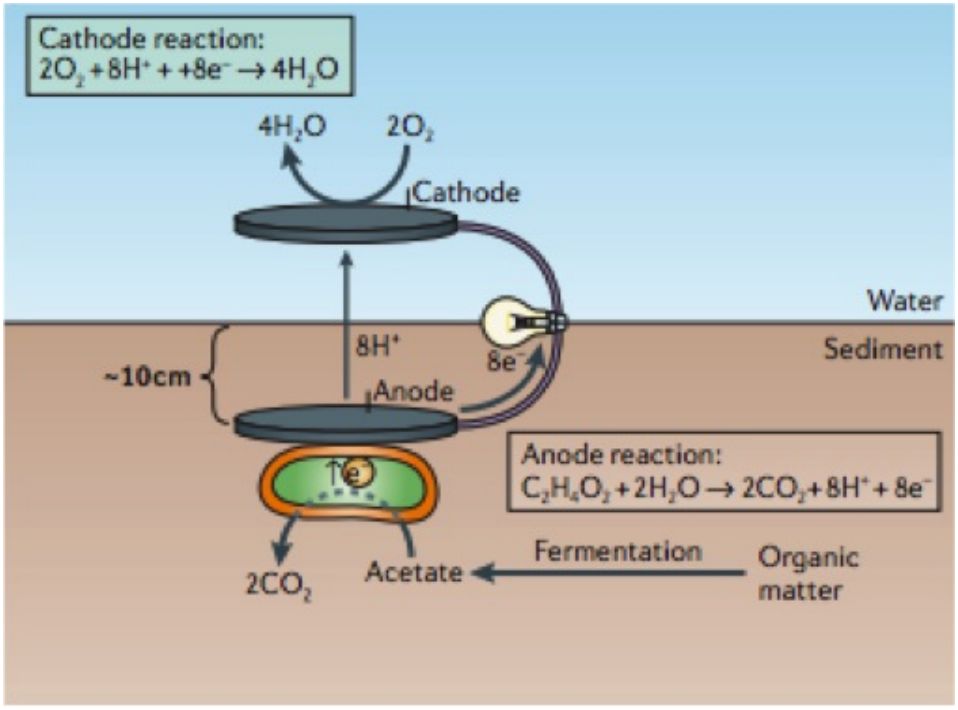

Figure 8.1: Schematic of a Benthic Microbial Fuel Cell [Lovley, 2006]

8.2 Substrate cross-conduction effect

This phenomenon was firstly observed with fuel cell when multiple cells share the same electrolyte membrane, connected in series to build voltage. Lower open circuit voltage and output current than should be expected are reported in [O'Hayre et al., 2003], leading to a performance degradation phenomenon. The flow of a parasitic cross-currents between stacked cells (dubbed membrane cross-conduction) are proposed as the cause for this loss phenomenon. A performance degradation phenomenon was also observed in two MFCs units electrically connected in series and hydraulically connected by substrate flow [Zhuang and Zhou, 2009] linked to substrate cross-conduction between cells' electrodes, creating ''antagonistic paths'' that negatively affect electrical performance [Aelterman et al., 2006a, Ieropoulos et al., 2008, Wang and Han, 2009, Ledezma et al., 2013a]. In a stack of two MFCs linked in series, the

cathode of MFC_1 (named C_1) is electrically connected to the anode of MFC_2 (named A_2). Essentially, the cathode of MFC_1 and the anode of MFC_2 form a shorted, leakage fuel cell as shown in Fig. 8.2. The value of the parasitic current due to substrate cross-conduction depends on the substrate resistance between the electrodes in parasitic fuel cell according to the Ohm's law and can be approximated by (8.1)

$$R_e = \rho \frac{l}{s} \tag{8.1}$$

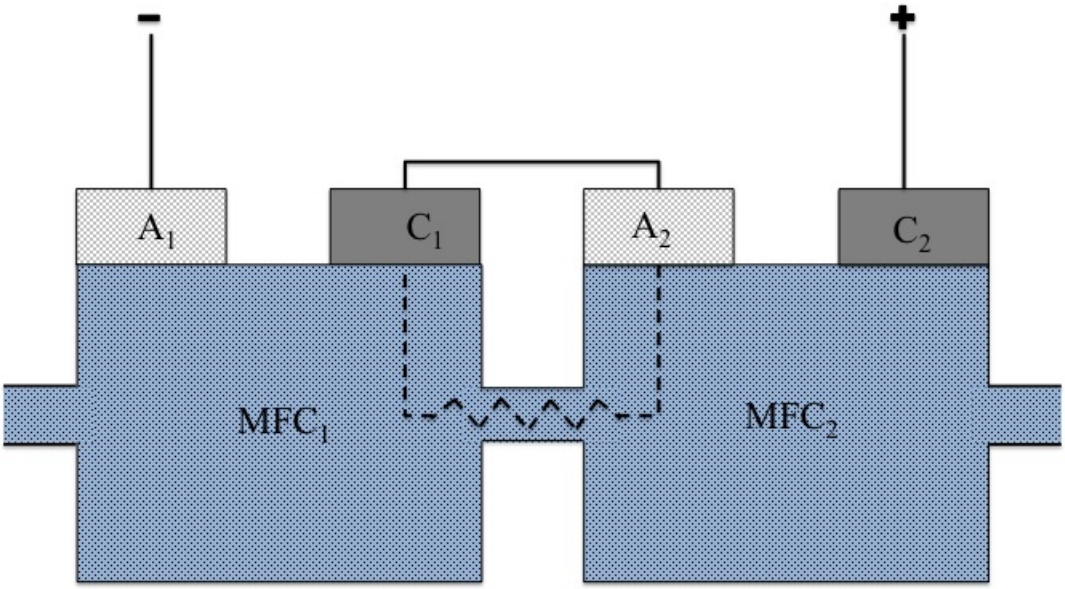

Figure 8.2: Illustration of substrate cross-conduction effect between serially connected MFCs [Zhuang and Zhou, 2009]

where ρ is the resistivity of the electrolyte, l is the distance between the electrodes and s is the cross-sectional area of substrate flow. In theory the resistance can be increased by enhancing the resistivity of the substrate (ρ). However, a higher resistivity could lead to a higher internal resistance of MFC and would consequently degrade the global performance of MFC. Extending the distance between the electrodes (l) or reducing the cross-sectional flow area (s) seem to be adjustable for increasing the resistance but would affect the mass flow rate.

To overcome this performance degradation phenomenon, several approaches were suggested by researchers in the conventional fuel cell field: thickening the membrane to increase the resistance (in a

double chamber MFC), decreasing the potential difference between unit cells, etc [O'Hayre et al., 2003]. However, many of them cannot be applied to MFC systems due to special characteristics and design. As the low resistance between the hydraulically connected cells caused ionic cross conduction, increasing the solution resistance can be one way to overcome it. In [Zhuang and Zhou, 2009], it was found that the voltage losses decrease with increasing the distance between the electrodes. The voltage losses were disappeared when the two individual cells were connected with a 20 cm tube of 0.3 cm internal diameter. Losses due to the cross-conduction were studied in six 2-chamber MFCs under continuous-flow configured as a vertical cascade [Ledezma et al., 2013b]. The output power was 97.6% lower than that produced under batch mode. The separation distance was increased up to 250 cm without significant improvement on the performance.

8.3 Performance analysis of hydraulically-connected MFCs

In this part, the effect of the hydraulic coupling on a stack of MFCs was practically studied. Four continuous-flow MFCs are configured and tested under different electrical connections.

8.3.1 Construction of the MFC-Cascade system

The MFC units are designed to allow a continuous flow of substrate using a carbon fiber brush anode and an air cathode. A PVC draining tube is used to form the reactor of 0.7 L. From the anode side, the cover was drilled and a ball valve (I.D. 13 mm) was employed to hydraulically connect the MFCs and to control the substrate flow between MFCs. A transparent garden hose (I.D. 15 mm) was used to connect the MFCs. MFCs are placed on a shelf. To give the ability to the study as the function of the distance between the connected MFCs, the shelf was chosen to be adjustable. In the first time, the distance between the connected MFCs was measured to be 15 cm. The schematic diagram, photographic and auxiliary equipments of the test set-up are shown in Fig. 8.3.a and b. Two tanks of 40 L are used at the top and the bottom. In such a system, the fluid flow was mostly gravity driven, with the need to pump only to the top tank.

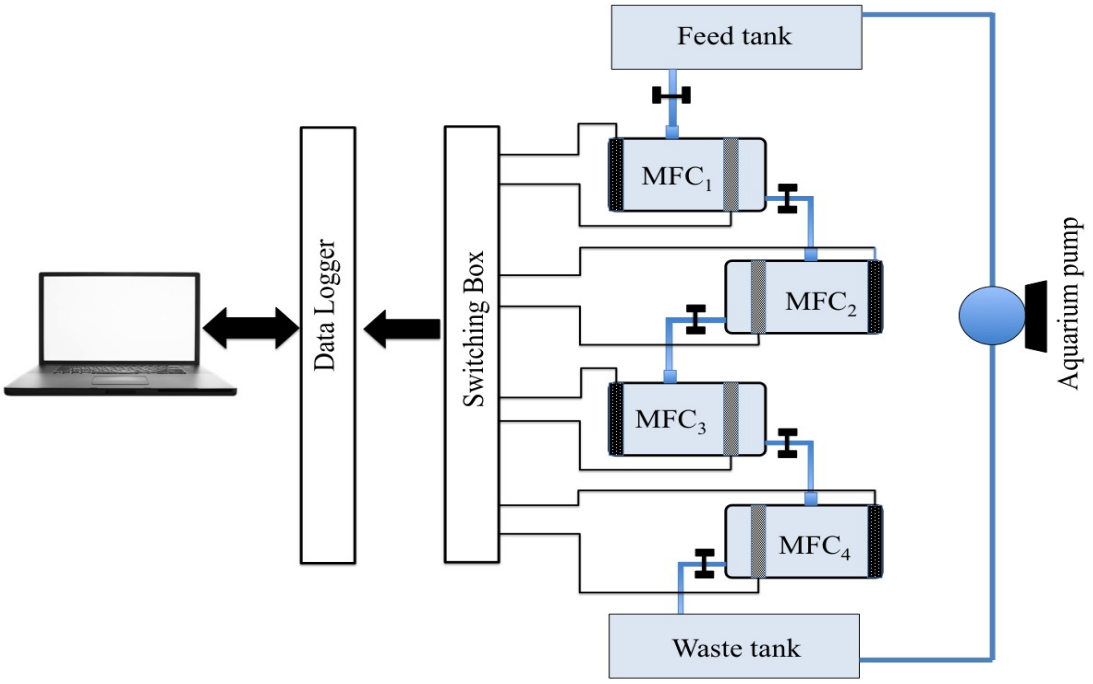

(a)

(b)

Figure 8.3: Stacked MFCs, Schematic diagram of the stack assembly (a) and picture of the test set-up (b).

8.3.2 Operation

The MFCs were operated at a room temperature of 18 ±3 °C. The MFCs are inoculated separately with wastewater sample from a wastewater plant and fed with 1 g/L of sodium acetate. MFCs voltages were monitored during biofilm development. After 10 days, the output voltages were visible and equal 208, 281, 314, 350 mV respectively. The MFCs are then characterized and the maximum power point were 180, 607, 234, 483 µW respectively. As discussed before, these non-uniformities between the MFCs are caused by different factors: the microbial activity, fabrication procedure, materials and operation condition. After 15 days, the output voltages reached their maximum equal to 552, 605, 690, 695 mV for MFC_1, MFC_2, MFC_3 and MFC_4 respectively. At the 25 days, the MFCs were supposed discharged and therefore recharged with 1g/L of sodium acetate to process the test. After the stabilization, MFCs were characterized and their characteristics static are given in Fig. 8.4[1].

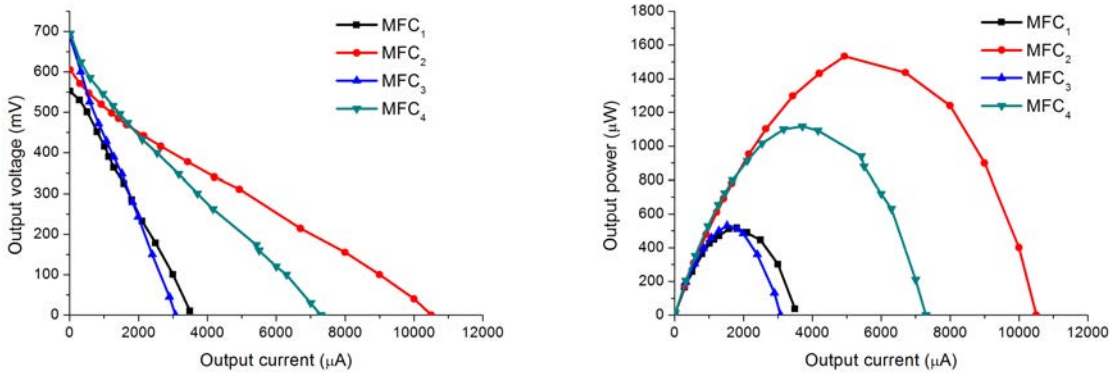

(a) (b)

Figure 8.4: Polarization (a) and power (b) curves of 4 MFCs in the stack under the conditions of hydraulic and electric isolation

8.3.2.1 Hydraulically insulated operation

After estimating the individual performance of each cell in the stack, the MFCs were connected in series and left to stabilize. After stabilization, a polarization sweep was performed, as expected the open circuit voltage of the stack is equal to the sum of the open circuit of all MFCs in the stack (2542 mV). The output power is not equal to the sum of MPP of the MFCs because of the non-uniformities of MFCs and it is equal to 2850 µW, which means 77.13 % of ratio of maximum achieved power.

[1] All the experiments were achieved at 3 min sampling rate

A parallel connection of the MFCs can improve the ratio of maximum achieved power to 83.35 %. The output voltage in this case is the same for all MFCs and equal to 574 mV. The maximum current delivered by the parallel stack is 22 mA which is 4 times higher than in the serial stack as shown in Fig. 8.5. As discussed before, a parallel connection of MFCs is not suitable for energy harvesting because of the low input voltage.

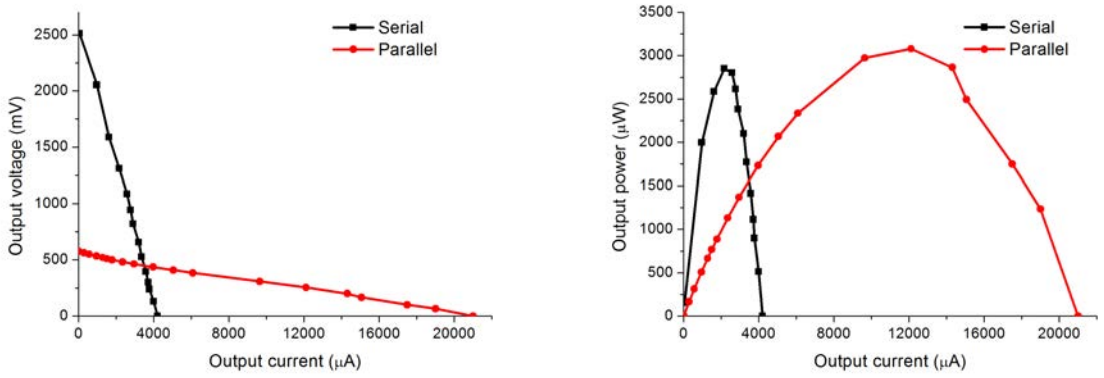

(a) (b)

Figure 8.5: Experimental polarization (a) and power (b) curves for the stack of 4 MFCs connected in series and parallel without hydraulic couplings

8.3.2.2 Hydraulic coupling with a low flow rate

The serial stack of MFCs was disconnected and the valves were controlled to assure a flow rate of 10 L/h, corresponding to a hydraulic retention time (HRT) of 0.07 h. The output voltages of all MFCs are monitored. A decrease in the open circuit voltage output was observed while increasing the flow rate. After stabilization, the voltage of MFC_1 and MFC_2 increased about of 17 mV, 10 mV respectively but the voltage of MFC_3 and MFC_4 decreased of 33 mV and 13 mV respectively. The experiments were repeated many time, almost the same results were found. That could be explained by the cumulative degradation of the nutrient supply, brought by feeding the stack only at the top cell (Fig. 8.3). The MFCs are then characterized and the results are shown in Fig. 8.6. The maximum power points of MFCs are 592, 1547 μW for MFC_1, MFC_2 and 407, 1078 μW for MFC_3, MFC_4 respectively.

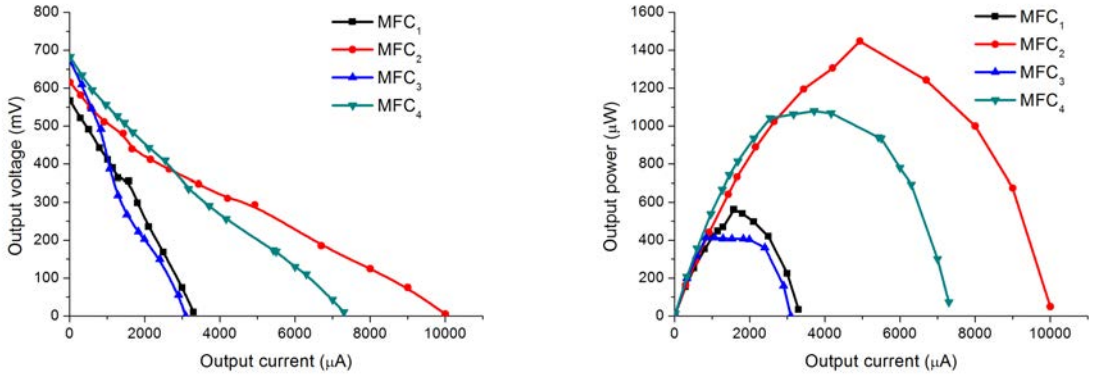

(a) (b)

Figure 8.6: Experimental polarization (a) and power (b) curves of the 4 MFCs under hydraulic connection with a flow rate of 10 L/h

A serial stack was achieved with a flow rate of 10 L/h. The open-circuit voltage for each MFC in the stack decreases and consequently the total voltage of the stack decreases. After stabilization, the open circuit voltages of the MFCs have decreased of 66, 50, 7 and 19 mV for MFC_1, MFC_2, MFC_3 and MFC_4 respectively due to the cross-conduction losses as shown in Tab. 8.1. A polarization sweep was applied and Fig. 8.7 presents the statics characteristics of each MFC in the stack. In term of power, the losses were 166, 260, 88 and 43 μW for MFC_1, MFC_2, MFC_3 and MFC_4 respectively. At about 2.5 mA of output current, the voltage of MFC_1 and MFC_3 have been reversed what limits the output power. The ratio of maximum achieved power in this case is 68.7%. The application of SC balancing circuit on the system compensates the losses caused by the non-uniformities and increases the efficiency to reach 82%.

Table 8.1: Open circuit voltage before and after the serial association of MFCs with a 10 L/h flow rate

Voltages (mV)	MFC_1	MFC_2	MFC_3	MFC_4
Before the serial association	567	615	675	682
After the serial association	501	565	668	663
Voltage drops	66	50	7	19

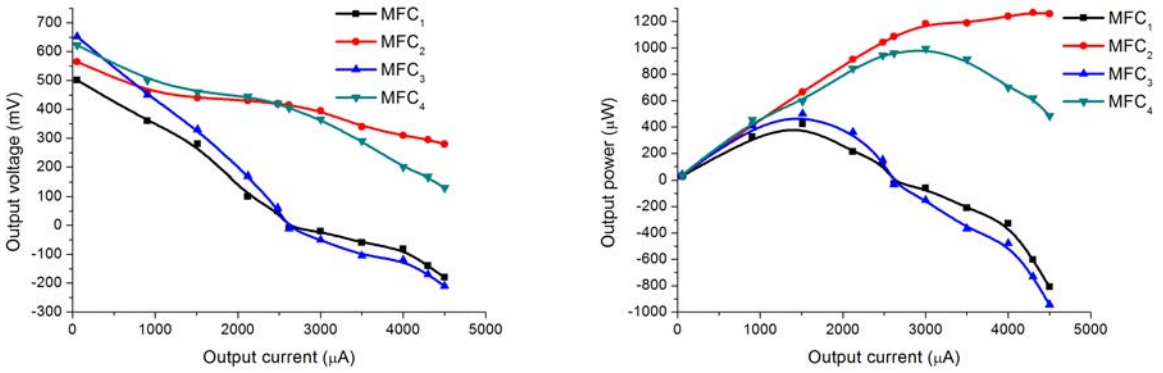

(a) (b)

Figure 8.7: Experimental polarization (a) and power (b) curves of 4 MFCs in the serial stack under hydraulic connection with a flow rate of 10 L/h

MFCs were then disconnected and left to stabilize under the hydraulic coupling. Contrary to the previous case, connecting the MFCs in parallel offers an output power lower than in the serial stack as shown in Fig. 8.8. The performance of MFCs in the stack is not identical what means that anodes and cathodes of the cells have different potentials. The cathodes of the parallel-connected stack form a shorted, leakage fuel cells, as also for the connected anodes. These two shorted MFCs can be modeled as shown in Fig. 8.9. The hydraulic coupling, in this case, creates ‘‘antagonistic paths’’ that negatively affects the electrical performance.

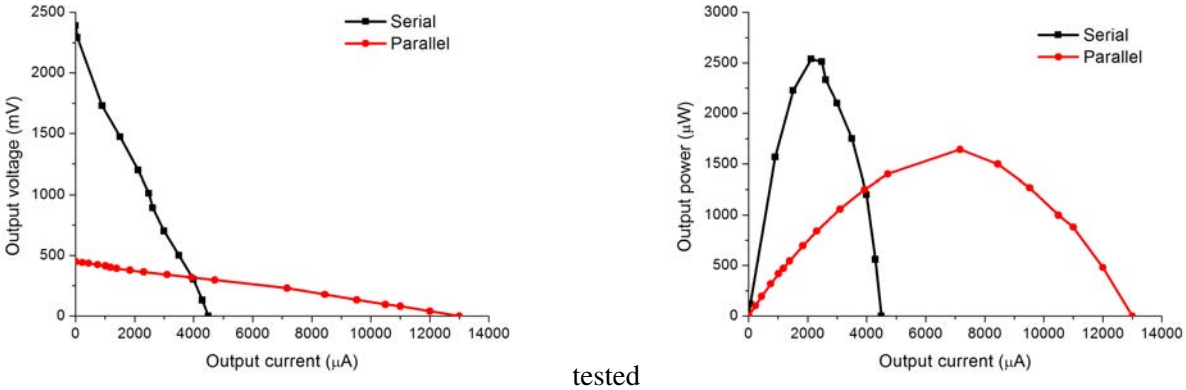

(a) tested (b)

Figure 8.8: Experimental polarization (a) and power curves (b) for the stack of 4 MFCs connected in series and parallel under a hydraulic coupling (10 L/h)

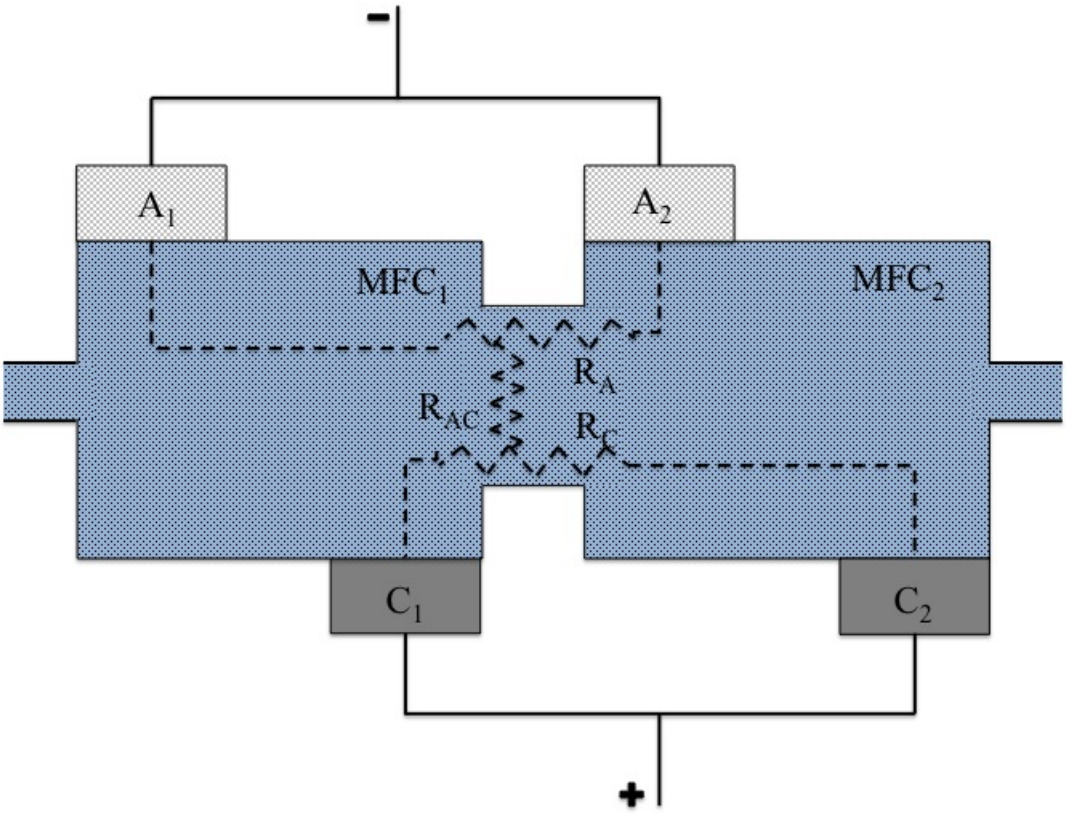

Figure 8.9: Illustration of substrate cross-conduction effect between the parallel-connected MFCs

8.3.2.3 Hydraulic coupling with a high flow rate

The flow rate was controlled to be 45 L/h and all experiments have been repeated. Even if the MFCs are electrically isolated, a high flow rate decreases significantly the open circuit voltages. After stabilization, the open circuit voltages were measured to 343, 485, 445 and 421 mV for MFC_1, MFC_2, MFC_3 and MFC_4 respectively. To the authors' best knowledge, this phenomenon is not discussed in literature. Losses may be explained by a charge leakage caused by the flow through the cathode due to proton flow and/or oxygen leakage, along with the flow, from the cathode to a subsequent anode which will function as a terminal electron acceptor for organisms instead of the anode.

The electrical characterization of the MFCs presented in Fig. 8.10 shows that maximum output powers are also negatively affected. They are 203 μW (39.3% of the initial power), 882 μW (57.53% of the initial power), 219 μW (41.3% of the initial power) and 426 μW (38.1% of the initial power) for MFC_1, MFC_2, MFC_3 and MFC_4 respectively.

With the large flow through the cathode, there were a 32%, 53%, 36% and 45% overall increase in internal resistance for MFC_1, MFC_2, MFC_3 and MFC_4 respectively with the hydraulic coupling compared to hydraulically isolated MFCs with values of 195 Ω (147 Ω hydraulically isolated), 95 Ω (62 Ω

hydraulically isolated), 312 Ω (228 Ω hydraulically isolated) and 150 Ω (103 Ω hydraulically isolated) respectively[1].

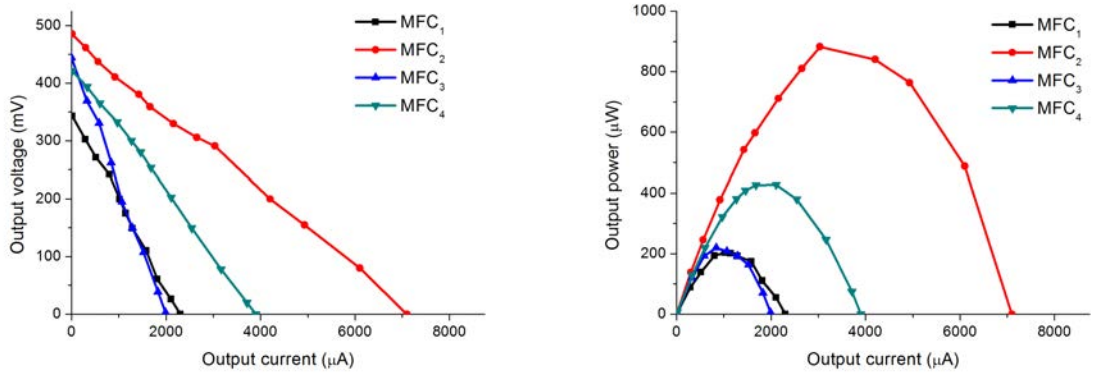

(a) (b)

Figure 8.10: Experimental polarization (a) and (b) power curves for the 4 MFCs electrically isolated under a hydraulic coupling (45 L/h)

The MFCs are then connected in a series stack. The open circuit voltages become 301 mV (54.5% of the initial voltage), 458 mV (75.7% of the initial voltage), 408 mV (59.1% of the initial voltage) and 307 mV (44.1% of the initial voltage) for MFC_1, MFC_2, MFC_3 and MFC_4 respectively. Fig. 8.11 shows the static characteristics of the 4 MFCs when connected in a serial stack under continuous flow 45 L/h. Taking MFC_1 as an example, the initial open circuit voltage is 552 mV (Fig. 8.4), a voltage drop of 209 mV is caused by increase the internal resistance and charge leakage (Fig. 8.10) and 42 mV is the voltage drop caused by the cross-conduction losses (Fig. 8.11). At a current higher than 1.5 mA, the voltages of MFC_1 and MFC_3 have been reversed. The ratio of maximum achieved power in this case is 23.8%. While a parallel connection of the MFCs offers an efficiency of 22.15%, lower than the efficiency of the serial stack as shown in the Fig. 8.12.

[1] Internal resistances are calculated from the slope of the polarization curve in the linear region

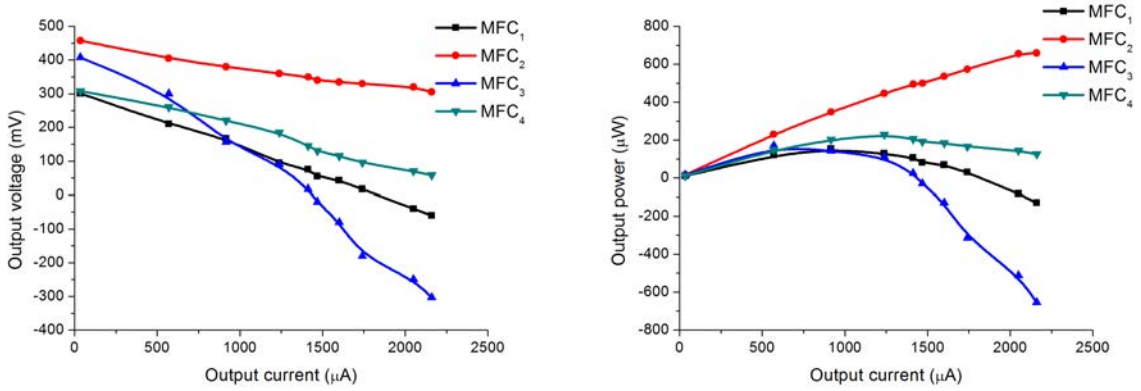

(a) (b)

Figure 8.11: Experimental polarization (a) and (b) power curves for the 4 MFCs serially connected under a hydraulic coupling (45 L/h)

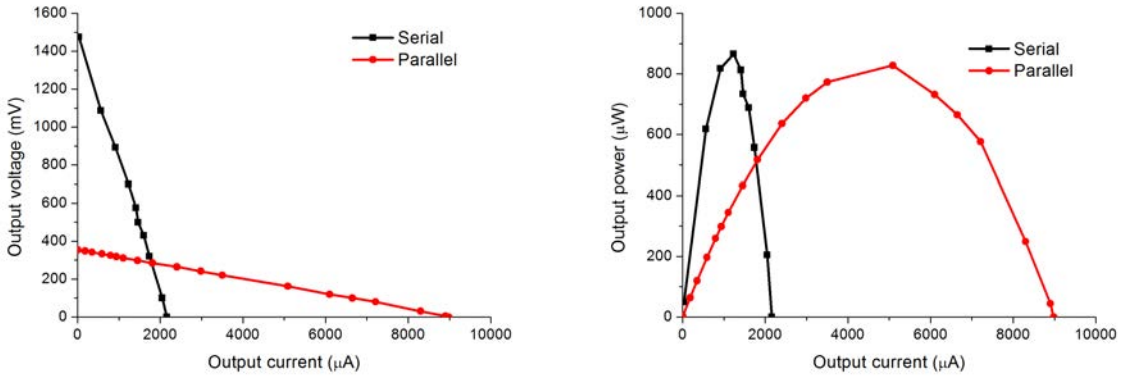

(a) (b)

Figure 8.12: Experimental polarization (a) and (b) power curves for the stack of 4 MFCs connected in series and parallel under a hydraulic coupling (45 L/h)

8.3.2.4 A hydraulically coupled stack without negative effect

From the previous discussion, it can be found that increasing the flow rate increases the losses (the stack under 10 L/h has an efficiency of 68.6% while under 45 L/h it has 23.8%). The flow rate is still decreased until the effect of charge leakage disappeared. The flow rate is measured and it was about 1 L/h. The stack is thus tested under 1 L/h flow rate. The open circuit voltage is 2500 mV and the ratio of maximum achieved power is 76.8% as shown in Fig. 8.13. The performance of the stack with a flow rate of 1 L/h is almost equal in performance to the stack hydraulically insulated. A stack with a flow rate of 1 L/h can benefit from the continuous flow of the organic matter without a negative effect on the performance.

The total efficiency can be improved by compensating the non-uniformities between the connected MFCs. This issue was studied in chapter 7. It was found that adding voltage balancing circuit to the serial stack, especially the switched-capacitor circuit, can improve significantly the efficiency. The application of this circuit has been tested, an efficiency of 91.3% has been achieved. Fig. 8.14 presents the characteristics of the stack with SC balancing circuit.

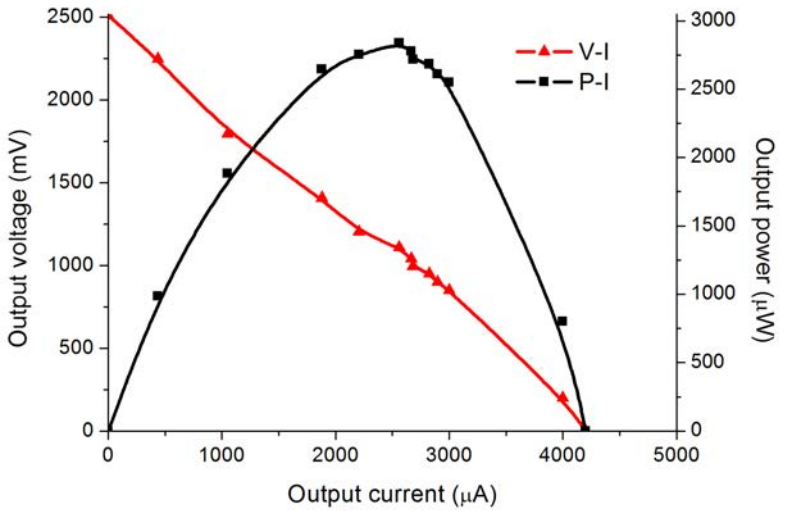

Figure 8.13: Experimental polarization and power curves for the stack of 4 MFCs connected in series under hydraulic coupling (1 L/h)

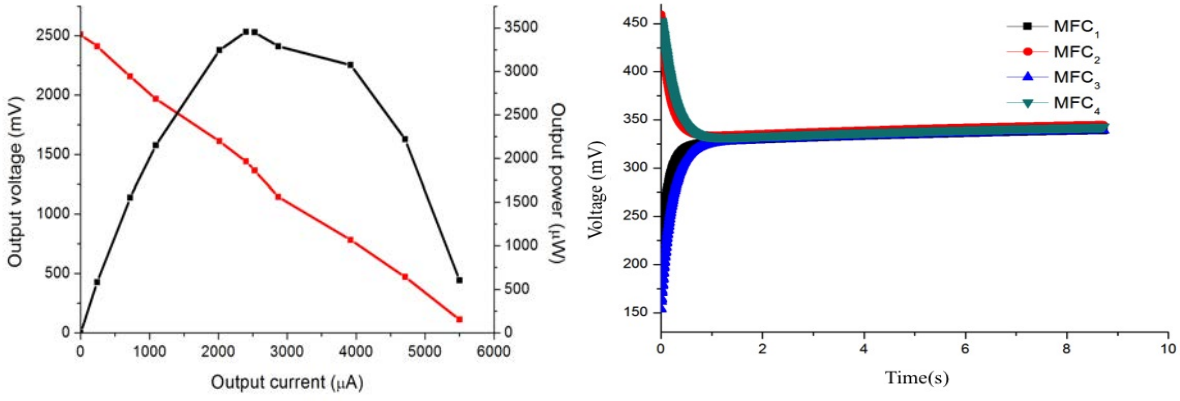

(a) (b)

Figure 8.14: Experimental polarization and power curves for the stack of 4 MFCs connected in series with the application of SC voltage balancing circuit under hydraulic couplings (1 L/h) (a), the voltage of the 4 MFCs in the stack (b)

The flyback converter, studied in chapter 6, is then connected to MFCs as shown in Fig. 8.15. The polarization and power curves at the output of the converter are presented in Fig. 8.16. The converter achieves 22.1 V in open circuit conditions and 4.46 V at MPP for a load of 7 kΩ. The experimental ratio of maximum achieved power is 78.16%.

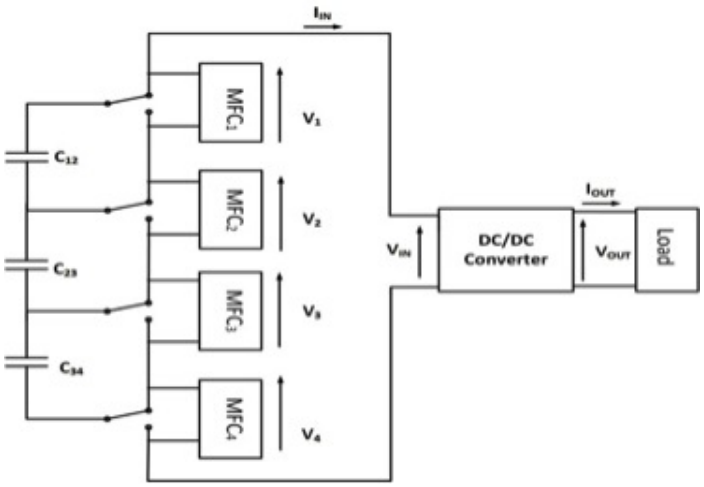

Figure 8.15: Schematic of the SC circuit and the converter applied to the stack of 4 serially-connected MFCs (hydraulic connections are not presented)

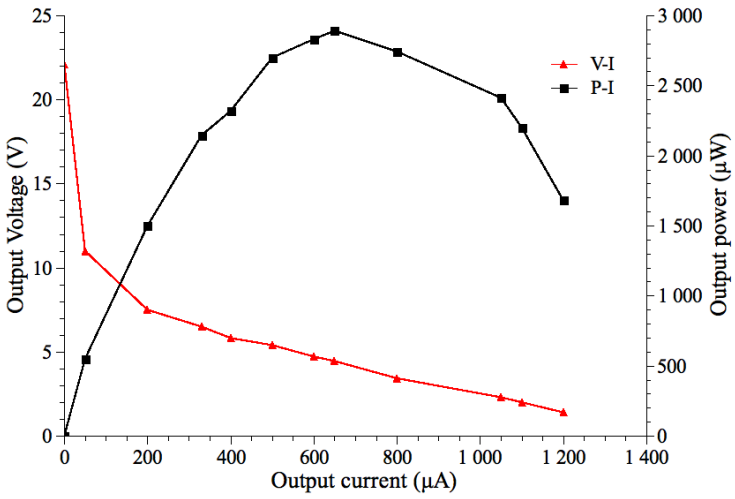

Figure 8.16: Experimental polarization and power curves for the stack of 4 MFCs connected in series under a hydraulic coupling (1 L/h) with the application of SC voltage balancing circuit and the flyback converter

8.4 Conclusion

Operating MFCs in a batch mode is critical because it is facing limitations like the substrate concentration. This problem can be solved by assuring a continuous flow of organic matters in the MFCs. The effect of the hydraulic coupling is investigated on a stack of non-uniform MFCs. The system was studied under different values of flow rate. With a medium value of flow rate (10 L/h), a drop in the open circuit voltage is observed for each MFC even if the MFCs were electrically isolated. Connecting the MFCs in series creates an additional drop caused by substrate cross-conduction effects. These losses increase as the flow rate increases. This can be explained by a charge leakage caused by the flow through the cathode against the proton flow. The oxygen leakage, with the flow, from the cathode to the anode can increase these losses. The oxygen in this case acts as an electron acceptor for microorganisms instead of the anode. A flow rate of 1 L/h is a threshold value to this phenomenon. A balancing circuit is still required to compensate the effect of non-uniformities in the serial stack. Applying the voltage balancing circuit and the flyback converter on the stack of MFCs under a flow rate of 1 L/h presents the most efficient energy harvesting system.

Part III

Field applications of microbial fuel cells

Chapter 9

Literature review

Contents

The energy produced by MFCs can be used in many domains. MFCs can be used as alternative electrical source to supply low power electronic systems. In wastewater treatment, they were considered to be used for treating wastewater. Producing hydrogen instead of electricity is also possible using MFCs. MFCs could be used as biosensor to measure the biological oxygen demand.

9.1 Electricity generation

Electricity generation from biofuel cells is a novel additional solution to existing energy harvesting potential. Chemical energy of the biomass can be converted directly by the oxidization of molecules into electrical energy [Rao JR Richter GJ, 1976]. Research on biofuel cells in the last 20 years has been oriented on "green" electricity production from natural substrates. A photosynthetic bioelectrochemical cell was constructed in [Tsujimura et al., 2001]. The maximum electrical power was about 0.3–0.4 W/m^2 of electrode surface. The efficiency of the light energy conversion was 2–2.5%. Power densities of about 0.7 W/m^2 are published in [Park DH, 2003] using a Mn^{4+}-graphite anode and a Fe^{3+} -graphite cathode and activated sludge fed with glucose in a one-compartment fuel cell. The output current was 14 mA, 0.45 V potential, 1.75 mA/m^2 current density. A comparison between two-compartment and one-compartment fuel cells showed that the electricity produced in the last one is higher for the same value of voltage. Four cells were connected into one block and tested in [Korneel Rabaey, 2003] with plain graphite electrodes (Morgan). The system was tested with different loading rates from 1.5 to 3.5

g/L of glucose. A coulombic efficiency up to 89% occurred for 0.5 g/L loading rate at powers up to 3.6 W/m^{2}of electrode surface which is a five fold higher than reported. In [Rosenbaum M, 2006], it has been reported current densities up to 6 mA/cm^2 at 0.2 V oxidation potential and 97% coulombic efficiency.

These developments on microbial fuel cells show that MFCs energy production is still low. However this energy may be sufficient to supply low-power consuming applications such as wireless sensors. Powering applications with a higher consummation from the output power of MFCs is possible by storage in capacitor bank acting as energy accumulators. The system then can be able to intermittently supply the application. [Ieropoulos I, 2003] used a bank of six capacitors for powering his first biologically inspired robot EcoBot I. The energy produced by eight MFCs was stored in these capacitors to power the robot. A 0.816F (120 x 6800μF electrolytic capacitors 6.3V) was used in the same way for supplying EcoBot III. The first demonstration of a MFC as a viable power source has been studied by [Tender et al., 2008]. MFCs are used to supply a meteorological buoy with an average power consumption of 18 mW. They employed two benthic microbial fuel cells with 24 mW (230 kg, 1.3 m^3) and 36 mW (16 kg, 0.03 m^3) to supply the buoy although it is not practical solution due to high cost implementation and significant weight. An intermittently supply of a wireless sensor of 2.5 W has been realized by a complex power management system supplied by a single sediment MFC (S-MFC) producing 3.4 mW average continuous power [Donovan et al., 2011]. Electric energy has been extracted from the SMFC, stored in a high-capacity ultracapacitor (100 F) and used to power a wireless sensor in [Zhang et al., 2011]. A power management unit consists of a charge pump and a DC/DC converter in this study. Power management system with two DC/DC converters to continuously power an underwater hydrophone from a sediment microbial fuel cell was studied in [Donovan et al., 233]. Powering a wireless sensor for several hours from a sediment-MFC was also reported in [Yohann R.J. Thomas, 2013]. After set-up of the experiments, the system was able to supply the sensor continuously for 100 min. After 100 min, the output energy was not enough to maintain the output voltage. However the intermittent operation was still possible for 15 h.

Other researches showed that the MFCs can be implanted in a human body to deliver continuing and protective power for implantable medical devices (IMDs). Several researches reported that glucose fuel cells are the most important cells to implantable application. An important research in the United States sponsored by Artificial Heart Program of the United States National Heart and Lung Institute, studied the feasibility of powering an artificial heart (4.5 W) from an implantable glucose fuel cell based on the reaction of glucose to gluconic acid [Appleby and Wolfson, 1973]. A microbial fuel cell (MFC) was adapted to be implanted in a human transverse colon [Patil, 2013]. After a couple of months, the MFC had 550 mV at open circuit voltage condition and 72.3 mW.m^{-2} maximum power density without a notable impact on human body.

9.2 Wastewater treatment

Huge amount of wastewater from starch, industrial and agriculture operations are produced annually. Although the wastewater treatment plants are large consumers of energy, required for the operation, the energy potential contained in wastewater exceeds by many folds the energy used to treat it. Some Wastewater Treatment Plants WWTPs produce the total energy they need to operate. A research in the United States showed that the annual costs of treatment of the household wastewater (46 trillion liters) is $25 billion and the electricity required constitutes 1.5% of the electricity used by the nation [DC, 2005]. Logan has reported that the U.S. household wastewater produced in one year contains 0.11, 0.3 and 0.1 quad (short for "quadrillion British thermal units") organic matter, animal wastes, and food processing respectively [Logan, 2004a]. While the electricity required by wastewater treatment is 0.6 quad. Therefore the energy produced by the WWTP could be enough to supply these stations [AGENCY, 2013, Logan, 2004a]. Microbial fuel cells offer the possibility for the conversion of wastewater organic materials into electricity by the metabolism of bacteria. A high efficiency can be obtained by MFCs in WWTPs using wastewater rich in organic matters such as sanitary wastes, food processing wastewater, swine wastewater and corn stover [Yang et al., 2013, Zuo et al., 2006]. For continuous electricity production from WWTP, the MFC must have a large surface area for biofilm formation. High concentrations of particles in the wastewater may cause clogging in the reactor. However that can be avoided by high porous reactors [Cheng et al., 2006a]. Thus a two-compartment design is difficult to apply in wastewater. A single chamber MFC is more adapted to both energy harvesting and continuously water treatment. Lui et al. presented the first demonstration for energy harvesting in WWTP by suing a single chamber microbial fuel cell SCMFC consisted of a single cylindrical chamber (388 mL) containing eight anode placed in a concentric arrangement about a single cathode [Liu and Ramnarayanan, 2004]. The MFC was fed with domestic wastewater to produce 25 mW/m^2 with 0.23 V at MPP. A Multiple Anode/Cathode Granular Activated Carbon Microbial Fuel Cell configuration (MAC-GACMFC) in continuous flow mode at a wastewater treatment plant using municipal wastewater as the substrate was developed in [liB2011]. The reactor was constructed with many anodes (graphite rods) and cathodes (carbon cloth) with different configurations. A power density of 750 mW/m^2 was obtained. Energy harvesting in WWTP by MFCs could be illustrated in Fig. 9.1 [Li et al., 2014].

9.3 Biohydrogen

Hydrogen has been considered to be a good alternative source of energy for other forms of fuels (fossil fuel) since the 1970s. Hydrogen has the highest energy potential of any common fuel by weight. About half of current hydrogen production is derived from fossil fuel (natural gas, coal, heavy oils) and from water by electrolysis or steam reforming [Balat and KÄśrtay, 2010]. Steam reforming is based on separated hydrogen atoms from carbon atoms in methane. While electrolysis involves applying an electric current through water to separate water into hydrogen and oxygen. Hydrogen can be also produced

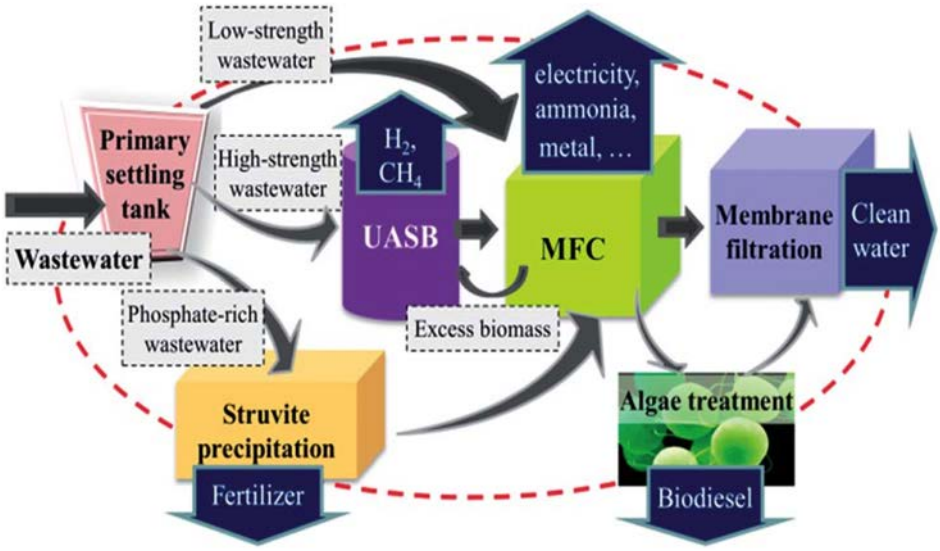

Figure 9.1: Process flow of a hypothetical MFC-centered hybrid process for wastewater [Li et al., 2014].

from biomass rich in carbohydrates by biological fermentation [Oh and Logan, 2005]. For example the fermentation of 1 mole of glucose can produce 4 mole of hydrogen as showed by (9.1).

$$C_6H_{12}O_6 + 2H_2O \rightarrow 4H_2 + 2CO_2 + 2C_2H_4O_2 \tag{9.1}$$

Returning to the half-reaction occurring at the anode (9.2), acetate will be oxidized at the anode producing protons and electrons. The electrons travel to the cathode electrode, where normally, in the presence of oxygen, they combine with oxygen and protons to form water as shown in (9.3). The anode potential is $\sim$ -300 mV vs +804 mV for the cathode.

$$C_2H_4O_2 + 2H_2O \rightarrow 2CO_2 + 8e^- + 8H^+ \tag{9.2}$$

$$8H^+ + 2O_2 + 8e^- \rightarrow 4H_2O \tag{9.3}$$

Forming hydrogen in fuel cell requires a potential greater than 410 mV while 1800-2000 mV is needed for water hydrolysis [Levin et al., 2004]. Producing hydrogen at the cathode of MFC, in the absence of oxygen, is possible by applying an external voltage greater than 110 mV, in practice voltages higher

than 250 mV are required due to overpotential at the electrode [HONG LIU, 2005]. In this way, we can generate hydrogen from the protons and the electrons from organic matter as shown in9.4.

$$8H^+ + 8e^- \rightarrow 4H_2 \tag{9.4}$$

The advantage of hydrogen production in this way is that the microbial fuel cell provides a renewable source for hydrogen production from the organic matter. In addition, it reduces the energy required to produce hydrogen compared to hydrogen production by other means (0.6 kWh/m^3 of hydrogen from the microbial oxidation against 4.5-5 kWh/m^3 form water electrolysis) [HONG LIU, 2005]. Virtually any type of biodegradable organic matter could be used to produce hydrogen in a MFC. Implanting MFCs in a WWTP may produce hydrogen with wastewater treatment to help offset the costs of wastewater treatment as well as provide a contribution in the hydrogen production field or produce the required electricity for water treatment.

9.4 Biosensor

A biosensor is a device that combines microorganisms with a transducer to produce a measurable signal such as current or potential proportional to the substrate concentration in fields as diverse as environmental monitoring, defense, food processing and safety. Many transducers could be used as biosensors such as Bioluminescence [Rensing C, 2003] and Fluorescence [KARUBE and WILSON, 1992]. In these biosensors, the emission of bioluminescence and fluorescence is directly proportional to the concentration. MFCs have been widely employed as biosensors for measuring biochemical oxygen demand (BOD) and water toxicity. Biochemical oxygen demand (BOD) is a measure of the content of biodegradable organic matter in water. The linear relationship between the output current density of MFCs and organic carbon content of the wastewater as shown in Fig. 9.2 what makes MFCs work as BOD biosensors [Chang et al., 2004, Peixoto et al., 2011]. A MFC-based BOD biosensor has many advantages over other types of BOD biosensors. They have a long-term stability, high reproducibility, fast response, good sensitivity and wide linear range [Dai and Choi, 2013]. MFC biosensors suffer from the low sensitivity because of the low power generated by MFCs. An MFC with voltage input of 0.2 V was used to overcome these limitations and to obtain maximum current generation [Modin and Wilén, 2012].

9.5 Conclusion

MFCs have shown great potential as a novel energy harvesting technology that can provide cheap, consistent, maintenance-free and stable power for long periods of time. Despite the low power densities of MFCs, the energy can be employed in many fields such as medical, communication, environment, detecting and monitoring. Implanted medical devices are a major application of the MFC using glucose in

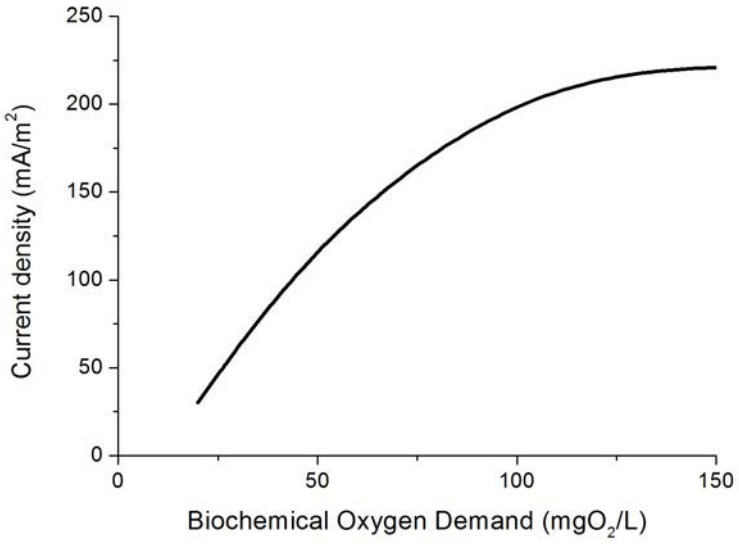

Figure 9.2: Current density generation in the MFC-based BOD biosensor as a function of initial BOD concentration [Peixoto et al., 2011]

human body and oxygen from blood to supply biomedical devices, reducing the need for routine surgery for the replacement of batteries. The ability to convert organic substrates into electricity and the linear relationship between the output current of MFCs and organic carbon content of the wastewater makes possible to use microbial fuel cells (MFCs) as a transducer in biosensors to measure concentrations. An application of energy harvesting from MFCs for powering a sensor will be presented in the next chapter.

Chapter 10

MFC as power supply of a low-power sensor

Contents

In this part, we will exploit the available energy in MFC for powering a practical application. The application could be a low-power consuming system or a storage system (ex. supercapacitor). Practically these applications require voltages higher than the output voltage of MFC. Powering an application requires first an analytical study of the behavior of this application and the study its consumption. In this section, a temperature sensor is used to be powered by MFC.

10.1 The sensor

Monitoring the natural systems (measuring PH, temperature…etc.) in remote locations (desert, under sea) where there is no suitable continuous power source is a challenge. A sensor network consists of spatially distributed sensors to monitor physical or environmental conditions and to cooperatively transit their data through a server to a main location. These can be used in a number of applications such as environmental monitoring (e.g. fire detection, air pollution monitoring, temperature monitoring), industrial monitoring (e.g. health monitoring system) or agricultural monitoring (e.g. sun exposition, humidity monitoring). Each system has typically several parts: one or several sensors, an energy source,

a power management circuit to interface the energy source and data transmission system. Usually one or more batteries are used to supply this system. Besides these batteries have limited life-time, they are made from a variety of chemicals to power their reactions. Some of these chemicals, such as nickel and cadmium, are extremely toxic and can cause damage the environment. A solution for powering these systems is to use natural energy. A large number of transducers are proposed as an alternative to batteries: solar, thermal, vibrational or electromagnetic transducers [Roundy et al., 2004]. MFC can be also an alternative energy source for powering a monitoring system, particularly in areas where it is difficult to access the system to replace batteries (river or deep-water).

An example of these systems is temperature sensor ‘‘Temp101A Data Logger, MadgeTech, Inc., Contoocook, NH, USA). The sensor is to be powered by 3.6 V lithium battery. Energy requirement of the sensor for normal operation, after start up, is around 0.9 mJ for one data processing cycle. This power can be supplied by one MFC. While it requires around 120 mJ at start-up, what can't be delivered by one MFC. At start-up the sensor consumes more than 2 mA to be compared with some hundreds µA in steady state. A power management unit is therefore required to step-up the voltage and assure the start-up of the sensor. Powering the sensor by multiple MFCs associated in series appears as a good solution. Generally during the experiments, large dispersions in electrical characteristics were noted even if MFCs were constructed in the same conditions. Serial association of a number of non-uniform MFCs presents several issues. First the hydraulic couplings when MFCs are sharing the same electrolyte, result in a poor energy recovery [Zhuang and Zhou, 2009]. A parasitic current flow in the parasitic fuel cell composed by the cathode of a first cell and the anode of a second one and through the electrolyte, causes a voltage loss in the stack. Increasing the distance between the fluidically linked MFCs may avoid the cross conduction problem [Kim et al., 2012, Winfield et al., 2011]. A twin-cell was built by joining two tubular MFCs connected with a 20 cm rubber tube (internal diameter= 0.3 cm): there was no voltage loss [Zhuang and Zhou, 2009]. The dispersions between generators lead to non-optimal stack efficiency because the associated cells are crossed by the same current and are not able to operate at Maximum Power Point (MPP). The weakest cell could suffer from voltage inversion and absorb the energy instead of producing it as detailed in chapter 7. Voltage balancing circuit has been introduced to avoid this phenomenon as discussed previously. In the following section, a commercially-available power management unit will be used to supply continuously the sensor in the first experiment. In the second one, the flyback converter will be tested to supply the sensor from one MFC.

10.2 Source

In this experiment, 2-single chambered MFC are used. The MFCs were previously used in our experiments; the biofilm was already developed. The MFCs are inoculated with wastewater treatment plant located in LIMONEST. The initial output voltages were about 150 mV. MFCs are then fed with 0.7 g of sodium acetate (1g of acetate/liter), (Sodium acetate, Sigma-Aldrich Chimie S.a.r.l, $C_2H_3NaO_2$, 82.03

g/mol, PN 71183). MFCs were connected to a load of 1 MΩ. After one hour, voltage steps were observed. After about one day, the output voltages reached their maximum and stable values. Figure 10.1 shows polarization and power curves of the 2 MFCs. MFC_1 and MFC_2 have 0.934V and 0.785 V open circuit voltage respectively and 1152 µW and 1108 µW output power at MPP respectively. These results show that the output voltage at the maximum power point is about 50% of the open circuit voltage. The dispersion between the two MFCs is explained by the non-uniform manufacturing process or microbial heterogeneities during inoculation and finally difference in microbial activities.

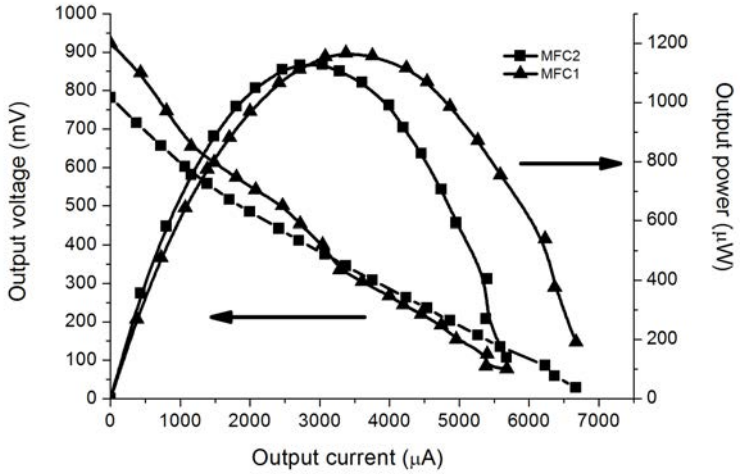

Figure 10.1: Polarization and power curves for MFC_1 and MFC_2

10.3 Converter

Energy harvested from a single MFC or a stack of connected MFCs requires a power management unit to step-up the low voltage to acceptable voltage levels and to control the operating point. A power management unit (PMU) used with a microbial fuel cell meets several design challenges. The main drawback of semiconductor technologies (generally CMOS for low-power applications) is that the required supply voltage is above the operation voltage of a MFC (300-500 mV). Many commercial converters with a start-up voltage suitable for MFCs and good efficiency such as TPS61200, appear promising for energy harvesting from MFCs. The issue with these converters is that when the voltage of MFC reaches the required start-up voltage, the consumed current exceeds what the MFC can supply. Consequently the output voltage of MFC drops and it will not be able to start-up the converter.

A low power DC/DC boost converter (3x3 mm^2) from Texas Instruments (bq25504) appears as a good PMU for this application. It has a low start-up voltage (330 mV) and once started, it continues to operate down to V_{IN} = 80 mV. It features a high efficiency around 85% at 100 µW of input power.

An input voltage regulation prevents the collapse of the MFC output voltage. The converter output voltage can be programed according to the sensor requirements. An adjustable integrated dynamic MPPT permits an optimal energy capture. It is adjusted to 50% of the MFC open circuit voltage (Fig. 10.1). The converter was realized on a 5x4 cm^2 PCB as shown in Fig. 10.2. The sampling ratio of the open circuit voltage for the control of MPP was externally programmed using a resistive division ratio of 0.5 connected to the pin VOC_SAMP. The converter was tested with a simple electrical model of MFC, i.e. a DC voltage source serially connected with a resistance according to the internal impedance of the MFC. Figure 10.3 presents input and output voltage and efficiency of the converter bq25504 for different load. The converter presents a satisfying efficiency higher than 80%.

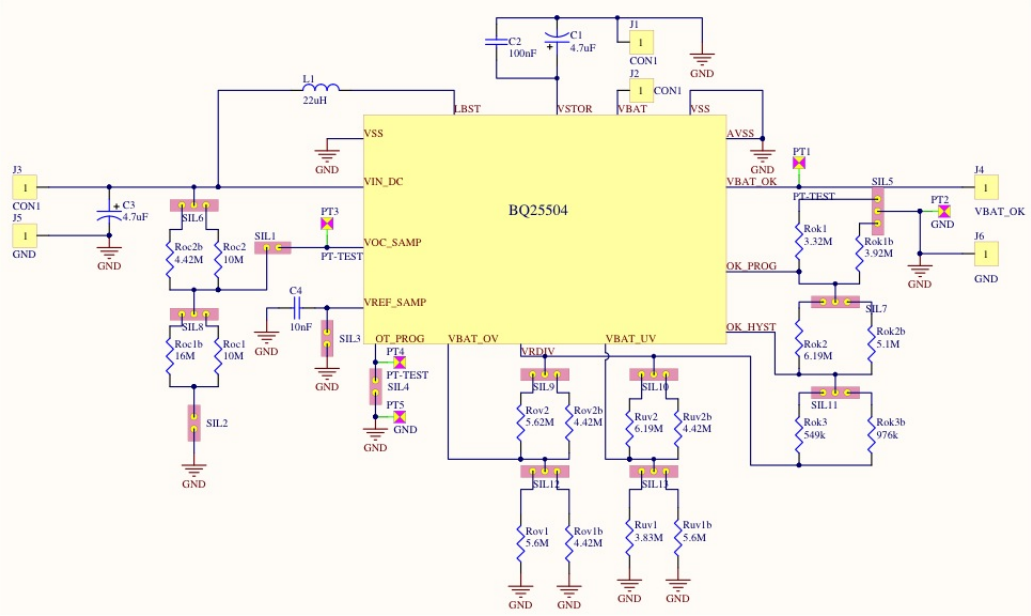

Figure 10.2: Schematic of the converter bq25504

The custom-designed power management system consists of capacitors and a DC/DC converter (bq25504) as shown in 10.4. A capacitor C_1 is connected directly to MFC_1 to filter the output voltage fluctuation. This system will not be able to start-up the sensor. A second capacitor at the output of the converter is required to store the required energy for the sensor start-up. The capacitor has to insure that the voltage at the end of the sensor start- up is higher than 3.17 V. This capacitor C_2 can be evaluated as detailed in (10.1).

$$W_s = \frac{1}{2} C_2 (V_{reg}^2 - V_d^2) \tag{10.1}$$

Where W_s is the sensor start-up energy, V_{reg} is the regulated output voltage of the DC/DC converter and V_d is the minimum voltage at the end of the start-up operation.

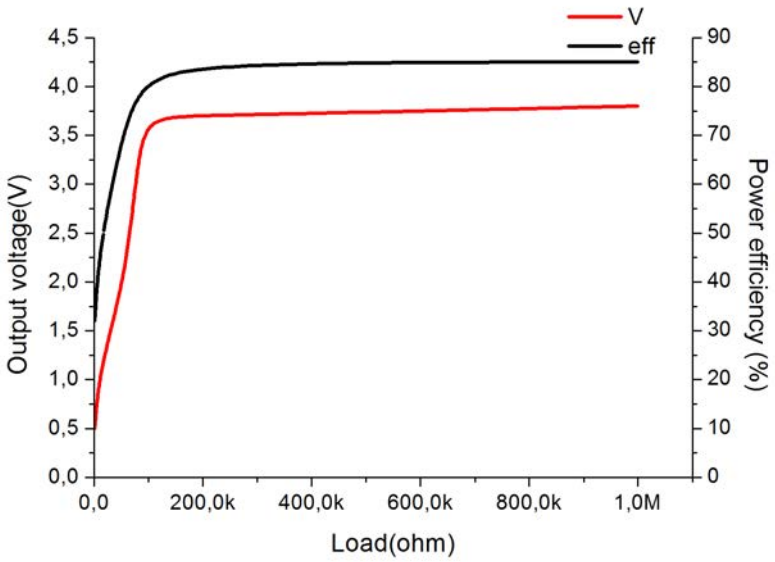

Figure 10.3: Characteristics of the source with bq25504 associated to an ideal MFC

A capacitor of 68 mF is able to store the necessary energy and assure the start-up of the sensor without decreasing the voltage below 3.17 V at the end of start-up. The MFC needs slightly less than 10 min to charge capacitor C_2 to 3.6 V. During start-up, the voltage of capacitor C_2 decreases from 3.6 V to 3.2 V and the voltage is regulated again later to 3.6 V as shown in Fig. 10.5.

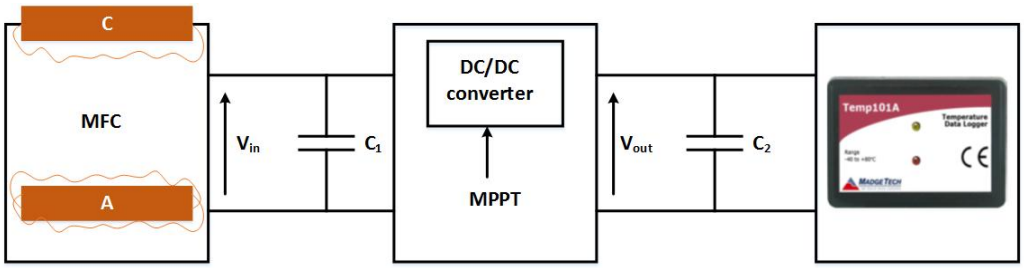

Figure 10.4: Schematic of a simple power management system with one MFC

10.4 Proposed solutions for powering the sensor

10.4.1 MFCs in battery-mode

In this case, each reactor is filled with wastewater and fed with acetate and closed. There is no hydraulic coupling between MFCs.

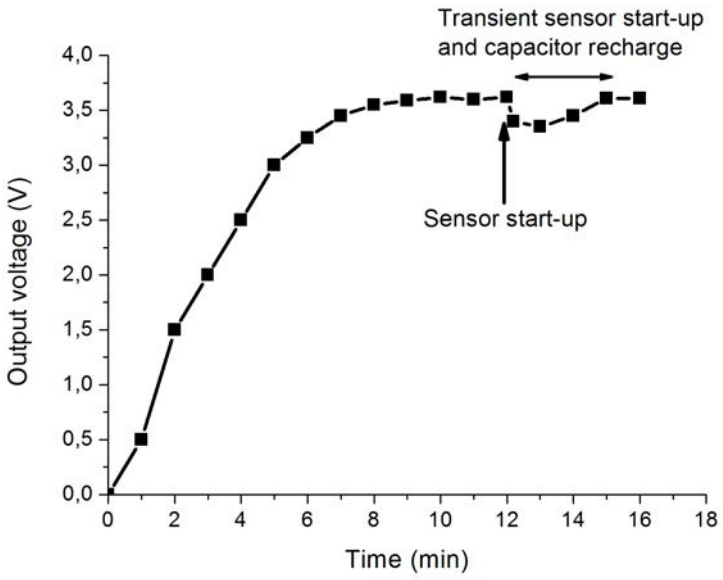

Figure 10.5: Voltage of output capacitor C_2

In the first experiment, MFC_1 is connected to the converter to power the sensor. Figure 10.6 presents the voltage of MFC_1 during data recording (Vin), the converter output voltage (Vout) and the measured data from the sensor T(°C). MFC_1 was able to power the sensor for 2 days. After 10 hours of operation, the converter output voltage starts to decrease slowly. After 40 hours, the output voltage reaches 3.5 V for 520 mV of input voltage. After that MFC_1 voltage decreases to 230 mV at 53 hours of operation and the DC/DC converter output voltage crosses the threshold voltage of 3.17 V when the sensor stops to operate. Therefore MFC_1 is disconnected of the converter and MFC_2 is connected. During switching time, capacitor C_2 can supply the sensor. MFC_1 voltage can increases rapidly again to reach 750 mV after 5 hours while MFC_2 gives the necessary energy to the sensor. MFC_2 is also capable to power the system for almost the same period as MFC_1. Figure 10.6 presents the voltage of MFC_2 during data recording (Vin), the converter output voltage (Vout) and the measured data T(°C).

Considering that the maximum electrical energy accessible with the MFC is about 2 kJ/g of acetate, the energy conversion efficiency in this experiment is unfortunately less than 5% seen from the sensor operation. That means 95% of available energy from 1 g of acetate could not be extracted during one cycle of operation. This energy is in fact not consumed and can be extracted after a relaxing time is offered to MFCs.

A continuous powering could be achieved by alternatively connect the MFCs (MFC_1 and MFC_2) as shown in Fig. 10.7. One MFC supplies the sensor for 2 days while the second MFC is in the relaxing mode. Manual switching is used in this test every 2 days up to 20 days. A decrease in the MFC voltage was noted at the end of this period of 20 days. Voltages of MFC_1 and MFC_2 are 420 mV and 515 mV respectively at the end of the last relaxing time. MFC voltage is therefore no longer able to reach its

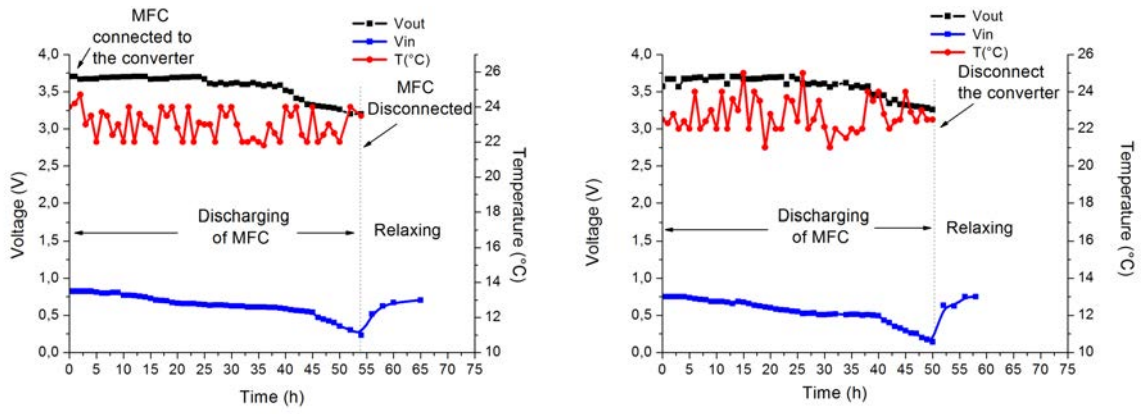

Figure 10.6: Voltages waveforms during data recording for 2 days (discharging) and relaxing time (recharging) when the sensor is powering by MFC_1 (a) and by MFC_2 (b)

initial voltage at the end of the relaxing time. In addition, when connected to the sensor, MFCs voltages drop more quickly. The output voltage of the converter therefore could no more exceed 3 V. This may be explained by a lack of fuel in MFCs. The MFCs were thus recharged by 1g/L of acetate at the end of experiments. The open-circuit voltage of MFC_1 and MFC_2 reach again 0.8 V and 0.77 V respectively. The converter output voltage comes back to 3.5 V. Figure 10.8 presents the evolution of input converter voltage (Vin: voltage of connected MFC), its output voltage (Vout) and the voltage during relaxing time (Vr). In this operation the extracted energy is about 50% of the original available energy in the MFC. Figure 10.9 presents a picture for the complete system and the recorded temperature by the sensor during the experiment period.

10.4.2 Continuous mode

Practically, these applications can be employed in wastewater treatment planet for measuring PH or temperature. In this case, MFCs work under a continuous-flow mode that assures a continuous substrate feed.

In lab-scale experiments, to build a continuous-flow mode system, a hydraulic connection mode of the twin-cell was realized using a peristaltic pump (Watson-Marlow Pumps Group, France). An individual recirculation loop for substrate feed and discharge was used as presented in Fig. 10.10. A flow rate of 10 mL/min of the substrate (containing 1g of sodium acetate per liter), corresponding to a hydraulic retention time (HRT) of 1.16 h, was controlled to be continuously fed to the individual MFC. The sensor is then supplied by connecting alternatively 2 MFCs as described previously (each MFC supply the sensor during two days). The system is able to continuously and autonomy supply the sensor. Figure 10.11 presents the evolution of the converter input voltage (Vin), its output voltage (Vout) and the voltage during relaxing time (Vr). MFCs were able to reach their initial voltage levels at the end of

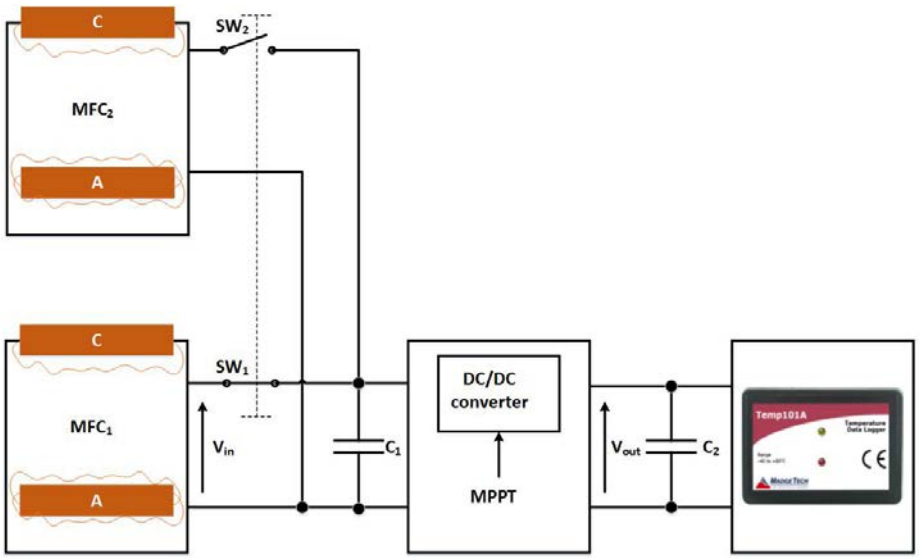

Figure 10.7: Schematic of power management system with 2 MFCs

relaxing time and the voltage at the end of work time is still greater than the shutdown voltage of the converter.

10.5 Powering the sensor with a Flyback converter

The main drawback of the commercial converter is that the input current is important which decreases the MFC output voltage in two days. That may be explained by a non-accurate MPPT operation. However this converter is designed for thermal electric generator (TEG) energy harvesting. The non-immediate mechanisms in the MFC are clearly shown in the output voltage during relaxing time. When the MFC is disconnected from the converter, the voltage takes some times to reach again the open circuit value. To prove the latter fact, MFC_2 was connected to a load of 140 Ω for 600s (equal to the internal resistance of MFC_2) after that the load was disconnected. The output voltage across the load was recorded using a TEKTRONIX oscilloscope. Figure 10.12-a shows the voltage of MFC_2 when it is connected to a load of 140 Ω and the evolution of this voltage after disconnected the load. The output voltage across the connected load decreases slightly from the open circuit voltage to a steady-state operation voltage (370 mV). When the load is disconnected, the output voltage increases slowly to reach 95% of the open circuit voltage value after 25 min. The maximum power point tracking implemented in the PMU circuit disables the converter for 256 ms to measure a new voltage value of reference. This time is thus too small compared to the MFC dynamics. Furthermore the sampled voltage reference is refreshed each 16 s while no change in the characteristics of the MFC will occur during this short time. This creates more losses in the circuit for no benefit from MPPT point-of-view. This test was realized by disconnecting the MFC from the load every 16 s for a short time (almost 300 ms). The measured “output voltage” equals

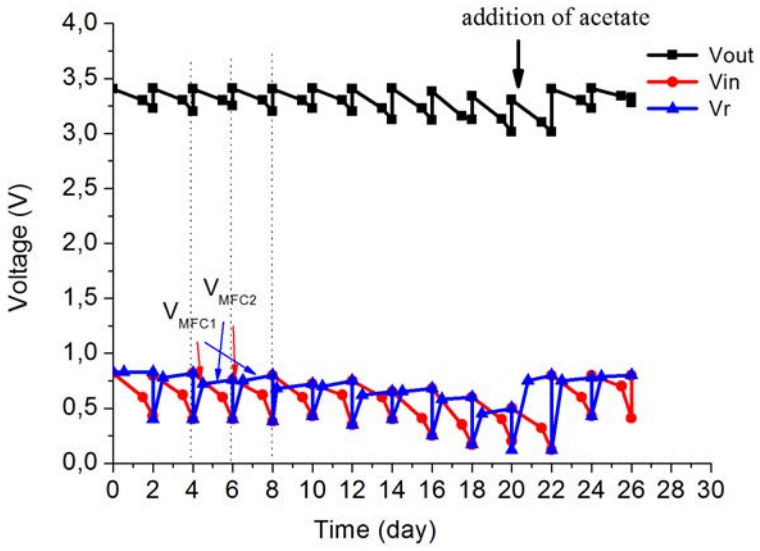

Figure 10.8: Voltages waveforms during data recording by switching MFC_1 and MFC_2

420 mV (Fig. 10.12-b), what means that the measured "open-circuit voltage" is in fact equal to 53% of the real open-circuit value. The commercial circuit is not adapted for MPPT issue for energy harvesting from MFCs.

The flyback converter, described in chapter 6, is designed and optimized for energy harvesting from MFCs. A MPPT method is implemented in this converter by adapting the input impedance of the converter. The converter was tested with MFCs and the efficiency was about 72%. This converter could be tested to supply the sensor. One MFC is continuously fed using the peristaltic pump: one channel was used to feed the MFC and another channel to discharge as presented in Fig. 10.13. A flow rate of

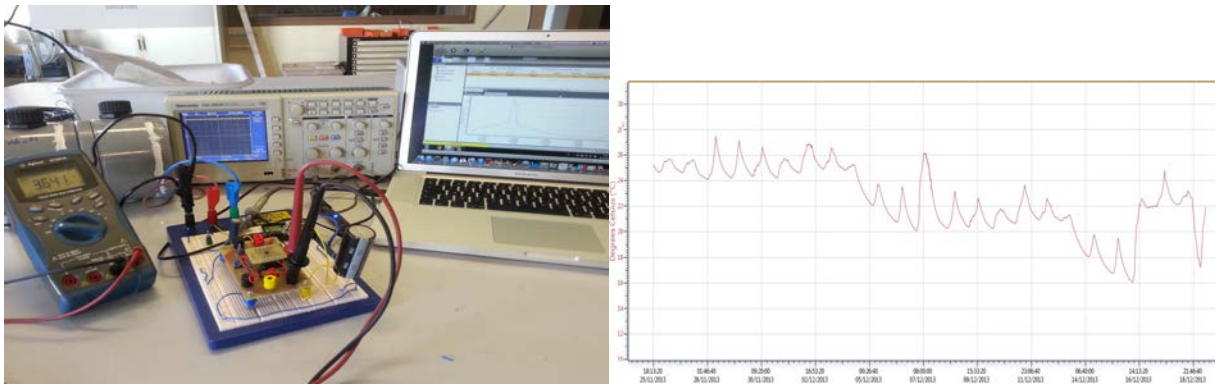

Figure 10.9: Picture for the complete system (left) and the recorded temperature by the sensor during the experiment period (right)

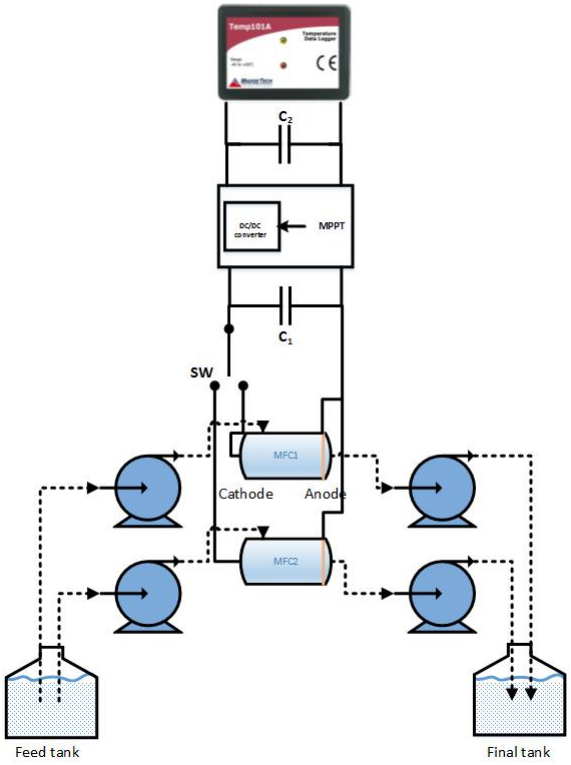

Figure 10.10: Schematic set-up for fluidic and electrical configurations of 2 MFCs for continuous operation

10 mL/min of the substrate (containing 1g of sodium acetate per letter), corresponding to a hydraulic retention time (HRT) of 1.16 h, was controlled to continuously feed the MFC. A super capacitor of 1.5 F (MGC, JAPAN) was connected at the converter output to hide the variation of the input voltage of the sensor. A zener diode 1N5228B was connected in parallel with the super capacitor to protect the sensor against overvoltage. The capacitor takes about 14h to reach 3.3 V and still increases until it reaches 3.6 V after 20h. Fig. 10.14 shows the variation of voltages during data recording. Optimizing the value of this capacitor can decrease the charge time. The converter input voltage varies between 0.43 and 0.48 V what proves that the implemented MPPT achieves a good performance. The impedance matching scheme limits the MFC output current and the converter controls the input voltage to be about 50% of the MFC open- circuit voltage. This system can supply the sensor without any action to switch or to feed the MFC. Comparing the reactor volume with the flow rate proves that the acetate at the output of the MFC fluidic link is not fully consumed. This energy could be harvested by another MFC to increase the total efficiency of the system.

This study can be extended to involve all the monitoring, communication and control systems in WWTP. In a WWTP, the continuous-flow of the organic matter is naturally assured. An example of this application is to replace the energy source for the equipments in the inaccessible areas by the energy pro-

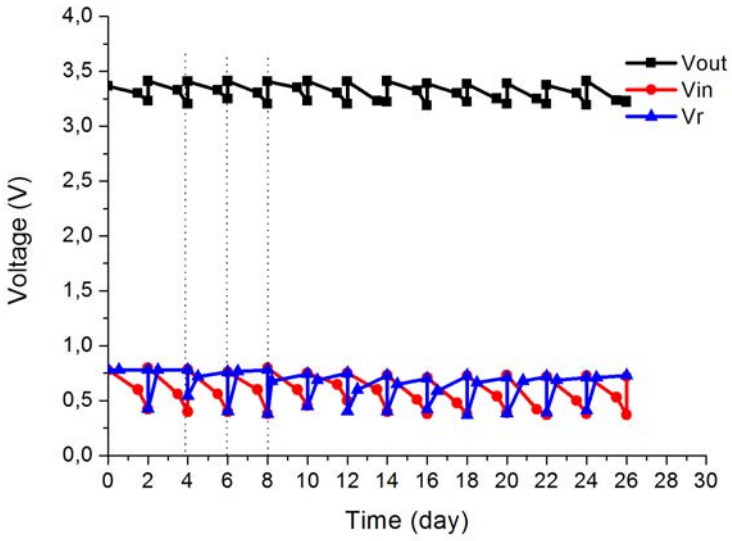

Figure 10.11: Voltages waveforms during data recording by switching MFC_1 and MFC_2 in continuous operation mode

duced by MFCs. These MFCs could be installed near the devices. The advantage is to remove batteries for the battery-powered equipments and to shorten the cables for the externally powered equipments. The output of these systems could be wirelessly transmitted or connected to a data logger. Powering a sensor from the energy of a MFC can be extended to design a system to control the air and water qualities in a WWTP. One sensor, for example RFCO2RHTemp2000A, is to measure air parameters as carbon dioxide, humidity and temperature. Another sensor is to record water pH and temperature (pHTemp2000). A sensor Level1000 is used also to measure water level. The information from these sensors is to be collected by data loggers and transmitted to a remote server that can take actions. The number of MFCs required to supply the system depends on the characteristics of the used MFCs and therefore the volume and the electrode surface. Table 10.1 presents the power consumption of these sensors and the number of MFCs reactors that are required to supply those sensors. A mini-generator of 13 liters composed of 18 MFCs would be sufficient to supply the system that can monitor air quality (CO2, humidity and temperature) and water quality (pH, temperature and water level).

Figures 10.15 and 10.16 represent the possible architectures of the monitoring system supplied by MFCs. There are two possibilities either using a power management unit for each sensor or using one flyback converter with multi-coil secondary transformer. In the two cases, MFCs are serially connected and a voltage balancing circuit is required to compensate for the non-uniformities between the associated MFCs as discussed previously.

Table 10.1: Monitoring system

Devices	Description	Average power	Number of MFCs to associate
RFCO2RHTemp2000A	CO2, humidity and temperature	10 mW	13
pHTemp2000	pH and temperature	1.2 mW	2
Level1000	Water level	2 mW	3
	Total power	13.2 mW	18

10.6 Conclusion

In this chapter, a power management unit including two capacitors and a commercial DC/DC converter was presented to supply a temperature sensor. The converter was realized and tested. One MFC with a power of 1.5 mW/L/g of acetate was able to supply continuously the sensor and the data has been recorded for two days. After this period, the MFC appears as discharged but in fact is not. A minimum relaxing time of 5 hours is required for the MFC to recover. A continuous powering was achieved by connecting alternatively two MFCs. Each MFC supplies the sensor for two days while the second one recovers. In this low-cost configuration, the system was able to supply the sensor for 20 days. After that the MFC output voltages decrease significantly. An addition of acetate is required regularly for enrichment of fuel offered to electrochemical microorganisms. A continuous feeding of both cells, as a simulation of a wastewater treatment plant, is realized by using a pump with a flow rate of 10 mL/min. Using a converter with non-adapted MPPT leads to a non-optimal energy harvesting from MFCs. An MPPT algorithm based on the impedance matching was integrated in the DCM flyback converter. The system is tested with one MFC in a continuous flow mode. The converter with the implemented MPPT achieves good performances to power the sensor from one MFC. In this way the system insures a continuous and autonomous operation of the sensor.

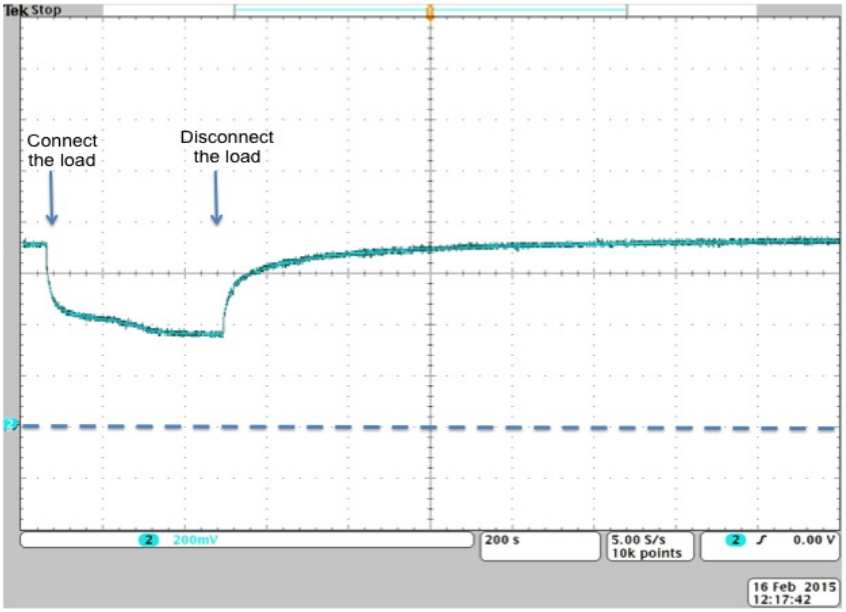

(a)

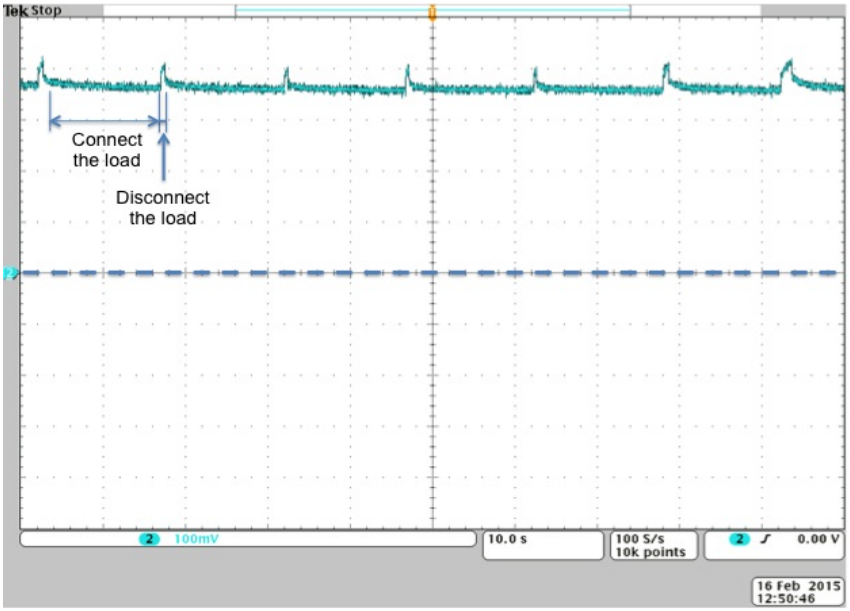

(b)

Figure 10.12: Output voltage of MFC_2 when it is connected and disconnected to a load of 140 Ω (a) and during MPPT operation (b)

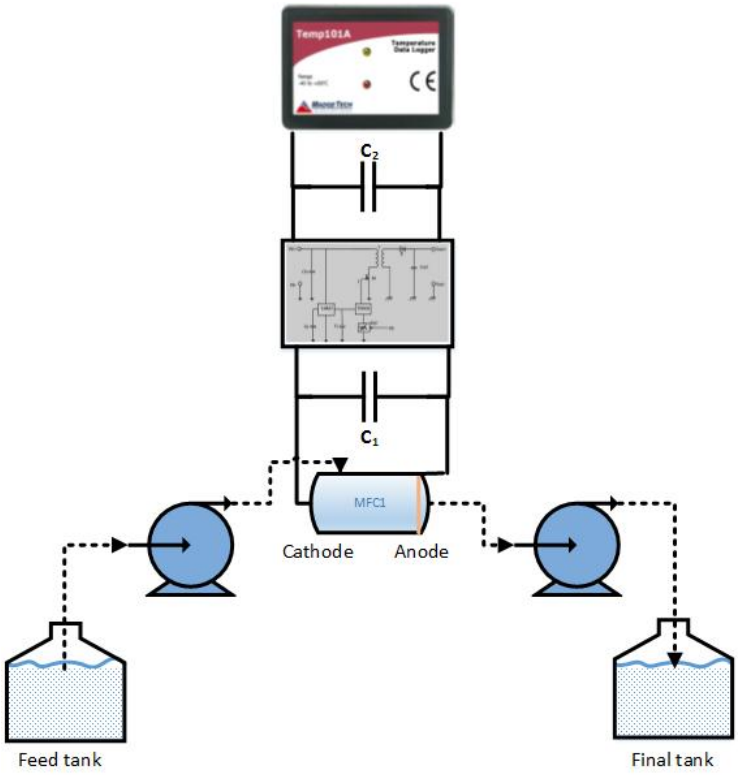

Figure 10.13: Schematic of the set-up for fluidic and electrical configurations of one MFC to power the sensor through a flyback converter

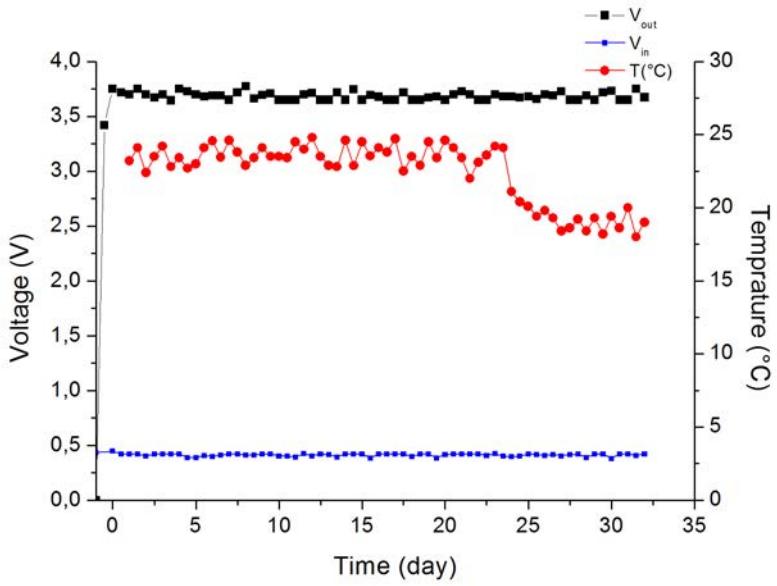

Figure 10.14: Voltages waveforms during data recording when the sensor is powered by MFC_1 through the flyback converter

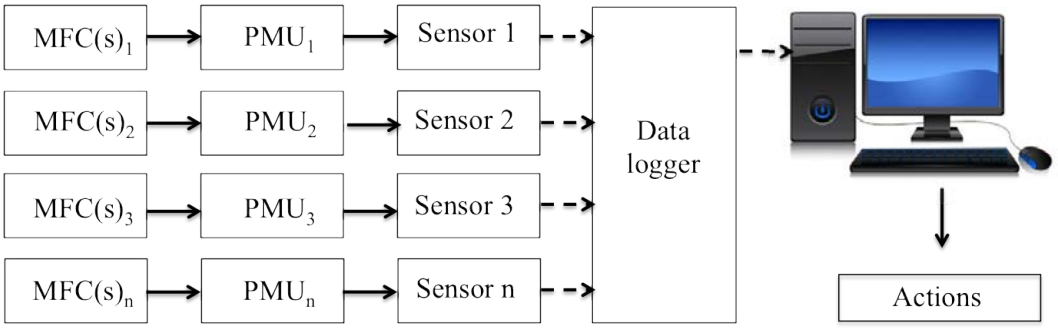

Figure 10.15: MFCs-powered monitoring system- topology 1

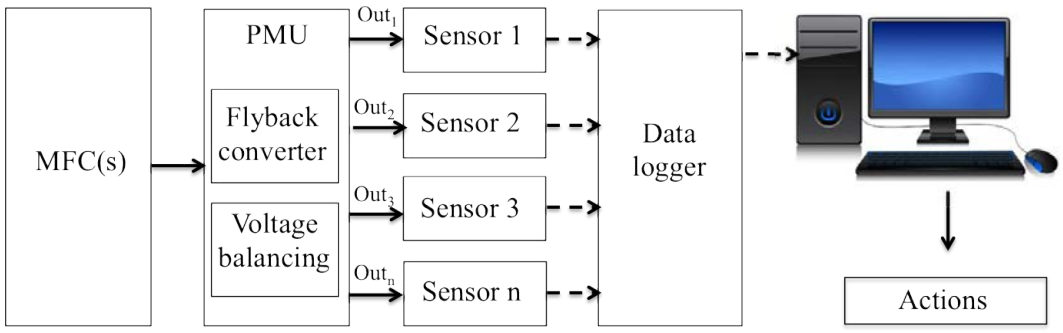

Figure 10.16: MFCs-powered monitoring system- topology 2

Chapter 11

General conclusions and perspectives

Contents

11.1 General conclusion

Large-scale ambient energy (e.g. solar, wind) is widely available and is to be efficiently captured and used. Besides, energy harvesting from naturally 'wasted' energy may be useful for recovering even a small fraction of the energy demand. That would have a significant economic and environmental impact.

This thesis focussed on energy harvesting from MFCs to supply low power systems from local sources where organic matters are available (i.e. local wastewater treatment plant). The available energy can be used for powering wireless sensor networks. In order to achieve this objective, several contributions to energy harvesting research from MFCs are made in this work and presented as follows:

MFCs are studied as micro-generators in Part 3. The parameters which define their performances are studied to discuss their operation and their performances. Literature study leads to develop an electrical model that describes the internal interactions and performance of MFCs. The internal losses of MFCs and the different voltage drops were evaluated. The ohmic losses limit the performance of MFCs. Design optimization is required to decrease the internal resistance. The quantification of the internal resistance of MFC validates the assumption that the MFC produces the maximum power when the internal resistance equals the external resistance. The implementation of a maximum power point tracking is thus possible by impedance emulation. A non-immediate response of the change of the operating condition was explained by a capacitive effect. Therefore a short sample rate can lead to overestimation in static characteristics evaluation. A minimum time of 3 minutes is necessary to adjust bacteria behavior to the change in the operating condition. The model was studied as a function of the substrate concentration.

The effect of the concentration of substrate showed that a concentration of 1 g/L is the optimal concentration for energy production in the lab-scale. Lower or higher concentration will lead to increase the internal resistance and performances degrade. Increasing the operation temperature increases the bacteria activity, decreases the internal resistance and improves the performances.

Energy harvesting from MFCs requires a power management unit that steps-up the voltage and controls the operation of the MFCs. An autonomous, low input-voltage, self-starting, isolated flyback converter was designed and optimized for energy harvesting from MFCs. The operation of the converter in a discontinuous conduction mode allows the control of the internal resistance of the flyback and thus controls the operation of the MFCs. The designed converter is suitable for energy harvesting from one MFC as from a stack of MFCs. The low power produced by one MFC limits the possible applications. Association of MFCs can scale-up the output power of the associated MFCs to the desired level. However the performances of the stack face by non-uniformities of the MFCs. A switched-capacitor voltage balancing circuit transfers the energy from the weakest MFC(s) to the strongest MFC(s) and improves the performances of the stack. In a wastewater treatment plant, MFCs could not be hydraulically isolated. A leakage charge between the associated MFCs will decrease the global efficiency. The flow rate has to be controlled to eliminate this problem. A flow from one cathode to one anode causes additional losses due to the oxygen leakage.

Even with the small amount of energy available from one MFC, it is still enough to supply an autonomous sensor. It was found that using a non-adaptive MPPT converter can negatively affect the characteristics of MFCs. A sensor was continuously supplied by alternatively connecting 2 MFCs. Each MFC supplies the sensor for two days. The flyback converter was able to continuously supply the sensor from the energy harvested from one continuously-fed MFC. The concept of grid-off, battery-less system powered by a stack of MFCs was presented. This could be a good application in a wastewater treatment plant to supply the monitoring system or also to supply the low power application of a building from a local or a building-integrated WWTP.

11.2 Scientific perspectives

Energy harvesting from MFCs was already presented as an alternative source to eliminate batteries in low power applications. The low power densities limit the application of MFCs. More works focus on the materials, microbiology, chemistry and electrochemistry to enhance the performances. Optimizing the design of MFCs and the materials may also decrease the internal resistance and improve the performances. Another research direction is to determine the limitation of the performances of MFCs with respect to the reactor volume. Many researches showed that the technology still face economic challenges. Reliability and durability studies have to be achieved to prove that MFCs are a profitable business in a long term.

In term of power conversion and control, the integration of the flyback converter with the switched-capacitor voltage balancing circuit is the most important perspective. The efficiency of these circuits is validated using discrete prototypes. The integration of the converter and the balancing circuit would allow to better optimize losses.

It will be interesting to realize experiments with a generator composed of a huge number of MFCs in a real WWTP to discover the limitations of the number of MFCs in a stack and to extrapolate the available energy in WWTP and the possible applications. The system may be completed by other energy harvesters. These systems may also be tested in a building-integrated WWTP to be a part of the "intelligent building". In this case, a relatively high power could be envisaged from a large-scale MFC. A power production of 70 W/m^3 can be produced from wastewater using a suitable design of MFCs. A wastewater volume of 1.5 m^3 is required to achieve the equivalent of a photovoltaic panel (e.g. SPM100P-TS-F, from SOLARTECH) of 100 W. Supposing that the unit volume is about 0.7 liter, a number of 2150 MFCs is required to reach a power level of 100 W. Assuming that the number of MFCs in a serial stack is limited, MFCs are divided in stacks of serially-connected MFCs to achieve the voltage level (40V). These stacks may then be connected in parallel to achieve the required current as shown in Fig. 11.1. To achieve higher voltage, the output of these converters can also be connected in series to reach the required voltage and build one module (like the essence of the project MICONET2). These modules would then be associated in parallel to offer the required current as shown in Fig. 11.2.

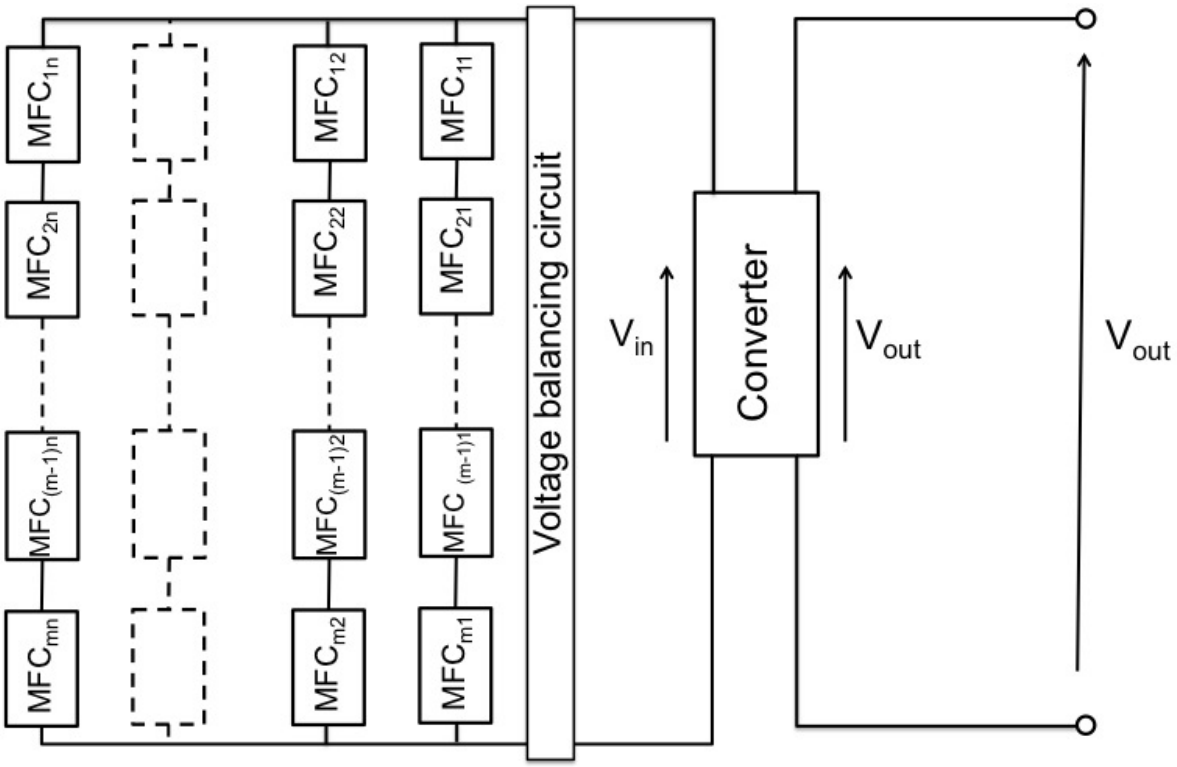

Figure 11.1: Schematic 1 of a large-scale MFC association

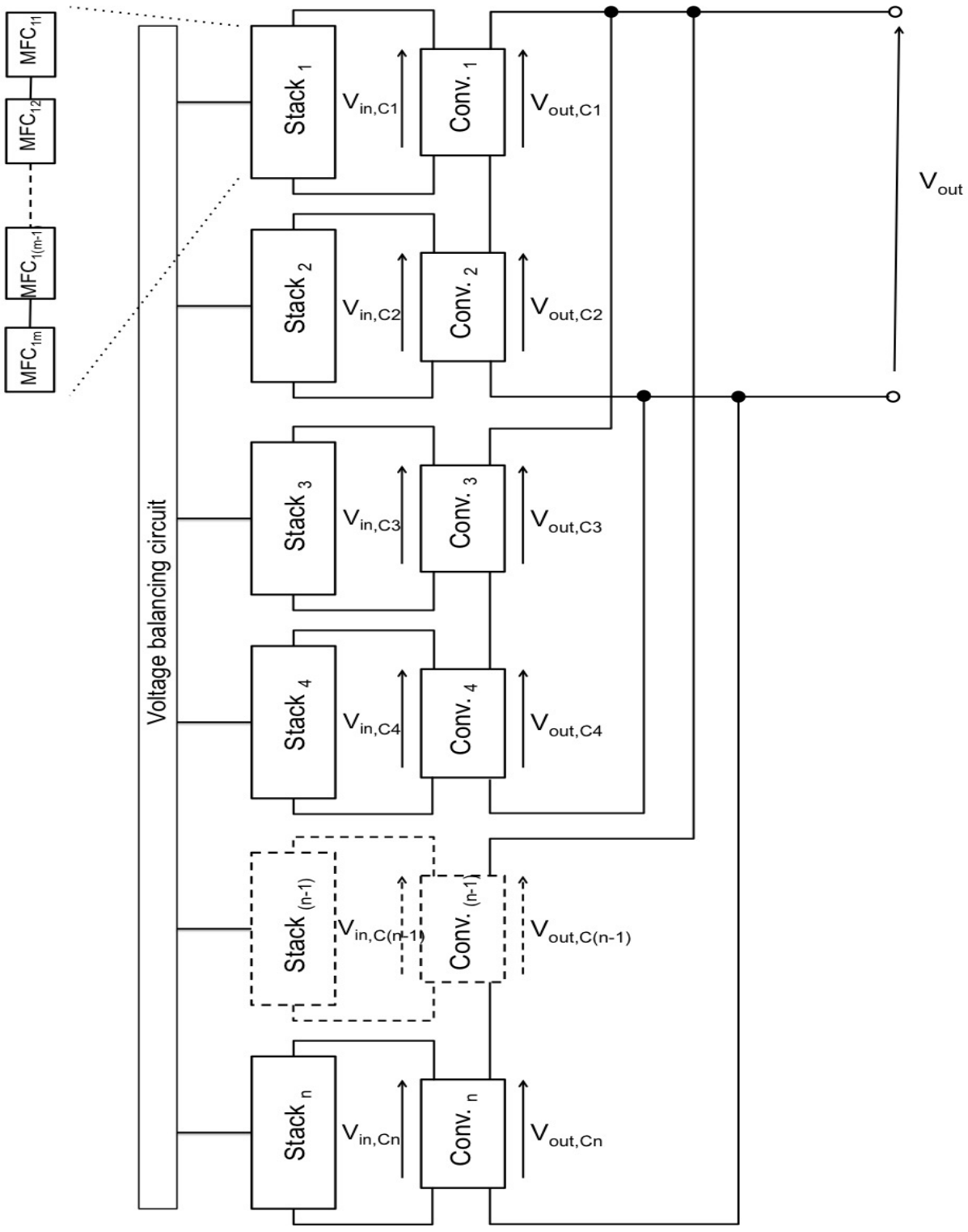

Figure 11.2: Schematic 2 of a large-scale MFC association

Bibliography

[Adami, 2013] Adami, S.-E. (2013). Optimisation de la récupération d'énergie dans les applications de rectenna.

[Adami et al., 2011] Adami, S.-E., Degrenne, N., Vollaire, C., Allard, B., Buret, F., and Costa, F. (2011). Autonomous ultra-low power DC/DC converter for Microbial Fuel Cells. In *Proceedings of ICECS*, pages 398–401. IEEE.

[Aelterman et al., 2006a] Aelterman, P., Rabaey, K., Clauwaert, P., and Verstraete, W. (2006a). Microbial fuel cells for wastewater treatment. *Water Science & Technology*, 54(8):9.

[Aelterman et al., 2006b] Aelterman, P., Rabaey, K., and Verstraete, W. (2006b). Continuous Electricity Generation at High Voltages and Currents Using Stacked Microbial Fuel Cells. 40(10):3388–3394.

[AGENCY, 2013] AGENCY, U. E. P. (2013). Energy efficiency in water and wastewater facilities. Technical report, U.S. ENVIRONMENTAL PROTECTION AGENCY.

[Ahn and Logan, 2010] Ahn, Y. and Logan, B. E. (2010). Effectiveness of domestic wastewater treatment using microbial fuel cells at ambient and mesophilic temperatures. *Bioresource technology*, 101(2):469–475.

[Allen and Bennetto, 1993] Allen, R. M. and Bennetto, H. P. (1993). Microbial fuel-cells. *Applied Biochemistry and Biotechnology*, 39-40(1):27–40.

[Amiel et al., 2011] Amiel, C., Nawawi-Lansade, D., and Sorensen, K. (2011). An optimal solution to achieve the energy neutral waste water treatment plant. *Water Pract Technol*, 6(4).

[An et al., 2015] An, J., Kim, B., Chang, I. S., and Lee, H.-S. (2015). Shift of voltage reversal in stacked microbial fuel cells. *Journal of Power Sources*, 278:534–539

[Appels et al., 2008] Appels, L., Baeyens, J., Degrève, J., and Dewil, R. (2008). Principles and potential of the anaerobic digestion of waste-activated sludge. *Progress in energy and combustion science*, 34(6):755–781.

[Appleby and Wolfson, 1973] Appleby, A., D. N. and Wolfson, S. (1973). Implantable power system for an artificial heart. *U.S Patents*, (3774243).

[Arnold, 2007] Arnold, D. P. (2007). Review of microscale magnetic power generation. *Magnetics, IEEE Transactions on*, 43(11):3940–3951.

[Asumadu et al., 2005] Asumadu, J., Haque, M., Vogel, H., and Willards, C. (2005). *Precision battery management system*, volume 2. IEEE.

[Balat and KÄśrtay, 2010] Balat, H. and KÄśrtay, E. (2010). Hydrogen from biomass–present scenario and future prospects. *International Journal of Hydrogen Energy*, 35(14):7416–7426.

[Bard and Faulkner, 1981] Bard, A. J. and Faulkner, L. R. (1981). *Electrochemical methods - Fundamentals and applications*, volume 125.

[Bard et al., 1985] Bard, A. J., Parsons, R., and Jordan, J. (1985). *Standard potentials in aqueous solution*, volume 6. CRC press.

[Baughman and Ferdowsi, 2008] Baughman, A. C. and Ferdowsi, M. (2008). Double-tiered switched-capacitor battery charge equalization technique. *Industrial Electronics, IEEE Transactions on*, 55(6):2277–2285

[Beeby et al., 2006] Beeby, S. P., Tudor, M. J., and White, N. (2006). Energy harvesting vibration sources for microsystems applications. *Measurement science and technology*, 17(12):175 –195.

[Biffinger and Ringeisen, 2008] Biffinger, J. C. and Ringeisen, B. R. (2008). Engineering microbial fuels cells: recent patents and new directions. *Recent patents on biotechnology*, 2(3):150–155

[Bond et al., 2002] Bond, D. R., Holmes, D. E., Tender, L. M., and Lovley, D. R. (2002). Electrode-reducing microorganisms that harvest energy from marine sediments. *Science*, 295(5554):483–485

[Bonfiglio and Roessler, 2009] Bonfiglio, C. and Roessler, W. (2009). A Cost Optimized Battery Management System with Active Cell Balancing for Lithium Ion Battery Stacks. *Methods*, pages 304–309.

[Böttner, 2002] Böttner, H. (2002). Thermoelectric micro devices: current state, recent developments and future aspects for technological progress and applications.

[Bradford, 2006] Bradford, T. (2006). *Solar revolution: the economic transformation of the global energy industry*, volume 1. the MIT Press.

[Bullen et al., 2006] Bullen, R. A., Arnot, T. C., Lakeman, J. B., and Walsh, F. C. (2006). Biofuel cells and their development. *Biosensors and Bioelectronics*, 21(11):2015–2045.

[Cadar et al., 2010] Cadar, D., Petreuş, D., Pătărău, T., and Ă, N. P. (2010). Electronics and Telecommunications ACTIVE BALANCING METHOD FOR BATTERY CELL EQUALIZATION Electronics and Telecommunications. 51(2):1–5.

[Canfield JH, 1963] Canfield JH, Goldner BH, L. R. (1963). utilisation of human wastes as electrochemicals fuels. Technical report, NASA Technical report, Magna Corporation, Anaheim, CA.

[Cao et al., 2008] Cao, J., Schofield, N., and Emadi, A. (2008). Battery balancing methods: A comprehensive review. In *Vehicle Power and Propulsion ...*, pages 3–8.

[Ceraolo et al., 2003] Ceraolo, M., Miulli, C., and Pozio, A. (2003). Modelling static and dynamic behaviour of proton exchange membrane fuel cells on the basis of electro-chemical description. *Journal of Power Sources*, 113(1):131 – 144.

[Chakraborty, 2004] Chakraborty, S.; Jain, A. M. N. (2004). Novel converter topology and algorithm for simultaneous charging and individual cell balancing of multiple li-ion batteries. *Telecommunications Energy Conference, 2004. INTELEC 2004. 26th Annual International*, pages 248–253.

[Chang et al., 2004] Chang, I. S., Jang, J. K., Gil, G. C., Kim, M., Kim, H. J., Cho, B. W., and Kim, B. H. (2004). Continuous determination of biochemical oxygen demand using microbial fuel cell type biosensor. *Biosensors and Bioelectronics*, 19(6):607–613.

[Chapin et al., 1954] Chapin, D. M., Fuller, C. S., and Pearson, G. L. (1954). A new silicon pâĂŘn junction photocell for converting solar radiation into electrical power. *Journal of Applied Physics*, 25(5):676–677.

[Chávez-Ramírez et al., 2010] Chávez-Ramírez, A. U., Muñoz-Guerrero, R., Durón-Torres, S. M., Ferraro, M., Brunaccini, G., Sergi, F., Antonucci, V., and Arriaga, L. G. (2010). High power fuel cell simulator based on artificial neural network. *International Journal of Hydrogen Energy*, 35(21):12125–12133.

[Cheng et al., 2006a] Cheng, S., Liu, H., and Logan, B. E. (2006a). Increased power generation in a continuous flow mfc with advective flow through the porous anode and reduced electrode spacing. *Environmental Science & Technology*, 40(7):2426–2432. PMID: 16646485.

[Cheng et al., 2006b] Cheng, S., Liu, H., and Logan, B. E. (2006b). Power densities using different cathode catalysts (Pt and CoTMPP) and polymer binders (nafion and PTFE) in single chamber microbial fuel cells. *Environmental science & technology*, 40(1):364–9.

[Cheng et al., 2011] Cheng, S., Member, S., Jin, Y., Rao, Y., Arnold, D. P., and Member, S. (2011). An Active Voltage Doubling AC / DC Converter for Low-Voltage Energy Harvesting Applications. *Power*, 26(8):2258–2265.

[Choi and Chae, 2011] Choi, S. and Chae, J. (2011). A series array of microliter-sized microbial fuel cell. In *Proceedings of MEMS*, pages 1289–1292. IEEE.

[Chong et al., 2009] Chong, M.-L., Sabaratnam, V., Shirai, Y., and Hassan, M. A. (2009). Biohydrogen production from biomass and industrial wastes by dark fermentation. *International Journal of Hydrogen Energy*, 34(8):3277 – 3287.

[Chung and Ho, 2003] Chung, H.S.-H.; Tse, K. H. S. M. C. and Ho, M. (2003). A novel maximum power point tracking technique for solar panels using a sepic or cuk converter. *IEEE Transactions on Power Electronics*, 18(3):717–724.

[Cohen, 1931] Cohen, B. (1931). The bacterial Culture as an Electrical Half-Cell. *Journal of bacteriology*, 21:18–19.

[COMMISSION, 2010] COMMISSION, E. (2010). Energy 2020 a strategy for competitive, sustainable and secure energy. Technical Report SEC(2010) 1346, EUROPEAN COMMISSION.

[Dai and Choi, 2013] Dai, C. and Choi, S. (2013). Technology and applications of microbial biosensor. *Open Journal of Applied Biosensor*, 2:83–93.

[Damaschke, 1997] Damaschke, J. M. (1997). Design of a low-input-voltage converter for thermoelectric generator. *IEEE Transactions on Industry Applications*, 33(5):1203–1207.

[Daowd et al., 2011] Daowd, M., Omar, N., Bossche, P. V. D., and Mierlo, J. V. (2011). A Review of Passive and Active Battery Balancing based on MATLAB/Simulink. xx(September).

[DC, 2005] DC, H. (2005). Microbe power. *Environ Health Persp*, 113(11):754–757.

[Degrenne, 2012] Degrenne, N. (2012). *Power management for microbial fuel cells*. PhD thesis, Ecole central de Lyon,.

[Degrenne et al., 2012a] Degrenne, N., Allard, B., Buret, F., Adami, S.-E., Labrousse, D., Vollaire, C., and Morel, F. (2012a). A 140 mV Self-Starting 10 mW DC / DC Converter for Powering Low-Power Electronic Devices from Low-Voltage Microbial Fuel Cells. *Journal of low-power electronics*, 8(4):485–497.

[Degrenne et al., 2012b] Degrenne, N., Buret, S. F., and Allard, B. (2012b). Power Management for Microbial Fuel Cells Presentation outline Introduction.

[Degrenne et al., 2013] Degrenne, N., Ledezma, P., Bevilacqua, P., Buret, F., Allard, B., Greenman, J., and Ieropoulos, I. A. (2013). Bioresource Technology Bi-directional electrical characterisation of microbial fuel cell. *Bioresource Technology*, 128:769–773.

[Deng et al., 2010] Deng, Q., Li, X., Zuo, J., Ling, A., and Logan, B. E. (2010). Power generation using an activated carbon fiber felt cathode in an upflow microbial fuel cell. *Journal of Power Sources*, 195(4):1130 – 1135.

[Deterre et al., 2014] Deterre, M., Lefeuvre, E., Zhu, Y., Woytasik, M., Boutaud, B., and Dal Molin, R. (2014). Micro blood pressure energy harvester for intracardiac pacemaker. *Microelectromechanical Systems, Journal of*, 23(14):651–660.

[Donovan et al., 233] Donovan, C., Dewan, A., Heo, D., Lewandowski, Z., and Beyenal, H. (233). Journal of power sources. *2013*, 79–85(7):Microbial fuel cell; Power management; Sensor; Remote monitoring.

[Donovan et al., 2011] Donovan, C., Dewan, A., Peng, H., Heo, D., and Beyenal, H. (2011). Power management system for a 2 . 5 W remote sensor powered by a sediment microbial fuel cell. *Journal of Power Sources*, 196(3):1171–1177.

[Du et al., 2007] Du, Z., Li, H., and Gu, T. (2007). A state of the art review on microbial fuel cells: A promising technology for wastewater treatment and bioenergy. *Biotechnology advances*, 25(5):464–82.

[Dumas et al., 2008] Dumas, C., Basseguy, R., and Bergel, A. (2008). Electrochemical activity of geobacter sulfurreducens biofilms on stainless steel anodes. *Electrochimica Acta*, 53(16):5235 – 5241.

[Dumas et al., 2007] Dumas, C., Mollica, A., Féron, D., Basséguy, R., Etcheverry, L., and Bergel, A. (2007). Marine microbial fuel cell: Use of stainless steel electrodes as anode and cathode materials. *Electrochimica Acta*, 53(2):468 – 473.

[Edwards et al., 2008] Edwards, P., Kuznetsov, V., David, W., and Brandon, N. (2008). Hydrogen and fuel cells: Towards a sustainable energy future. *Energy Policy*, 36(12):4356 – 4362. Foresight Sustainable Energy Management and the Built Environment Project.

[Einhorn et al., 2011] Einhorn, M., Permann, R., Kral, C., Conte, F. V., Guertlschmid, W., Blochberger, T., Kumpusch, R., and Fleig, J. (2011). Current Equalization of Serially Connected Battery Cells for a Possible Second Life Application. *Management*, pages 1–5.

[Erable and Bergel, 2009] Erable, B. and Bergel, A. (2009). First air-tolerant effective stainless steel microbial anode obtained from a natural marine biofilm. *Bioresource Technology*, 100(13):3302 – 3307.

[Esram and Chapman, 2007] Esram, T. and Chapman, P. L. (2007). Comparison of Photovoltaic Array Maximum Power Point Tracking Techniques. *IEEE Transactions on Energy Conversion*, 22(2):439–449.

[Fan et al., 2007] Fan, Y., Liu, H., and Hu, H. (2007). Enhanced Coulombic efficiency and power density of air-cathode microbial fuel cells with an improved cell configuration. *Journal of Power Sources*, 171(2):348–354.

[Fang et al., 2010] Fang, L., Liu, Z., Li, X., Yang, Q., Zheng, Y., and Jia, B. (2010). [electricity generation by the microbial fuel cells using the supernatant fluid of microwave pretreated sludge as fuel]. *Huan jing ke xue= Huanjing kexue/[bian ji, Zhongguo ke xue yuan huan jing ke xue wei yuan hui" Huan jing ke xue" bian ji wei yuan hui.]*, 31(10):2518–2524.

[Femia and Vitelli, 2005] Femia, N.; Petrone, G. S. G. and Vitelli, M. (2005). Optimization of perturb and observe maximum power point tracking method. *Power Electronics, IEEE Transactions on*, 20(4):963 – 973.

[Fradler et al., 2014] Fradler, K. R., Kim, J. R., Boghani, H. C., Dinsdale, R. M., Guwy, A. J., and Premier, G. C. (2014). The effect of internal capacitance on power quality and energy efficiency in a tubular microbial fuel cell. *Process Biochemistry*, 49(6):973 – 980.

[Ghoreyshi et al., 2011] Ghoreyshi, A. A., Jafary, T., Najafpour, G. D., and Haghparast, F. (2011). Effect of Type and Concentration of Substrate on Power Generation in a Dual Chambered Microbial Fuel Cell. pages 1174–1181.

[Gilbert and Balouchi, 2008] Gilbert, J. M. and Balouchi, F. (2008). Comparison of energy harvesting systems for wireless sensor networks. *international journal of automation and computing*, 5(4):334–347.

[Gonzalez del Campo et al., 2013] Gonzalez del Campo, a., Lobato, J., Cañizares, P., Rodrigo, M., and Fernandez Morales, F. (2013). Short-term effects of temperature and COD in a microbial fuel cell. *Applied Energy*, 101:213–217.

[Gorby and Fredrickson, 2006] Gorby, YA, S. Y. J. M. K. R. D. M. A. D. T. B. I. C. B. K. K. K. D. C. S. R. M. R. D. S. E. H. L. S. D. E. D. K. G. P. K. W. S. I. B. L. K. N. and Fredrickson, J. (2006). Electrically conductive bacterial nanowires produced by shewanella oneidensis strain mr-1 and other microorganisms. *Proceedings of the National Academy of Sciences of the United States of America*, 103(30):11358–11363.

[Greenman et al., 2011] Greenman, J., Ieropoulos, I., and Melhuish, C. (2011). *Modern Aspects of Electrochemistry*, volume 52, pages 239–290. Springer New York.

[Grgić et al., 2009] Grgić, D., Ungan, T., Kostić, M., and Reindl, L. M. (2009). Ultra-low input voltage DC-DC converter for micro energy harvesting. In *Proceedings of PowerMeMs*, pages 265–268.

[Guo, 2010] Guo, H.-J. (2010). Review and critical analysis of the research papers published till date on maximum power point tracking in wind energy conversion system. *Energy Conversion*, 1:4075–4082.

[Gurung et al., 2012] Gurung, A., Kim, J., Jung, S., Jeon, B.-H., Yang, J. E., and Oh, S.-E. (2012). Effects of substrate concentrations on performance of serially connected microbial fuel cells (MFCs) operated in a continuous mode. *Biotechnology letters*, 34(10):1833–9.

[HaoYu et al., 2007] HaoYu, E., Cheng, S., Scott, K., and Logan, B. (2007). Microbial fuel cell performance with non-pt cathode catalysts. *Journal of Power Sources*, 171(2):275 – 281.

[He et al., 2008] He, Z., Huang, Y., Manohar, A. K., and Mansfeld, F. (2008). Bioelectrochemistry Effect of electrolyte pH on the rate of the anodic and cathodic reactions in an air-cathode microbial fuel cell. *Bioelectrochemistry*, 74(1):78–82.

[He et al., 2005] He, Z., Minteer, S. D., and Angenent, L. T. (2005). Electricity generation from artificial wastewater using an upflow microbial fuel cell. *Environmental science & technology*, 39(14):5262–7.

[He et al., 2006] He, Z., Wagner, N., Minteer, S. D., and Angenent, L. T. (2006). An upflow microbial fuel cell with an interior cathode: assessment of the internal resistance by impedance spectroscopy. *Environmental science & technology*, 40(17):5212–7.

[Heilmann J, 2006] Heilmann J, L. B. (2006). Production of electricity from proteins using a microbial fuel cell. *Water Environ Res*, 78(7):531–537.

[Hernandez and Newman, 2001] Hernandez, M. E. and Newman, D. K. (2001). Extracellular electron transfer. 58(11):1562–1571.

[HONG LIU, 2005] HONG LIU, STEPHEN GROT, A. B. E. L. (2005). Electrochemically assisted microbial production of hydrogen from acetate. *Environ. Sci. Technol*, 39:4317–4320.

[Hong Liu and Logan, 2005] Hong Liu, S. C. and Logan, B. E. (2005). Power generation in fed-batch microbial fuel cells as a function of ionic strength, temperature, and reactor configuration. *Environ. Sci. Technol.*, 39(14):5488–5493.

[Hoogers, 2014] Hoogers, G. (2014). *Fuel cell technology handbook*. CRC press.

[Ieropoulos et al., 2008] Ieropoulos, I., Greenman, J., and Melhuish, C. (2008). Microbial fuel cells based on carbon veil electrodes: Stack configuration and scalability. *International Journal of Energy Research*, 32(13):1228–1240.

[Ieropoulos et al., 2010] Ieropoulos, I. A., Winfield, J., and Greenman, J. (2010). Small Scale Microbial Fuel Cells and Different Ways of Reporting Output. *Image (Rochester, N.Y.)*, 28(9):1–9.

[Ieropoulos I, 2003] Ieropoulos I, Greenman J, M. C. (2003). Imitating Metabolism : Energy Autonomy in Biologically Inspired Robots. *Proceedings of the 2nd International Symposium on Imitation in Animals and Artifacts*, pages 191–194.

[Imtiaz and Khan, 2011] Imtiaz, A. M. and Khan, F. H. (2011). A Low-Cost Time Shared Cell Balancing Technique for Future Lithium-Ion Battery Storage System Featuring Regenerative Energy Distribution. *Current*, pages 792–799.

[Inc., 1999] Inc., M. W. C. (1999). In research needs to optimize wastewater resource utilization. *Watanabe, M. E., Ed.; Water Environment Research Foundation (WERF), New York*.

[Instruments, 2001] Instruments, T. (2001). Inductor and flyback. Technical report, Texas Instruments.

[Ivanov et al., 2010] Ivanov, I., Vidaković-Koch, T., and Sundmacher, K. (2010). Recent advances in enzymatic fuel cells: experiments and modeling. *Energies*, 3(4):803–846.

[Jacques K, 1999] Jacques K, Lyons TP, K. D. (1999). *The alcohol textbook*. Wiltshire: Redwood Books, 3rd edition.

[Jadhav and Ghangrekar, 2009] Jadhav, G. S. and Ghangrekar, M. M. (2009). Performance of microbial fuel cell subjected to variation in pH, temperature, external load and substrate concentration. *Bioresource technology*, 100(2):717–723.

[Jang et al., 2004] Jang, J. K., Pham, T. H., Chang, I. S., Kang, K. H., Moon, H., Cho, K. S., and Kim, B. H. (2004). Construction and operation of a novel mediator- and membrane-less microbial fuel cell. *Process Biochemistry*, 39(8):1007–1012.

[Jeon et al., 2005] Jeon, Y., Sood, R., Jeong, J.-H., and Kim, S.-G. (2005). Mems power generator with transverse mode thin film pzt. *Sensors and Actuators A: Physical*, 122(1):16–22.

[Jiang et al., 2005] Jiang, X., Polastre, J., and Culler, D. (2005). Perpetual environmentally powered sensor networks. *Information Processing in Sensor Networks, 2005. IPSN 2005. Fourth International Symposium on*, pages 463–468.

[Kalogirou, 2004] Kalogirou, S. A. (2004). Optimization of solar systems using artificial neural-networks and genetic algorithms. *Applied Energy*, 77(4):383 – 405.

[KARUBE and WILSON, 1992] KARUBE, I., T. A. K. I. and WILSON, G. (1992). *Biosensors: Fundamentals and Applications*. Mir Publishers, Moscow, Russia.

[Kasa and Iwamoto, 2000] Kasa, N.; Iida, T. and Iwamoto, H. (2000). Maximum power point tracking with capacitor identifier for photovoltaic power system. *Power Electronics and Variable Speed Drives, 2000. Eighth International Conference on (IEEE Conf.)*, pages 130,135.

[Kausar et al., 2014] Kausar, A. Z., Reza, A. W., Saleh, M. U., and Ramiah, H. (2014). Energizing wireless sensor networks by energy harvesting systems: Scopes, challenges and approaches. *Renewable and Sustainable Energy Reviews*, 38:973–989 1364–0321.

[Khaled et al., 2015] Khaled, F., Ondel, O., Allard, B., and Buret, F. (2015). Voltage balancing strategies for serial connection of microbial fuel cells. *Eur. Phys. J. Appl. Phys.*, 71(1):10904.

[Khanna and Das, 2013] Khanna, N. and Das, D. (2013). Biohydrogen production by dark fermentation. *Wiley Interdisciplinary Reviews: Energy and Environment*, 2(4):401–421.

[Kim et al., 2012] Kim, D., An, J., Kim, B., Jang, J. K., Kim, B. H., and Chang, I. S. (2012). Scaling-up microbial fuel cells: configuration and potential drop phenomenon at series connection of unit cells in shared anolyte. *ChemSusChem*, 5(6):1086–91.

[Kim et al., 1999] Kim, H. J., Park, H. S., Hyun, M. S., Chang, I. S., Kim, M., and Kim, B. H. (1999). A mediator-less microbial fuel cell using a metal reducing bacterium, shewanella putrefaciens. *Microbial. biotechno.*, 9:365–367.

[Kim and Kim, 2011] Kim, J. and Kim, C. (2011). A Regulated Charge Pump With a Low-Power Integrated Optimum Power Point Tracking Algorithm for Indoor Solar Energy Harvesting. *Circuits and Systems II: Express Briefs, IEEE Transactions on*, 58(99):1–5.

[Kim et al., 2008] Kim, J. K., Oh, B. R., Shin, H.-J., Eom, C.-Y., and Kim, S. W. (2008). Statistical optimization of enzymatic saccharification and ethanol fermentation using food waste. *Process Biochemistry*, 43(11):1308–1312

[Kim et al., 2007] Kim, J. R., Jung, S. H., Regan, J. M., and Logan, B. E. (2007). Electricity generation and microbial community analysis of alcohol powered microbial fuel cells. *Bioresource Technology*, 98(13):2568 – 2577.

[Kim et al., 2010] Kim, J. R., Premier, G. C., Hawkes, F. R., Rodríguez, J., Dinsdale, R. M., and Guwy, A. J. (2010). Modular tubular microbial fuel cells for energy recovery during sucrose wastewater treatment at low organic loading rate. *Bioresource Technology*, 101(4):1190 – 1198.

[Kim et al., 2011a] Kim, K.-Y., Chae, K.-J., Choi, M.-J., Ajayi, F. F., Jang, A., Kim, C.-W., and Kim, I. S. (2011a). Enhanced coulombic efficiency in glucose-fed microbial fuel cells by reducing metabolite electron losses using dual-anode electrodes. *Bioresource technology*, 102(5):4144–4149.

[Kim et al., 2011b] Kim, T., Qiao, W., and Qu, L. (2011b). Series-Connected Self-Reconfigurable Multicell Battery. *Electrical Engineering*, pages 1382–1387.

[Kobayashi et al., 2006] Kobayashi, K., Takano, I., and Sawada, Y. (2006). A study of a two stage maximum power point tracking control of a photovoltaic system under partially shaded insolation conditions. *Solar Energy Materials and Solar Cells*, 90(18–19):2975 – 2988. 14th International Photovoltaic Science and Engineering Conference 14th International Photovoltaic Science and Engineering Conference.

[Korneel Rabaey, 2003] Korneel Rabaey, Geert Lissens, S. D. S. . W. V. (2003). A microbial fuel cell capable of converting glucose to electricity at high rate and efficiency. *Biotechnology*, 25:1531–1535.

[Larminie and Dicks, 2003] Larminie, J. and Dicks, A. (2003). *Fuel cell systems explained*. John Wiley & Sons, 2nd edition.

[Larrosa-Guerrero et al., 2010] Larrosa-Guerrero, A., Scott, K., Head, I., Mateo, F., Ginesta, A., and Godinez, C. (2010). Effect of temperature on the performance of microbial fuel cells. *Fuel*, 89(12):3985 – 3994.

[Ledezma et al., 2014] Ledezma, P., Degrenne, N., Bevilacqua, P., Buret, F., Allard, B., Greenman, J., and Ieropoulos, I. (2014). Dynamic polarisation reveals differential steady-state stabilisation and capacitive-like behaviour in microbial fuel cells. *Sustainable Energy Technologies and Assessments*, 5(0):1 – 6.

[Ledezma et al., 2013a] Ledezma, P., Greenman, J., and Ieropoulos, I. (2013a). MFC-cascade stacks maximise COD reduction and avoid voltage reversal under adverse conditions. *Bioresource Technology*, 134:158–165.

[Ledezma et al., 2013b] Ledezma, P., Greenman, J., and Ieropoulos, I. (2013b). MFC-cascade stacks maximise COD reduction and avoid voltage reversal under adverse conditions. *Bioresource Technology*, 134:158–165.

[Lee et al., 2008] Lee, H.-S., Parameswaran, P., Kato-Marcus, A., Torres, C. I., and Rittmann, B. E. (2008). Evaluation of energy-conversion efficiencies in microbial fuel cells (MFCs) utilizing fermentable and non-fermentable substrates. *Water research*, 42(6-7):1501–1510.

[Lee, 2005] Lee, Y.-S. C.-Y. D. G.-T. C. S.-C. Y. (2005). Battery equalization using bi-directional cuk converter in dcvm operation. *Power Electronics Specialists Conference*, pages 765–771.

[Levin et al., 2004] Levin, D. B., Pitt, L., and Love, M. (2004). Biohydrogen production: prospects and limitations to practical application. *International Journal of Hydrogen Energy*, 29(2):173 – 185.

[Li et al., 2009] Li, J., Zheng, G., He, J., Chang, S., and Qin, Z. (2009). Hydrogen-producing capability of anaerobic activated sludge in three types of fermentations in a continuous stirred-tank reactor. *Biotechnology advances*, 27(5):573–577.

[Li et al., 2014] Li, W.-W., Yu, H.-Q., and He, Z. (2014). Towards sustainable wastewater treatment by using microbial fuel cells-centered technologies. *Energy and Environmental Science*, 7(3):911–924.

[Liu et al., 2005a] Liu, H., Cheng, S., and Logan, B. E. (2005a). Production of electricity from acetate or butyrate using a single-chamber microbial fuel cell. *Environmental science & technology*, 39(2):658–62.

[Liu et al., 2005b] Liu, H., Cheng, S., and Logan, B. E. (2005b). Production of electricity from acetate or butyrate using a single-chamber microbial fuel cell. *Environmental science & technology*, 39(2):658–662.

[Liu and Logan, 2004] Liu, H. and Logan, B. E. (2004). Electricity Generation Using an Air-Cathode Single Chamber Microbial Fuel Cell in the Presence and Absence of a Proton Exchange Membrane. 38(14):4040–4046.

[Liu and Ramnarayanan, 2004] Liu, H. and Ramnarayanan, R. (2004). Production of Electricity during Wastewater Treatment Using a Single Chamber Microbial Fuel Cell. *Environmental Science & Technology*, 38(7):2281–2285.

[Liu et al., 2009] Liu, Z., Liu, J., Zhang, S., and Su, Z. (2009). Study of operational performance and electrical response on mediator-less microbial fuel cells fed with carbon- and protein-rich substrates. *Biochemical Engineering Journal*, 45(3):185 – 191.

[Logan et al., 2007] Logan, B., Cheng, S., Watson, V., and Estadt, G. (2007). Graphite Fiber Brush Anodes for Increased Power Production in Air-Cathode Microbial Fuel Cells. *Environmental Science & Technology*, 41(9):3341–3346.

[Logan, 2004a] Logan, B. E. (2004a). Harvesting energy from wastewater treatment. Penn State University.

[Logan, 2004b] Logan, B. E. (2004b). Peer reviewed: extracting hydrogen and electricity from renewable resources. *Environmental science and technology technology*, 38(9):160A–167A.

[Logan, 2008] Logan, B. E. (2008). *Microbial Fuel Cells*. New Jersey: John Wiley and Sons, Inc.

[Logan, 2012] Logan, B. E. (2012). Essential data and techniques for conducting microbial fuel cell and other types of bioelectrochemical system experiments. *ChemSusChem*, 5(6):988–94.

[Logan et al., 2006] Logan, B. E., Hamelers, B., Rozendal, R., Schröder, U., Keller, J., Freguia, S., Aelterman, P., Verstraete, W., and Rabaey, K. (2006). Microbial fuel cells: methodology and technology. *Environ. Sci. Technol.*, 40:5181–5192.

[Logan et al., 2005] Logan, B. E., Murano, C., Scott, K., Gray, N. D., and Head, I. M. (2005). Electricity generation from cysteine in a microbial fuel cell. *Water Research*, 39(5):942–952

[Longlong Zhang and Wölfle, 2010] Longlong Zhang, W. G. H. and Wölfle, W. (2010). A new approach to achieve maximum power point tracking for pv system with a variable inductor. *2010 2nd IEEE International Symposium on Power Electronics for Distributed Generation Systems*, pages 948 – 952.

[Lovley, 2006] Lovley, D. R. (2006). Microbial fuel cells: novel microbial physiologies and engineering approaches. *Current opinion in biotechnology*, 17(3):327–332.

[Luigi, 1791] Luigi, G. (1791). De viribus electricitatis in motu musculari commentarius. *Bologna, Italy, Ex typographia Instituti Scientiarum*.

[Marcus et al., 2007] Marcus, A. K., Torres, C. I., and Rittmann, B. E. (2007). Conduction-based modeling of the biofilm anode of a microbial fuel cell. *Biotechnol. Bioeng*, 98(6):1171–1182.

[Martin et al., 2010] Martin, E., Savadogo, O., Guiot, S. R., and Tartakovsky, B. (2010). The influence of operational conditions on the performance of a microbial fuel cell seeded with mesophilic anaerobic sludge. *Biochemical Engineering Journal*, 51(3):132–139.

[Mateu et al., 2007] Mateu, L., Pollak, M., and Spies, P. (2007). Step-up converters for human body energy harvesting thermogenerators. *Technical Digest PowerMEMS*, pages 213–216.

[Mathuriya and Sharma, 2010] Mathuriya, A. S. and Sharma, V. N. (2010). Bioelectricity production from various wastewaters through microbial fuel cell technology. 2(2009):133–137.

[Middaugh et al., 2006] Middaugh, J., Cheng, S., Liu, W., and Wagner, R. (2006). How to Make Cathodes with a Diffusion Layer for Single-Chamber Microbial Fuel Cells.

[Min et al., 2005] Min, B., Cheng, S., and Logan, B. E. (2005). Electricity generation using membrane and salt bridge microbial fuel cells. *Water research*, 39(9):1675–86.

[Min and Logan, 2004] Min, B. and Logan, B. E. (2004). Continuous electricity generation from domestic wastewater and organic substrates in a flat plate microbial fuel cell. *Environmental science & technology*, 38(21):5809–14.

[Minh and Takahashi, 1995] Minh, N. Q. and Takahashi, T. (1995). *Science and technology of ceramic fuel cells*. Elsevier.

[Minnich et al., 2009] Minnich, A., Dresselhaus, M., Ren, Z., and Chen, G. (2009). Bulk nanostructured thermoelectric materials: current research and future prospects. *Energy and Environmental Science*, 2(5):466–479.

[Minteer et al., 2007] Minteer, S. D., Liaw, B. Y., and Cooney, M. J. (2007). Enzyme-based biofuel cells. *Current opinion in biotechnology*, 18(3):228–234

[Mitcheson et al., 2004] Mitcheson, P. D., Miao, P., Stark, B. H., Yeatman, E., Holmes, A., and Green, T. (2004). Mems electrostatic micropower generator for low frequency operation. *Sensors and Actuators A: Physical*, 115(2):523–529.

[Modin and Wilén, 2012] Modin, O. and Wilén, B.-M. (2012). A novel bioelectrochemical bod sensor operating with voltage input. *Water Research*, 46(1):6113–6120.

[Mohan et al., 2008] Mohan, S. V., Babu, V. L., and Sarma, P. (2008). Effect of various pretreatment methods on anaerobic mixed microflora to enhance biohydrogen production utilizing dairy wastewater as substrate. *Bioresource Technology*, 99(1):59–67

[Moo et al., 2003] Moo, C., Hsieh, Y., Tsai, I., and Cheng, J. (2003). Dynamic charge equalisation for series-connected batteries. *IEE Proceedings-Electric Power Applications*, 150(5):501–505 1359–7043.

[Moo, 2010] Moo, W. H. K.-S. N. J.-H. H. C.-S. (2010). Charge equalization of battery power modules in series. *Power Electronics Conference (IPEC), 2010 International*, pages 1568–1572.

[Mukhopadhyay and Forssell, 2005] Mukhopadhyay, K. and Forssell, O. (2005). An empirical investigation of air pollution from fossil fuel combustion and its impact on health in india during 1973–1974 to 1996–1997. *Ecological Economics*, 55(2):235–250

[Nagayoshi and Kajikawa, 2007] Nagayoshi, H.; Tokumisu, K. and Kajikawa, T. (2007). Evaluation of multi mppt thermoelectric generator system. *Thermoelectrics, 2007. ICT 2007. 26th International Conference on*, pages 318–321.

[Ndegwa and Thompson, 2001] Ndegwa, P. and Thompson, S. (2001). Integrating composting and vermicomposting in the treatment and bioconversion of biosolids. *Bioresource Technology*, 76(2):107 – 112.

[Nishijima et al., 2000] Nishijima, K., Sakamoto, H., and Harada, K. (2000). A pwm controlled simple and high performance battery balancing system. pages 517–520.

[Oh and Logan, 2005] Oh, S. and Logan, B. E. (2005). Hydrogen and electricity production from a food processing wastewater using fermentation and microbial fuel cell technologies. *Water Research*, 39(19):4673 – 4682.

[Oh et al., 2009] Oh, S. E., Kim, J. R., Joo, J.-H., and Logan, B. E. (2009). Effects of applied voltages and dissolved oxygen on sustained power generation by microbial fuel cells. *Water science and technology : a journal of the International Association on Water Pollution Research*, 60(5):1311–7.

[O'Hayre et al., 2003] O'Hayre, R., Fabian, T., Lee, S.-J., and Prinz, F. B. (2003). Lateral Ionic Conduction in Planar Array Fuel Cells. *Journal of The Electrochemical Society*, 150(4):A430.

[Oliveira et al., 2013] Oliveira, V., Simões, M., Melo, L., and Pinto, A. (2013). Overview on the developments of microbial fuel cells. *Biochemical Engineering Journal*, 73:53–64.

[Pant et al., 2010] Pant, D., Van Bogaert, G., Diels, L., and Vanbroekhoven, K. (2010). A review of the substrates used in microbial fuel cells (MFCs) for sustainable energy production. *Bioresource technology*, 101(6):1533–1543.

[Park et al., 2007] Park, H.-s., Kim, C.-e., and Moon, G.-w. (2007). Two-Stage Cell Balancing Scheme for Hybrid Electric Vehicle Lithium-Ion Battery Strings. *Science*, pages 273–279.

[Park DH, 2003] Park DH, Z. J. (2003). Improved fuel cell and electrode designs for producing electricity from microbial degradation. *Biotechnol. Bioeng*, 81:348–355.

[Pascual, 1998] Pascual, C. (1998). "Switched capacitor system for automatic battery equalization," US Patent 5,710,504.

[Patil, 2013] Patil, S.; Mulla, A. K. S. (2013). A Single Chamber microbial fuel cell as power supply for implantable medical devices. *Energytech, 2013 IEEE*, pages 1–4.

[Paul and Liu, 2012] Paul, E. and Liu, Y. (2012). *Biological sludge minimization and biomaterials/bioenergy recovery technologies*. John Wiley and Sons.

[Peixoto et al., 2011] Peixoto, L., Min, B., Martins, G., Brito, A. G., Kroff, P., Parpot, P., Angelidaki, I., and Nogueira, R. (2011). In situ microbial fuel cell-based biosensor for organic carbon. *Bioelectrochemistry*, 81(2):99 – 103.

[Pennsylvania, 2004] Pennsylvania, T. (2004). Electricity Generation Using an Air-Cathode Single Chamber Microbial Fuel Cell in the Presence and Absence of a Proton Exchange Membrane. 38(14):4040–4046.

[Pham et al., 2009] Pham, T. H., Aelterman, P., and Verstraete, W. (2009). Bioanode performance in bioelectrochemical systems: recent improvements and prospects. *Trends in biotechnology*, 27(3):168–178

[Pi Changming and Wenhong, 2010] Pi Changming, Yan Wei, Z. K. and Wenhong, L. (2010). Dcm, fsm, dead time and width controllers for a high frequency high efficiency buck dc-dc converter over a wide load range. *Journal of Semiconductors*, 31.

[Picard, 2010] Picard, J. (2010). Under the hood of flyback smps designs. *Power Supply Design Seminar SEM1900, Topic 1*, (SLUP261).

[Picioreanu et al., 2007] Picioreanu, C., Head, I. M., Katuri, K. P., van Loosdrecht, M. C. M., and Scott, K. (2007). A computational model for biofilm-based microbial fuel cells. *Water research*, 41(13):2921–40.

[Picioreanu et al., 2008] Picioreanu, C., van Loosdrecht, M. C. M., Katuri, K. P., Scott, K., and Head, I. M. (2008). Mathematical model for microbial fuel cells with anodic biofilms and anaerobic digestion. *Water science and technology : a journal of the International Association on Water Pollution Research*, 57(7):965–71.

[Pinto et al., 2010] Pinto, R. P., Tartakovsky, B., Perrier, M., and Srinivasan, B. (2010). PERFORMANCE ANALYSES OF MICROBIAL FUEL CELLS OPERATED IN SERIES. (Dycops):533–538.

[Potter, 1911] Potter, M. C. (1911). Electrical Effects Accompanying the Decomposition of Organic Compounds. *Proceedings of the Royal Society of London. Series B,*, 84(571):260–276.

[Puig et al., 2010] Puig, S., Serra, M., Coma, M., Cabré, M., Balaguer, M. D., and Colprim, J. (2010). Effect of ph on nutrient dynamics and electricity production using microbial fuel cells. *Bioresource technology*, 101(24):9594–9599.

[Rabaey et al., 2005a] Rabaey, I., Ossieur, W., Verhaege, M., and Verstraete, W. (2005a). Continuous microbial fuel cells convert carbohydrates to electricity. *Water science and technology : a journal of the International Association on Water Pollution Research*, 52(1-2):515–23.

[Rabaey et al., 2004] Rabaey, K., Boon, N., Siciliano, S. D., Verhaege, M., and Verstraete, W. (2004). Biofuel Cells Select for Microbial Consortia That Self-Mediate Electron Transfer. 70(9):5373–5382.

[Rabaey et al., 2005b] Rabaey, K., Clauwaert, P., Aelterman, P., and Verstraete, W. (2005b). Tubular microbial fuel cells for efficient electricity generation. *Environmental science & technology*, 39(20):8077–8082.

[Raghavulu et al., 2009] Raghavulu, S. V., Mohan, S. V., Goud, R. K., and Sarma, P. (2009). Effect of anodic ph microenvironment on microbial fuel cell (mfc) performance in concurrence with aerated and ferricyanide catholytes. *Electrochemistry Communications*, 11(2):371 – 375.

[Rai et al., 2004] Rai, C. L., Struenkmann, G., Mueller, J., and Rao, P. G. (2004). Influence of ultrasonic disintegration on sludge growth reduction and its estimation by respirometry. *Environmental Science Technology*, 38(21):5779–5785. PMID: 15575300.

[Ramadass and Chandrakasan, 2011] Ramadass, Y. K. and Chandrakasan, A. P. (2011). A Battery-Less Thermoelectric Energy Harvesting Interface Circuit With 35 mV Startup Voltage. *IEEE Journal of Solid-State Circuits*, 46(1):333–341.

[Randall, 2003] Randall, J. (2003). *On ambient energy sources for powering indoor electronic devices*. PhD thesis, Ecole Polytechnique Federale de Lausanne, Lausanne, Switzerland.

[Rao JR Richter GJ, 1976] Rao JR Richter GJ, V. F. W. (1976). Performance of glucose electrodes and characteristics of different biofuel cell constructions. *Bioelectrochem. Bioenerg.*, 3(139-150).

[Rasi et al., 2007] Rasi, S., Veijanen, A., and Rintala, J. (2007). Trace compounds of biogas from different biogas production plants. *Energy*, 32(8):1375–1380.

[Raty, 2010] Raty, T. D. (2010). Survey on contemporary remote surveillance systems for public safety. *Systems, Man, and Cybernetics, Part C: Applications and Reviews, IEEE Transactions on*, 40(5):493–515.

[Reguera et al., 2005] Reguera, G., McCarthy, K. D., Mehta, T., Nicoll, J. S., Tuominen, M. T., and Lovley, D. R. (2005). Extracellular electron transfer via microbial nanowires. *Nature*, 435(7045):1098–1101.

[Reimers CE, 2001] Reimers CE, Tender LM, F. S.-W. W. (2001). Harvesting energy from the marine sediment-water interface. *Environ. Sci. Technol.*, 35(1):192–195.

[Rensing C, 2003] Rensing C, M. R. (2003). Issues underlying use of biosensors to measure metal bioavailability. *Ecotoxicol. Environ. Safety*, 65(1):140–147.

[Rismani-Yazdi et al., 2008] Rismani-Yazdi, H., Carver, S. M., Christy, A. D., and Tuovinen, O. H. (2008). Cathodic limitations in microbial fuel cells: An overview. *Journal of Power Sources*, 180(2):683 – 694.

[Rosenbaum et al., 2011] Rosenbaum, M., Aulenta, F., Villano, M., and Angenent, L. T. (2011). Cathodes as electron donors for microbial metabolism: which extracellular electron transfer mechanisms are involved. *Bioresource Technology*, 102(1):324–333.

[Rosenbaum M, 2006] Rosenbaum M, Schroder U, S. F. (2006). Investigation of the electrocatalytic oxidation of formate and ethanol at platinum black under microbial fuel cell conditions. *Solid State Electrochem*, 10:872–878.

[Roundy et al., 2004] Roundy, S., Steingart, D., Frechette, L., Wright, P., and J (2004). Power sources for wireless sensor networks. *Sensor Networks*, 2920:1–17.

[Roundy et al., 2003] Roundy, S., Wright, P. K., and Rabaey, J. (2003). A study of low level vibrations as a power source for wireless sensor nodes. *Computer Communications*, 26(11):1131 – 1144. Ubiquitous Computing.

[Rozendal et al., 2008] Rozendal, R. A., Hamelers, H. V. M., Keller, J., Rabaey, K., and Buisman, C. J. N. (2008). Towards practical implementation of bioelectrochemical wastewater treatment. *Trends in Biotechnology*, 26(8):450–459.

[S P Matova and van Schaijk, 2011] S P Matova, R Elfrink, R. J. M. V. and van Schaijk, R. (2011). Harvesting energy from airflow with a michromachined piezoelectric harvester inside a helmholtz resonator. *J. Micromech. Microeng.*, 21(10):1–6.

[Samuel Raj. B, 2013] Samuel Raj. B, Jebakumar Solomon. R.D, P. A. K. (2013). Production of electricity from agricultural soil and dye industrial effluent soil using microbial fuel cell. *International Journal of Research in Engineering and Technology*, 2(10):140–148.

[Sangeetha and Muthukumar, 2013] Sangeetha, T. and Muthukumar, M. (2013). Influence of electrode material and electrode distance on bioelectricity production from sagoâĂŘ processing wastewater using microbial fuel cell. *Environmental Progress and Sustainable Energy*, 32(2):390–395

[Schröder, 2007] Schröder, U. (2007). Anodic electron transfer mechanisms in microbial fuel cells and their energy efficiency. *Physical chemistry chemical physics : PCCP*, 9(21):2619–2629.

[Sealy, 2008] Sealy, C. (2008). The problem with platinum. *Materials Today*, 11(12):65 – 68.

[Shannon et al., 2008] Shannon, M. A., Bohn, P. W., Elimelech, M., Georgiadis, J. G., Marinas, B. J., and Mayes, A. M. (2008). Science and technology for water purification in the coming decades. *Nature*, 452(7185):301–310.

[Sharma and Li, 2010] Sharma, Y. and Li, B. (2010). Optimizing energy harvest in wastewater treatment by combining anaerobic hydrogen producing biofermentor (hpb) and microbial fuel cell (mfc). *International Journal of Hydrogen Energy*, 35(8):3789 – 3797.

[Shen and Wang, 1994] Shen, H. and Wang, Y.-T. (1994). Modeling hexavalent chromium reduction in escherichia coli 33456. *Biotechnol. Bioeng.*, 43:293–300.

[Shibata et al., 2001] Shibata, H., Taniguchi, S., Adachi, K., Yamasaki, K., Ariyoshi, G., Kawata, K., Nishijima, K., and Harada, K. (2001). *Management of serially-connected battery system using multiple switches*, volume 2. IEEE.

[Shin et al., 2010] Shin, J.-W., Seo, G.-S., Chun, C.-Y., and Cho, B.-H. (2010). Selective flyback balancing circuit with improved balancing speed for series connected lithium-ion batteries. *Power Electronics Conference (IPEC), 2010 International*, pages 1180–1184.

[Silicon.labs, 2014] Silicon.labs (2014). A 1v/1microa easy-to-use resistor-tuned silicon oscillator/timer, ts3001.

[Singh et al., 2010] Singh, D., Pratap, D., Baranwal, Y., Kumar, B., and Chaudhary, R. (2010). Microbial fuel cells: a green technology for power generation. *Annals of Biological Research*, 1(3):128–138

[Smith, 2008] Smith, A. M. (2008). Prospects for increasing starch and sucrose yields for bioethanol production. *The Plant Journal*, 54(4):546–558

[Speltino et al., 2010] Speltino, C., Stefanopoulou, A., and Fiengo, G. (2010). Cell Equalization In Battery Stacks Through State Of Charge Estimation Polling. pages 5050–5055.

[Stevens, 1999] Stevens, J. (1999). Optimized thermal design of small thermoelectric generators. *Proceedings of 34th Intersociety Energy Conversion Eng. Conference. Society of Automotive Engineers*, (1):2564.

[Stillwell et al., 2010] Stillwell, A. S., Hoppock, D. C., and Webber, M. E. (2010). Energy recovery from wastewater treatment plants in the united states: a case study of the energy-water nexus. *Sustainability*, 2(4):945–962.

[Stojmenovic, 2005] Stojmenovic, I. (2005). *Handbook of sensor networks: Algorithms and architectures*, volume 49. John Wiley and Sons.

[T. Paing and Popovic, 2008] T. Paing, J. Shin, R. Z. and Popovic, Z. (2008). Resistor emulation approach to low-power rf energy harvesting. *IEEE Transactions on Power Electronics*, 23(3):1494–1501.

[Taylor, 2004] Taylor, R. J. (2004). Optimization of a discontinuous conduction mode flyback for acoustical energy harvesting.

[Tender et al., 2008] Tender, L. M., Gray, S. A., Groveman, E., Lowy, D. A., Kauffman, P., Melhado, J., Tyce, R. C., Flynn, D., Petrecca, R., and Dobarro, J. (2008). The first demonstration of a microbial fuel cell as a viable power supply : Powering a meteorological buoy. 179:571–575.

[Tender, 2002] Tender, L. M., R. C. E. S. H. A.-H. D. E. B. D. R. L. D. A. P. K. R. C. (2002). Harnessing microbially generated power on the seafloor. *Nature Biotechnology Nature Biotechnology*, 20:821–825.

[Ter Heijne et al., 2011] Ter Heijne, A., Schaetzle, O., Gimenez, S., Fabregat-Santiago, F., Bisquert, J., Strik, D. P. B. T. B., Barriere, F., Buisman, C. J. N., and Hamelers, H. V. M. (2011). Identifying charge and mass transfer resistances of an oxygen reducing biocathode. *Energy Environ. Sci.*, 4:5035–5043.

[Thauer and Jungermann, 1977] Thauer, R. K. and Jungermann, K. (1977). Energy Conservation in Chemotrophic Anaerobic bacteria. *Bacteriological reviews*.

[Thompson and Phillips, 2009] Thompson, S. P. and Phillips, T. S. (2009). *Dynamo-Electric Machinery; A Manual for Students of Electrotechnics*. BiblioBazaar.

[Thurston C. F. and L., 1985] Thurston C. F., Bennetto H. P., D. G. M.-M. J. R. R. S. D. and L., S. J. (1985). Glucose metabolism in a microbial fuel cell. stoichiometry of product formation in a thionine-mediated proteus vulgaris fuel cell and its relation to coulombic yields. *J. Gen. Microbiol.*, 131(1393–1401).

[Tiquia-Arashiro, 2014] Tiquia-Arashiro, S. M. (2014). *Thermophilic Carboxydotrophs and their Applications in Biotechnology*. Extremophilic Bacteria Extremophilic Bacteria. Springer International Publishing, 1 edition.

[Torres et al., 2007] Torres, I., Rittmann, B. E., and Marcus, A. K. (2007). Conduction-Based Modeling of the Biofilm Anode of a Microbial Fuel Cell. 98(6):1171–1182.

[Tran HT, 2010] Tran HT, Ryu JH, J. Y. O. S. C. J. P. D. A. D. (2010). Continuous bioelectricity production and sustainable wastewater treatment in a microbial fuel cell constructed with non-catalyzed granular graphite electrodes and permeable membrane. *Water Sci Technol.*, 61(7):1819–1827.

[Tsujimura et al., 2001] Tsujimura, S., Wadano, A., Kano, K., and Ikeda, T. (2001). Photosynthetic bioelectrochemical cell utilizing cyanobacteria and water-generating oxidase. *Enzyme and Microbial Technology*, 29(4-5):225–231.

[U. Song, 2010] U. Song, E. L. (2010). "resources, conservation and recycling environmental and economical assessment of sewage sludge compost application on soil and plants in a landfill. *Conserv. Recycl.*, 54:1109–1116.

[Veerachary Mummadi and Uezato, 2002] Veerachary Mummadi, S. T. and Uezato, K. (2002). Voltage-based maximum power point tracking control of pv system. *IEEE Transac- tions on Aerospace and Electronic Systems*, 38:262–270.

[Vighetti et al., 2010] Vighetti, S., Lembeye, Y., Ferrieux, J., and Barbaroux, J. (2010). PHOTOVOLTAIC MODULE AND SHADOW: STUDY AND INTEGRATION OF A CURRENT BALANCING SYSTEM. In *Proceedings of EUPVSEC*, pages 4139 – 4143.

[Vikrant.A.Chaudhari, 2005] Vikrant.A.Chaudhari (2005). *Automatic peak power tracker for solar pv modules using dspacer software*. PhD thesis, Deemed University, maulana azad national institute of technology (Deemed University).

[Visser and Vullers, 2013] Visser, H. J. and Vullers, R. J. (2013). Rf energy harvesting and transport for wireless sensor network applications: Principles and requirements. *Proceedings of the IEEE*, 101(6):1410–1423

[Wang and Han, 2009] Wang, B. and Han, J.-I. (2009). A single chamber stackable microbial fuel cell with air cathode. *Biotechnology letters*, 31(3):387–393.

[Wang et al., 2012] Wang, H., Park, J.-D., and Ren, Z. (2012). Active energy harvesting from microbial fuel cells at the maximum power point without using resistors. *Environmental science & technology*, 46(9):5247–52.

[Wang X, 2009] Wang X, Cheng S, F. Y. M. M. S. T. L. B. (2009). Use of carbon mesh anodes and the effect of different pretreatment methods on power production in microbial fuel cells. *Environ Sci Technol.*, 43(17):6870–6874.

[Wasynczuk, 1983] Wasynczuk, O. (1983). Dynamic behavior of a class of photovoltaic power systems. *IEEE Trans. Power App. Syst.*, 102(9):3031–3037.

[Watanabe, 2008] Watanabe, K. (2008). Recent Developments in Microbial Fuel Cell Technologies for Sustainable Bioenergy. *Journal of Bioscience and Bioengineering*, 106(6):528–536.

[Watson and Logan, 2011] Watson, V. J. and Logan, B. E. (2011). Analysis of polarization methods for elimination of power overshoot in microbial fuel cells. *Electrochemistry Communications*, 13(1):54–56.

[Wen et al., 2009] Wen, Q., Wu, Y., Cao, D., Zhao, L., and Sun, Q. (2009). Electricity generation and modeling of microbial fuel cell from continuous beer brewery wastewater. *Bioresource technology*, 100(18):4171–5.

[West and Krein, 2000] West, S. and Krein, P. (2000). Switched-capacitor systems for battery equalization. *IEEE Modern Techniques and Technology (MTT 2000). Proceedings of the VI International Scientific and Practical Conference of Students, Post-graduates and Young Scientists,*, pages 57—59.

[Williams, 1960] Williams, R. (1960). Becquerel photovoltaic effect in binary compounds. *The journal of Chemical physics*, 32(5):1505–1514.

[Win et al., 2011] Win, K. K., Dasgupta, S., and Panda, S. K. (2011). An optimized MPPT circuit for thermoelectric energy harvester for low power applications. In *Proceedings of ECCE Asia*, pages 1579–1584. IEEE.

[Winfield et al., 2011] Winfield, J., Ieropoulos, I., Greenman, J., and Dennis, J. (2011). Investigating the effects of fluidic connection between microbial fuel cells. *Bioprocess and biosystems engineering*, 34(4):477–84.

[Wu et al., 2012] Wu, P. K., Biffinger, J. C., Fitzgerald, L. A., and Ringeisen, B. R. (2012). A low power DC / DC booster circuit designed for microbial fuel cells. *Process Biochemistry*, 47(11):1622–1628.

[Xiao et al., 2011] Xiao, B., Yang, F., and Liu, J. (2011). Enhancing simultaneous electricity production and reduction of sewage sludge in two-chamber {MFC} by aerobic sludge digestion and sludge pretreatments. *Journal of Hazardous Materials*, 189(1–2):444 – 449.

[Xiao and Dunford, 2004] Xiao, W. and Dunford, W. (2004). A modified adaptive hill climbing mppt method for photovoltaic power systems. *Power Electronics Specialists Conference*, 3:1957,1963.

[Xie et al., 2013] Xie, L., Shi, Y., Hou, Y. T., and Lou, A. (2013). Wireless power transfer and applications to sensor networks. *Wireless Communications, IEEE*, 20(4):140–145

[Xu et al., 2012] Xu, Y., Rojas-cessa, R., and Grebel, H. (2012). Allocation of Discrete Energy on a Cloud-Computing Datacenter using a Digital Power Grid. pages 615–618.

[Yahiro et al., 1964] Yahiro, A., Lee, S., and Kimble, D. (1964). Bioelectrochemistry: I. enzyme utilizing bio-fuel cell studies. *Biochimica et Biophysica Acta (BBA) - Specialized Section on Biophysical Subjects*, 88(2):375 – 383.

[Yang et al., 2013] Yang, F., Ren, L., Pu, Y., and Logan, B. E. (2013). Electricity generation from fermented primary sludge using single-chamber air-cathode microbial fuel cells. *Bioresource technology*, 128:784–787

[Yang et al., 2012] Yang, F., Zhang, D., Shimotori, T., Wang, K.-C., and Huang, Y. (2012). Study of transformer-based power management system and its performance optimization for microbial fuel cells. *Journal of Power Sources*, 205:86 – 92.

[Yohann R.J. Thomas, 2013] Yohann R.J. Thomas, Matthieu Picot, A. C. O. B. O. S. F. B. (2013). A single sediment-Microbial Fuel Cell powering a wireless telecommunication system. 241:703–708.

[Yu et al., 2012] Yu, J., Park, Y., Cho, H., Chun, J., Seon, J., Cho, S., and Lee, T. (2012). Variations of electron flux and microbial community in air-cathode microbial fuel cells fed with different substrates. *Water Science and Technology*, 66(4):748–753.

[Yuan, 2011] Yuan, Y., Z. S. X. N. Z. L. (2011). Microorganism-immobilized carbon nanoparticle anode for microbial fuel cells based on direct electron transfer. *Applied microbiology and biotechnology*, 89(5):1629–1635.

[Zhang et al., 2011] Zhang, F., Tian, L., and He, Z. (2011). Powering a wireless temperature sensor using sediment microbial fuel cells with vertical arrangement of electrodes. *Journal of Power Sources*, 196(22):9568–9573.

[Zhang and Halme, 1995] Zhang, X.-c. and Halme, A. (1995). MODELLING OF A MICROBIAL FUEL CELL PROCESS Xia-Chang Zhang and Aarne Halme Automation Technology Laboratory, Helsinki University of Technology, 02150 ESPOO, FINLAND. 17(8):809–814.

[Zhao and Kugel, 1996] Zhao, Q. and Kugel, G. (1996). Thermophilic/mesophilic digestion of sewage sludge and organic wastes. *Journal of Environmental Science and Health Part A*, 31(9):2211–2231.

[Zhu et al., 2013] Zhu, X., Tokash, J. C., Hong, Y., and Logan, B. E. (2013). Controlling the occurrence of power overshoot by adapting microbial fuel cells to high anode potentials. *Bioelectrochemistry*, 90(0):30 – 35.

[Zhuang and Zhou, 2009] Zhuang, L. and Zhou, S. (2009). Electrochemistry Communications Substrate cross-conduction effect on the performance of serially connected microbial fuel cell stack. *Electrochemistry Communications*, 11(5):937–940.

[Zuo et al., 2006] Zuo, Y., Maness, P.-C., and Logan, B. E. (2006). Electricity production from steam-exploded corn stover biomass. *Energy and Fuels*, 20(4):1716–1721.